UNIVERSITÀ DI PARMA

UNIVERSITA' DEGLI STUDI DI PARMA

DOTTORATO DI RICERCA IN
INGEGNERIA CIVILE E ARCHITETTURA

CICLO XXXIV

Automatic detection of landslide events for risk management and early warning procedures

Coordinatore:
Chiar.mo Prof. Sandro Longo

Tutore:
Chiar.mo Prof. Andrea Segalini

Co-tutore:
Chiar.mo Prof. Marian Drusa

Dottorando: Alessandro Valletta

Anni Accademici 2018/2019 – 2020/2021

Table of contents

List of Figures

List of Tables

Chapter 1. Introduction

1.1. Significance of the problem

During the last century, the influence of anthropogenic activities on the environment has become more and more impactful. This trend can be attributed mainly to the substantial growth of the human population: the results involve increased urbanization, industrial and construction activities, and the realization of an ever-growing network of transport infrastructures (Guzzetti, 2005). All these actions are inevitably correlated to an intensive exploitation of the available land, as well as a negative impact on climate change due to the ever growing demand of resources. As a consequence, a sensible increase of the occurrence of natural hazards has been observed, with heavy socio-economic impacts on local communities. According to data reported by the UNDRR (United Nations Office for Disaster Risk Reduction), a total of 281 disasters were recorded in 2018, affecting 61.7 million people and resulting in over 10700 lives lost (UNDRR, 2019).

Over the years, several international reports and policy documents have underlined this issue, raising awareness on the environmental degradation as one of the main driving forces behind the risk related to natural hazards (Depietri, 2020). The Millennium Ecosystem Assessment, initiated in 2001 and presented in 2005, evidenced the increased vulnerability of human populations to natural hazards caused by environmental degradation, and the importance of an appropriate management of ecosystems as a tool to reduce it (Reid, 2005). The Thematic Strategy for Soil Protection, produced by the European Commission in 2006, highlighted the serious problem posed by soil degradation and reports a series of community actions taken by several countries to address and discuss this issue (these include the United Nation Convention to Combat Desertification, the Protocol on Soil Protection under the Alpine Convention, the Kyoto Protocol, and the Convention on Biological Diversity).

Among the different typologies of natural hazards, landslides are included in the Thematic Strategy as one of the main threats to European soils. The term *landslide* includes a wide variety of phenomena and can be generally defined as a movement of a mass of rock, debris, or earth down slope, under the influence of gravity (WP/WLI, 1991). The range of landslide events is particularly diversified, encompassing small rock falls as well as large movements of soil involving millions of cubic meters of material, and their evolution in terms of velocity spans over fourteen orders of magnitude. Moreover, these phenomena are strongly correlated with other type of natural hazards, such as heavy rainfalls, earthquakes, floods, tsunamis, and volcanic eruptions (Casagli et al., 2017). A consequence of this connection is the underestimation of the socio-economic impact of these phenomena, which are usually not separated for the triggering actions represented by other natural hazards. The concerning outcome is a potential reduction of awareness regarding landslide risk (Sassa and Canuti, 2008).

Nonetheless, in recent years the worldwide scientific community has increasingly focused its attention on several approaches and methodologies for landslide risk reduction. A prime example is the SafeLand project, funded by EU and ran from 2010 to 2012, aimed to develop quantitative risk assessment and management tools and strategies for landslides across Europe.

Spanning over 5 Thematic Areas and 21 Work Packages, the large-scale research project involved 27 institutions from 13 European countries coordinated by the Norwegian Geotechnical Institute in Norway. The results of this collaboration were disseminated through a series of deliverable and reports, detailing several aspects of the investigated topic.

Another instance is represented by the report realized in 2018 by ISPRA (Istituto Superiore per la Protezione e la Ricerca Internazionale – Institute for Environmental Protection and Research) to provide an updated overview on landslide and flood hazard and risk on the Italian territory. Among European countries, Italy is one of the most affected by landslides (Figure 1), with a total of 620'808 occurrences included in the national database, corresponding to roughly 2/3 of the total number of landslides in Europe. The report evidenced the high exposure in terms of population, buildings, industries, and cultural heritage, highlighting the increasing trend of significant events on the Italian territory (Trigila et al., 2018).

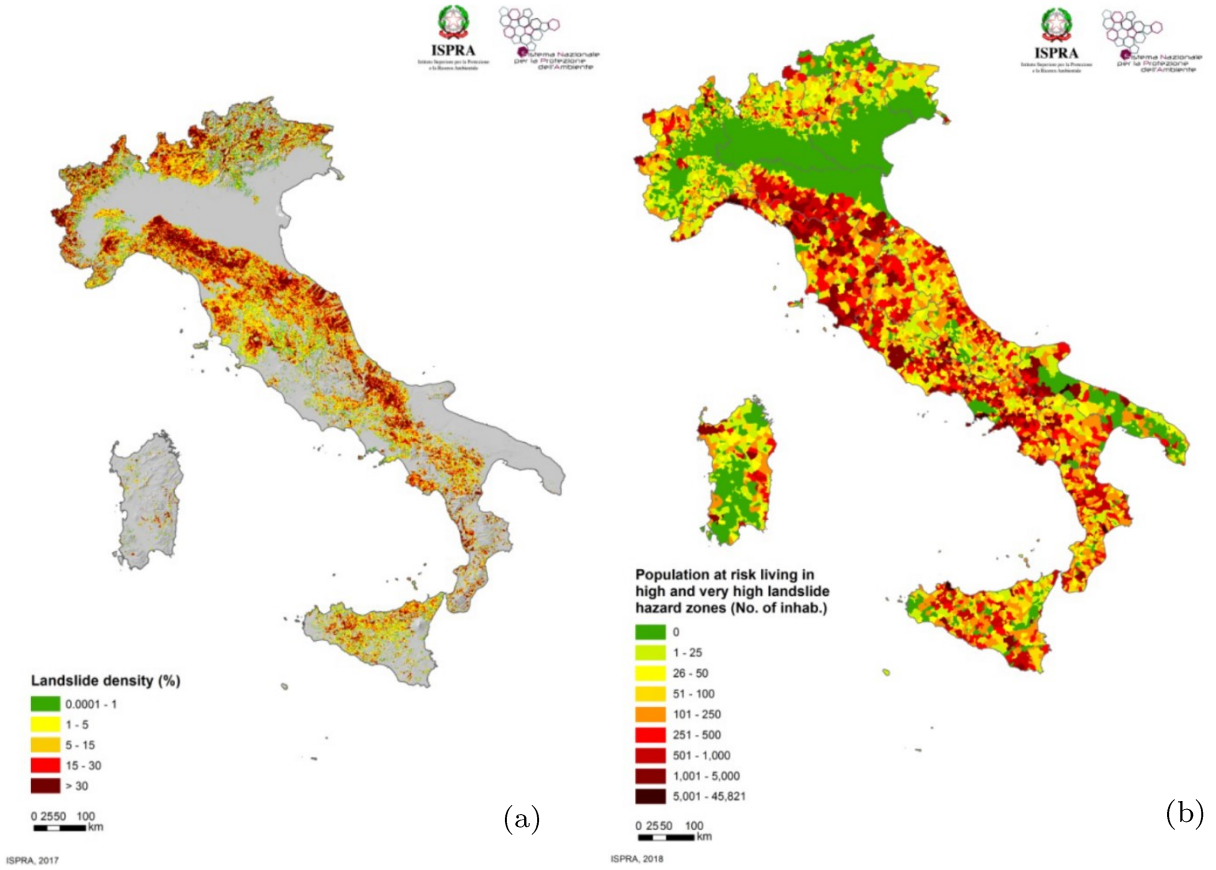

Figure 1. (a) Landslide density, calculated as the ratio between landslide area and total area referred to a 1x1 km grid; (b) Population at risk living in high and very high landslide hazard zones, defined by the River Basin District authorities (Trigila et al., 2018)

1.2. Work structure

Starting from these considerations, the work here presented aims to introduce new methodologies for landslide risk management and early warning purposes. In particular, the main objective of this thesis involves the automatic analysis of monitoring data in order to identify the occurrence of potentially critical events and consequently disseminate appropriate alert messages.

The first chapter is dedicated to the presentation of the main theoretical elements on which the work is based. This involves the introduction of the concept of Landslide Early Warning System and its main components, with particular attention to landslide monitoring devices and failure forecasting methodologies. The second chapter descends from the previous one, exploring the advantages of automatic monitoring systems based on Internet of Things technologies. The chapter focuses especially on the improved performances of these techniques in term of ability to achieve high sampling frequencies and integrate different sensor typologies for a multi-parameter monitoring approach.

The following chapters represent the core of the research project, focusing on the algorithms developed for the identification and assessment of potentially critical landslide events. Chapter 4 describes a criterion based on the analysis of displacement monitoring data to determine the presence of an accelerating trend. The algorithm follows a multi-level structure for the analysis in order to define the beginning of the acceleration phase, together with the dataset displaying this pattern. The following Chapter introduces a classification process intended to be applied to the outcome of the previous algorithm. The methodology relies on the evaluation of three different parameters, dependent of the dataset features and the results deriving from failure forecasting analyses, to assess the alert level for the identified event. Chapter 6 introduces two different procedures to define alert thresholds starting from available monitoring data. The first methodology is based on the forecasting model known as Inverse Velocity Method and integrates a normalization operation applied to monitoring outcomes. The objective is to provide a dimensionless parameter for the definition of generalized threshold values. The second algorithm introduces the concept of equivalent displacement, defined as the displacement generated in a time interval equal to the one showed by the potentially critical event. The process aims to compare the displacement produced by the event of interest with equivalent displacements referred to previously sampled data, to determine if the observed movement deviates significantly from the trend displayed by already available measurements.

Finally, Chapter 7 entails the aspect related to the dissemination of relevant information obtained from the previously described methodologies. For this purpose, two different algorithms were realized exploiting the *Matlab Report Generator™* toolbox. The first one is dedicated to the creation of a periodic monitoring report, including all relevant outcomes recorded over a predefined time period by instrumentation installed on site. The second one is a 1-page bulletin, generated in correspondence of the identification of a critical landslide event and delivered in near-real time for early warning applications. It contains only the essential information needed to understand if the observed phenomenon is evolving towards a hazardous state.

Chapter 2. Landslides Early Warning Systems (LEWS)

Early Warning Systems (EWS) represent a relevant option for effective disaster risk reduction, especially in those cases where structural measures are not viable for economical or practical reasons, or if they are unable to guarantee the safety of areas interested by instability phenomena.

A wide number of definitions and characterizations are present in the literature. As stated by Medina-Cetina and Nadim (2008), early warning systems are "monitoring devices designed to avoid, or at least to minimize, the impact imposed by a threat on humans, damage to property, the environment, or/and to more basic elements like livelihoods". According to another definition provided by UNDRR (United Nations Office for Disaster Risk Reduction, formerly known as UNISDR – United Nations International Strategy for Disaster Reduction), early warning systems should be designed to "empower individuals and communities threatened by hazards to act in sufficient time and in an appropriate manner to reduce the possibility of personal injury, loss of life and damage to property and the environment" (UNISDR, 2006). This definition was updated and integrated in 2016 with the following description: "An integrated system of hazard monitoring, forecasting and prediction, disaster risk assessment, communication and preparedness activities systems and processes that enables individuals, communities, governments, businesses and others to take timely action to reduce disaster risks in advance of hazardous events" (United Nations, 2016).

Several authors over the years have proposed different EWS general schemes, trying to summarize the key activities that should always be included in the design process of a landslide-oriented Early Warning System. According to UNISDR (2006), complete and effective EWS should include four components: risk knowledge, monitoring and warning service, dissemination and communication, and response capability (Figure 2a). The correct functioning of the entire system depends on these elements, and a weakness in a single one of these could result in the failure of the entire system.

An alternative structure was proposed by Di Biagio and Kjekstad (2007), which employed a flow diagram to highlight four main sequential activities: monitoring, analysis and forecasting, warning, and response (Figure 2b). According to the authors, the key issue to have an effective EWS lies in the identification, monitoring, and measurement of the events preceding a landslide occurrence. In particular, the precursors identification is essential for the correct choice of the most appropriate monitoring sensors.

By elaborating these two approaches, Intrieri et al. (2013) presented a new diagram that describes the EWS structure as a balanced combination of four components: design, monitoring, forecasting, and education (Figure 2c). The first phase involves the identification of the needs and vulnerabilities of the population at risk, as well as any obstacle to the action planned in the EWS. It also includes the determination of geo-indicators, i.e., geologic and meteorologic conditions that caused the landslide activation. The monitoring stage begins during the previous step, in order to provide preliminary information regarding the landslide behaviour. After the completion the design phase, the instrumentation becomes fully active, and the

monitoring activity enters the so-called operational phase. Forecasting is regarded by the authors as the most critical element of a LEWS, both for its importance and the issues related to the definition of reliable thresholds and the formulation of meaningful predictions. In particular, it is underlined the problem represented by false alarms, which can be reduced but never completely eliminated from the early warning process. Lastly, the education phase is focused on the community at risk and aims to increase the knowledge regarding the risk perception and the correct actions to prevent damages or losses.

An alternative representation, in the form of a wheel-like scheme, was proposed by Calvello et al. (2015). After the definition of the system scale and objectives, it is necessary to detail the required skills, the activities to be performed, the means to be used, and the basic elements of the system (Figure 2d). This approach underlines the necessity of a synergic collaboration between technical and social skills, with the objective of defining efficient processes and making the EWS an effective risk reduction tool, respectively.

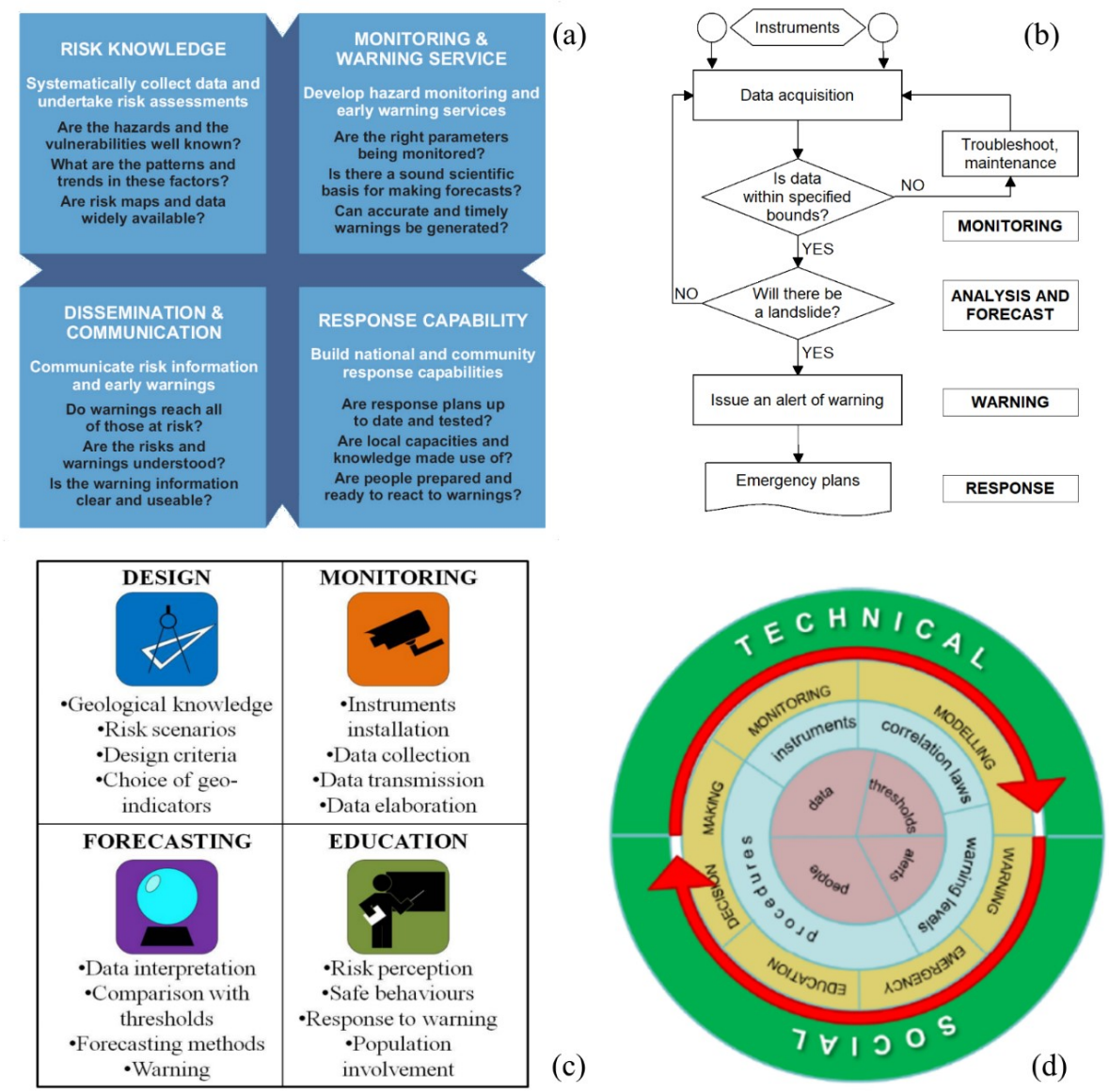

Figure 2. Schematic representations of LEWS structures, as proposed by: (a) UNISDR, 2006; (b) Di Biagio and Kiekstad, 2007; (c) Intrieri et al., 2013; (d) Calvello et al., 2015

The application scale is a fundamental component in the EWS design process, and it is frequently used as a reference to categorize the different systems. The most popular classification approach involves the definition of "local" and "regional" systems (Piciullo, 2016). EWSs operating at local scale are intended for site-specific applications, focusing on a slope-scale analysis of the instability phenomenon. Due to their site-specific nature, they are strongly affected by several factors related to the addressed case study. An interesting contribution to the design process of local EWSs, tackling both practical and technical aspects, is included in a deliverable of the SafeLand European project (Bazin, 2012), while many other examples of local early warning systems are available in literature (Froese and Moreno, 2014; Loew et al., 2017; Manconi and Giordan, 2015; Michoud et al., 2013; Oppikofer et al., 2009; Tarchi et al., 2003; Thiebes, 2012, among others).

On the other hand, regional warning systems are applied over appropriately defined areas, affected by diffuse instability problems. They are used when the exact location of future landslides is unknown, and typically involve the prediction and monitoring of meteorological variables. In particular, as evidenced in Piciullo et al. (2018), rainfall events have been widely used as the critical parameter to set up thresholds and plan emergency measures at regional scale. The same authors present a slightly different terminology, defining as "territorial" (Te-LEWS) the systems applied to the possible occurrence of several landslides at large scale. In this context, the adjective is intended to provide a more general definition to include all EWSs employed over a wide area, spanning from a river catchment to regions or nations. A detailed and extensive description of several warning systems designed for large geographical areas can be found in Guzzetti et al. (2020).

Regardless of the classification systems adopted, it is possible to identify a series of features and criteria that any EWS must fulfil (Stähli et al., 2015):

- Easy of implement: it is essential to achieve limited complexity, both in technical and communication-related aspects.
- Comprehensible and manageable: the interpretation of the EWS outcomes and components (e.g., thresholds, predictions, alert messages, etc.) should be as easy as possible for those in charge of the emergency management.
- Redundancy: it is fundamental to not rely on single sensors and transmission lines, and a multi-parametric and redundant system should be preferred.
- Precision: the system should be able to measure the critical parameters with an adequate precision.
- Autonomy: the power supply must be designed to support all operations with minimal maintenance and keeping the system functionality even in remote areas.
- Robustness: instrumentation must be able to withstand severe environmental conditions, taking into account a range external influences depending on the specific application.
- Affordability: the acquisition and operation costs should be balanced according to the expected risk reduction.

2.1. Risk assessment

Within the framework of natural hazards mitigation, risk assessment is a complex task that involves the combination of a wide range of techniques and methods. The synergic coordination between different expertise in the working fields of geology, geomorphology, engineering, and environmental technologies (among the others) is the foundation for the achievement of such an important objective (Guzzetti, 2005). Risk management processes plays a key role in the modern world, where the rapid growth of population and anthropic activities have generated problems related to the availability of territory. This has led to an increase of susceptibility to potentially catastrophic natural phenomena such as landslides, floods, volcanic eruptions, etc.

The description and the main goals of the landslide risk evaluation activity derives from a well-known report published by Varnes and the IAEG Commission on Landslides and other Mass-Movements, which presents the following definition: "Landslide risk evaluation aims to determine the expected degree of loss due to a landslide (specific risk) and the expected number of live lost, people injured, damage to property and disruption of economic activity (total risk)" (Varnes, 1984).

Due to its inherent complexity, landslide risk is usually determined starting from the evaluation of its components. A largely accepted formulation describes the risk as a function of three parameters, namely hazard, vulnerability, and elements at risk.

Landslide hazard (H) is defined as a description of the magnitude (M) and probability of occurrence (P) of a potentially damaging phenomenon within a certain time period of time and within a given area (Fell, 1994):

$$H = P * M \tag{I}$$

In this context, the term "magnitude" refers to the volume of material which may fail, the velocity of the movement during failure, and the potentially affected area (Crozier, 1995; Hunt, 1984). A simplified definition associates this component to the volume of displaced material. For example, the International Geotechnical Societies' UNESCO Working Party on World Landslide Inventory (WP/WLI, 1990) proposed an approximate formulation to evaluate the landslide volume under the hypothesis of a rotational slide:

$$\frac{1}{6}\pi * D_r * W_r * L_r \tag{II}$$

where:

- D_r is the maximum depth of rupture below the original ground surface
- W_r is the maximum width between flanks of landslide perpendicular to length L_r
- L_r is the minimum distance from the toe of the rupture surface to the landslide crown

On the other hand, the "probability" component can be described as the probability that a specific landslide will occur within a given period of time, and it usually ranges between 0 and 1. It is strictly related to slope stability analyses, since it is possible to assess the probability of failure according to the Factor of Safety evaluated by the procedure.

For what concern the vulnerability (V), Varnes (1984) defined it as the potential degree of loss to a given element (or set of elements) at risk resulting from the occurrence of a natural phenomenon featuring a given magnitude. The range of values varies between 0 (no damage) to 1 (total loss). According to Fell (1994), it is possible to describe the vulnerability as a product of different components, as reported in the following formulation:

$$V = V_S * V_T * V_L \quad \text{(III)}$$

where:

- V_S is the likelihood of spatial impact
- V_T is the likelihood of temporal impact
- V_L is the likelihood of loss of life of an individual occupant in the impacted element

It is worth noting that, although human losses are of primary importance compared to damages related to infrastructures and anthropic elements, scientific literature concerning the vulnerability of people to landslide was less common if compared to building-related damage analyses. The reasons for this derive from the difficulty to measure reliably all factors related to the human behaviour, such as situational awareness and decision-making abilities (Eidsvig et al., 2014). Moreover, it could be argued that human losses induced by a landslide event are often related to the collapse of occupied building, thus resulting in an indirect vulnerability (Jakob et al., 2012). However, it is possible to observe an increase of research activities focusing on this aspect in more recent years (some examples can be found in Assis Dias et al., 2020; Lin et al., 2017; Nor Diana et al., 2021; Pollock and Wartman, 2020).

These components allow to define the specific risk R_s as the expected degree of loss experienced by a given element due to the occurrence of a specific natural phenomenon. According to this definition, proposed by Varnes (1984) and approved by UNDRO (Office of the United Nations Disaster Relief Coordinator), the specific risk can be described as the product of hazard and vulnerability:

$$R_S = H * V \quad \text{(IV)}$$

Finally, the elements at risk (E) include the population, properties, infrastructures, and all the economic activities located in the area potentially affected by a specific event, thus being defined as a sum of every individual feature involved in the phenomenon evolution (Fell, 1994). The definition of this coefficient is strictly related to the scale of the investigation.

It this then possible to define the total risk R_T as the product of specific risk and elements and risk, representing the expected physical and social damage caused by the occurrence of a particular natural phenomenon (Varnes, 1984):

$$R_T = R_S * E = H * V * E \quad \text{(V)}$$

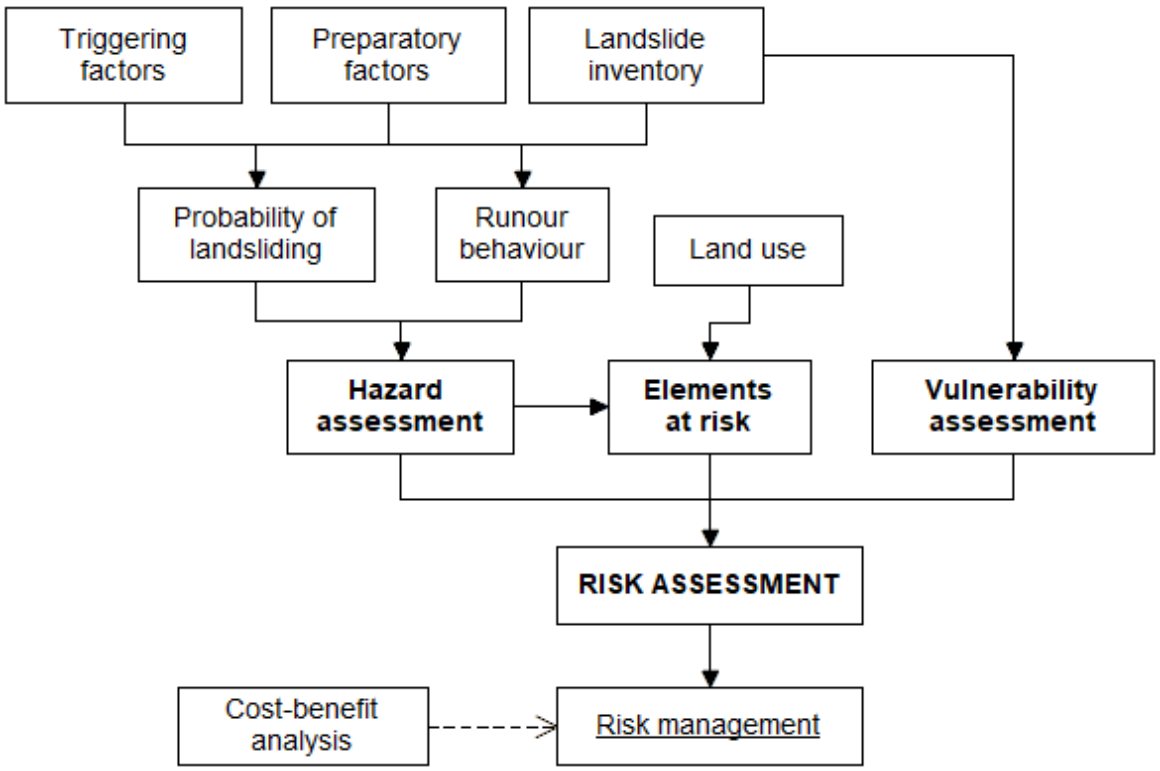

Figure 3. Example of a general framework for landslide risk assessment and management (modified after Dai et al., 2002)

When attempting to evaluate landslide risk, two main methodologies are usually employed: quantitative (probabilistic) approaches, and qualitative (heuristic) approaches. Quantitative analyses exploit numerical data and mathematical methods in order to estimate probabilities related to persons injured, structural damages, disruption of economic activities, etc., thus defining probabilistic levels of individual and collective risk. Their application often requires a catalogue of landslides, the compilation of which can be extremely difficult and time consuming. Moreover, the completeness, time span, and reliability of these lists play a key role in the reliability of the quantitative risk assessment procedure (Guzzetti, 2005). The qualitative risk assessment approach can be employed as an alternative to this methodology, in particular to design landslide scenarios based on qualitative ratings. This involves the description of hypothetical landslide events, including their effects on population and properties, in order to establish a probability of occurrence. In both cases, it should always be taken into account that the precision and reliability of the risk analysis depends on whether all components have been considered properly, and on the quality and reliability of the available data (VanDine et al., 2004).

2.2. Landslide monitoring

The monitoring activity of slope instabilities and landslides has gained increasing importance in recent years. The necessity to study and describe their evolution over time comes from their highly destructive effect on civilian population and infrastructures (Angeli et al., 2000). Additionally, field instrumentation is vital to the practice of geotechnics if compared to most other branches of engineering in which people have a much greater control of the materials involved in their activities (Dunnicliff, 1988). In the interests of mitigating the outcomes of such devastating events, the monitoring activity should aim to provide useful data to correctly identify impending failures and to design adequate mitigation measures. Among the others, these strategies shall comprise protective engineering measures and emergency planning, hazard mapping and assessment, and near-real time monitoring (Savvaidis, 2003). The main objectives of a landslide monitoring system can be summarized as follows:

- Evaluation of the phenomenon frequency, probability, and magnitude
- Database creation
- Definition of important parameters and relationships between them
- Formulation of forecasting hypotheses
- Determination of the mitigation measures efficiency and sustainability
- Dependence on meteorological and hydraulic conditions
- Numerical model realization and implementation

As reported by Dunnicliff et al. (2012), a geotechnical monitoring programme carries a considerable number of benefits, including damage minimization, performance improving, and state-of-knowledge advancing. The acknowledgement of these advantages, together with significant improvements experienced in several technological fields, has led to the development of a wide range of innovative devices able to guarantee an accurate and reliable sampling activity of significant parameters. However, it should always be remembered that a correct system design is mandatory to achieve reliable results. In fact, unappropriated instruments located in unfavourable positions could provide low quality information and misleading results (Segalini et al., 2017a). Moreover, because of the variability of landslide types and processes, investigation objectives, field conditions, and due to the still progressing technological development of monitoring sensors, no standardization can be adopted as a universal solution for landslide monitoring (Arbanas et al., 2014).

For these reasons, the design process of a monitoring program should be tackled with the utmost attention to all details, following a systematic approach to the planning process. As noted by Dunnicliff (1988), “full benefit can be achieved from geotechnical instrumentation programs only if every step in the planning and execution process is taken with great care”.

The same author proposed a series of steps, constituting a guideline for the development of a monitoring program:

- Define the project conditions
- Predict mechanism that control the behaviour
- Define the geotechnical questions that need to be answered
- Define the purpose of the instrumentation
- Select the parameter to be monitored
- Predict magnitudes of change
- Conceptualize remedial actions
- Assign tasks for the different project phases (design, construction, operation)
- Select the most appropriate instruments
- Select the location for each device to be installed on-site
- Plan recording of factors that may influence measured data
- Establish procedures for ensuring the correctness of monitoring readings
- List the specific purpose of each instrument
- Prepare the budget
- Write instrument procurement specifications
- Plan the installation procedure
- Plan regular calibration and maintenance of the system
- Plan data collection, processing, presentation, interpretation, reporting, and implementation
- Write contractual arrangements for field instrumentation services
- Update the budget in light of all previous steps

2.2.1. Traditional instrumentation

Over the years, various instruments have been applied to monitor the most relevant physical entities, dealing both with direct and indirect techniques. Despite following different design and purposes depending on the specific system, these tools share some features that are peculiar of the so-called “traditional” approach. In particular, they mainly rely on a manual and/or optical acquisition, requiring the presence of an operator on-site to acquire the monitored data or, alternatively, to collect the already recorded measures. Low acquisition frequency is another characteristic of these tools, typically ranging from some days to weeks and even months, since the operator availability and monitored site accessibility are mandatory for the data acquisition procedure, and both of those cannot be always guaranteed. On the other hand, this particular feature allows for an easier data elaboration, storage, and management, due to the limited number of measures sampled by the instrumentation. Additionally, in these cases, the energy requirements are generally low, and the power supply design does not pose relevant issues.

Conversely, the limited data availability makes it particularly difficult to implement meaningful statistical procedures intended to verify and improve the quality of the measured values, since their application to inadequate datasets can lead to non-significant and misleading results. Additionally, this property affects the possibility to assess cause-effect relationships

between different quantities, which is notably more difficult to achieve when data availability over time is limited. Moreover, a low sampling rate is not suitable for early warning procedures, where the availability of larger datasets is strongly suggested when applying forecasting methods (Valletta et al., 2019). This is a particularly important aspect since the effectiveness of a EWS is extremely relevant in risk management and mitigation operations.

As previously observed, one of the key features to be considered during the choice of the most appropriate monitoring device is the parameter of interest. In the geotechnical field, the knowledge of water level and ground displacements are among the most relevant factors to take into account. It is worth noting that traditional instrumentation is usually dedicated to the sampling of a specific physical quantity, with sensors designed to measure certain parameters.

Manual inclinometer

Inclinometers are used to determine the magnitude, rate, direction, depth, and type of landslide movement, helping in the identification of the potential sliding surface (Stark and Choi, 2008). Introduced in the market for the first time in the late 1950s, the slope inclinometer is nowadays a well-known and widely used device to describe the behaviour of a landslide.

The instrument integrates one or two force-balanced servo-accelerometers in order to measure the inclination of the casing with respect to the vertical direction; the most common version consists of a biaxial probe containing two perpendicular accelerometers. Since the device measures rotations at specified points, it is unable to detect translational movements. The system is generally constituted by a circular casing with two pairs of orthogonal grooves, acting as guides for the probe wheels (Figure 4a). The casing is inserted inside a vertical borehole, which must be deep enough to reach the stable zone located under the potential zone of movement in order to provide a meaningful description of differential displacements.

The measure is performed by lowering the probe at the bottom of the inclinometer and raising it incrementally with a predefined space interval, until the top of the casing is reached. During this procedure, one of the servo-accelerometers records the tilt in the plane of the inclinometer that tracks the longitudinal grove, while the other one measures the tilt in the plane perpendicular to the wheels. This operation is repeated twice for each set of grooves, for a total of four different directions of movement (commonly named A0, A180, B0, and B180, as in Figure 4b). A portable readout unit connected to the probe with an electrical cable collects and stores monitoring data, which have to go through a subsequent elaboration process in order to obtain the physical quantity of interest. This process is performed for the first time shortly after the inclinometer installation, in order to determine the initial shape of the casing and define the reference reading (known as “zero reading”). The difference between zero reading and subsequent measurements allows to calculate the differential displacements along the vertical direction and provide an insight to the magnitude, rate, direction, depth, and type of movement (Stark and Choi, 2008; Terzaghi and Peck, 1996).

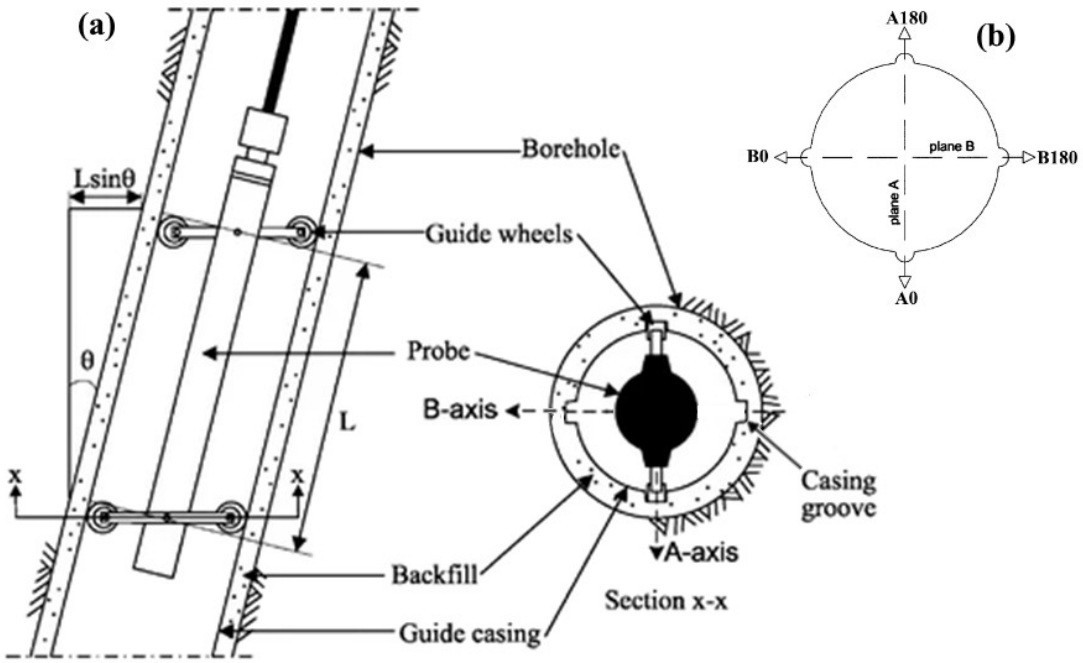

Figure 4. (a) schematic of the manual inclinometer device and casing; (b) identification of the four reference grooves in the inclinometer casing (modified after Stark and Choi, 2008)

All these operations, starting from the casing placement to monitoring data sampling and processing, should always be performed with great attention in order to minimize all possible random or systematic errors that could arise during the measurement execution (Ganjalipour, 2021; Green and Mikkelsen, 1988; Mikkelsen, 2003).

Extensometer

Extensometers are devices used in numerous practical applications to measure the changing distance between two specific points, thus describing the longitudinal deformation of the monitored element. When applied to landslide displacements, these points may be located on the surface to measure the opening of a tension cracks, or to identify the detachment of blocks from a rock mass. Alternatively, the extensometer can be installed in a borehole to measure differential displacements at specific depths (Eberhardt, 2013).

Several technologies have been exploited to produce different type of extensometers, ranging from traditional ones requiring an optical reading to more recent, electrical-based sensors relying on vibrating wire electronics or fibre optic elements. One of the most popular design in landslide monitoring is the wire extensometer, a simple and low-cost device that allow the measurement of relative displacements between a point located in stable ground, and another one identified on the moving landslide mass. Depending on the specific case study, the fixed point can be defined on the landslide surface or at the base of a borehole.

In the first case, the extensometer is usually installed across tension cracks to measure their opening over time according to the wire lengthening and shortening (Bonnard and Steinmann, 1990; Coe et al., 2003). In the second case, the reference point is located at the bottom of a borehole reaching the stable surface under the moving landslide (Angeli et al., 1988; Corominas

et al., 2000; Mentes, 2012). It is worth noting that a proper interpretation of wire extensometer data requires an adequate knowledge of the general pattern of the movement. In fact, there is no direct relationship between the landslide displacements and the wire length variation, which gives only punctual and one-dimensional information (Gracchi, 2019).

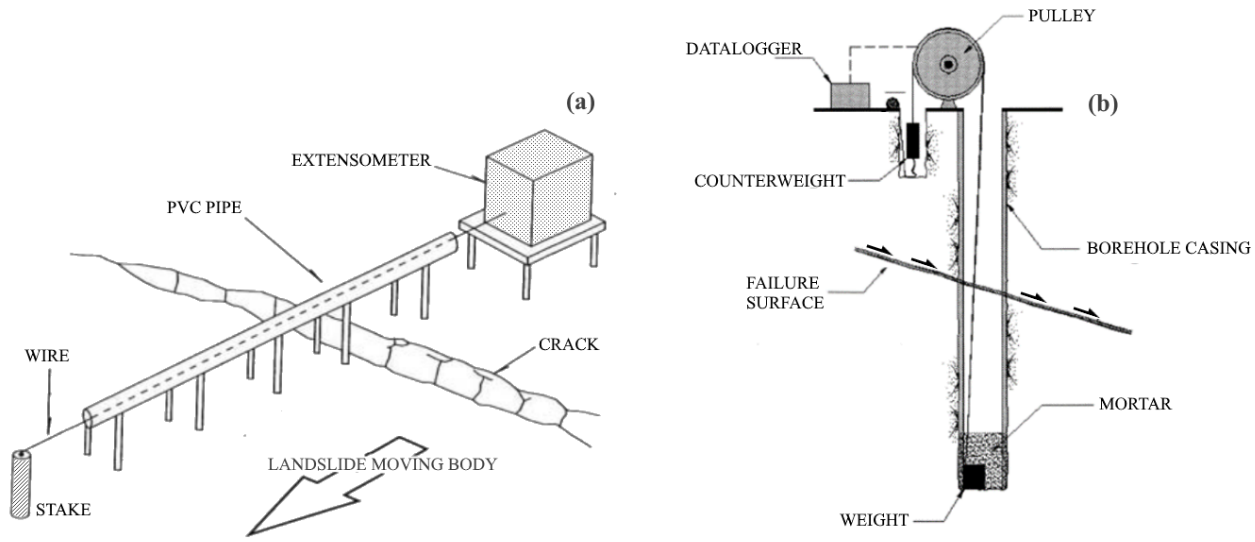

Figure 5. Schematic representation of wire extensometers with different installation approaches: (a) surface wire extensometer; (b) borehole wire extensometer (modified after Corominas et al., 2000; Karnawati et al., 2010)

Piezometer

Piezometers are extremely valuable tools when there is the need to measure pore water pressure and ground water level variations, which represent two of the most important parameters in the assessment of slope stability conditions (Van Asch et al., 2007). They also give information on the seepage pattern, zones of potential piping, and help in the definition of the ground water flow net.

The simplest and most traditional configuration is the open standpipe, usually combined with a Casagrande piezometer. It consists of a porous filter placed inside a borehole drilled into the soil to a previously determined depth intercepting the water table. The borehole is filled with gravel and presents a slotted portion in correspondence of the water table position, while the top sealing is provided by a cement and bentonite plug. The Casagrande piezometer tip is typically surrounded by sand and connected to the surface by a pair of plastic pipes. Water level measurements are usually performed by using an acoustic dip meter, and the pore pressure is equal to the height of the water above the measuring point (i.e., the centre of the porous filter). An alternative and more modern approach relies on electrical pressure transducers in order to monitor the parameters of interest. It consists of a cylindrical stainless-steel casing, a porous filter, and an electric sensor able to measure pore water pressure variations experienced by a membrane (Tremblay, 1989).

Depending on the design choice, the piezometer can be used to measure pore pressure in saturated soils (absolute piezometer), or to evaluate groundwater levels in wells and open

standpipes (relative piezometer). Moreover, the working principle depends on the typology of the transducer integrated in the device. In the case of a pneumatic piezometer, the instrumentation involves a valve, a flexible diaphragm, and it requires a supply of pressurized gas to counterbalance the pore water pressure acting on the filter. The readings are obtained when these two components reach an equilibrium condition. Piezometers based on vibrating wire technology integrate a magnetic, high-tensile strength, stretched wire plucked by a coil magnet. This component is anchored to the instrument body and is connected to a diaphragm sensible to pressure variations. As soon as pore water pressure changes, it influences the wire tension and, in turn, affects its vibrating frequency. This parameter is related to pressure differentials and can be read by using an appropriate datalogger. Lastly, strain gauge piezometers integrate an electrical resistance in order to measure the membrane deflection. The pressure is computed by reading the strain gauges signal, usually in 4-20 mA or 0-10 mV, and converting it with appropriate calibration equations.

Compared to Casagrande piezometers, electrical transducers can be set up for remote and automatic readings, resulting in a more efficient monitoring activity. Moreover, they show a shorter time response, making them more suitable for applications where a timely measurement of the hydrodynamic response is needed (Dunnicliff, 1988; Terzaghi and Peck, 1996).

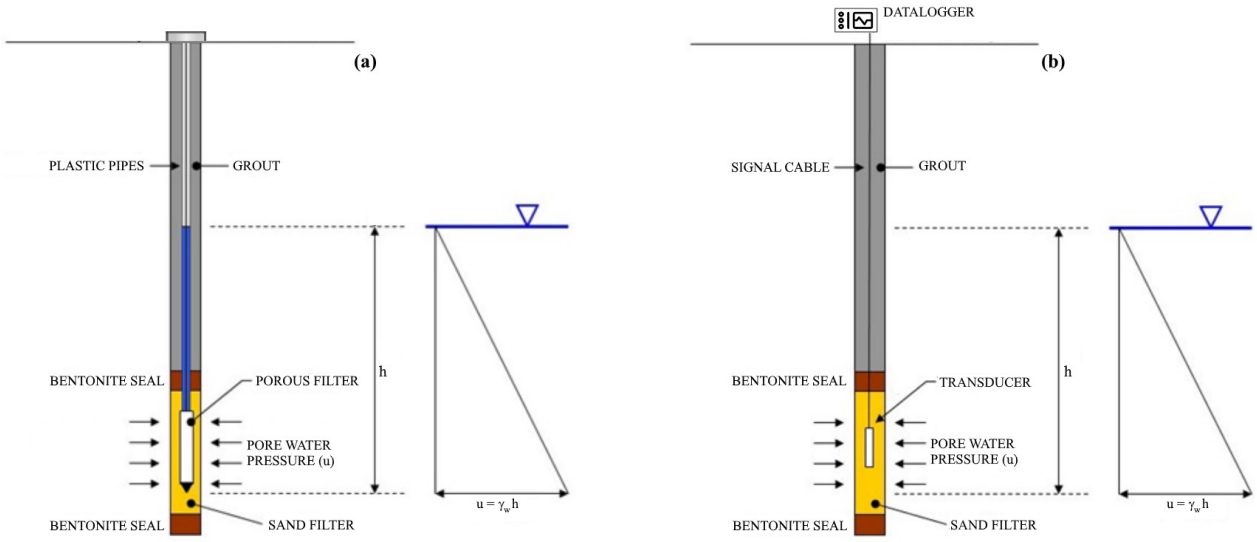

Figure 6. Components and installation of (a) Casagrande piezometer; (b) electric piezometer (modified after Prasad and Dixit, 2020)

2.2.2. Innovative instrumentation

In more recent years, geotechnical sensors have undergone considerable improvements regarding accuracy, efficiency and reliability. As a result, starting from the second half of 20th century, a series of innovative monitoring devices have been designed and produced, thanks to the introduction and widespread of latest-generation technologies. Notably, recent studies have focused their attention on improving automation and data elaboration procedures thanks to the integration of advanced algorithms and communication structures based on the Internet of Things approach (e.g., Bai et al., 2020; Carri et al., 2021; Wrzesniak and Giordan, 2017).

Furthermore, the development of these systems is often based on the combination of different traditional sensors, an approach that considerably improve the results reliability (Arbanas et al., 2013).

With respect to traditional instrumentations, the main features of innovative tools are the ability to operate automatically, the presence of remote-control features, and the possibility to monitor the parameters of interest with a considerably higher sampling frequency. These properties are closely related, presenting a series of advantages that play a key role in the design and planning of a landslide monitoring system. A remote and automated procedure, aimed to acquire and elaborate monitoring data, is extremely useful since it simplifies the operator's task. For what concern the increased sampling frequency, the most obvious improvement relates to the possibility of following the phenomenon evolution over time with greater detail and precision. Moreover, it allows to create a large database of monitored values, which is particularly useful in order to apply meaningful statistical analyses and to identify cause-effect relationships between different physical quantities (Carri, 2019). Another advantage is the possibility to integrate Early Warning processes thanks to the improved data availability. In fact, a system featuring high sampling frequencies and automated acquisition procedures is suitable for a near-real time approach, which can prove to be a key element to guarantee a timely and effective response to emergencies (Smethurst et al., 2017).

However, it should be pointed out that innovative systems often require an increased amount of power resources in order to work properly a provide the aforementioned advantages. For example, the energy supply of a monitoring device that needs to guarantee a sampling frequency in the range of hours, or even minutes, must be carefully designed and dimensioned (Reid et al., 2008). In fact, a sudden power failure can have extremely dangerous consequences, leading to a monitoring system shutdown and loss of information regarding potentially critical event (Segalini et al., 2017a)

Another aspect to be considered is the development of an adequate visualization platform, which becomes necessary to properly display the large amount of monitoring data produced by automatic instrumentation. On this regard, web-based environments are experiencing an increasing success thanks to the possibility to implement user-friendly interfaces and interactive elements to access all monitoring data in a continuously updated system (Frigerio et al., 2014; Pumo et al., 2015).

Remote Sensing

The application of remote sensors constitutes a relevant asset in landslide monitoring and is nowadays a well-regarded and widespread approach for several case studies. Within the category of remotely-based monitoring tools are included all those devices that do not need to be installed in contact with the area of interest in order to record data. While these sensors are limited to surface measures, remote sensing offers the possibility to observe an extended area without being influenced by the deformations acting on the monitored element. This approach

is especially useful when applied to natural phenomena featuring significant heterogeneity in terms of geomorphological and hydrogeological characteristics. Some of the most frequently used remote sensing tools are briefly described below.

Photogrammetry

Among the remote sensing approaches, photogrammetry is arguably one of the oldest approaches developed to control the evolution of landslides and has been used since long time either in its aerial and ground-based configuration (Roncella et al., 2014). The methodology is based on the acquisition of multiple optical images of the area of interest at different times, and the recognition of specific elements (named Control Points) that are present in each image. Knowing the camera parameters, it is possible to exploit these CPs in order to georeference the images, making it possible to identify displacements experienced by the monitored element.

Despite the arising of new technologies based on laser and radar sensors, photogrammetry is still a prominent technique in landslide investigation, especially in its aerial configuration based on Unmanned Aerial Vehicles (UAV, Figure 7). Some of its applications include the identification of topographic features of the slope (Lane et al., 2000; Walstra et al., 2007), the creation of Digital Elevation Models (Stumpf et al., 2015; Uysal et al., 2015), and the evaluation of morphological surface changes induced by mass movements (Fabris, 2019; Marsella et al., 2012).

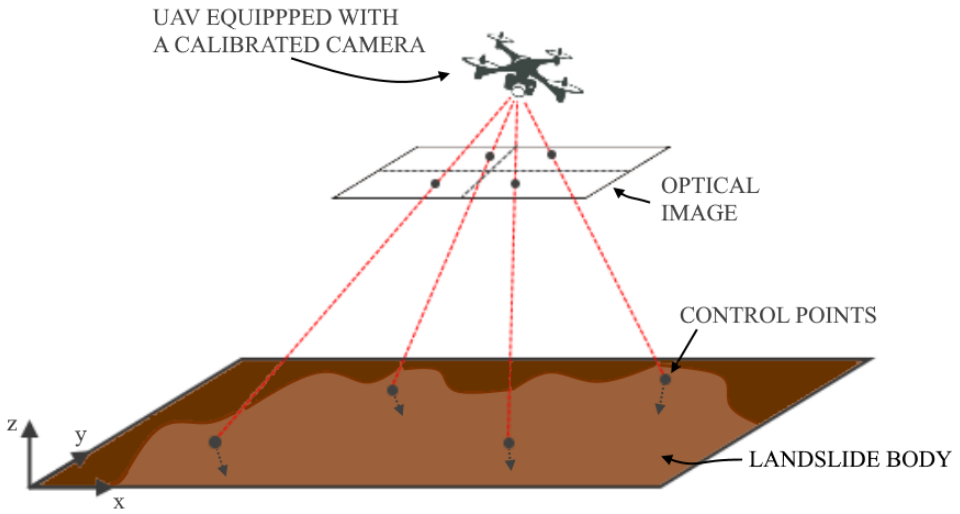

Figure 7. Image acquisition and detection of ground Control Points on a moving landslide body, by means of an UAV equipped with a calibrated camera

Laser Scanner

The Laser Scanner is a device able to collect a dense array of points thanks to an active laser sensor (Figure 8). This instrument can be set to scan automatically the area of interest and generate a point cloud where each point is defined by a set of 3D coordinates. For each scanned point, in is possible to determine its position and distance with respect to the device by evaluating the time of flight between the impulse generated and received by the sensor. The result of the data elaboration and processing is a three-dimensional model of the monitored

object (Jaboyedoff and Derron, 2020). The comparison of models created at different moments in time gives a measure of displacement occurred in the selected time interval. Moreover, it is possible to choose the sampling frequency according to the case, thus obtaining 3D models featuring several degrees of detail.

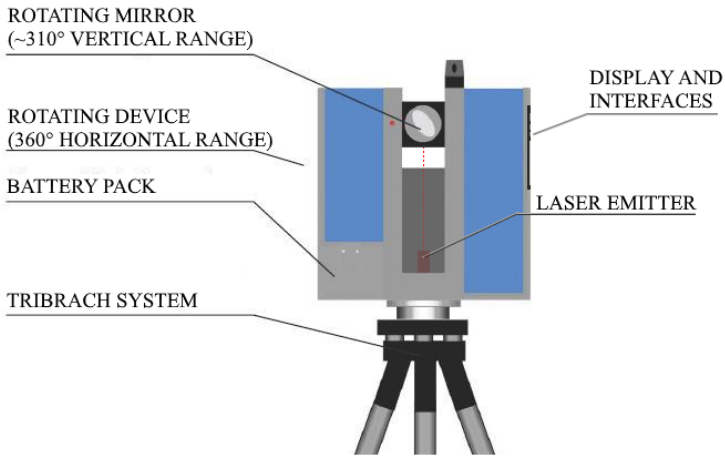

Figure 8. Main components of a terrestrial laser scanner device (modified after MicroGeo Srl)

Some of the most frequent application of this technology include the creation of digital terrain models for landslide mapping (Ardizzone et al., 2007; Gazibara et al., 2019), the evaluation of volumes mobilized by debris flow or rockfall events (Rengers et al., 2021; Scheidl et al., 2008), and the characterization of rock faces that would be difficult to access by other means (Gigli et al., 2014; Mavrouli et al., 2015).

Robotic Total Station

A Total Station is an electronic/optical device composed by a theodolite and an electronic distance meter (EDM), integrated with a dedicated microprocessor. The combination of these sensors permits to measure horizontal angles, vertical angles, and the distance of the monitored element from the station point, thus obtaining the position of the object itself. Control points are usually materialized by prisms, which reflect the Total Station signal more reliably, and improve the measures precision and accuracy. The so-called Robotic Total Station (RTS) was developed in order to remove the need of an operator on-site to control the instrumentation (Figure 9). To achieve this objective, the device equips a series of servomotors for automatically rotating the instrument and the horizontal and vertical plane. Moreover, an Advanced Tracking Sensor (ATS) in installed for tracking the prisms placed on site (Savvaidis, 2003). This approach allows to automate the monitoring process, significantly improving the system's efficiency.

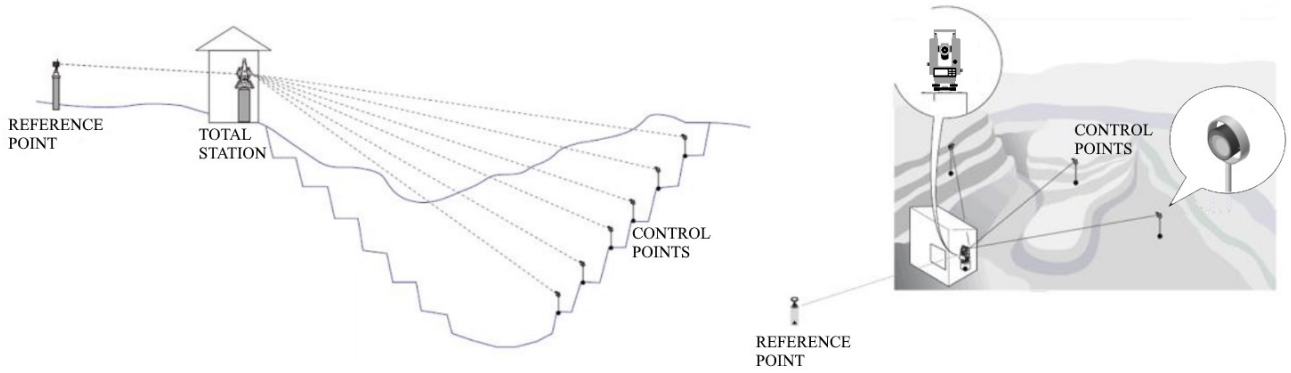

Figure 9. Main components of a monitoring system based on a robotic total station and multiple control points (modified after Kalybekov et al., 2018)

In the landslide monitoring framework, RTS is used to measure with great accuracy the displacement of specific points of interest located on the slope surface, and it is frequently used in synergy with other monitoring devices to provide a complete description of the monitored element behaviour (Castagnetti et al., 2013; Corsini et al., 2013; Lienhart, 2017).

Interferometric Synthetic Aperture Radar (InSAR)

Interferometric Synthetic Aperture Radar (InSAR) technology is a well consolidated monitoring approach for measuring ground motion. Its working principle relies on an active sensor designed to acquire Synthetic Aperture Radar (SAR) images of a specific area, produced by reflecting the radar signal and measuring the two-way travel time back to the receiving sensor. SAR interferometry exploits two images acquired at different times to evaluate the surface displacement that occurred in that time span. Nowadays, InSAR technology is used in two different configurations: satellite-based and ground-based.

Satellite-based InSAR (Figure 10) dates back to the early 90's, when the European Space Agency launched the first satellite for Earth observation, the ERS-1. During the years, this technique has been extensively studied and applied, resulting in the development of several approaches for the interpretation of radar images. One of the most advanced and accurate is the Persistent Scatter Interferometry (PSI), which takes advantage of the presence of so-called persistent scatterers, i.e., natural and artificial elements that provide a constant and characteristic radar reflection over time. A wide range of PSI algorithms has been developed over the years, depending on the baseline configuration, the pixel selection criterion, and the deformation model used in the process (Crosetto et al., 2016). The sampling period of satellite interferometry varies depending on the satellites used and their revisiting time, i.e., the time needed to frame the same area after a previous passage. After the launching of Sentinel-1a and Sentinel-1b, in 2014 and 2016 respectively, the minimum time interval has been reduced to 6 days (Raspini et al., 2019). While this sampling frequency could prove inadequate for early warning activities, it is definitely suited for monitoring activities related to long-term displacements, historical analyses, landslide mapping and characterization, and surveying of very large areas (some examples can be found in Barra et al., 2016; Crippa et al., 2020; Miele et al., 2021; Reyes-Carmona et al., 2020; Tofani et al., 2013).

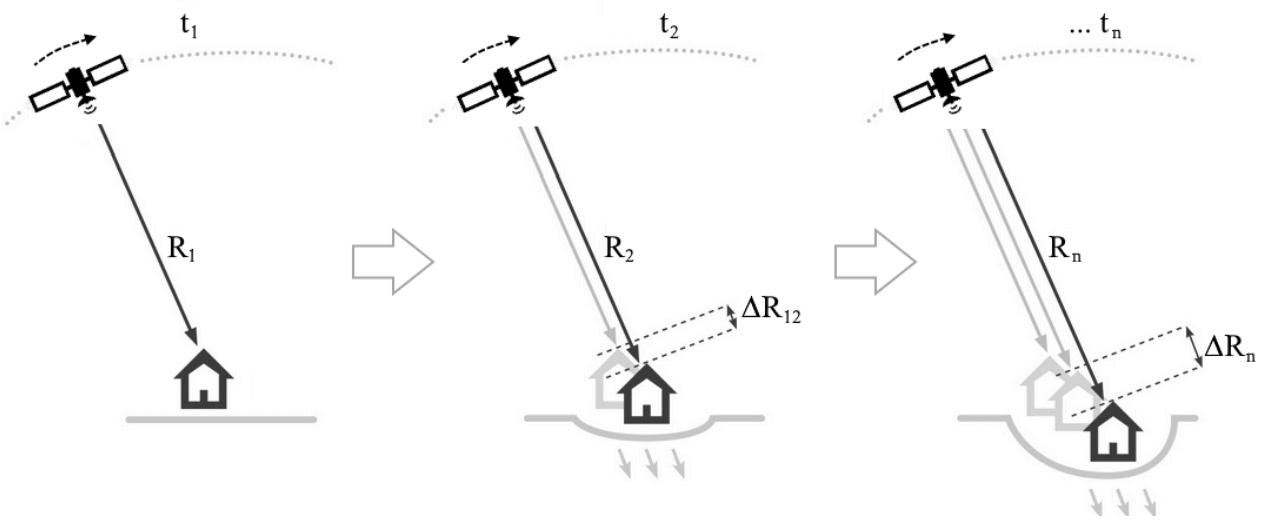

Figure 10. Working principle of the satellite-based SAR interferometry (modified after Wilson et al., 2019)

The ground-based interferometry technique (known as GB-InSAR) exploits the very same working principle described for the satellite-based version. In this configuration, it relies on the correlation of different radar images acquired by a sensor appropriately located in front of the monitored object in an area not influenced by the instability phenomenon. The device is composed of an active sensor, able to transmit and receive radar signals thanks to two different antennas, acquiring images by moving along a horizontal rail that allows extremely precise movements (Figure 11).

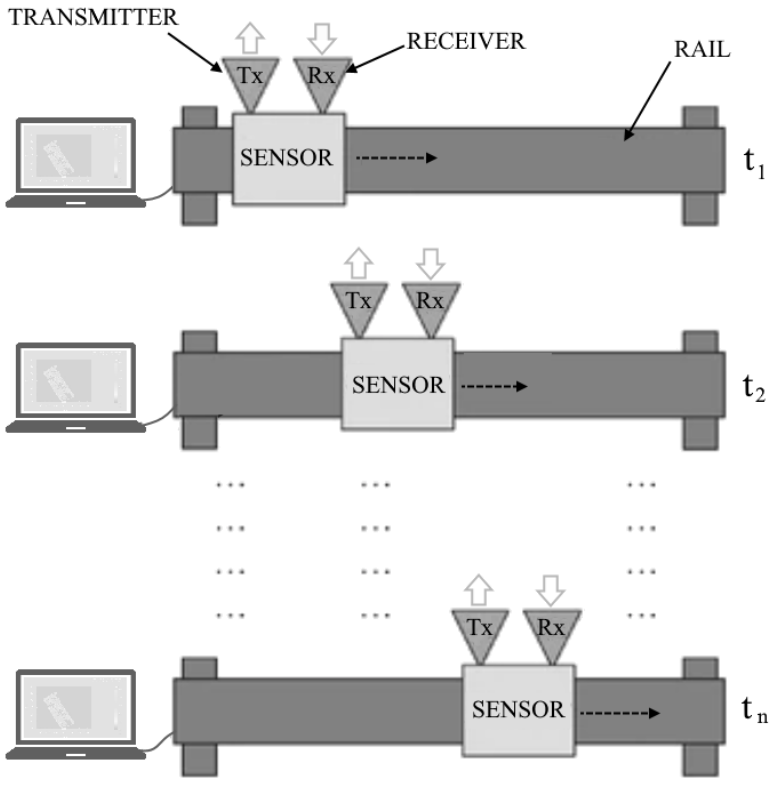

Figure 11. Schematic representation of the ground-based InSAR working principle (modified after Bozzano et al., 2011)

The sensor obtains 2D images of the monitored surface, thus allowing the evaluation of displacements along line of sight (LOS) of the instrument by comparing the phase signal difference of each pixel between images acquired at different times (Mazzanti et al., 2015a). Compared to its spaceborne counterpart, GB-InSAR is able to reach very high sampling frequency, collecting a new radar image every few minutes (Frodella et al., 2016). This feature, together with the ability to survey very wide areas, makes it a very successful device for early warning activities and to monitor fast landslides, especially when combined with other survey techniques (Bozzano et al., 2011; Carlà et al., 2017a; Crosta et al., 2017; Di Matteo et al., 2017; Mazzanti et al., 2018; Zheng et al., 2019).

Direct Monitoring

A different set of innovative instruments follows the so-called "direct" approach, which identifies a monitoring tool installed on-site in contact with the area of interest. While these systems are not comparable to remote sensing devices for what regards the spatial extent of the monitored area, their sampling ability is not limited to the slope surface, and they can collect detailed information at different depths. Usually, these tools are designed around the integration of various sensors measuring different physical quantities, thus allowing to provide an improved measurement framework thanks to their multi-parametric and redundant properties.

A brief description of some of the most frequently used innovative monitoring tools following the "direct" approach is reported in the following paragraphs.

TDR (Time Domain Reflectometry)

TDR technology represents a particular case in the landslide monitoring framework. In fact, even if the core working principle has been employed since the 1930s in several sectors (e.g., electrical engineering), its application for the automated monitoring of unstable slopes is relatively recent (Drusa and Bulko, 2016).

A Time Domain Reflectometry system basically consists of two components: a coaxial cable installed in a borehole and coupled to the surrounding rock, and a dedicated cable tester with the ability to generate electrical pulses in form of electro-magnetic waves along the device length (Figure 12). Since the propagation velocity of the signal is constant, the distance is determined by measuring the time between initiation of the pulse and detection of its reflection. In this configuration, the coaxial cable works like a continuous sensor able to identify any change in the geometry caused by deformations of the monitored element, according to the return time of the reflected signal. Information about the type and amount of deformation can be inferred from the analysis of the pulse recorded by the control unit, therefore helping in the identification of the potential sliding surface of the monitored landslide. It is worth noting that TDR technology is able to determine the exact position of the observed deformation zone, while the displacement magnitude can be assessed with a semi-quantitative approach (Singer et al., 2006).

Moreover, the same working principle can be applied for the measurement of the water table elevation. This operation relies on the difference in the signal propagation through mediums, such as air and water, presenting distinct values of dielectric constant. Because of this feature, it is possible to identify a change in the TDR waveform at the interface point, thus determining the water level depth (Moret et al., 2004).

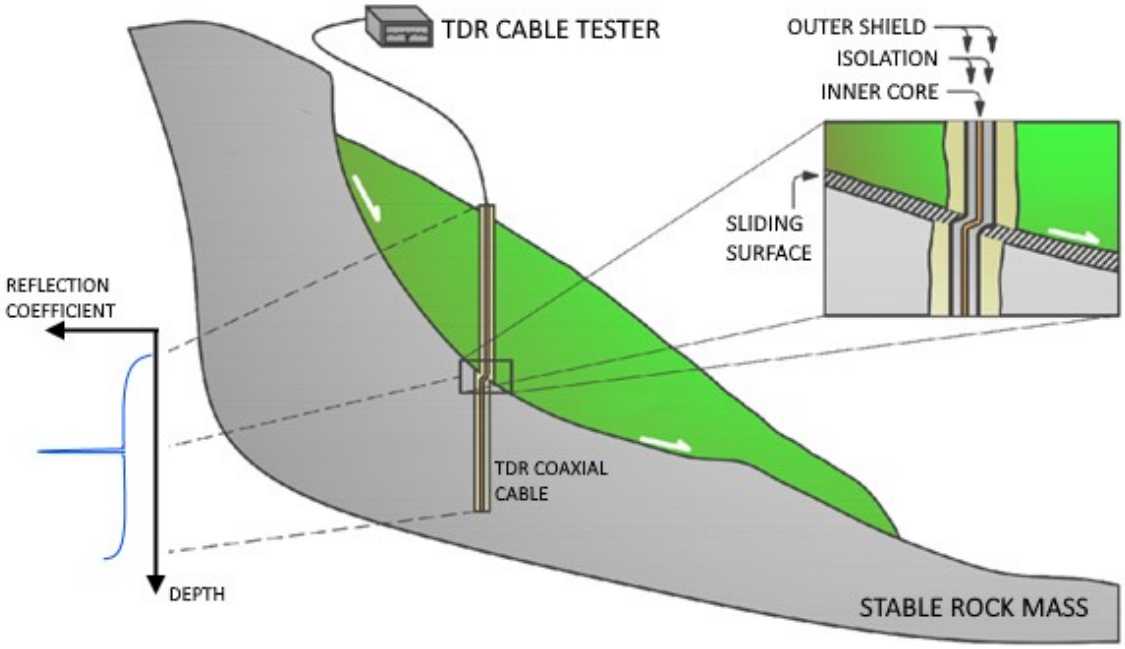

Figure 12. Basic setup of a TDR system for landslide monitoring (modified from Drusa and Bulko, 2016)

AIS (Automatic Inclinometer System)

The Automatic Inclinometer System (AIS) is a mechanized inclinometer designed by Research Institute for Hydrogeological Prevention and Protection – CNR IRPI (IT) with the goal to automatize the measurement conventionally carried out by an operator. The system consists of a traditional inclinometer probe equipped with 2D servo-accelerometers or MEMS, and integrates an electric motor to drive the device up and down inside the casing. Additionally, it comprises a load cell to control the probe mobility, and an encoder to record the position of the probe inside the borehole (Allasia et al., 2020). The measuring phase follows the same working principle of a traditional inclinometer, where the electrical actuator controls the probe downlift and uplift operations. Data are stored in the probe memory unit and transmitted to a control unit at the top of the borehole thanks to a wireless connection. A software processes the data, checking also the system integrity and sending warning messages if slope movements exceed a predetermined threshold (Lollino et al., 2002).

DMS (Differential Monitoring of Stability)

Differential Monitoring of Stability (DMS) is a patented tool produced by CSG S.r.l. (IT) designed for continuous control of potentially unstable areas. This device is pre-assembled at the factory in the form of an instrumented column that connects the required number of modules, and is designed to monitor landslides and geotechnical structures (Lovisolo and Della

Giusta, 2005). Each module is 1-metre long and can be equipped with 2D MEMS, piezometer, thermometer or triaxial accelerometer sensors. A dedicated readout unit automatically collects data from each DMS column, and transmits them to the monitoring center, where they are stored and elaborated by a proprietary software.

SAA (Shape Accel Array)

Shape Accel Array (SAA) is a patented geotechnical instrumentation developed by Rensselaer Polytechnic Institute (USA) and Measurand Inc. (NB - Canada). The device comprises an array of rigid segments connected with flexible joints, and equipped with a set of three orthogonal MEMS sensors to measure changes in the apparent gravitational field due to movement of the array (Swarbrick and Clarke, 2015). Each Shape Array is installed inside a small diameter access tube and follows the same working principle of in-place inclinometers, using raw tilt data collected by the sensors to compute displacements at predefined depths (Dasenbrock et al., 2012). The entire procedure is managed by a control unit that automatically queries sensors in near-real time and periodically upload results on a web platform, disseminating alert messages at the overcoming of a predefined threshold.

MUMS (Modular Underground Monitoring System)

One of the most recent approaches to innovative direct-monitoring instrumentation is represented by MUMS (Modular Underground Monitoring System) technology, developed by ASE S.r.l. (IT). Due to its prominent role in the development of all methodologies included in this work, Chapter 3.1 of this thesis will be devoted to an in-depth description of the working principle of this monitoring device.

2.3. Failure forecasting methods

The prediction of a landslide occurrence is a particularly relevant task from both a scientific and social point of view. Accurate time-of-failure forecasting plays a key element to develop an efficient Early Warning System, allowing to avoid or at least reduce damage and human losses. However, this is known to be one of the most challenging problems regarding slope stability analysis, due to the large number of factors and parameters influencing landslide behaviour and its triggering. For this reason, this topic has been the main focus of several studies carried out over the years to address the possibility to predict a landslide collapse starting from monitoring data.

The main concept of most kinematic-based failure forecasting methods relates to the assumption that slope displacements approaching failure follow a continuous acceleration, described by a creep curve (Tavenas and Leroueil, 2011). According to the classical interpretation of creep theory (Varnes, 1982), it is possible to differentiate three stages: the first one (primary creep) shows a decreasing of the strain rate, the second one (secondary) features a constant strain rate, and the third (tertiary) presents an increasing creep rate, ultimately leading to rupturing (Figure 13).

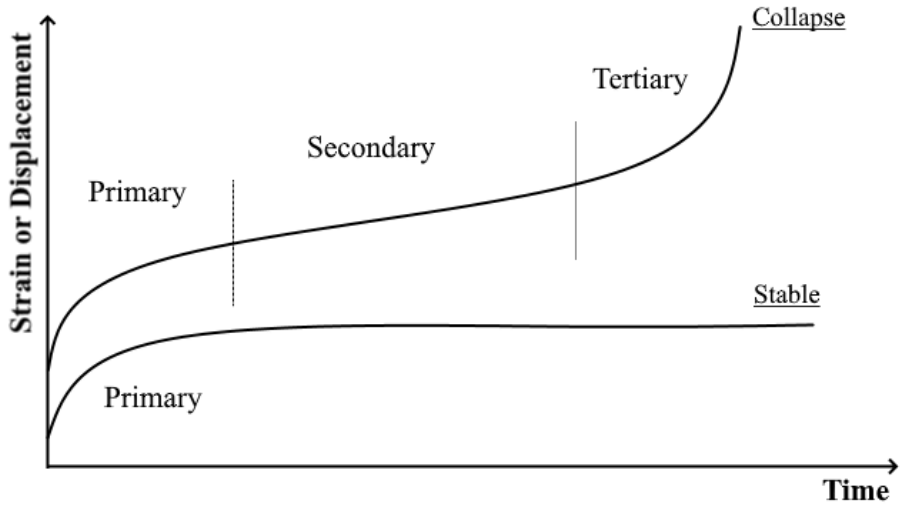

Figure 13. Creep curve representing the relationship between strain (or displacement) and time in stable and collapsing configurations

It is possible to identify two main groups of kinematic based time-of-failure prediction methods (Intrieri et al., 2019):

- Empirical methods: these approaches usually extrapolate the time-of-failure prediction thanks to geometrical procedures starting from displacement rate data
- Semi-empirical methods: the basis of these methods is a general equation that relates displacement rate and acceleration data

This chapter reports a summary of some of the main approaches developed over the years to address the failure forecasting topic. A more in-depth discussion can be found in Federico et al. (2012) and Intrieri et al. (2019).

2.4. Empirical methods

A first approach to failure forecasting was presented in the early 1960s, when Saito and Uezawa (1961) proposed a method based on the comparison between displacement records and creep rupture curves. The approach was firstly introduced by the authors to be applied on secondary creep curves, and relied on a formulation to evaluate the time left to failure t_L according to the value of strain rate:

$$\log_{10} t_L = 2.33 - 0.916 \log_{10} \dot{\varepsilon} \pm 0.59 \qquad \text{(VI)}$$

Saito (1969) lately extended this approach to tertiary creep trends, introducing a graphical methodology to evaluate the time-of-failure. According to the procedure described by the author, based on geometrical arguments, three points (namely A1, A2, and A3) can be selected on a displacement curve in order to have an equal difference of displacement. By drawing a line parallel to the x-axis and passing through A2, it is possible to identify the projection of A1 and A3 on it, named A'1 and A'3 respectively. The point M identifies the midpoint if the segment A'1A2, while the point N refers to segment A'1A'3. Finally, it is possible to evaluate

the time-of-failure as the abscissa of the intersection of a line passing through A'1 and N', and another line parallel to the x-axis and passing through M'.

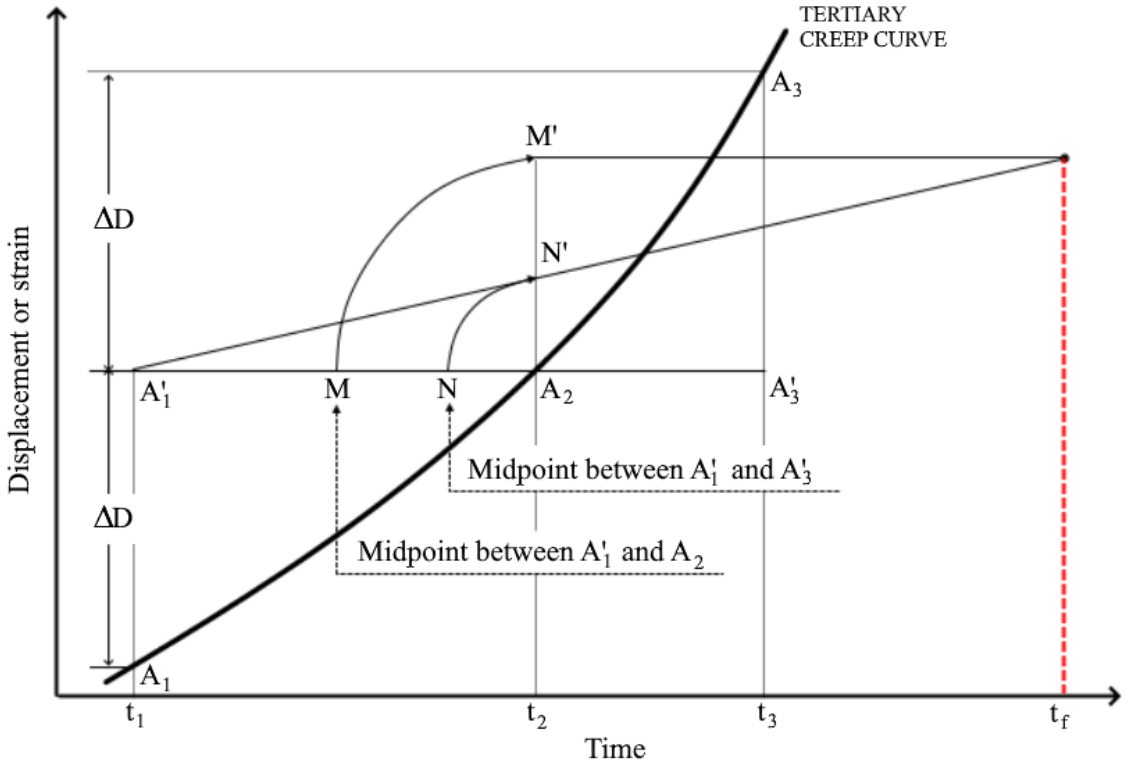

Figure 14. Saito's graphical approach to determine the time of failure from a tertiary creep trend (modified after Saito, 1969)

The geometrical procedure can be described through the following numerical formulation:

$$t_f = \frac{t_2^2 - t_1 t_3}{2t_2 - (t_1 + t_3)} \qquad \text{(VII)}$$

where t_1, t_2, and t_3 are time coordinates of the corresponding A-point. Some examples of successful applications of this method can be found in Saito (1979).

Among the failure forecasting approaches based on the creep theory, the inverse velocity method (IVM) introduced by Fukuzono (1985) is by far one of the most used thanks to its ease of application and successful results. This method relies on a graphical approach to be applied on the tertiary creep phase, when the landslide undergoes acceleration starting from a specific time instant t_0 (defined onset of acceleration, OOA) where velocity v starts increasing asymptotically. It is then possible to produce an inverse of velocity $1/v$ versus time t plot, where the accelerating trend corresponds to a line whose extrapolation intersects the time axis at $1/v \to 0$ ($v \to \infty$). The intersection point identified with this procedure represents the time-of-failure t_f (Figure 15).

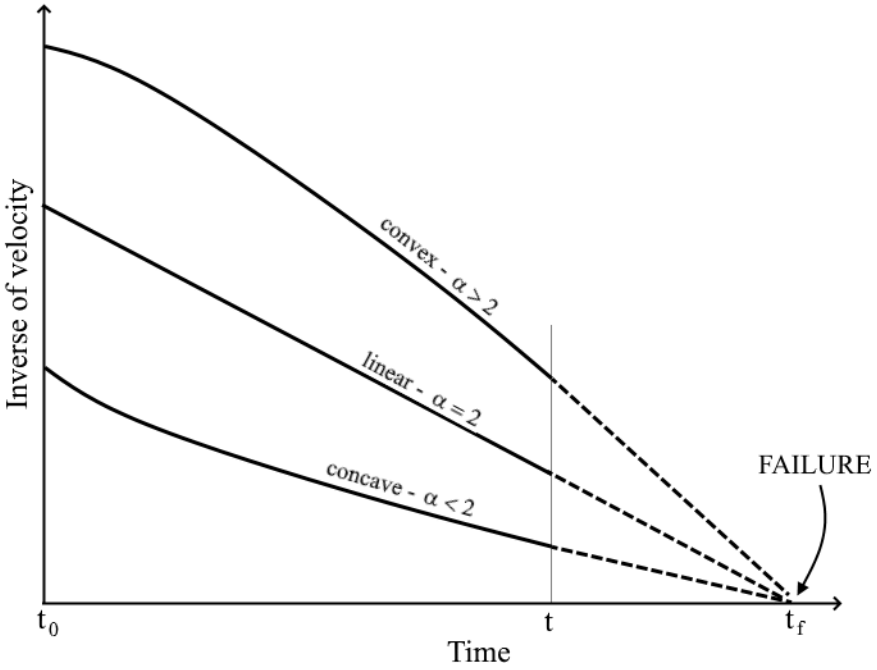

Figure 15. Inverse-velocity vs time relationship preceding slope collapse, and graphical methodology to identify the landslide time of failure (modified after Fukuzono, 1985)

From an analytical point of view, the author showed that pre-failure conditions can be described by a power law equation that involves the logarithm of velocity of the surface displacement and the logarithm of the acceleration:

$$\frac{d^2t}{dt^2} = A\left(\frac{dx}{dt}\right)^{\alpha} \tag{VIII}$$

where x represents the slope surface displacement and t is the time, while A and α are dimensionless constant parameters. Under the assumption of an infinite velocity at collapse, it is possible to use the following formulation to predict the time of failure:

$$\frac{1}{v} = \left(A(\alpha - 1)(t_f - t)\right)^{\frac{1}{\alpha - 1}} \tag{IX}$$

In this formulation, v represents velocity and t_f the time of failure. The trend of the $1/v - t$ plot depends on parameter alpha, which controls the linearity or non-linearity of the curve. As reported by Fukuzono (1985), this parameter ranges from 1.5 to 2.2 for natural slopes, but lower values can be obtained in case of slopes influenced by man-made structures (Bozzano et al., 2014). For $\alpha = 2$ the resulting curve follows a linear trend, while different values lead to concave ($\alpha < 2$) or convex ($\alpha > 2$) curves. Since this parameter typically does not differ much from 2, the hypothesis of linearity is generally considered a good assumption to evaluate the time of failure, provided that the dataset is updated constantly to identify the onset of trend changes (Rose and Hungr, 2007). In this case, it is possible to use the following simplified equation to obtain the failure time:

$$t_f = \frac{t_2\left(\frac{1}{v}\right)_1 - t_1\left(\frac{1}{v}\right)_2}{\left(\frac{1}{v}\right)_1 - \left(\frac{1}{v}\right)_2} \quad \text{(X)}$$

The effectiveness of this method has been proven by various studies concerning retrospective analysis of different cases, such as open pit mines (Carlà et al., 2017a), experimental man-made slopes (Petley, 2004), and catastrophic natural events (Kilburn and Petley, 2003). However, it should be taken into account that its application must be carefully evaluated depending on the specific case. Guidelines and suggestions provided by several authors include the necessity to include data pre-processing to reduce the influence of natural and instrumental noise (Dick et al., 2015), and the importance of employing high sampling frequency monitoring tools to detect rapid displacements and trend variations (Carlà et al., 2017b)

A more recent addition to failure forecasting procedures is the SLO method, presented by (Mufundirwa et al., 2010). Starting from a formulation introduced by Fukui and Okubo (1997) to represent strain divergence in the terminal phase of creep failure in rocks, the authors proposed the following equation:

$$t\left(\frac{du}{dt}\right) = t_f\left(\frac{du}{dt}\right) - B \quad \text{(XI)}$$

where x represents the slope displacement, t is time, t_f is the time of failure, and B is a constant. By plotting this formulation in a $t(du/dt)$ vs du/dt reference system, the time of failure corresponds to the slope of the resulting line while B is the intercept. Case studies included in Mufundirwa et al. (2010) display reliable predictions, even if these results were more conservative if compared to those obtained with the IVM.

The ability of these methods to provide a reliable failure forecasting was investigated also by Intrieri and Gigli (2016), which applied the three approaches proposed by Saito (1961), Fukuzono (1985) and Mufundirwa et al. (2010) to different cases, also trying to assess the influence of different factors in the failure forecast process. The authors introduced a Predictability Index (PI), evaluated for each specific landslide monitored and ranging from 1 to 5, to indicate the effectiveness of each approach. The results showed a similar performance of the Saito and Fukuzono models, while the approach proposed by Mufundirwa generally proved to be less accurate. Additionally, the authors noted that the Saito and Fukuzono methods achieved different results in terms of quality with respect to the specific cases, underlining the independence and non-redundancy of these models.

2.5. Semi-empirical methods

Since constitutive relationships used in numerical modelling do not take into account the "time" element, there is no present knowledge concerning the physical description of the process leading to slope failure (Intrieri et al., 2019). Semi-empirical models are an alternative to purely phenomenological approaches to describe the different stages involved the collapse process.

The mathematical generalization of Fukuzono's method, proposed by Voight (1988, 1989), represents the best attempt to define a general law describing various forms of material failure:

$$\ddot{\Omega} = A\dot{\Omega}^{\alpha} \quad \text{(XII)}$$

In this formulation, A and α are empirical constants, while Ω is a generic measurable quantity describing the phenomenon. According to Voight (1988), Ω could be interpreted in terms of geodetic observations, seismic quantities, or geomechanical observations. For example, Ω could refer to surface displacements, which in turn allows to define $\dot{\Omega}$ as the velocity, and $\ddot{\Omega}$ as the acceleration. While Fukuzono considered an infinite velocity as the reference value to define the time of failure, according to Voight the collapse occurs when $\dot{\Omega}$ reaches a specific threshold $\dot{\Omega}_f$, leading to a more conservative prediction:

$$\dot{\Omega} = \left(A(\alpha - 1)\left(t_f - 1\right) + \dot{\Omega}_f^{1-\alpha}\right)^{\frac{1}{1-\alpha}} \quad \text{(XIII)}$$

An example of a procedure aimed to define this threshold can be found in Crosta and Agliardi (2002). It is also possible to introduce the Fukuzono's assumption by assuming the hypothesis $\dot{\Omega}_f \to \infty$, which leads to the following equation expressed in terms of t_f:

$$t_f = \left(\frac{\dot{\Omega}^{1-\alpha}}{A(\alpha - 1)}\right) + t \quad \text{(XIV)}$$

where $\dot{\Omega}$ refers to the velocity measured at time t.

The main issue in the application of Voight equations is related to the necessity of assessing the value of A and α constants, which cannot be performed with graphical methodologies. In particular, A shows a significant range of values, spanning over 4 orders of magnitude, while α displays more moderate variations and it is usually close to 2 (Intrieri et al., 2019; Segalini et al., 2018). A simplified solution consists of imposing α=2, similarly to the linearity hypothesis in Fukuzono theory.

An alternative solution was proposed by Hao et al. (2016), which discussed a theoretical derivation of Eq. XIII for $\alpha > 1$:

$$\dot{\Omega}\ddot{\Omega}^{-1} = (\alpha - 1)(t_f - t) \quad \text{(XV)}$$

This relation aims to forecast the time of failure by plotting $\dot{\Omega}\ddot{\Omega}^{-1}$ over time, and linearly extrapolating the trend line to intercept the x-axis, similarly to the procedure followed by the inverse velocity method, without the need to calibrate the parameter α.

2.6. Alert thresholds assessment

While the definition of warning thresholds does not involve directly a time of failure evaluation, it is an activity that can still be included in those methods aiming to identify a

change in the slope stability conditions before its final collapse, and can play a relevant role in the Early Warning design process.

In several cases, the threshold assessment process in completely empirical, relying on expert judgement and available monitoring data, and provides values suitable only for the specific landslide for which they are originally defined (Intrieri et al., 2019). Numerical modelling is another possible approach to assess warning levels for a specific landslide. These methods aim to compare displacements measured by monitoring tools installed on-site with displacements simulated by a reference model. If properly designed and calibrated, the model should be able to represent the behavior of the real slope, thus allowing to evaluate one or more alert thresholds corresponding to potentially critical evolution of the monitored parameters. This approach is quite challenging due to the large number of components to take into account in the modelling process, and the model is able to provide reliable results only for the specific landslide on which it has been calibrated (Intrieri et al., 2019). However, the recent technological improvements regarding the computational ability of modern calculators, and the increased availability of powerful modelling software integrating advanced algorithms, have significantly boosted the research activity in this specific field. The result is a great availability of scientific literature presenting numerical models based on a wide range of different approaches and methodologies, such as algorithms based on machine learning and neural networks (some examples can be found in Krkač et al., 2017; Li et al., 2018; Liu et al., 2021; Prakash et al., 2021; Singh et al., 2020; Zhou et al., 2018).

On the other hand, other methodologies have been developed over the years with the purpose to create a procedure not dependent from a specific case study. In these cases, the design process is based on failure forecasting methods (Carlà et al., 2017b; Crosta and Agliardi, 2002; Manconi and Giordan, 2016), or derives from a solid observational basis (Brox and Newcomen, 2003; Xu et al., 2011). Due to their degree of exportability, these methodologies can be integrated in different slope-scale EWS. Nonetheless, they tend to share the same issues affecting the methods from where they derive and should not be used in isolation with a “black-box” approach. In fact, at present, the most reliable approach appears to be the integration of more than one method in order to have a more complete description of the phenomenon (Intrieri et al., 2019).

Chapter 3. Innovative monitoring: the IoNH approach

Monitoring systems play a key role in the study and description of natural phenomena. They allow to obtain a wide range of different information for continuous and optimal management of infrastructures, landslides, and critical events in general. Traditionally, the technology involved in the geotechnical field has been characterized by a manual approach for what concerns the monitoring activity, specifically regarding both collection and on-site investigations. As detailed in the previous chapter, this methodology can be quite complex and time-consuming, particularly for sites difficult to access directly, and especially during hazardous events (e.g., intense rainfall, adverse meteorological conditions, etc.)

The technological improvements experienced in the last two decades have been a strong drive in the innovation of tools and sensors involved in geotechnical monitoring activities. The main goal is to produce a complete and efficient system featuring automatic procedures and characterized by improved accuracy, reliability, and durability.

One of the major advancements introduced by innovative instrumentations involves the integration of Internet of Things (IoT) technologies in the design process of automated monitoring systems. Numerous definitions have been provided over the years for this term, firstly introduced by Kevin Ashton in 1999 and attributed to the work of the Auto-ID Labs on networked radio-frequency identification (RFID) infrastructures at Massachusetts Institute of Technology (Kramp et al., 2013; Wortmann and Flüchter, 2015). The basic idea of this concept is the presence of a variety of objects and sensors, which are able to interact with each other through an appropriate network and cooperate to reach common goals (Atzori et al., 2010; Giusto et al., 2010). When it comes to landslide monitoring, the integration of IoT-based devices results in a multi-layered architecture, where each component of the system has a specific role and is essential in guaranteeing the system functionality and efficiency. Some studies presenting an application of the IoT concept in this work field can be found in Abraham et al. (2020), Chaturvedi et al. (2018), Gamperl et al. (2021), Giorgetti et al. (2016), Lo et al. (2020), Moulat et al. (2018), and many more.

While the architecture could be different from one case study to another depending on specific necessities and requirements, it is possible to identify some essential components for IoT-based monitoring systems (Figure 16):

- Perception layer: a network of connected sensors interacting with the environment and collecting data and information.
- Network Layer: this layer acts like a bridge between sensors and objects, transmitting the acquired information through specific protocols between different elements of the system, including the elaboration centre.
- Data layer: it involves the storage and elaboration of monitoring data, and it is an essential component in an IoT-based system to manage properly the large amount of data generated by an automatic system.

- Application layer: in this stage, monitoring outcomes are represented and made available for the end-user through dedicated services and/or applications.

In all these configurations, a significant advantage derives from the possibility to achieve a real-time or near-real-time monitoring approach through the integration of automated processes, which is a fundamental element in any monitoring system with early warning applications. Apart from landslides, underground excavation works is another sector where this feature has proven to be a useful component. For example, multi-parameter approaches have been introduced in subway construction sites, where an EWS based on single-sensor data and simpler models is not advised due to the high degree of complexity involved (Wang et al., 2015; Xie and Liu, 2017).

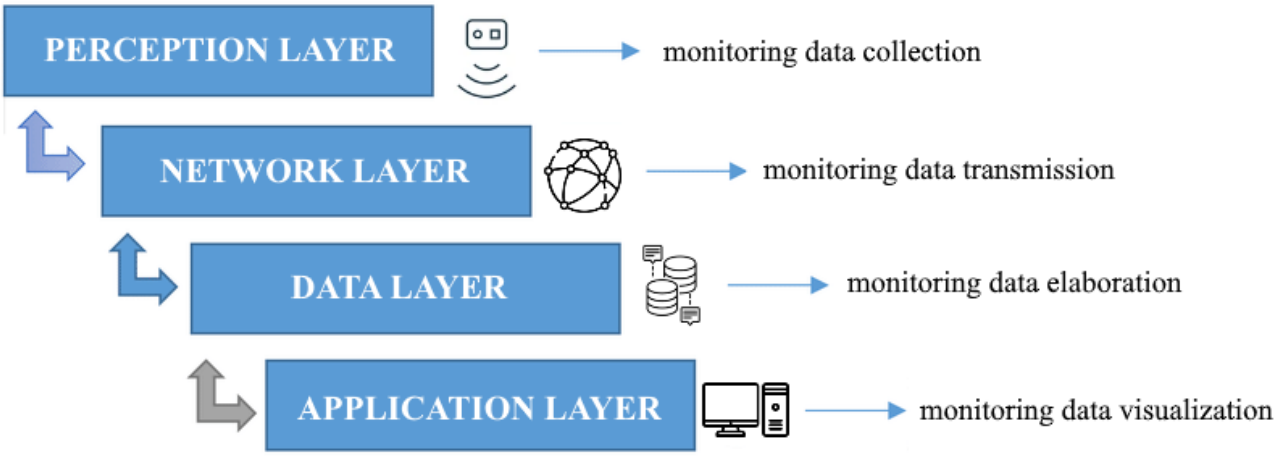

Figure 16. Simplified diagram of a 4-layer, IoT-based monitoring system

The implementation of IoT-based procedures is the core component of the Internet of Natural Hazards (IoNH) approach. IoNH represents a design concept where different components can interact and exchange data thanks to Internet connectivity by exploiting a bidirectional control of both sensors and control units (CU) placed in a specific monitoring site, taking advantage of a cloud-based database (DB), elaboration software, and representation platform. Equipped with appropriate technology, network-connected devices can be remotely controlled and accessed, thus creating an integrated and automated monitoring system with improved efficiency and performance (Segalini et al., 2021).

Figure 17 summarizes the working principles of the IoNH approach, highlighting the different components of the system, which will be presented and investigated in the following sections together with some examples to underline the approach advantages.

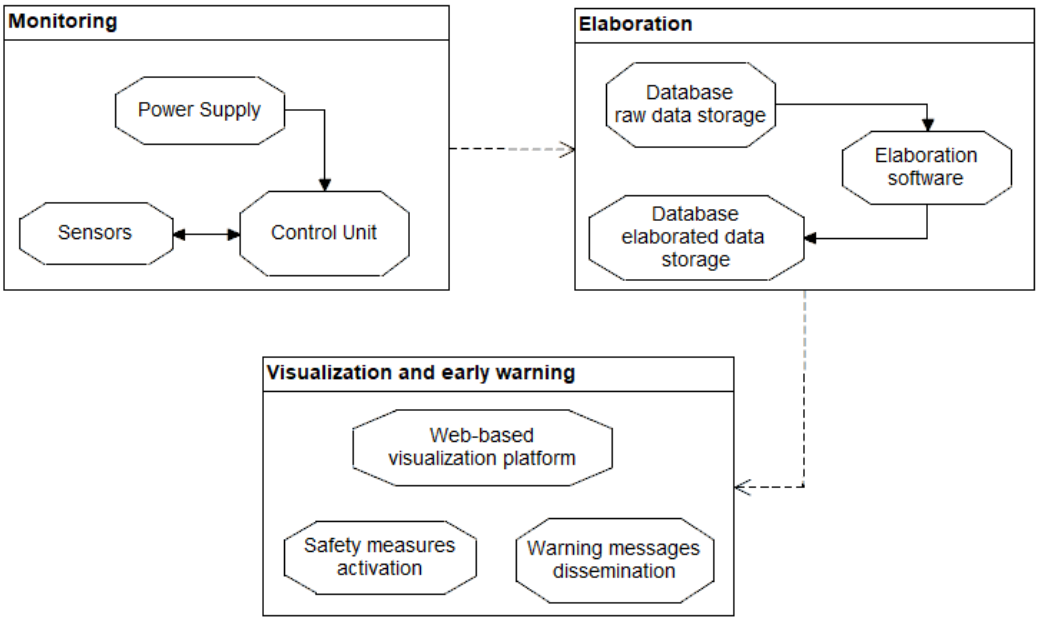

Figure 17. Schematic representation of the Internet of Natural Hazards (IoNH) approach (Carri et al., 2021)

3.1. Modular Underground Monitoring System (MUMS)

The IoNH approach is based on the experience acquired along 10 years of automatic geotechnical monitoring during the development, improvement and production of a new monitoring device called MUMS.

Modular Underground Monitoring System (MUMS) is a patented monitoring system designed and produced by ASE S.r.l. (IT). The instrumentation is composed of a series of epoxy resin nodes, called Links (Figure 18), connected by a quadrupole electrical battle and an aramid fibre cable. The result is an arbitrary long array of sensors, which can be located at specific distances according to specific requirements and can measure different parameters depending on the monitoring activity (Segalini and Carini, 2013). Originally designed as an automatic inclinometer, MUMS devices have been constantly improved and evolved over the years, and have been installed in several different sites, including landslides (Segalini et al., 2014; 2019a), underground constructions (Carri et al., 2019; Savi et al., 2019), geotechnical structures (A. Segalini et al., 2019b), and geothermal plants (Tinti et al., 2018).

Figure 18. Link of a MUMS Array

The instrumentation was born in 2011 with the idea to provide a new alternative to traditional measurement instrumentation. In particular, the design of the new system was focused on some critical aspects that characterize a manual inclinometer (Carri, 2019):

- Develop a completely automatic monitoring process to remove the need for an operator on-site to activate the instrumentation, improving the system efficiency and reliability.
- Include a data acquisition procedure able to reach high sampling frequencies together with the collection of multi-parameter data, allowing a direct correlation between displacements and triggering factors thanks to the availability of a large amount of monitoring outcomes.
- Remove any rigid mechanical connection between sensors, reducing uncertainties due to spiralling and creating a flexible instrumentation, easier to carry and install on-site.
- Change the data elaboration philosophy, removing any closed-box hardware filter in order to store the raw data and apply statistical tools. Raw data availability makes it possible to study and test new algorithms to improve the elaboration process.
- Optimize the electrical consumption in order to use smaller power units and reduce the impact on the landscape.

As previously stated, the structure of MUMS-based systems allows the integration of a wide selection of different digital and analog sensors. This characteristic is intended to provide a flexible and customizable system able to adapt to different contexts according to the parameters that need to be controlled.

The configuration designed to measures landslide displacements (Figure 19a) is called "Vertical Array" and relies on Micro Electro-Mechanical System (MEMS) sensors composed of an accelerometer, a magnetometer, and a thermometer. Additionally, it is possible to integrate an electrolytic tilt sensor for redundancy reasons and if a higher resolution is needed (Figure 19b). It is worth noting that MEMS have a 360° measuring range, while electrolytic cells feature a full-scale value of ±25°. Additionally, the structure of MUMS-based arrays permits the exploitation of different sensor typologies in the same array, such as piezometers to detect water level variations (Carri et al., 2016).

The data transmission relies on 4G, 3G or GPRS lines with a UMTS router. In the case of monitoring systems based on the IoNH structure, the elaboration process usually involves several variables and parameters, resulting in a quite complex and computationally expensive procedure. For this reason, the system is designed to transmit raw data only, and calculate the final results separately.

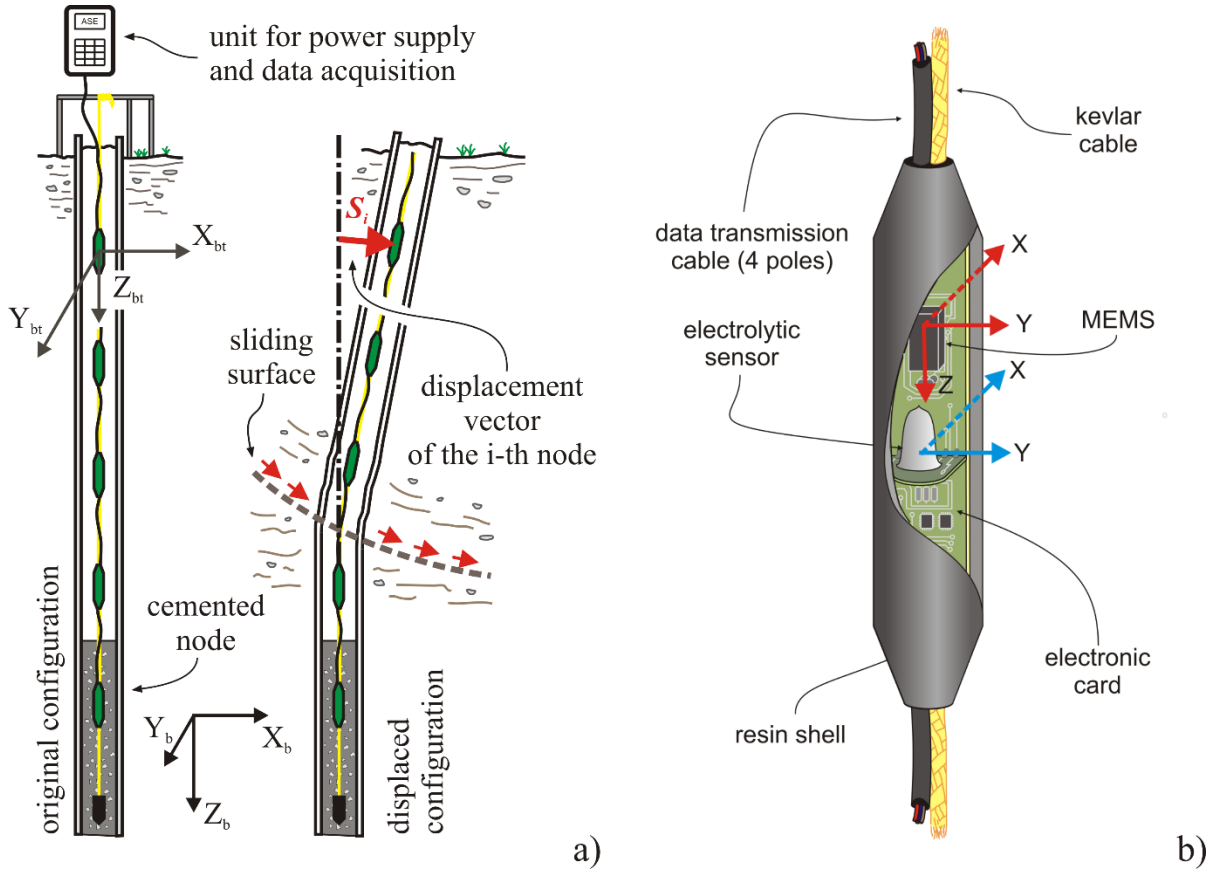

Figure 19. (a) Vertical Array working principle; (b) components of a Tilt Link HR 3D V.

The redundancy provided by this approach play a major role in data analysis and validation processes. An example of this importance is presented in the following case study where MUMS-based instrumentation was installed to monitor a reinforced soil retaining wall with the objective to control the displacement of the structure. Additionally, the system included an alert system based on a predefined, site-specific threshold calibrated on a 7-day time interval. The monitoring apparatus included two 15-metre long Vertical Arrays, each one composed of 15 Links integrating both MEMS and electrolytic tilt sensors. The monitoring activity started at the end of August 2017 and continued for 17 months until January 2019, when the retaining wall was demolished for safety reasons (Segalini et al., 2019b). During this time period, the presence of two different sensors measuring the same physical quantity at the same depth played a primary role in the monitoring data interpretation, in particular during an event occurred in July 2018 when one of the Array evidenced a consistent displacement at 14 metres of depth. Since the area interested by the movement was supposed to be stable, and the other device did not evidence any deformation at that specific depth, there could have been some doubts regarding the data reliability. However, the presence of both displacement sensors in the same Link allowed to observe a similar behaviour for both the MEMS and the electrolytic cell, with some difference in the displacement magnitude due to the different sensitivity of the two devices. As can be observed in Figure 20, both sensors recorded a movement starting on July 5th around 10.00 AM, resulting in a displacement of 18.6 mm according to the MEMS, and 16.9 mm according to the electrolytic tilt sensor.

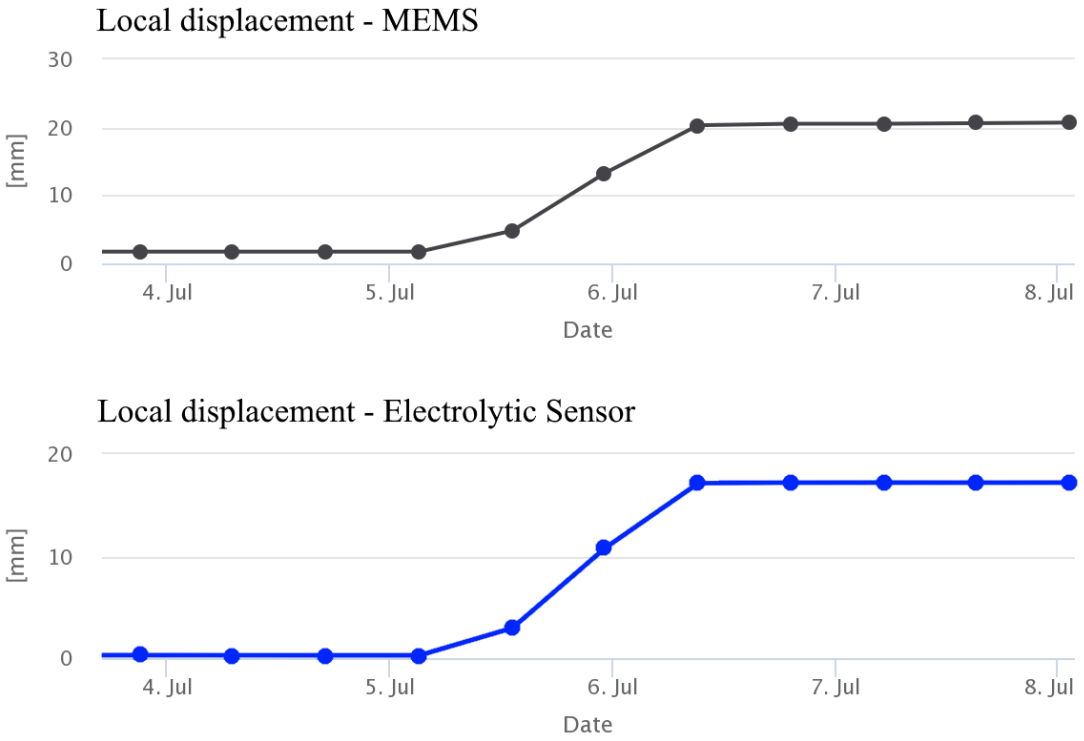

Figure 20. Displacement vs time trends recorded by MEMS and electrolytic tilt sensor at -14 m (Segalini et al., 2019b)

As previously discussed, another advantage deriving from the application of multi-parameter devices such as MUMS-based automatic inclinometers, is the identification of significant cause-effects relationships between different physical quantities. One of the most common and useful correlation involves the monitoring of rainfalls and water level variations, in order to verify their influence on the slope stability conditions. The following graphs present an example of this approach, referred to a monitored site where two different Vertical Arrays were equipped with piezometers (Piezo Link) in addition to displacement sensors (Tilt Link HR 3D V), allowing to receive information regarding the water table behaviour, while a rain gauge in close proximity of the area of interest provided rainfall data.

The event of interest occurred in January 2021, when both inclinometers recorded a significant displacement increase located at a depth of approximately 5 metres. In particular, for what concern Vertical Array #1, Tilt Link 29 (located at -5.0 m b.g.l.) measured a displacement of 10 mm, while the two piezometers integrated in the Array displayed an increase of the water level, resulting in a variation of 1.6 metres according to the Piezo Link located at -13.0 m, and 1.3 metres according to the Piezo Link installed at -19.0 m (Figure 21). On the other hand, Vertical Array #2 evidenced a displacement of 14 mm measured by Tilt Link 31, placed at a depth of 5.0 m, and the only piezometer integrated in the Array recorded a water level variation of 1.3 metres (Figure 22), displaying strong similarities with information recorded by Vertical Array #1.

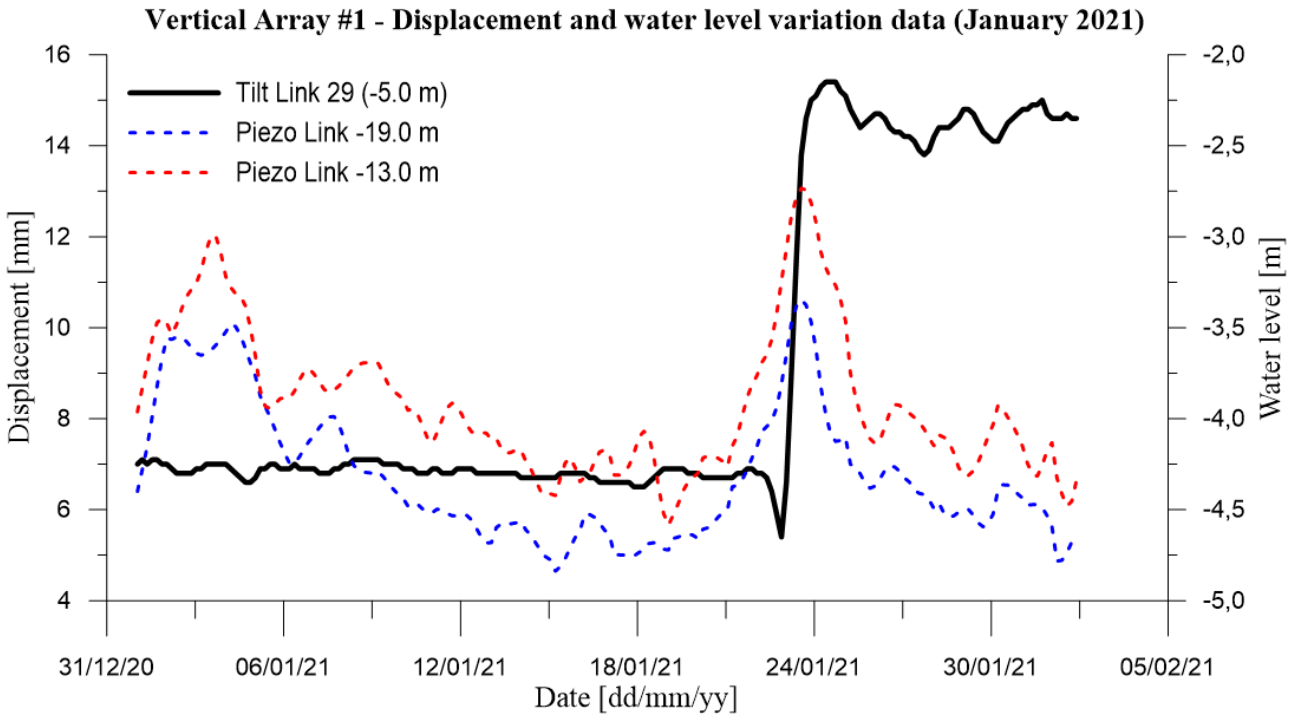

Figure 21. Correlation between displacements data and water level variations measured during January 2021 by sensors integrated in Vertical Array #1

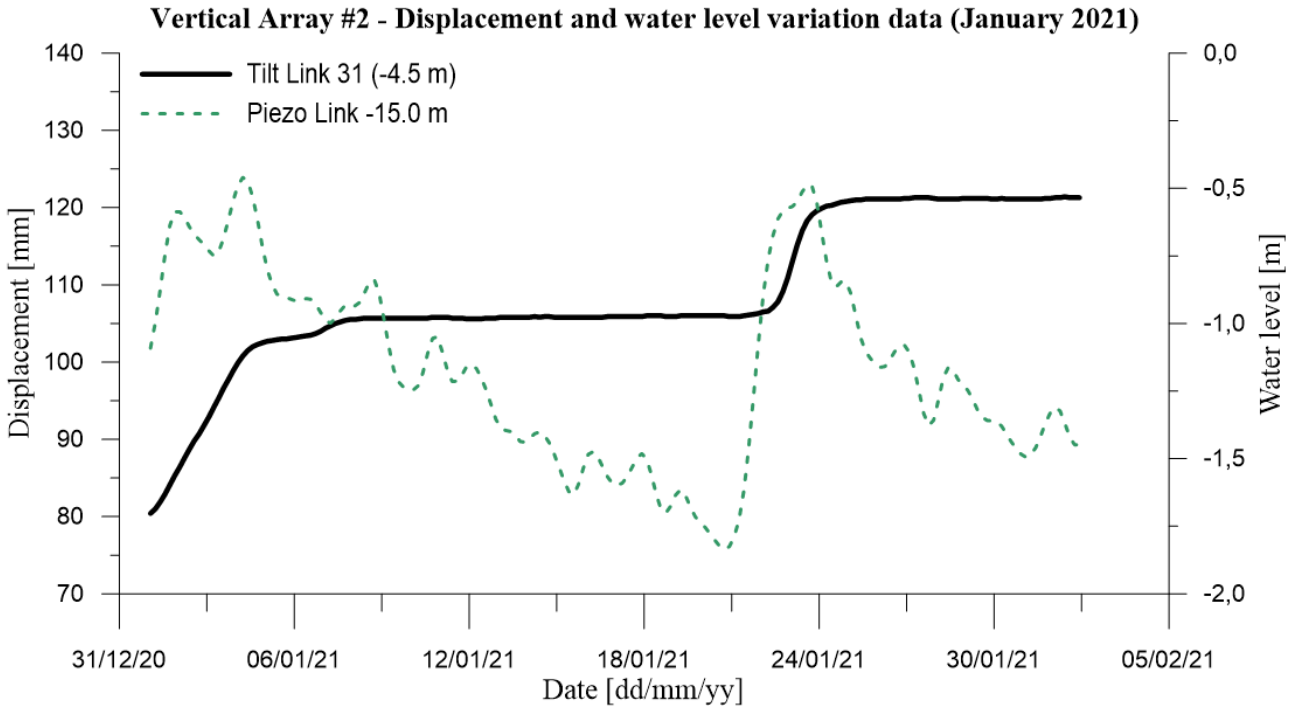

Figure 22. Correlation between displacements data and water level variations measured during January 2021 by sensors integrated in Vertical Array #2

In both cases, it is evident the correlation between the slope displacements and the water level variations, which in turn show a significant connection with rainfalls. In fact, as can be observed in Figure 23Figure 26, the main triggering event appears to be a particularly intense event that started on January 19th and continued for five days until January 24th, reaching its peak on January 22nd with 72.2 mm. By bringing together all information recorded by each

different device, it is possible to assume that the slope behaviour is strictly connected with rainfalls, and increments in slope displacements could be observed in correspondence of other intense events in the area of interest.

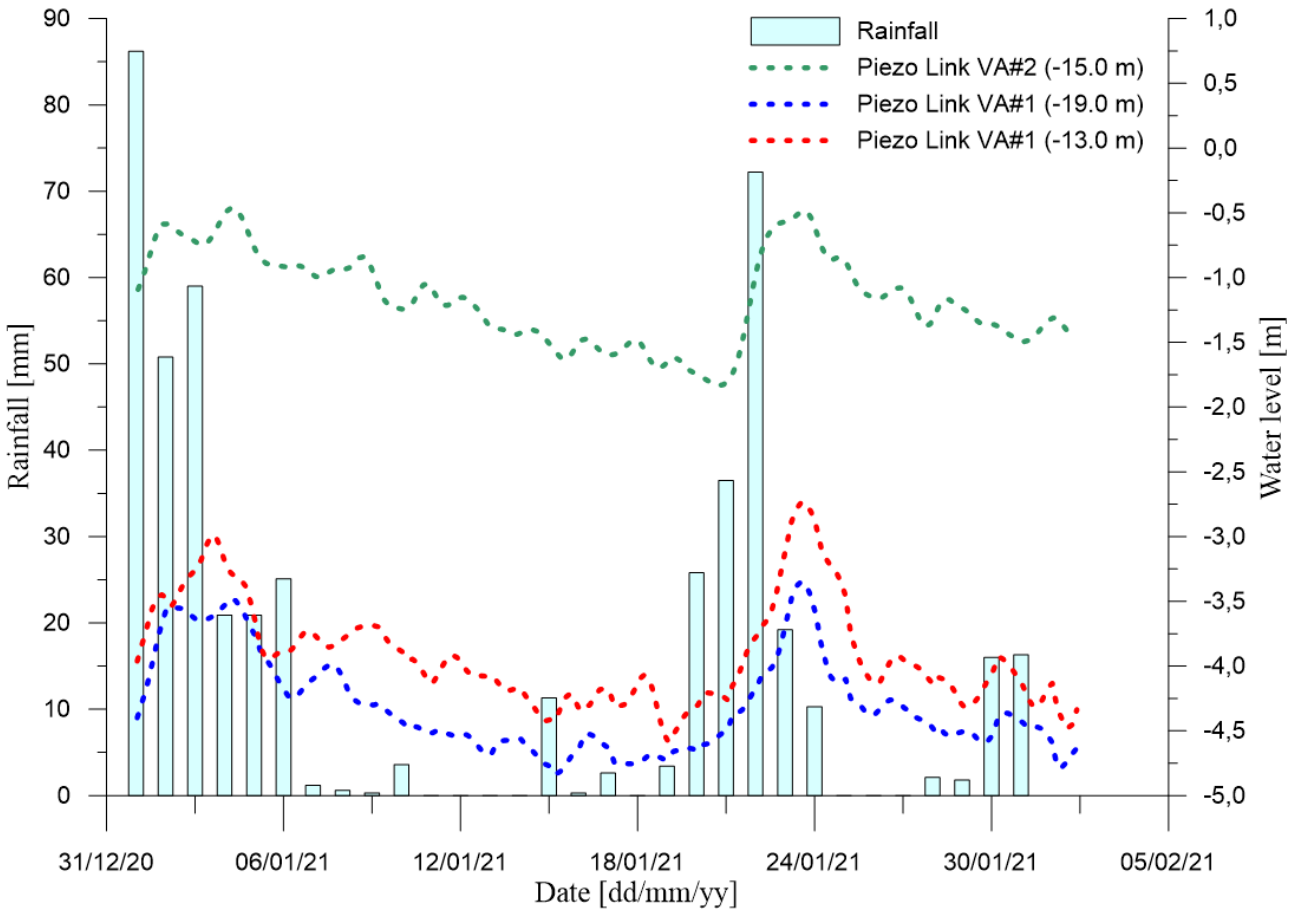

Figure 23. Correlation between rainfall data recorded by the rain gauge, and water level variation values recorded by the Piezo Links integrated in both Vertical Arrays installed on the monitored site

Another example of a possible application of multi-parameter sensors is the availability of useful information for a better interpretation of the phenomenon evolution. The data reported in Figure 24 refers to a monitored site where a tilt meter was placed on a building located close to a landslide, in order to identify possible interactions between the two elements. In particular, the MUMS-based device was able to provide data regarding the inclination of the monitored wall, and the temperature measured by a thermometer integrated in the same Link. This allowed to compare the trends displayed by the two physical quantities for a better understanding of the building behaviour in different time periods. Reported data refers to a full year of monitoring activity. This permits to observe how tilt and temperature data follow a very similar pattern, with the MEMS sensor displaying a counter-clockwise tilt as the temperature decreases approaching the winter season, and reversing the trend once the temperature starts to rise again. If only tilt data were available, the interpretation of monitoring outcomes would have been more difficult, with the possibility to assume the presence of a potential instability due to the tilt variation recorded by the sensors. However, the presence of two sensors allowed to correctly interpret the phenomenon, identifying the close relationship between temperature variations and tilt values measured by the MEMS.

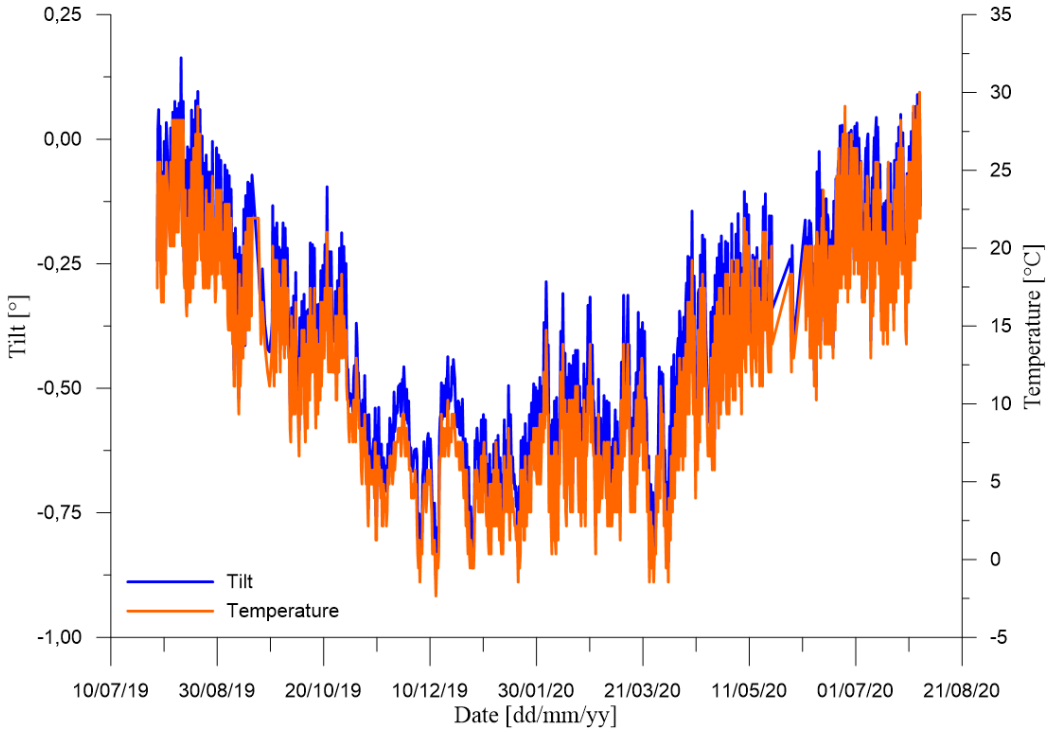

Figure 24. Comparison between tilt data and temperature recorded by a tilt meter installed on a building wall

The possibility to perform a cross-check between different physical quantities is an extremely useful feature when a monitoring system integrates sensors specifically designed to identify the occurrence of rapid critical events, such as rockfalls or debris flows. This task is usually performed by exploiting mechanical-electrical trigger sensors, which are able to perform predefined procedures after their activation. The example reported below refers to a case study where a complex monitoring system was installed to control the occurrence of debris flow events on a slope located in proximity of a road tunnel entrance. Among the different elements composing the system, it integrated several wire extensometers and tilt meters, a rain gauge, two cameras, and two mechanical triggers installed in specific areas of the slope. Thanks to the implementation of IoNH principles previously described, it was possible to create a networked structure where the identification of a potentially critical event leads to the automatic activation of other key elements of the system to acquire more information for a correct interpretation of the phenomenon. On August 16th, 2021, at 10:02 PM the software reported the activation of one of the mechanical triggers, arguably due to a small debris flow generated by a sudden cloudburst in the area, which was correctly detected by the rain gauge located on site. Following this report, a review of available monitoring data highlighted that one of the wire extensometers recorded a deformation of approximately 2.8 mm in correspondence of the trigger activation (Figure 25). Finally, one of the cameras provided an image of the area of interest, confirming the presence of a small flow generated by the rainfall event. The close interconnection between sensors, and the ability to operate automatically with a near-real time approach, gave to responsible authorities all information needed to identify the event and assess the phenomenon intensity, which ultimately did not cause any significant inconvenience to the road nearby.

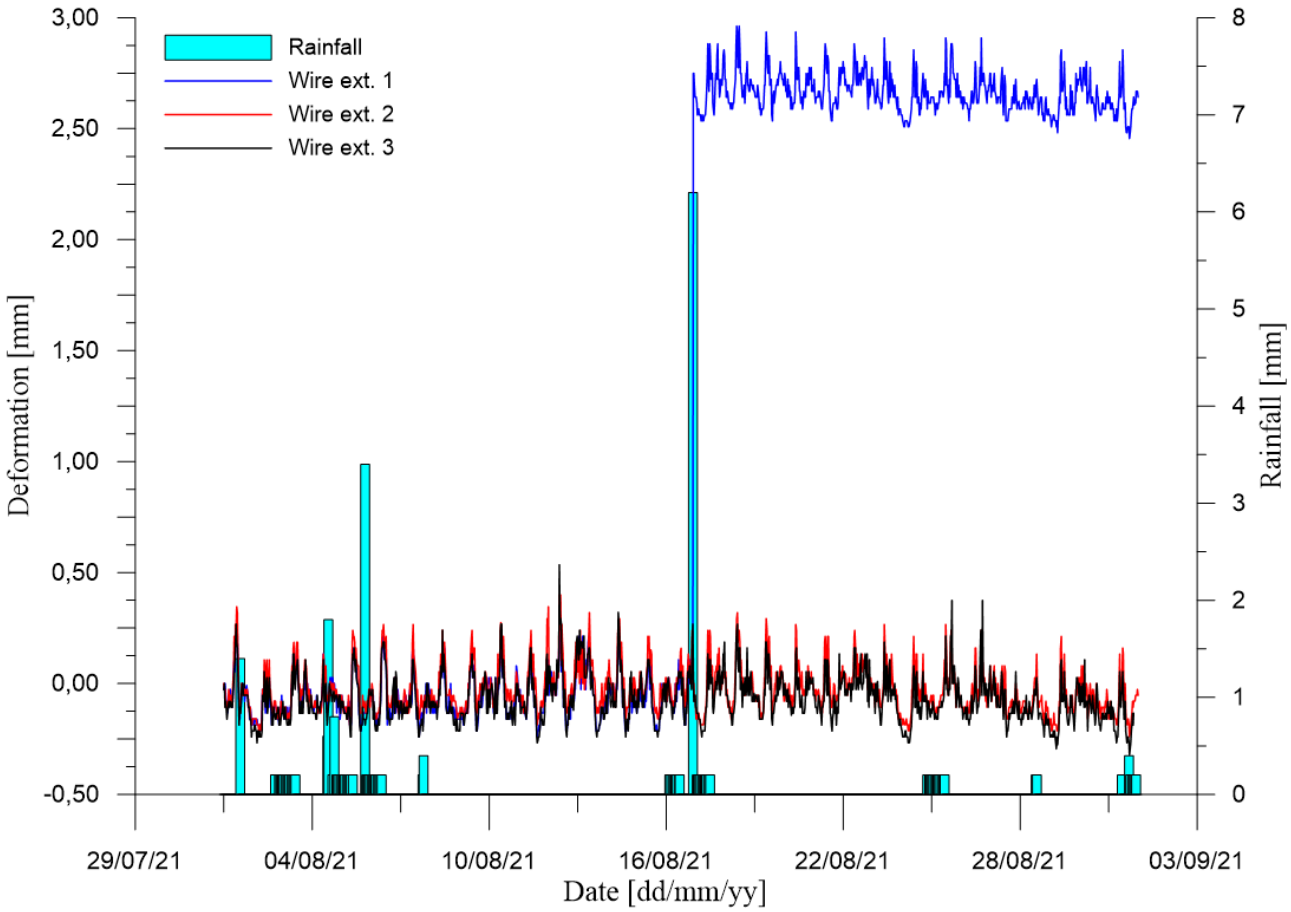

Figure 25. Monitoring data recorded by the rain gauge and three different wire extensometers on August 2021, evidencing the event that caused the activation of one of the trigger sensors present on site

3.2. Control unit and power supply

The entire system is operated by a control unit, which queries all connected sensors at a specified sample period and stores the values on an external memory unit. In addition to digital sensors, the datalogger is able to record any kind of traditional device featuring an analog output signal. As a result, it is possible to manage complex and diversified monitoring systems with a single control unit, database, software, and web platform. The power supply comes from a rechargeable lead battery, connected to a solar panel, or directly connected to the electrical line if available on site. Both these configurations are designed to provide a reliable power source, which is a mandatory necessity for any acquisition system, especially if it includes early warning procedures (Reid et al., 2008). For this reason, the battery level is always accessible on the visualization platform, and a routine integrated in the elaboration software analyses automatically sends warning messages if the recorded value is below a predefined threshold.

Two examples of the importance of this feature are presented hereafter. Figure 26a regards a case study where an array of 23 high-resolution thermometers was installed for the monitoring of soil temperature at different depths. A lead–acid battery connected to a solar panel provided the power supply to the monitoring system, set to acquire a new value every 10 minutes. After the tool installation, a prolonged period of adverse climate conditions severely affected the ability of the solar panel to properly recharge the battery. This event, together with the high sampling frequency required by this case study, induced a gradual depletion of the energy

supply. Once the battery voltage reached a level lower than a predefined threshold, the system issued a series of alert messages to highlight the problem. The system operativity was restored with the substitution of the battery and the upgrading of the solar panel with a more powerful one (Carri et al., 2021).

The example reported in Figure 26b concerns a monitoring system including a Vertical Array and a series of traditional analog devices to control the influence of a landslide on the nearby buildings. The site configuration allowed to connect the rechargeable battery directly to the electrical line to provide a continuous energy supply to the system. In May 2020, a heavy thunderstorm caused a blackout in the area of interest, leading to the temporary failure of the electrical line to which the battery was connected. As a result, the level vs time plot showed a rapidly decreasing trend as the monitoring activity progressed without the ability to recharge the battery. Once the automatic software reported the issue, it was possible to take action in order to reset the power supply and continue the data sampling operations regularly.

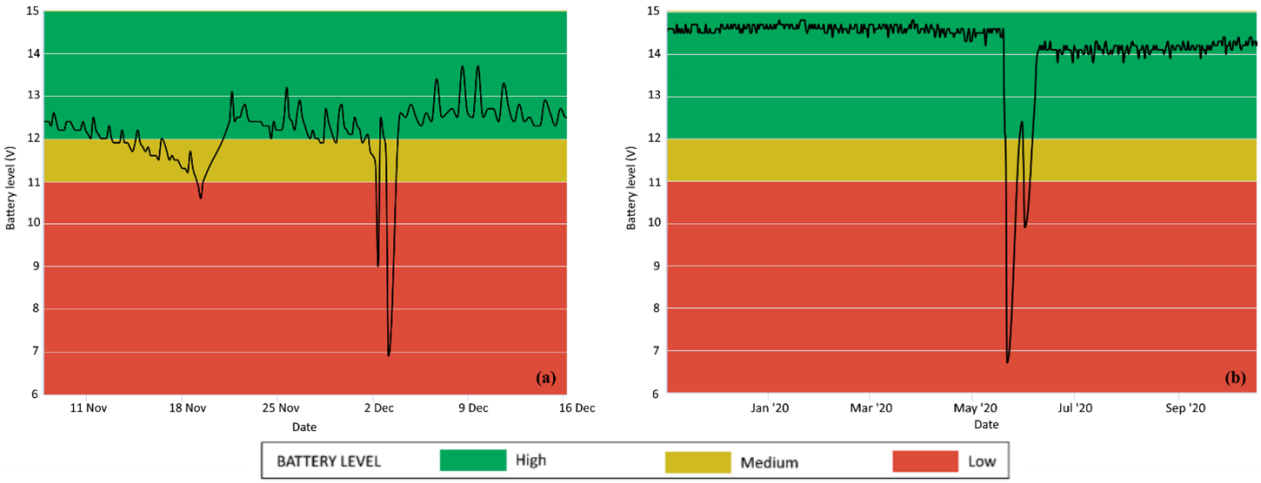

Figure 26. Two examples of battery level vs time plots indicating an issue in the power supply system

3.3. Elaboration and self-check controls

The elaboration software, specifically optimized for each different application of MUMS-based devices, has the main task to convert raw data (i.e., electrical signals sampled by sensors) into physical units, and calculates the final results after the application of a series of several self-check data controls. Such procedures are a fundamental component in elaboration processes designed for automated systems, since they are intended to guarantee the quality and reliability of the monitoring outcomes.

The software dedicated to the elaboration of monitoring data sampled by MUMS instrumentation takes advantage of several algorithms, intended for the verification of specific requirements connected to the parameters of interest. A brief discussion of the main self-check processes is presented below, while a more in-depth and complete explanation of their working principles and integration into MUMS elaboration software can be found in Carri (2019).

3.3.1. Spike noise and instrumental noise recognition

Spike noise (or impulse noise) is a sporadic and unpredictable electrical disturbance consisting of impulsive disorders in the signal, often induced by external factors, which heavily contaminate the acquired data (Zhang and Wu, 2017). When it comes to landslide monitoring, both accelerometer and magnetometer data are processed to identify any outliers. In this specific field of application, spikes could be related to earthquakes or traffic vibrations and, if not highlighted, may lead to false alarms.

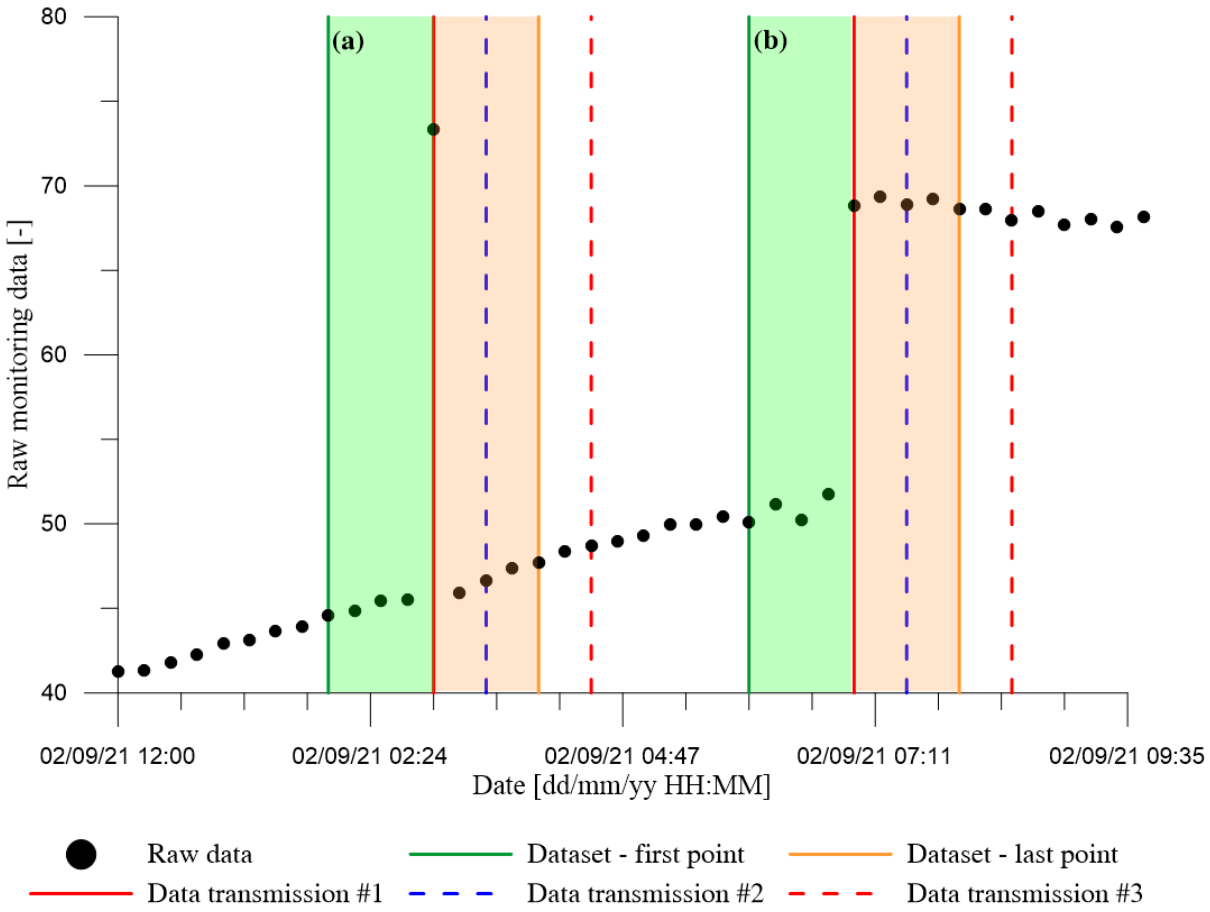

Figure 27. Raw data analysis, showing the procedure to determine the occurrence of (a) a spike event, and (b) an actual variation of monitoring data (modified from Carri et al., 2021)

While the removal of outliers and spike noise is a relevant topic in the data elaboration process, it should be reminded that such an operation causes a time-delay related to the complete dataset validation. In the example reported in Figure 27 reports a monitoring dataset characterized by a sample period of 15 min, a check analysis that considers 9 elements, and a data transmission frequency to the elaboration centre of 30 min. When the software starts the elaboration of newly acquired information, only a left-weighted de-spiking process is available for the calculation process, using a dataset which takes into consideration the previous 4 points (starting from the green lines in Figure 27) If the data to be evaluated does not follow the previous behaviour, the algorithm could potentially identify two different scenarios: the occurrence of a spike or the beginning of a new data trend (case (a) and case (b) respectively). The software must perform a preliminary real-time analysis that interprets one of the two mentioned cases, accordingly to the deviation from the median, which returns an information

with a 50% reliability compared to the fully available dataset. After 30 minutes, a new data transmission takes place (blue dashed line), adding new elements to the dataset previously investigated. The new elaboration takes advantage of these information, and the algorithm is able to make a first estimation of the nature of the data variation. The result has a higher confidence than the previous one, even if a degree of uncertainty is still present since the dataset is not complete. The following data transmission (occurring 30 minutes later, and represented by red dashed lines in Figure 27) provides the missing information to the analysed dataset, and confirms the outcomes previously obtained with a level of confidence equal to 100% with respect to the parameter set for the outlier identification procedure (i.e., 9 elements).

3.3.2. Coherence and variability of the gravity acceleration vector

The main component of any MUMS systems designed for landslide monitoring is a 3D MEMS sensors featuring three main elements, namely an accelerometer, a magnetometer, and a thermometer. Its three-dimensional working principle makes it is possible to reconstruct the magnetic field vector represented by gravity acceleration g, and the static nature of these measures allows controlling the vector coherence at every step, as in Equation XVI (a_x, a_y, a_z represent the three acceleration components).

This procedure helps in the identification and troubleshooting of malfunctions involving specific sensors of the Array by imposing a predefined threshold Δ_g, which should be defined according to the sensor technical features.

$$\frac{\sqrt{a_x^2 + a_y^2 + a_z^2}}{g} = 1 \tag{XVI}$$

$$\left| 1 - \frac{\sqrt{a_x^2 + a_y^2 + a_z^2}}{g} \right| \geq \Delta_g \tag{XVII}$$

The investigation of the instrumental gravity acceleration vector variability is performed on two consecutive readings performed by the same sensor at t and $t-1$. In this case, the analysis focuses on the identification of abnormally large variations according to a reference value ε_g, and provides a complementary check to the previous one.

$$\left| \frac{\sqrt{a_{x_t}^2 + a_{y_t}^2 + a_{z_t}^2}}{g} - \frac{\sqrt{a_{x_{t-1}}^2 + a_{y_{t-1}}^2 + a_{z_{t-1}}^2}}{g} \right| > \varepsilon_g \tag{XVIII}$$

3.3.3. Coherence and variability of the magnetic field vector

The presence of a magnetometer integrated in the MEMS gives the possibility to evaluate the coherence and the variability of the magnetic field recorded by the sensor. In fact, it is possible to reconstruct the resultant Earth magnetic field vector of the monitored site by exploiting the Latitude, Longitude, and altitude data, and to compare it with the vector

recorded by the instrumentation. The variability check follows the same principle presented for the gravity acceleration vector, and the identification of anomalies in the measurements performed by the instrumentation allows to take action in order to solve the issues during the elaboration process.

3.3.4. Coherence of node temperature

Due to the specific field of application, which involves the installation of underground instrumentation, the temperature is usually relatively stable and varies in a range of roughly 15 to 30 °C depending on the location of the monitored site and the depth at which the measure is recorded (e.g., Alam et al., 2015; Pouloupatis et al., 2011; Shah et al., 2019). For this reason, the thermometer integrated in the MEMS should return a value within a predefined range in order to consider as reliable the monitoring information collected by the sensor. For MUMS-based instrumentation, maximum (T_{max}) and minimum (T_{min}) temperature values are usually set as +80 °C and -20 °C, respectively.

$$T_{min} < T < T_{max} \tag{XIX}$$

3.3.5. Recognition of not-operating sensors

All the self-check analyses presented up to this point are intended to identify specific anomalies affecting a single value or a dataset. However, it may occur that a sensor does not work as intended and is unable to transmit new data to the control unit. In this case, the data logger is set to carry on the sampling process by querying the following nodes of the Array, while the malfunctioning Link returns a text code related to the undergoing issue. When the software identifies an error code, the last validate numerical value of the Link is reported to allow the continuation of the elaboration process, while the text code itself is preserved in order to perform the adequate troubleshooting operations.

3.4. Data visualization

The installation of a huge number of devices with multiparametric sensors requires adequate data management due to the amount of information generated by the instrumentation. Therefore, monitoring data availability and visualization should be considered fundamental elements in the design process of a monitoring system, aiming to simplify and optimize the accessibility and interpretation of the outcomes for the end user.

Following this principles, MUMS-based devices take advantage of an interactive web-based platform with private access, where results of interest are represented with different graphs, widgets, and tools, depending on the data typology. Moreover, monitoring values can be exported in common formats, such as images or text files, in order to perform further analyses. Web-based environments provide several advantages in terms of data browsing, thanks to the implementation of a dedicated user-friendly interface that allows to interact with a constantly updated workspace. The integration of modular elements gives the possibility to customize the platform according to the users' requests, in order to interact easily with monitoring data according to specific needs (e.g., selecting a time interval, displaying only specific results, browsing through different physical quantities, etc.).

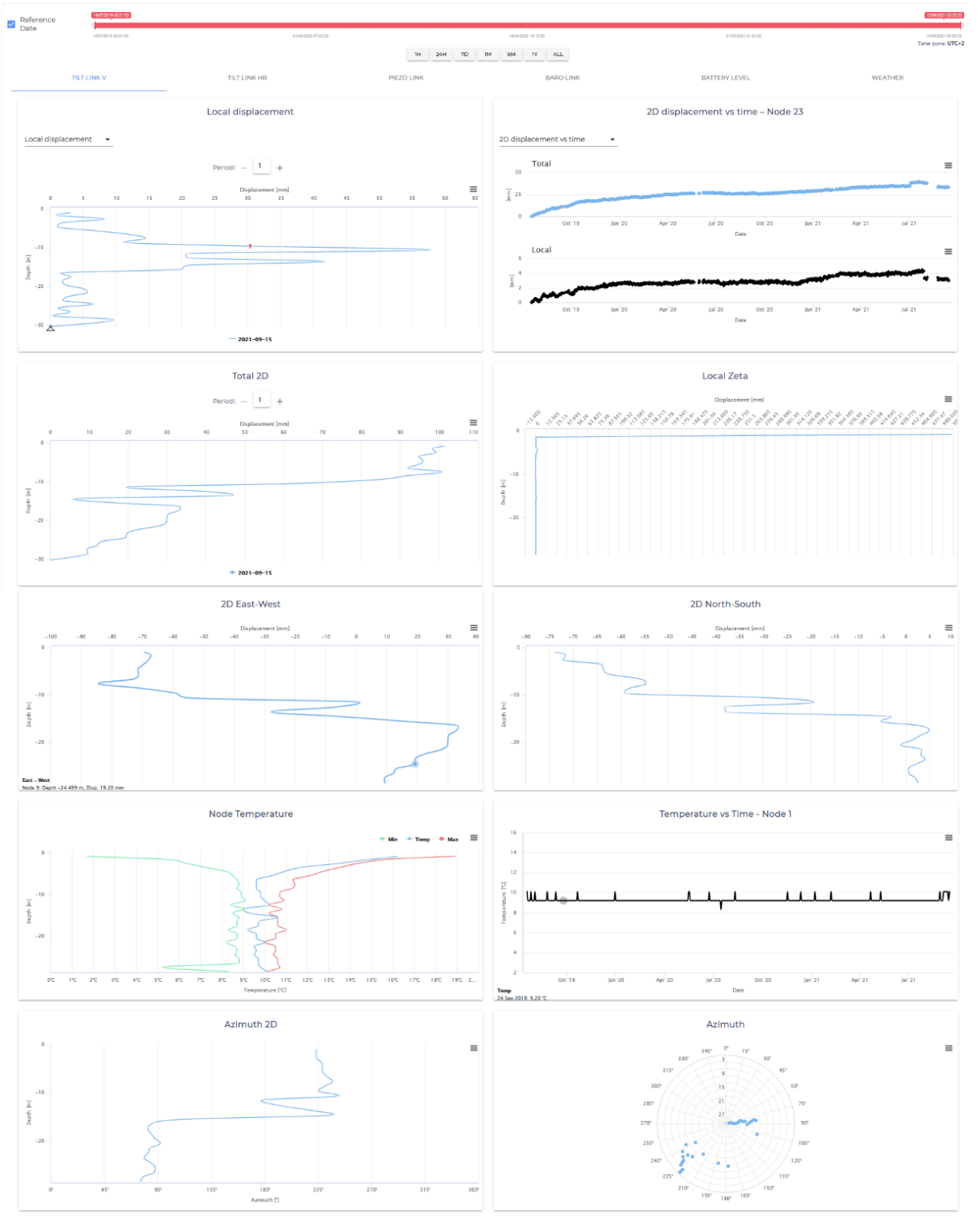

Figure 28. Structure of the web-based platform for Vertical Array instrumentation

Moreover, thanks to the enhanced connection provided by IoT elements integrated in the IoNH approach, it is possible to interact directly with the settings of the control unit installed on the monitored site, automatically changing configuration parameters like sampling period, or data transmission frequency, according to monitoring outcomes.

Chapter 4. Acceleration phase identification algorithm

As discussed in the previous chapters, assessing the landslide time of failure is a topic of major concern in the field of geological risk management, consequently leading to the development of several approaches to achieve this goal. According to Brabb (1993), it could be theoretically possible to avoid at least 90% of losses caused by landslide phenomena by identifying the problem before its critical evolution. Nonetheless, the ability to predict the future behaviour of a landslide remains a challenging task.

Among the several factors playing a role in the forecasting process, one of the most crucial and complex aspects is the definition of the dataset to be used to determine the phenomenon evolution. The importance of this task derives from the assumption that the behaviour preceding the collapse can be explained with a tertiary creep model. In fact, forecasting methods needs to be applied to this specific stage of the phenomenon evolution in order to provide reliable results. Consequently, a correct definition of the beginning of the actual acceleration phase could be fundamental to apply these methods correctly and, consequently, provide meaningful evaluations regarding the most probable event behaviour (Dick et al., 2015). According to this consideration, the definition of the landslide acceleration phase acquires a particularly relevant position among the several components forming an Early Warning System.

Traditionally, the identification of the onset-of-acceleration (OOA) and the following application of failure forecasting methods have been performed manually on the available monitoring dataset (e.g., Mazzanti et al., 2015b; Rose and Hungr, 2007; Voight and Kennedy, 1979). This approach, involving the first-hand evaluation of an expert, could provide highly accurate results, but it is definitely a sub-optimal solution when a timely warning is needed. This is mainly due to the lack of automation, which is a key component for an effective real-time EWS (Allasia et al., 2013)., However, as noted by Bozzano et al. (2018), a standard procedure to identify the beginning of the tertiary creep phase has yet to be defined. An interesting approach to solve this problem, introduced by Carlà et al. (2017b), involves the crossover between short-term and long-term moving averages (SMA and LMA, respectively) to identify a trend change in the raw data. According to the authors, the OOA point can be defined when the SMA line crosses above the LMA, representing the beginning of an uptrend behaviour. On the opposite, a downtrend occurs when the SMA line lies below the corresponding LMA line, thus representing the end of the acceleration phase.

As reported in previous chapters, the most successful failure forecasting methods have been able to provide good results under the hypothesis of a tertiary creep behaviour. For this reason, the selected dataset should contain only accelerating displacement data to improve the procedure reliability. This assumption highly influences the forecasting analysis outcomes and evidences the necessity to apply monitoring tools featuring high sampling rates and automatic acquisition procedures. In fact, a monitoring approach relying on manual acquisition is not suitable for these purposes, since the low sampling rate is unable to guarantee an adequate

description of the acceleration phase, which can take place in a time interval up to some hours (e.g., Bozzano et al., 2011; Carlà et al., 2017a).

In general, an expert operator should be able to identify the onset-of-acceleration through a manual check of the available monitoring data. However, the task is quite harder when a software has to recognize automatically the starting and progression of an accelerating phase with a real time or near-real time approach. Another factor that should be taken into account is the simultaneous monitoring of several different landslides, which nowadays is becoming more and more common thanks to the introduction of automatic instrumentation. In this context, the integration of highly detailed models and the manual elaboration of monitoring data would be hardly sustainable in terms of economical and computational resources.

The present chapter describes the design, calibration, and application of a methodology specifically developed to identify the beginning and evolution of a landslide acceleration phase. All the aspects previously covered were taken into consideration during the development of the proposed approach, addressing the advantages of an automated procedure and the possibility to apply it consistently to a large number of monitored sites. The main source of this chapter is Valletta et al. (2021).

4.1. Algorithm structure

The algorithm discussed in this section was developed with the objective to identify an increasing pattern in displacement rates through the analysis of the dataset trend according to four different criteria, applied with a "drop-down" structure. Given that the procedure is intended to work autonomously, this choice provides some relevant advantages. The main one is the possibility to stop the algorithm when a single condition is not fulfilled, which allows to optimize the expected time analysis. The impact of this choice becomes more and more relevant when dealing simultaneously with multiple devices featuring high sampling frequencies, which often results in an extremely large database of monitoring values to be elaborated at the same time. Additionally, a multi-criteria approach permits to impose conditions on each sub-routine individually, thus allowing to differentiate between mandatory requirements and other conditions featuring specific margins of tolerance. These aspects heavily influenced the design process of the proposed approach, trying to balance computational complexity and results reliability.

The fundamental hypothesis of the method is the presence of an observable transition from a linear to a non-linear behaviour. These correspond respectively to a constant and increasing displacement rate, which can be evaluated as follows:

$$v_j = \frac{S_j - S_{j-1}}{t_j - t_{j-1}} \qquad \text{(XX)}$$

Where v is the displacement rate recorded between j and $j-1$ readings, S is the displacement recorded at reading j by the monitoring instrumentation, and t_j is the date, expressed as a number, corresponding to reading j. The following sections describe in detail each single sub-condition, while Figure 29 summarizes the algorithm structure. Since its development, the

algorithm has been tested on a large number of MUMS-based monitoring devices featuring different sampling frequencies. However, from a conceptual point of view, the proposed methodology could be applied to any device intended to monitor slope displacements.

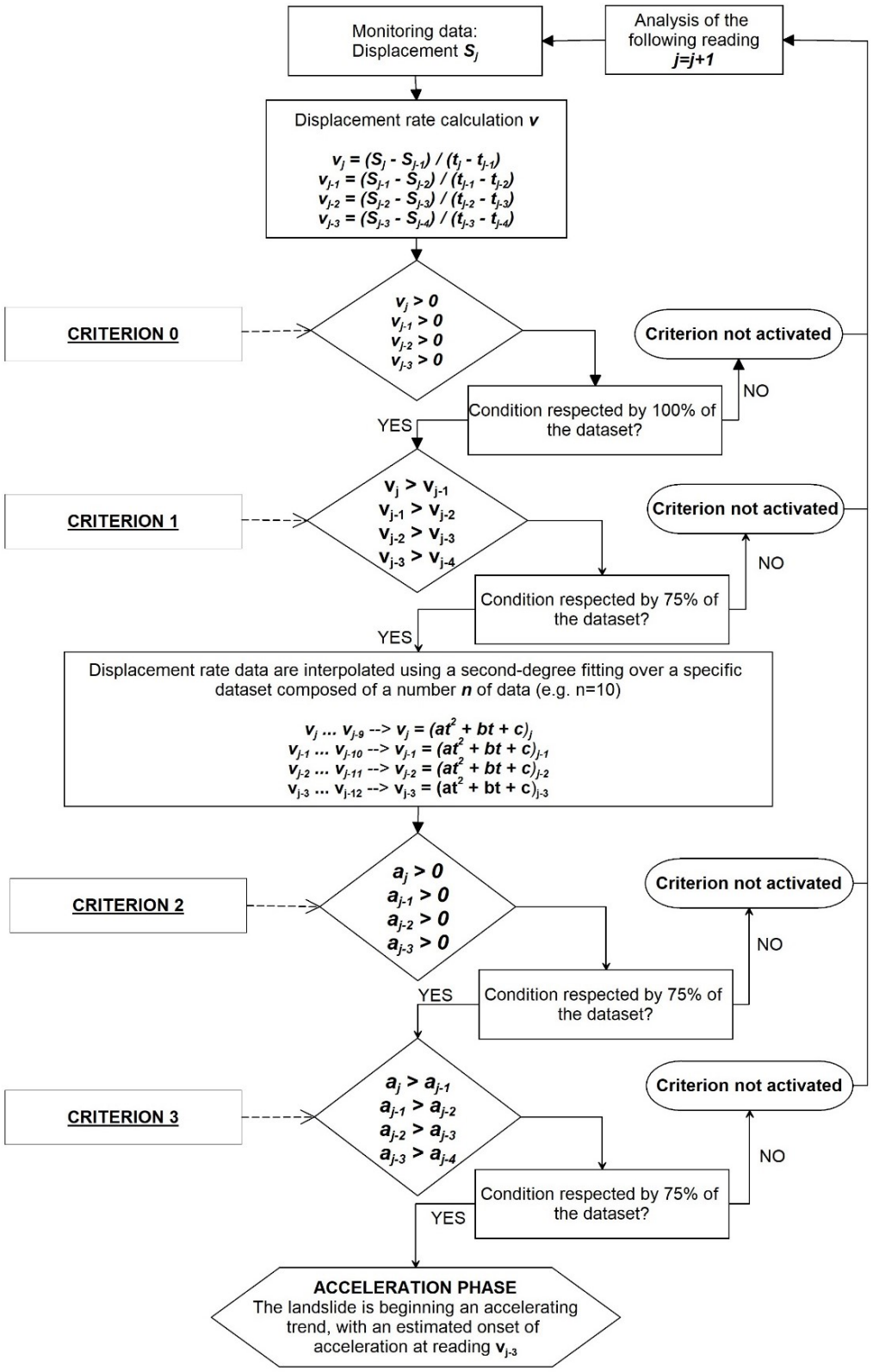

Figure 29: Flow chart of the multi-criteria algorithm, displaying each passage and the corresponding conditions (Valletta et al., 2021)

4.1.1. Criterion 0: positive displacement rate

Criterion 0 was included in the algorithm as a preliminary check on displacement rates extracted from the monitoring dataset. This mandatory condition requires four consecutive positive velocities (referred to reading j) to proceed with the following operations. This means that it is necessary to have a dataset composed of at least four displacement rate values (i.e., five displacement data) in order to continue the analysis. The introduction of this first step is particularly important to obtain meaningful results from the application of forecasting models, like IVM, to the selected dataset. In fact, a negative velocity would be meaningless in this context, effectively invalidating any result coming from the forecasting analysis.

$$\begin{cases} v_j > 0 \\ v_{j-1} > 0 \\ v_{j-2} > 0 \\ v_{j-3} > 0 \end{cases} \tag{XXI}$$

4.1.2. Criterion 1: increasing displacement rate

If Criterion 0 gives a positive result, the subsequent step focuses on the variation between two consecutive values in order to check if the displacement rate is displaying an actual accelerating trend. In this phase, data referred to readings j and $j-1$ are considered to compute the velocity variation Δv_j. The criterion is fulfilled if the $\Delta v > 0$ condition applies to at least the 75% of the considered dataset, which corresponds to three out of four consecutive displacement rate values.

$$\Delta v_j = v_j - v_{j-1} > 0 \tag{XXII}$$

This choice is intended to prevent errors deriving from anomalies in monitoring data, represented by outliers or spike noises, among the others. In fact, a too strict condition (such as the one applied to Criterion 0) could lead to the interpretation of a single negative result as an actual deceleration, thus stopping the procedure due to an undetected inconsistency in the dataset. On the other hand, the introduction of this tolerance margin makes it possible to carry on the analysis even if an anomalous value is present. Moreover, when dealing with monitoring devices featuring high sampling frequencies, it is sometimes possible to detect a temporary deceleration within a more consistent upward trend. In this context, a 100% validation condition of the dataset would interpret this behaviour as an actual deceleration, while its duration could be minimal when compared to the general trend of the landslide displacements.

4.1.3. Criterion 2: parabolic trend

The following condition is based on the assumption that displacement rates will display a non-linear behaviour during the acceleration phase. According to this hypothesis, Criterion 2 is intended to define a curve fitting the selected dataset, with the purpose to detect an upward trend. Taking as a reference the creep theory (as discussed in previous chapters), Criteria 1 and 2 aim to determine the initial transition from a linear trend, typically associated with a secondary creep stage, to a non-linear behaviour. Scientific literature focused on the evolution of potentially critical landslide events usually refers to a power law equation applied to

displacement rate data in order to describe the tertiary creep phase (e.g., Corcoran and Davies, 2018; Cruden and Masoumzadeh, 1987; Helmstetter et al., 2004; Voight, 1989). However, the calibration and testing of the proposed methodology evidenced how a power law function would not be suitable in an algorithm intended to interpolate a generic trend, since it gives reliable outcomes only when applied to the last phase of the phenomenon evolution.

To solve this problem, a fitting procedure involving a second-degree polynomial function was tested, with the objective to identify upward or downward trends in different datasets by studying the concavity direction. Figure 30 displays four different examples extracted from the testing process, presenting a comparison between two fitting approaches, namely power law and second-degree polynomial equation, performed on displacement rate data. This example refers to the time series #2 reported in Ryan and Call (1993). It is possible to observe how the fitting obtained with a parabolic equation accurately interpolates the monitoring data, displaying a concavity that correctly represents both an increasing (Datasets #1 and #2) and decreasing (Datasets #3 and #4) displacement rate trend. On the other hand, the power law model fails to provide an accurate representation of the dataset trends, not allowing a reliable interpretation of the landslide behaviour.

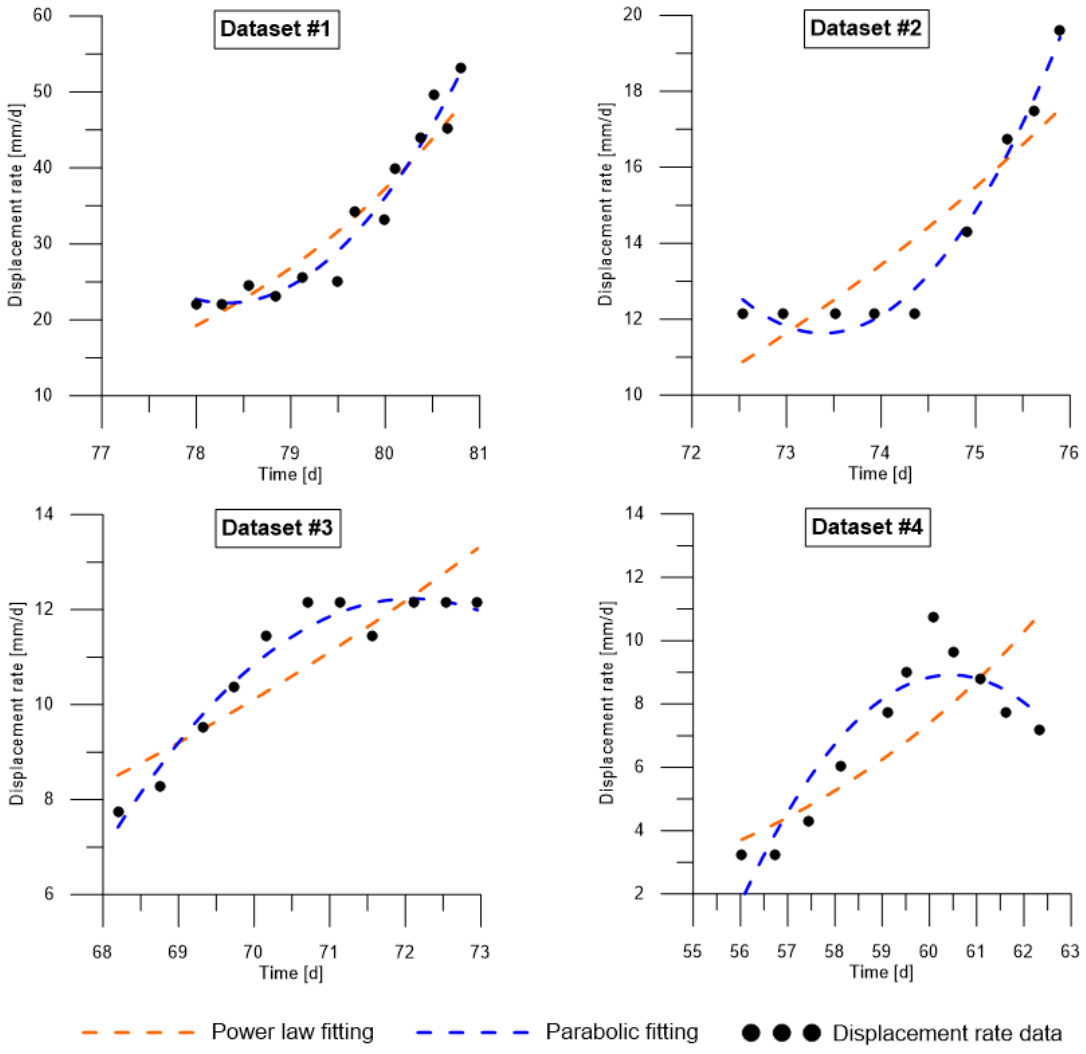

Figure 30: Comparison between two different fitting approaches, based on power law and parabolic equation, applied to four different displacement rate datasets (Valletta et al., 2021)

Table 1: Equations used for the parabolic and power law fitting procedures, together with the parameters resulting from their application to datasets reported in Figure 30

Dataset	Parabolic fitting $y = ax^2 + bx + c$			Power law fitting $y = ax^b$	
	a	b	c	a	b
#1	4.9507	-775.5021	30391.6446	8.8988E-049	26.0745
#2	1.2344	-181.1658	6658.9467	2.6346E-019	10.5431
#3	-0.3178	45.8235	-1639.4291	6.7969E-012	6.5973
#4	- 0.3631	43.9043	-1318.2098	1.0399E-017	10.039

Therefore, after fulfilling the previous Criterion 1, displacement rate data are interpolated using a parabolic fitting in order to determine the value of the a parameter that describes the concavity orientation:

$$y = ax^2 + bx + c \tag{XXIII}$$

where y refers to displacement rates and x represents time, expressed as a number. It is important to note that the most appropriate number of data to perform this operation may vary according to the specific case study, depending on parameters such as sampling frequency, instrumental noise, smoothing procedures, and other filters applied on monitoring data. The example in Table 2 refers to a case study where a fitting operation on a dataset composed of 10 displacement rates v was performed.

Table 2: Dataset considered for the Criterion 2, under the hypothesis of $n = 10$ data for the nonlinear interpolation

Referring dataset	First reading considered in the dataset	Last reading considered in the dataset	Concavity parameter
j	v_{j-9}	v_j	a_j
j-1	v_{j-10}	v_{j-1}	a_{j-1}
j-2	v_{j-11}	v_{j-2}	a_{j-2}
j-3	v_{j-12}	v_{j-3}	a_{j-3}

As previously assessed, the evaluation of the a coefficient of the interpolating curve is the main goal of this step. In fact, this parameter holds information regarding the curve concavity: a positive value identifies an upward concavity (i.e., an accelerating trend), while a downwards concavity features a value of $a < 0$ and corresponds to a decelerating pattern. In the proposed procedure, a positive value should be obtained in order to claim that an acceleration is taking place. If the condition is verified for at least the 75% of the dataset represented by j, $j-1$, $j-2$ and $j-3$ readings, Criterion 2 is fulfilled, and the analysis can advance to the following step.

4.1.4. Criterion 3: increasing concavity

The last step of the procedure takes into account the variation of the a coefficient between two consecutive readings. Specifically, the sign of Δa is studied to assess if the curve interpolating the monitoring data displays a more pronounced upward concavity compared to the previous one (i.e., the acceleration is increasing). While the previous conditions were designed to detect a transition between two different behaviours, namely secondary and tertiary creep stages, this particular criterion investigates a non-linear trend featuring increasing values. If a positive result is obtained from the application of Eq. XXIV., it is possible to state that the displacement rates trend is consistent with an increasingly accelerating pattern. Instead, a negative difference between two readings ($\Delta a < 0$) means that the curve is experiencing a transition towards a more linear trend, thus approaching a downwards concavity that represents a deceleration of slope movements.

$$\Delta a_j = a_j - a_{j-1} \tag{XXIV}$$

If Criterion 2 is activated at reading j, the analysis defines a dataset composed of four parameters and evaluates the variation of a starting from the first reading, namely the Δa_{j-3} reading. Similar to the two previous stages, a 75% success rate is required to fulfil the condition imposed for Criterion 3. If this last step returns a positive outcome, it could be assumed that an accelerating phase is taking place, and the $j-3$ reading could be taken as the OOA of the monitored event.

4.2. Parametric analysis

The validation of the proposed approach involved a parametric analysis, in order to evaluate the model performances under the variation of the main parameters implemented in the algorithm. In particular, the number of data points (d), the percentage limit, and the number of data (n) used in the model fitting procedure were considered during the process analysis.

In particular, Figure 31a and Figure 32a compare the reference dataset of $d = 4$ monitoring data, featuring a 3/4 rate limit (i.e., 75%), with a 5-point dataset characterized by two different rates, namely 3/5 (60%) and 4/5 (80%). Figure 31b and Figure 32b display the same reference case compared to a 6-point dataset with a rate of 4/6 (67%) and 5/6 (83%). Results reported in Figure 31 comes from the elaboration of the displacements recorded at the New Tredegar landslide (Bentley and Siddle, 2000), and are obtained by considering 10 monitoring data for the parabolic model fitting. Figure 32 follows the same approach, and takes as reference case study the Hogart Pit landslide (Brawner and Stacey, 1979).

By studying the analysis outcomes, it is possible to make the following considerations regarding the parameter influence on the algorithm:

- The OOA estimation is the same for all configuration, except for the $d = 6$, 4/6 model that placed the onset-of-acceleration one day earlier. Excluding this particular case, the beginning of the acceleration phase was assessed correctly according to the information available for the specific case studies.

- Increasing the number of data points (from 4 to 6) produced a progressively delayed fulfilment of the Criterion 3 condition, leading to a postponed assessment of the acceleration phase. This is a relevant downside in a methodology that is intended to provide timely evaluations for early warning purposes.
- Percentage limits higher than the reference value (i.e., 75%) did not display any relevant improvement in avoiding false positives. The only exception relates to the 83% rate in the $d = 6$ configuration, which however provided a notably delayed OOA estimation compared to the other configurations. On the other hand, values lower than 75% led to an increment of false positives for both $d = 5$ and $d = 6$.

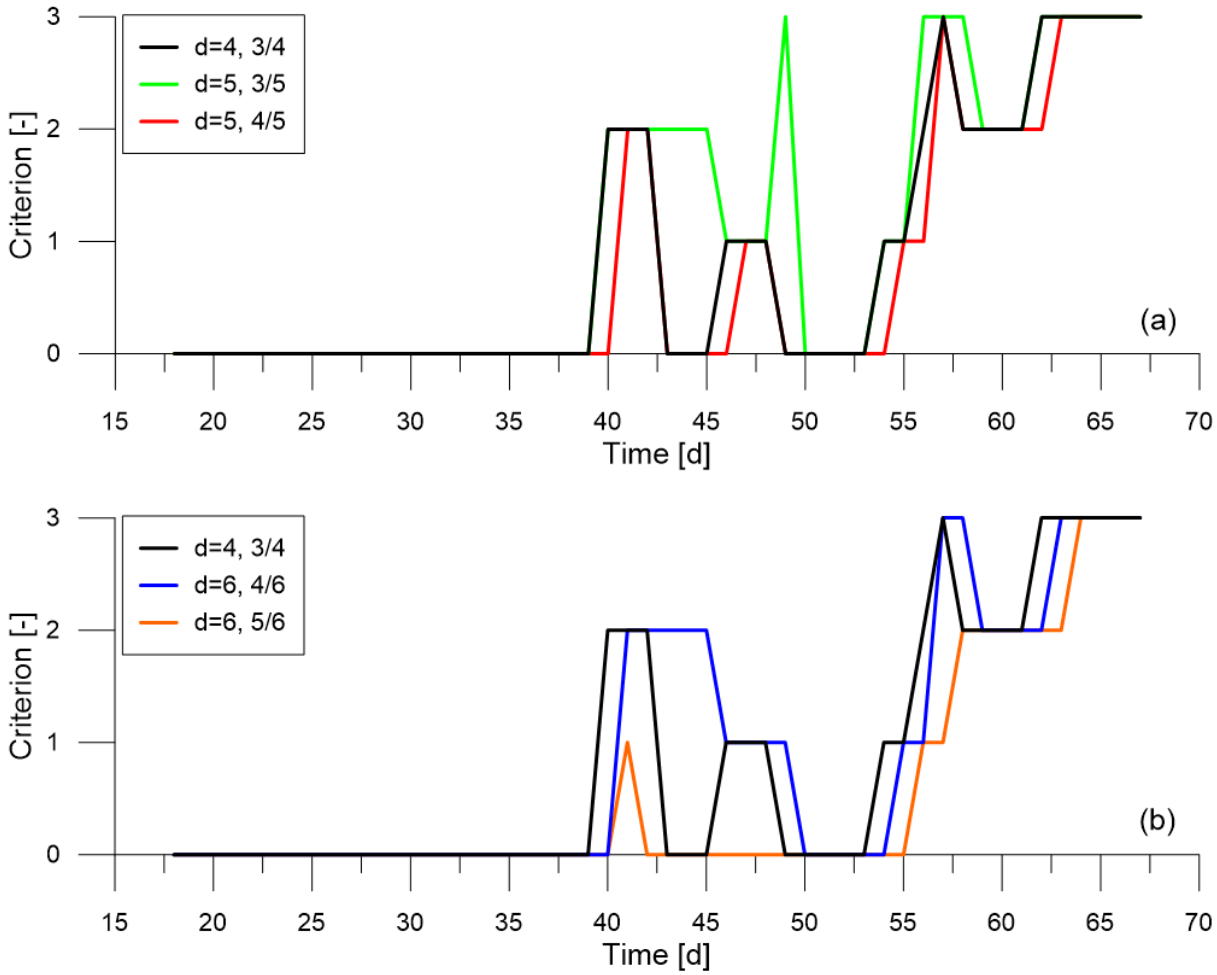

Figure 31: Parametric analysis of the New Tredegar landslide dataset, comparing the $d = 4$, 3/4 reference configuration with (a) $d = 5$, and (b) $d = 6$ configurations, including also different values for the percentage level parameter (Valletta et al., 2021)

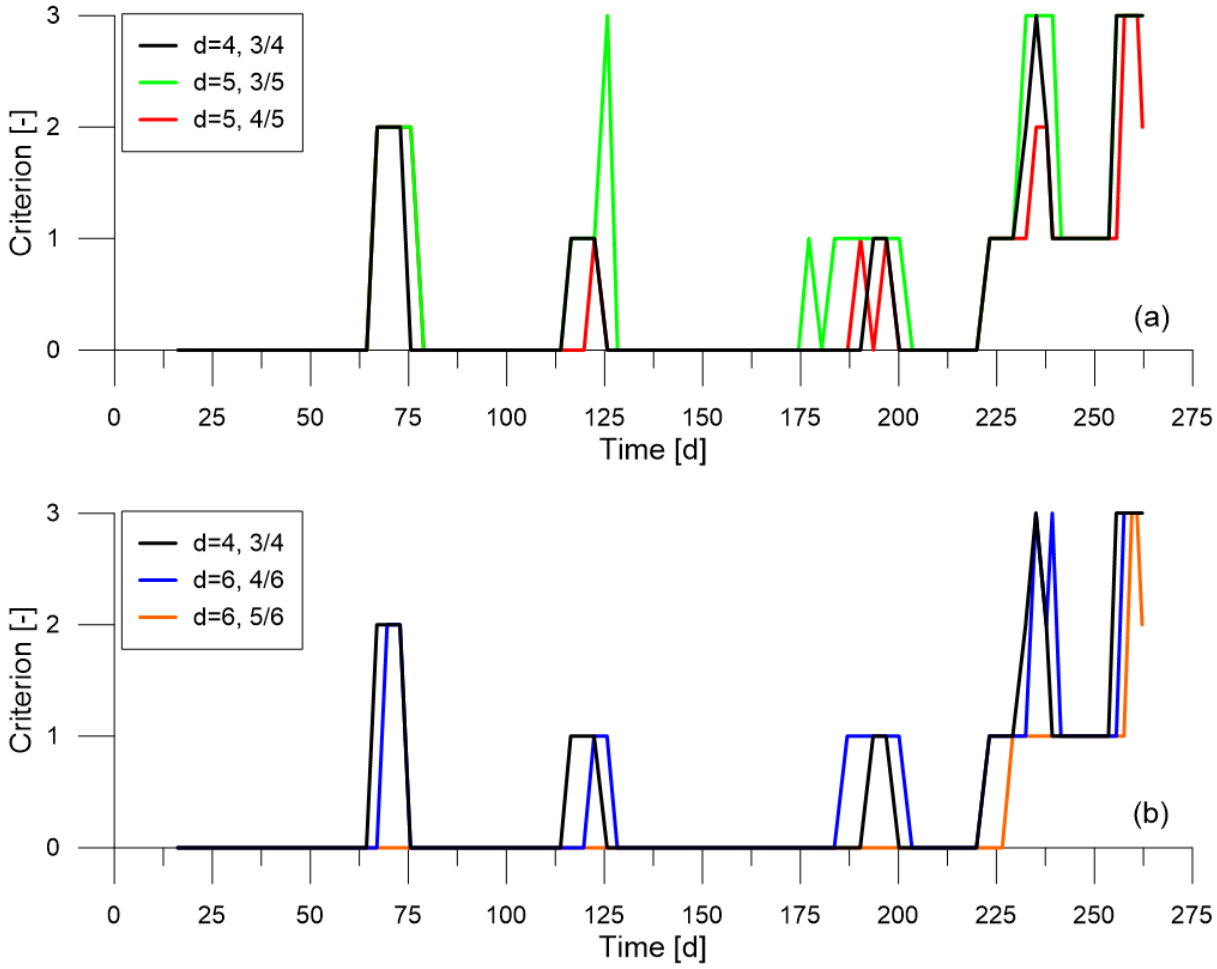

Figure 32: Parametric analysis of the Hogart Pit landslide dataset, comparing the $d = 4$, 3/4 reference configuration with (a) $d = 5$, and (b) $d = 6$ configurations, including also different values for the percentage level parameter (Valletta et al., 2021)

Figure 33a and Figure 33b provide the results of the parametric study performed on the number of monitoring data used in the parabolic model fitting, deriving respectively from the analysis of the New Tredegar landslide (Bentley and Siddle, 2000) and Ohto landslide (Suwa et al., 2010) datasets. Both these cases were processed by considering a $d = 4$, 3/4 configuration.

By observing the results of these elaborations, it is possible to notice the influence of the n parameter for what concern the occurrence of false positives. In particular, analyses performed with $n > 10$ evidenced a higher number of data points fulfilling the Criterion 3 conditions, generating a series of false positives before the actual onset of acceleration. Additionally, some false alarms caused by $n = 11$ and $n = 12$ configurations lasted for more than a single monitoring record (e.g., the event starting at $t = 41$ days in Figure 33a), which could lead to an even more severe misinterpretation of available data. For what concern $n = 8$ and $n = 9$ configurations, they were unable to provide a reliable assessment of the onset of acceleration. In fact, the elaborations did not always reach the required level during the critical acceleration phase, thus leading to an inaccurate OOA definition. An example of this behaviour can be observed in Figure 33b, where the analyses performed with datasets ranging from 10 to 12 points consistently fulfilled the Criterion 3 conditions after the OOA identification. On the

opposite, datasets featuring $n < 8$ displayed a much less stable behaviour, not allowing to provide a reliable OOA definition.

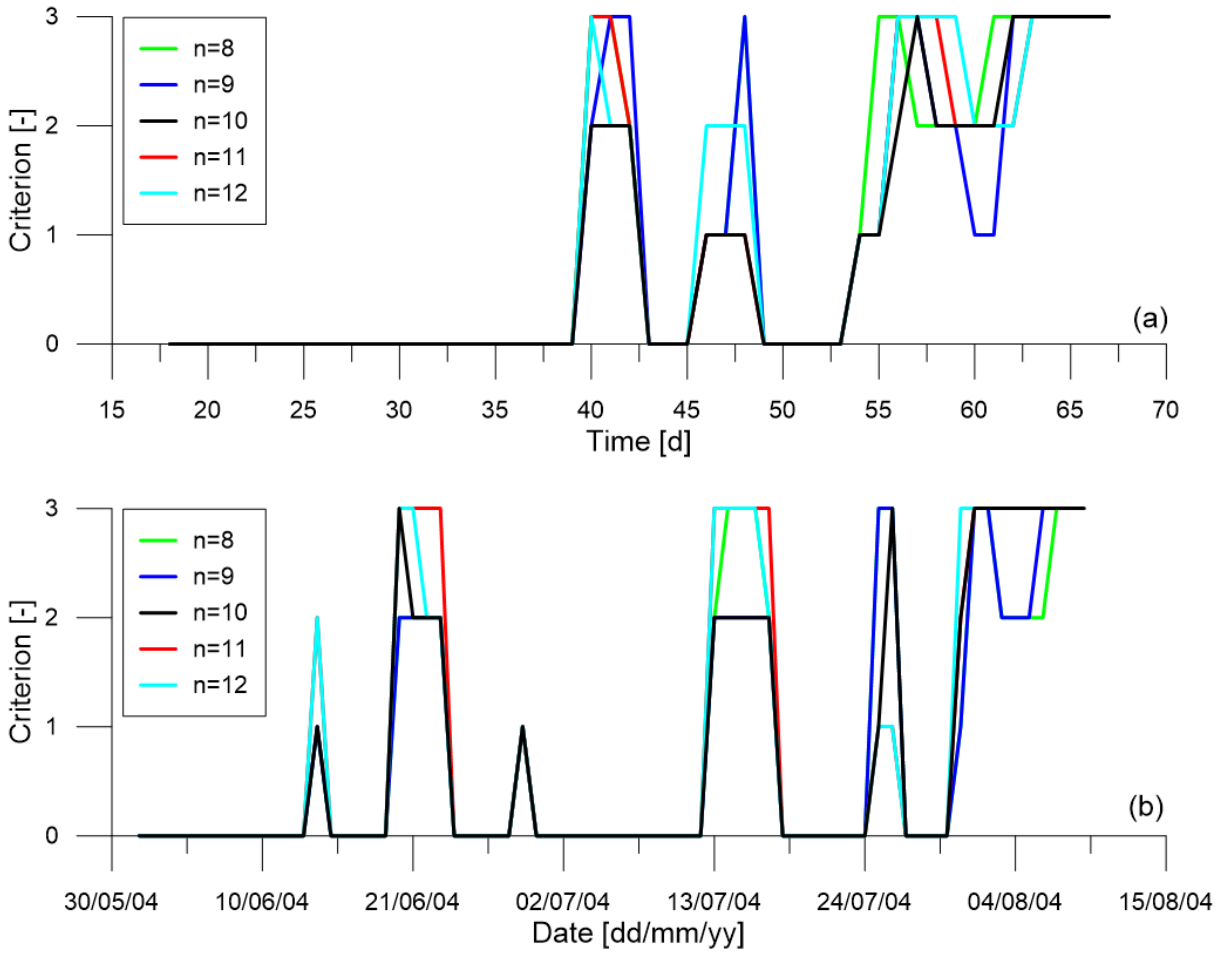

Figure 33: Parametric analysis of the (a) New Tredegar landslide and (b) Ohto landslide datasets, focusing on the number of monitoring data used for the parabolic fitting model (Valletta et al., 2021)

4.3. Case studies

As detailed in the previous sections, the application of the proposed procedure involves a real time or near-real time monitoring approach, aiming to identify potentially critical acceleration trends starting from available displacement data. In the following sections, three real case scenarios are presented to outline the algorithm implementation. Even if all monitoring data here presented come from historical events retrieved from scientific literature, the procedure is applied b simulating a real-time acquisition, since the algorithm provides a new result each time a sampled value is elaborated by the automatic software. The analysis was performed with the drop-down structure previously described, generating a new dataset for each single monitoring data. Displacement rate datasets were digitized from data reported in scientific literature, considering a daily sampling rate.

It is important to underline that, in order to perform the Criterion 2 procedure, a dataset composed of 10 displacement rate values ($n = 10$) was selected for all following case studies. Therefore, the minimum number of monitoring data to perform the complete analysis is 12 displacement values. In fact, the first displacement rate can be evaluated starting from the

second reading, and the Criterion 3 needs two non-linear interpolations to investigate the concavity parameter variation. Additionally, according to the results obtained in the parametric analyses, a 4-point dataset and a percentage limit of 75% were used for these elaborations.

4.3.1. Case Study #1: Ohto Landslide

This case study refers to a landslide occurred on August 10th, 2004, in Nara Prefecture, Japan (Suwa et al., 2010). According to the information retrieved from studies related to this event, the collapse took place during a particularly critical year due to prolonged rainfalls and typhoons that interested the entire country, which resulted in damaged structures and triggering of several landslides (Fujisawa et al., 2010). The event presented in this case study was first identified in January 2004, when a series of cracks appeared on a retaining wall along National Highway 168, near the Otomura village. As a result, several monitoring tools were installed on site, including extensometers to observe the displacement of the unstable slope, and a video camera to capture any motion displayed by the slope. Additionally, the system was able to send an automatic notification message at the overcoming of predefined thresholds. A sequence of typhoons occurring from late June prompted the planning of further investigations, and ultimately the National Highway was closed at 05:10 AM on August 8th when the creep velocity reached 4mm/2h. The landslide collapsed without claiming any victims 43 hours later, at 00:15 AM on August 10th, and involved a total volume of 0.2x10^{6} m^{3} of material (Suwa et al., 2010).

The displacement dataset obtained from the monitoring activity was used to verify the ability of the proposed method to identify correctly the acceleration phase that ultimately led to the landslide collapse (Figure 34). According to Suwa et al. (2010), monitoring data recorded by extensometers showed a constant displacement rate until July 31 when an acceleration was observed, meaning that the movement transitioned from a secondary to a tertiary creep phase. According to this observation, it is possible to take this date as the onset-of-acceleration reference value, since it marked the beginning of the accelerating phase that ultimately led to the slope collapse.

Figure 35 presents the outcomes obtained from the algorithm application to each single monitoring record included in the available dataset. In particular, the chart displays the landslide displacements and the corresponding verified sub-criteria as the monitoring activity continues. The process is repeated progressively for each sampled value, ultimately generating the displacement dataset acquired after the landslide collapse. As can be observed, despite the detection of some early activations, the algorithm identified correctly the acceleration phase. In particular, after the fulfilment of all conditions of the algorithm in correspondence of the measure recorded on August 1st, the procedure gives a positive result for all the following elaborated data. Consequently, according to the principles discussed in previous sections, it could be assessed that the onset of acceleration point can be placed on the displacement measured on July 29th, which is in good agreement with the OOA value available for this landslide from scientific literature.

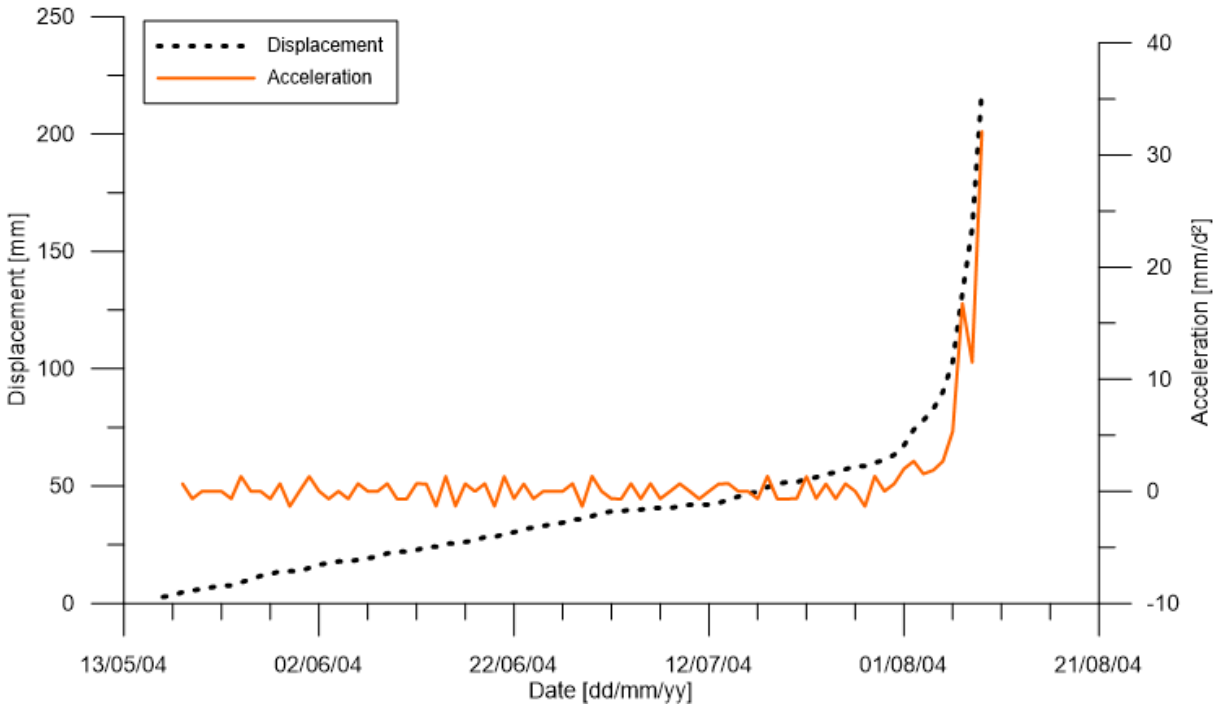

Figure 34: Displacement and acceleration curves for the Ohto landslide – dataset digitized from Suwa et al. (2010)

Moreover, a more in-depth analysis of each single condition evidences that the monitoring value measured on July 29th fulfilled only the Criterion 0, and it was included in the accelerating dataset thanks to the tolerance factor introduced in the algorithm. In fact, starting from July 30th, each single point verified all the conditions included in the proposed method. Therefore, this date could be taken as a more reliable OOA reference point, resulting in a value even closer to what Suwa et al. (2010) reported in their study.

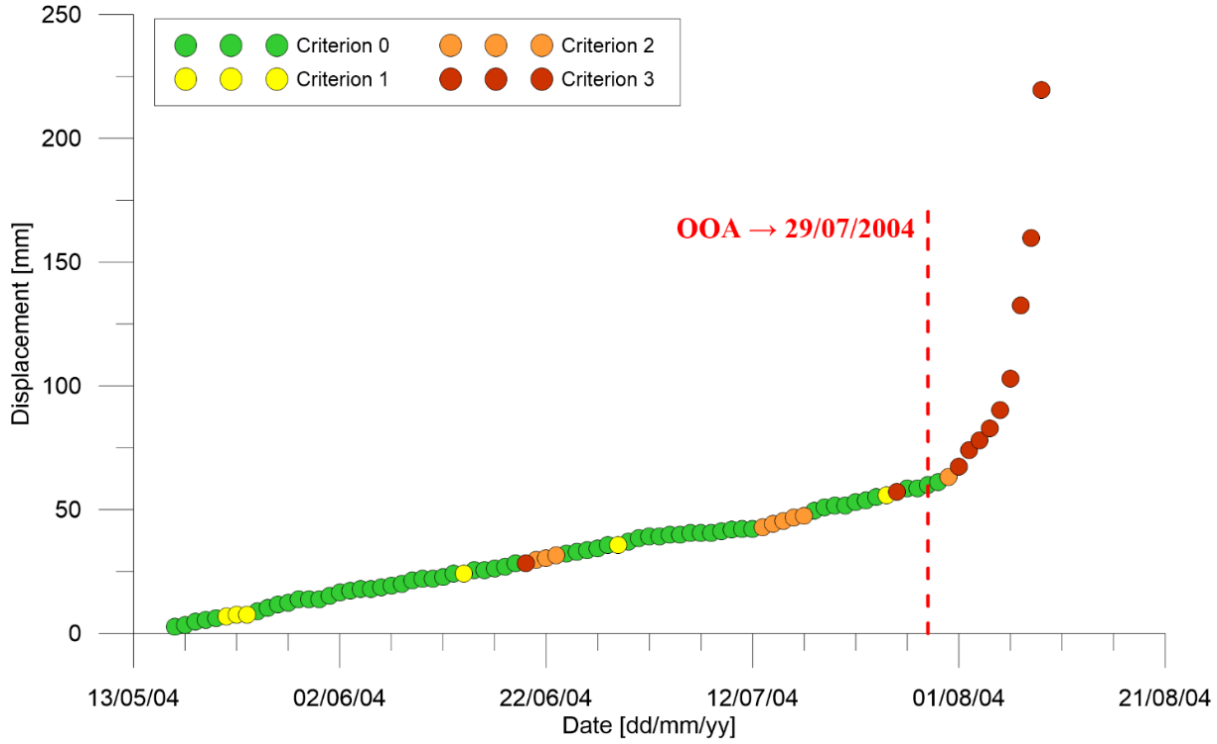

Figure 35: Results obtained from the application of the algorithm to the Ohto Landslide dataset (displacement data recorded during the monitoring period from May to August 2004)

4.3.2. Case Study #2: Agoyama Landslide

The second case study concerns a collapse occurred in December 1972, about 5 km to the northwest of Fukui City, Japan (Saito, 1979). According to the author, the landslide was 200 m wide, 80 m high, and 180 m in slope length. The triggering factor may be related to excavation works as borrow-pit performed at the foot of the slope. Starting from October 4th, early indications of instability were observed when a long, continued crack was identified on a hillside of Agoyama. This event led to the installation of a monitoring system in order to measure the landslide displacements. Additionally, the person in charge of the site received information on the phenomenon evolution following the execution of a forecasting analysis. Apparently, the analysis met some difficulties related to irregular movements in the final stage and partial failures of the landslide body. This resulted in a slightly anticipated prediction of the actual collapse, which happened on December 2nd at 01:30 AM.

As reported by Saito (1979), displacement recorded by the monitoring instrumentation installed on-site initially amounted to 10 mm per day, reaching 20 mm/d at the end of October, and ultimately escalating up to 100 mm/day after November 20th (Figure 36). On the basis of these information, the OOA reference date that will serve as a comparison for the algorithm application could be placed on the moment where displacement increased significantly before the collapse, i.e., on November 20th, 1972.

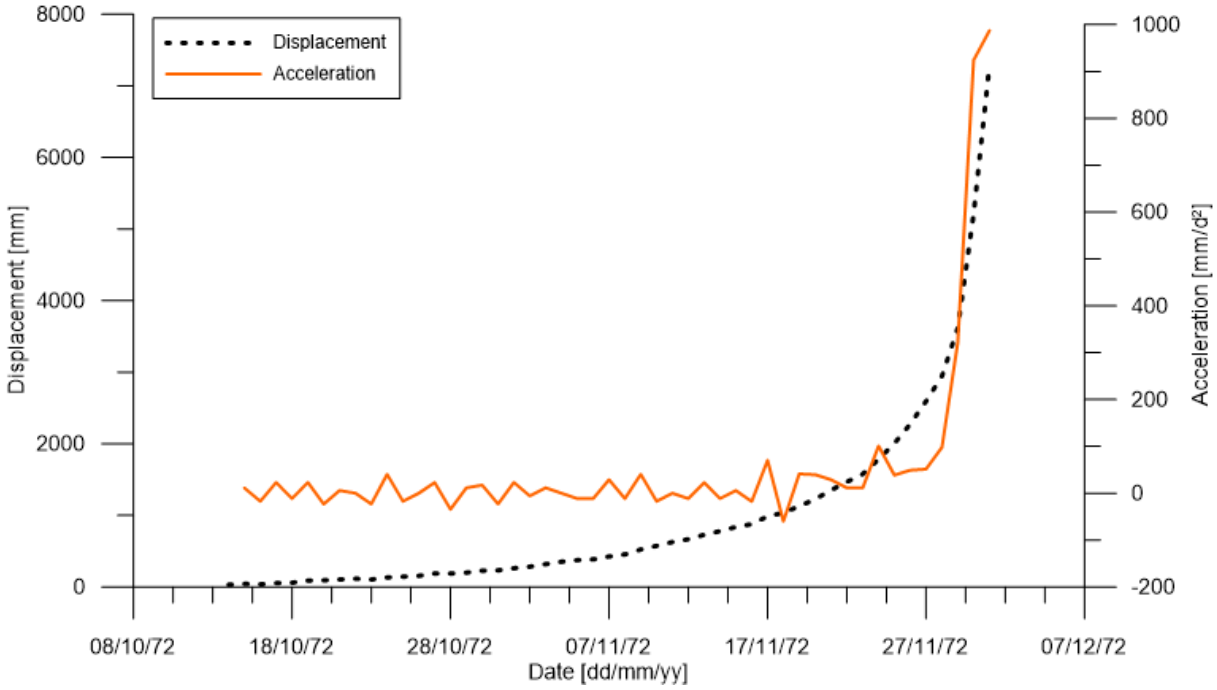

Figure 36: Displacement and acceleration curves for the Agoyama landslide – dataset digitized from Hayashi and Yamamori (1991)

Results represented in highlight the good performances of the proposed methodology, which correctly identified the accelerating trend that started from the displacement measured on November 23rd. According to this outcome, it is possible to define the OOA for this case study on November 20th, which corresponds to the reference value previously extrapolated from displacements described by Saito (1979).

An alternative interpretation of the analysis results could take into account the expansion of the accelerating dataset to include also the two measures obtained on November 20th and 21st. As can be observed in Figure 37, the former point represents an "interval" between the accelerating trend identified by the analysis, and the previous monitoring data that fulfil the Criterion 3 condition. It could be then argued that the measure recorded on November 21st, despite stopping at the condition imposed on Criterion 2, could be included in the larger accelerating dataset. This choice would place the onset of acceleration on November 18th, some days before the previous estimation, but still providing a good result in terms of definition of the accelerating trend.

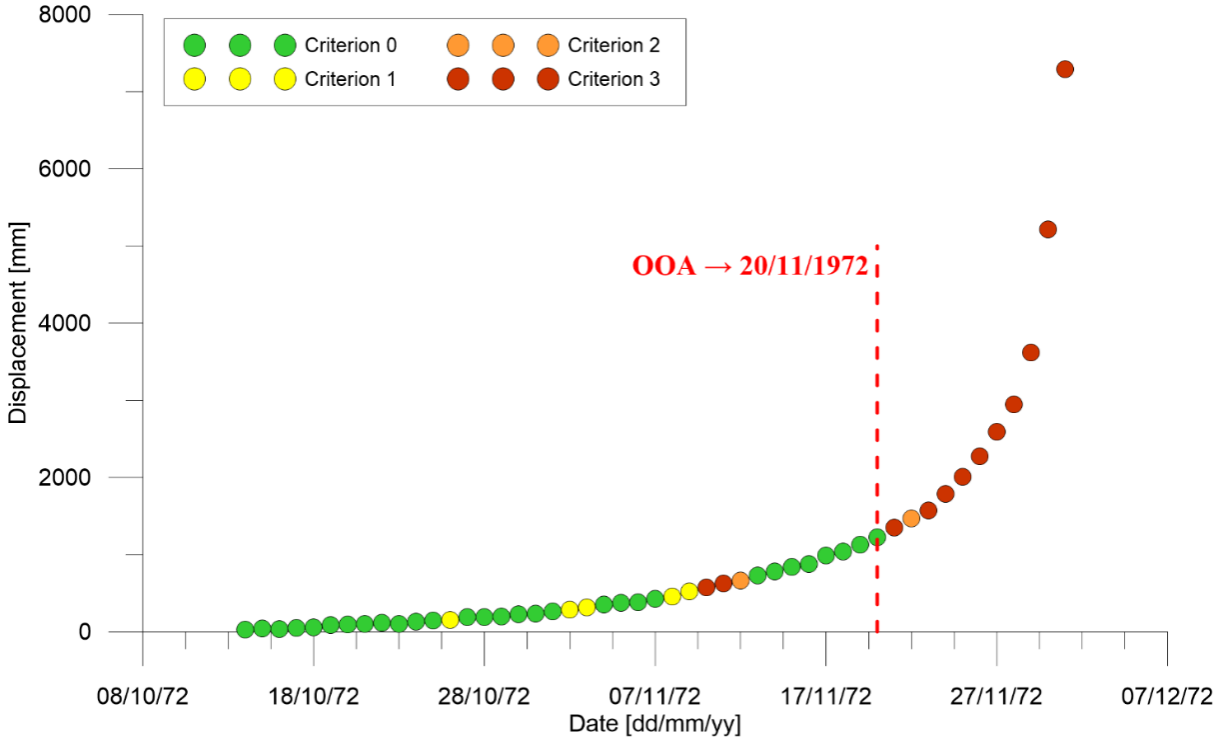

Figure 37: Results obtained from the application of the algorithm to the Agoyama Landslide dataset (displacement data recorded during the monitoring period from October to December 1972)

4.3.3. Case Study #3: Tuckabianna West Landslide

The third case study deals with a translational planar rockslide occurred in Tuckabianna West open pit mine, Australia. The collapse involved 1.2×10^5 m^3 of material and was likely triggered by excavation works (Glastonbury and Fell, 2002). Rockfall events were observed in the area 10 days before the main collapse. It should be noted that these minor events occurred before the beginning of the tertiary creep phase, which lasted approximately 6 days (Moretto et al., 2017). After the identification of a tension crack in the upper part of the slope, a series of surface surveys were activated in the interested area. However, as reported by Glastonbury and Fell (2002), mining activities were not stopped, and on-site works continued even during the acceleration phase.

For this case study, it was not possible to find a clear evaluation of the onset of acceleration that resulted in the slope collapse. For this reason, the OOA reference value was defined by taking into consideration all information reported by authors previously mentioned regarding

the phenomenon evolution. Therefore, the displacement data trend (Figure 38) and other considerations regarding the acceleration evolution over time were taken as a reference to identify the beginning of the accelerating phase between March 4th and 5th.

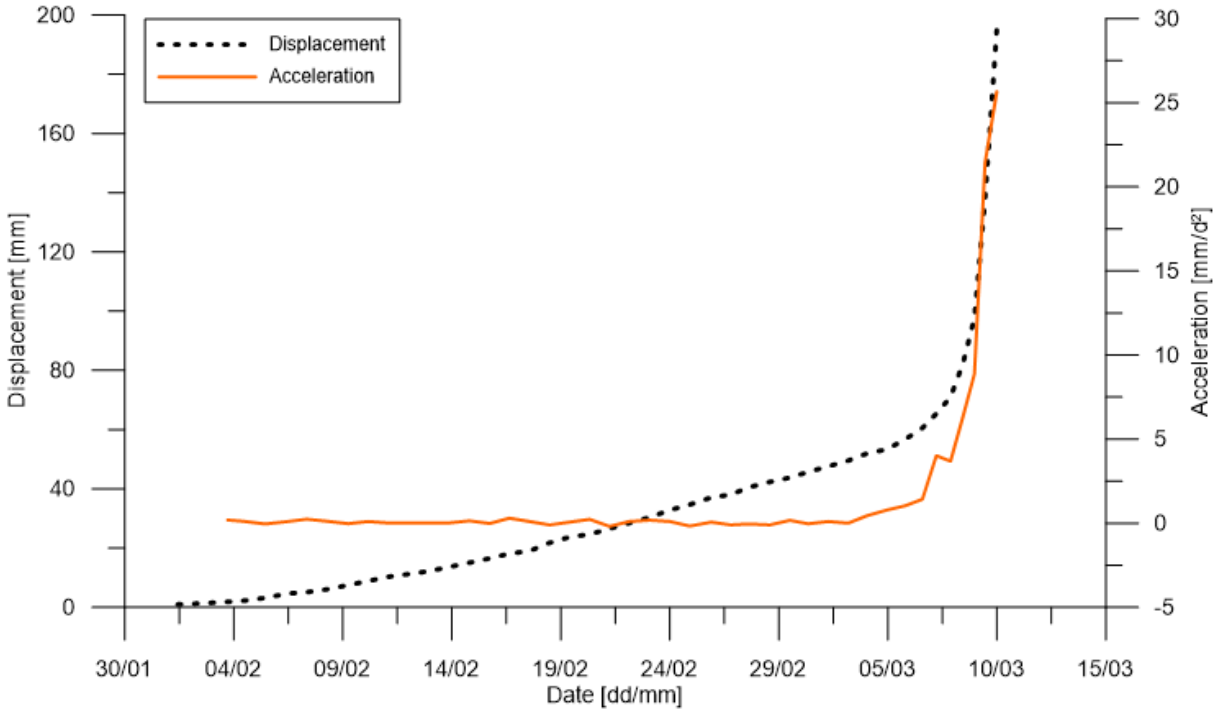

Figure 38: Displacement and acceleration curves for the Tuckabianna West landslide – dataset digitized from Glastonbury and Fell (2002)

Following the same process presented in previous case studies, the displacement dataset was elaborated by applying the algorithm to each monitoring data simulating a real-time acquisition. As evidenced by results reported in Figure 39, it is possible to observe a clear distinction between the constant velocity phase, characterized by a linear displacement trend, and the subsequent accelerating stage that ultimately led to the slope collapse. According to the outcomes provided by the software, the monitoring data sampled on March 4th is the first one to satisfy all conditions and achieve the Criterion 3 requirements, while the following three data do not go beyond the fulfilment of Criterion 2. However, starting from March 7th, the displacement trend showed a more evident accelerating behaviour, and each monitoring measure from this point onwards reached the level defined by Criterion 3. According to these outcomes, the OOA date for this case study could be placed approximately on March 4th, which is in good agreement with the reference value retrieved from available literature.

By observing the results coming from the algorithm application on these case studies, it is possible to identify a common behavior showed by every analysed dataset. Specifically, the first part of each displacement dataset is characterized by a linear trend (i.e., constant displacement rate) and is mostly limited by the Criterion 1 condition, which only requires an increasing displacement rate. On the other hand, the second part of the dataset presents an upward trend that consistently fulfil all conditions defined by the algorithm, effectively representing the accelerating stage of the landslide.

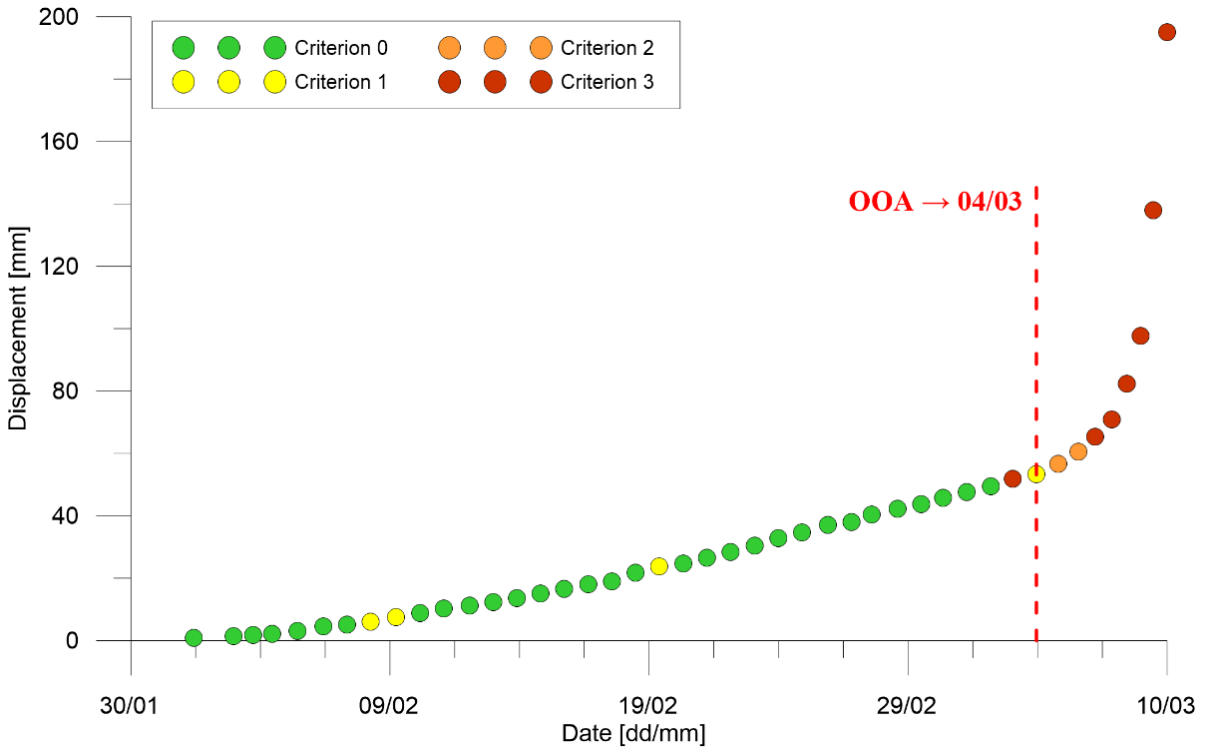

Figure 39: Results obtained from the application of the algorithm to the Tuckabianna West Landslide dataset (displacement data available starting from 1st February)

The algorithm proved to be an effective tool to identify the landslide acceleration phase, allowing to determine its starting point. However, it is possible to note the occurrence of some false positives in the analysis, represented by monitoring points that fulfilled all the conditions despite not being part of the critical acceleration phase. When investigating the causes responsible for these events, it should be taken into account that this approach is mainly based on geometrical arguments, trying to employ a non-linear interpolation to represent the monitoring dataset and forecast its evolution. For this reason, it is possible to attribute these inaccuracies to local fluctuations in the displacement dataset, displaying short upward trends that the algorithm could interpret as actual acceleration phases. Another element to take into account is the quality of the dataset generated by a digitizing process, which cannot be considered as accurate as the original monitoring dataset. Either way, it should be underlined that the false alarms generated during the algorithm application lasted no more than two consecutive measures, thereby resulting easily detectable when following datasets did not activate one of the algorithm sub-criteria.

Chapter 5. Classification algorithm

The procedure described in the previous chapter is aimed to determine if a monitoring dataset is displaying a set of features that are indicative of a potentially hazardous evolution of the landslide behaviour. However, as discussed in the case studies presentation, the methodology is not immune to false positives. In fact, it is possible for a landslide to show an accelerating trend lasting long enough to fulfil all conditions of the algorithm, without effectively leading to a collapse.

Regardless of the scale, an EWS should be designed to avoid as much as possible the occurrence of both false positive and missed alerts (Table 3). In fact, a false alert could result in the activation of emergency measures when the expected critical event does not occur, while a missed alert could lead to the underestimation of the occurring event, with no risk reduction actions taken when the hazard is triggered. Both these events are particularly problematic, since they can induce significant issues from a social, economic, and legal point of view. Some of the improvements that have been proposed to limit the occurrence of these issues include the implementation of different thresholds, and the integration of multiple sensors to achieve a redundancy in monitoring measurements (Klein and Coccia, 2020).

Table 3. Confusion matrix adapted to landslide early warning (modified from Klein and Coccia, 2020)

	No Threat	**Threat**
Alert	False positive (FP) → FALSE ALERT	True Positive (TP) → TRUE ALERT
No Alert	True Negative (TN) → NO ALERT	False Negative (FN) → MISSED ALERT

The procedure described in this chapter was conceived with the intent to limit the occurrence of false alerts produced by the acceleration criterion, by introducing a series of thresholds to classify the hazard level posed by an event previously identified from monitoring data. In particular, the methodology takes advantage of a multi-level system which allows to take into account both trends presenting a potentially critical behaviour, and minor events that could be still taken into account and analysed even without leading to the slope collapse. Because of this, this system is intended to work in synergy with the OOA identification algorithm, which has the task to define the dataset that should be processed through the multi-level procedure.

The main advantage coming from this approach lies on the possibility to provide an adequate dissemination of information related on the ongoing phenomenon, depending on the level reached by the observed event. Moreover, one the of objectives is to create a methodology designed to work simultaneously with a large number of monitoring system installed in different sites, featuring high sampling frequencies and automatic procedures for data acquisition. These features are typically connected with the necessity to manage large numbers of data at the same time, while pursuing at the same time the real or near-real time approach needed to have

an efficient and reliable landslide EWS. As previously underlined, these characteristics are usually associated with so-called innovative monitoring systems, which integrate the proper technologies to sustain the sampling rates required for these applications. The methodology development was conducted taking into account all these points, to find an adequate balance between results reliability and performance efficiency. The main source for this chapter is Valletta et al. (2020a).

5.1. Algorithm structure

The flow chard reported in Figure 40 summarizes the structure of the proposed multi-level algorithm, which starts from the acquisition of displacement data from monitoring tools installed on-site. It should be specified that the methodology design process was based on the dataset structure of MUMS-based devices, which have been described in previous chapters. Nonetheless, the approach is not intrinsically exclusive of this type of instrumentation, and could be easily adapted to suite other monitoring tools with similar structure and working principles.

The basis of the classification algorithm relies on the implementation of a failure forecasting model, and the subsequent study of different parameters characterizing the analysis performed on the dataset. In particular, a set of three parameters to be taken as a reference to define the alert level reached by the analysis has been defined:

- The determination coefficient R^2 obtained from the application of the failure forecasting model, namely the linear Inverse Velocity Method (IVM) introduced by Fukuzono (refer to Chapter 2.3 for further details on this methodology). As previously explained, the hypothesis of a linear trend of the inverse of velocity has been considered a good approximation to describe the landslide behaviour as the slope gets closer to the final collapse. Therefore, it could be assumed that the achievement of a good results in the linear interpolation of the dataset (i.e., a high determination coefficient value) could be indicative of a potentially hazardous event. Manconi and Giordan (2016) followed a similar approach to define operative thresholds based on the reliability of the forecasting analysis.

- The number of monitoring data included in the IVM analysis. The choice of this parameter come from the assumption that the landslide behaviour approximates a tertiary creep curve when approaching its failure. As a consequence, a dataset containing a high number of monitoring points could represents a trend consistently accelerating over time, which could be a sign of a critical developing event. While the OOA identification algorithm generates a 4-point dataset, the classification algorithm is able to expand the dataset by exploiting the same multi-criteria structure. Additional details are included in the following paragraphs.

- The number of sensors included in the IVM analysis after fulfilling all conditions imposed by the OOA identification algorithm. This parameter comes into plays since the methodology was originally designed for a monitoring system (i.e., MUMS-based instrumentation) integrating several sensors in the same array. The availability of

information regarding the landslide behaviour at different depths makes it possible to determine of the displacement identified by the software is limited to a local area of the slope, or if it involves several sections of the landslide. Therefore, a higher number of sensors displaying an accelerating trend could be an indication of the relevant magnitude of the detected event.

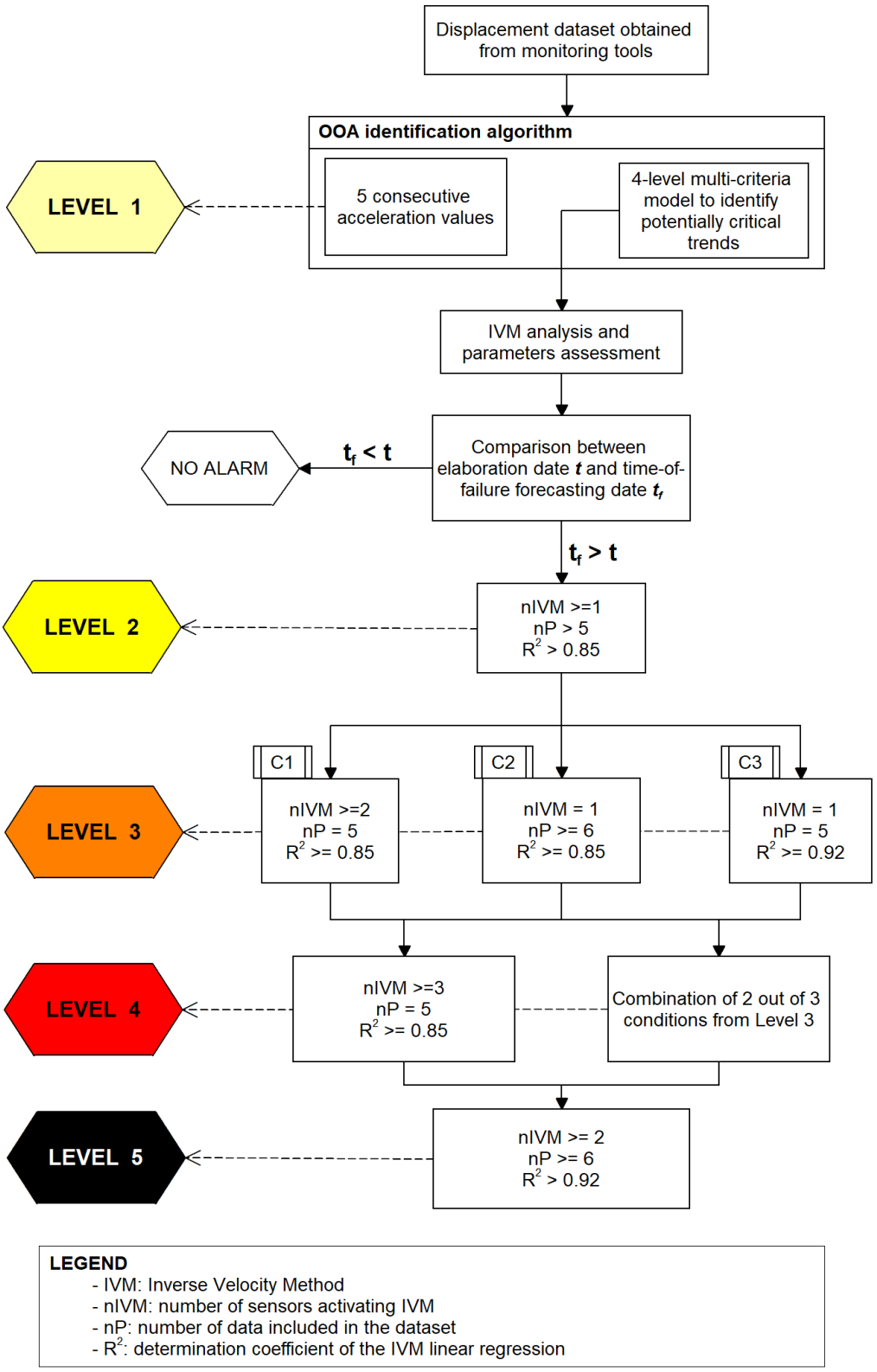

Figure 40. Flow diagram summarizing the alert classification algorithm structure

5.1.1. Forecasting analysis and dataset definition

If the OOA identification algorithm returns a positive outcome, the software performs a failure forecasting analysis by applying the Inverse Velocity Method under the hypothesis of linear inverse-velocity vs time trend. Generally, the outcome of this operation is an estimation of the time of failure t_f based on the available monitoring data. However, in this phase, the main objective IVM application allows is to determine the three parameters mentioned before, which are needed to assess the alert level for the event identified by the automatic software.

As previously discussed, forecasting models should be applied on an accelerating trend in order to provide reliable result. The determination of the proper dataset to use in this analysis derives from the application of the OOA identification algorithm previously described. However, the procedure is designed to work on a predefined number of data, checking progressively if new monitoring values are in accordance with the imposed conditions. On the other hand, at this stage of the analysis, a single dataset is needed to perform the failure forecasting analysis. For this reason, once the algorithm identifies the first 4-point dataset, the software continues the analysis by applying the same criteria to previous monitoring data, including in the dataset all previous values that fulfil the imposed conditions.

This dataset expansion process is described in Figure 41 and can be summarized as follows:

- Once the 4-point dataset is defined, a first prediction of the time of failure is performed by interpolating the monitoring data
- The software checks if the value of t_f is positive, i.e., it verifies that the result of the forecasting analysis indicates a later date than the moment when the analysis is performed. A negative result corresponds to a prediction located in the past, which has no utility for early warning purposes, and leads to the termination of the analysis. Such a case could appear when a moving average elaboration process is applied to monitoring data, inducing a slight change in previous values, and retroactively activating the criteria.
- Instead, if $t_f > 0$, the software evaluates the three parameters controlling the classification process, namely the regression coefficient of the IVM procedure, the number of sensors activating the forecasting model, and the number of monitoring data composing each dataset. Then, the algorithm performs another check based on the R^2 value, which should be equal or larger than 0.85 in order to continue the analysis.
- If $R^2 \geq 0.85$, and other monitoring data are available, the software applies the same process introduced in the OOA identification algorithm to verify if the dataset should be integrated with other points following the same accelerating trend. If the following monitoring value manages to fulfil all the conditions, it is included in the dataset and the process is repeated for next data, if there are any. However, if the analysed value does not satisfy every condition, it is not immediately discarded. Instead, the same analysis is performed on the following value and, with a positive result, both data are included in the dataset and the

analysis can continue. This process is intended to avoid the possibility to abort the entire procedure due to the presence of a single outlier in the monitoring dataset.

- Once there are no more data available, or the analysis returned two consecutive negative results, the final dataset is defined and a value of t_f is assessed, together with a new set of controlling parameters that will be used to determine the alert level generated by the event.

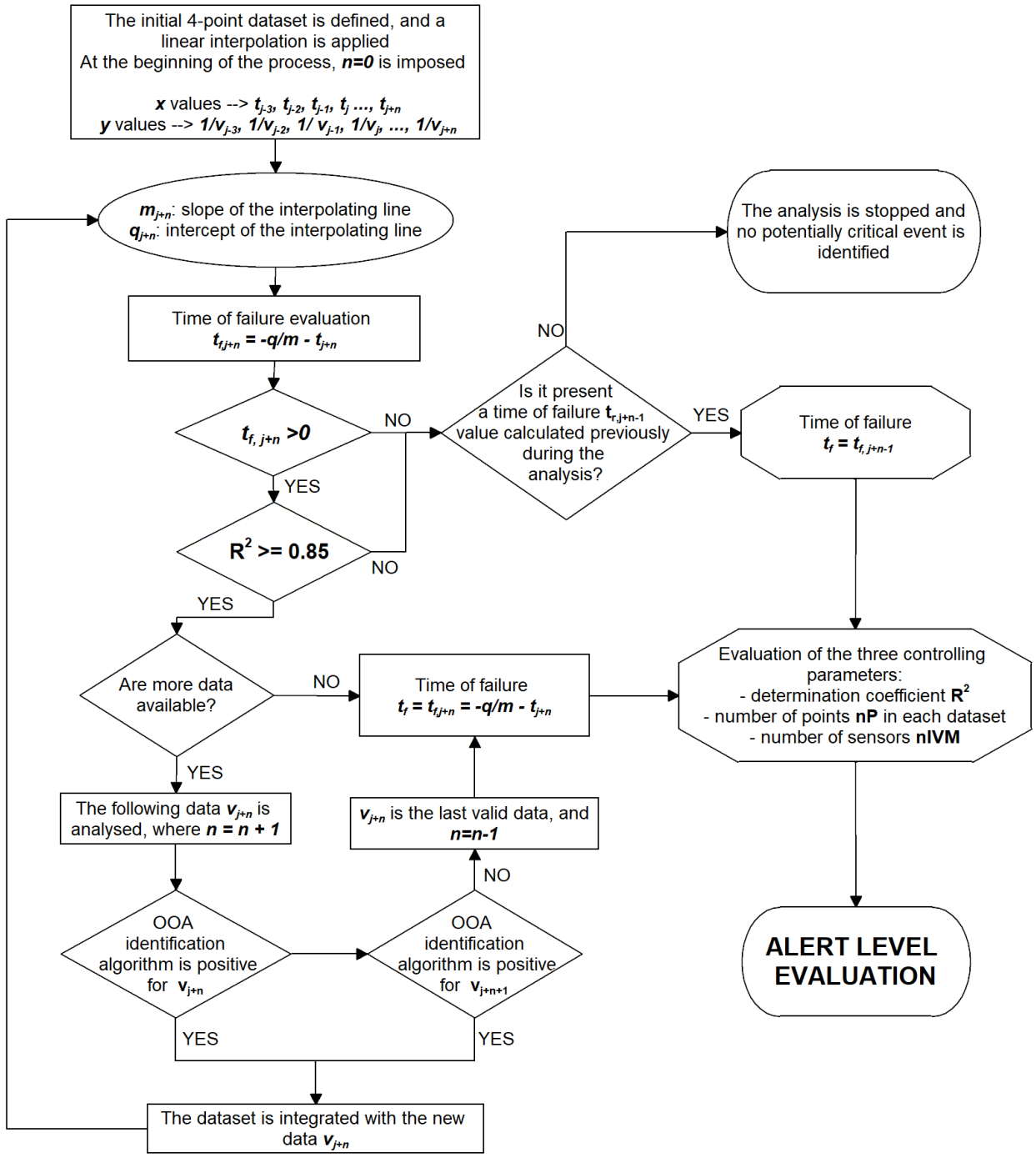

Figure 41. Flow chart describing the process from the assessment of the starting dataset to the evaluation of the time of failure and the parameters needed to determine the alert level generated by the event

5.1.2. Level definition

Level 1

Each time a new displacement value reaches the elaboration centre, the automatic software activates the OOA identification routine in order to verify if the displacement rate and acceleration data display a potentially critical trend. A positive outcome should be obtained from the analysis to continue the elaboration process.

However, in this stage, the automatic software performs a parallel analysis on an expanded dataset, which include the present value and a set of four acceleration data previously calculated. Level 1 is reached if the algorithm successfully identifies a continuous positive acceleration trend, represented by five consecutive acceleration values in the elaborated dataset. As can be noted, the condition needed to achieve this level depends only on the acceleration trend, and does not take into account other parameters or models. Therefore, the only information resulting from this step is a generic indication that the monitored site is currently displaying some type of activity, in contrast with a more stable behaviour (i.e., the devices are not detecting any movement).

Taking into account all considerations previously presented, if no higher levels are achieved in the analysis, a Level 1 should never be considered as an actual alert and should instead be seen simply as an "activity note" from the monitored site.

Level 2

Following the determination of an accelerating trend by the OOA identification algorithm, the process verifies if further points should be taken into account for the analysis by following the procedure described in Figure 41. In case of a positive result, the algorithm returns a set of values for the three parameters controlling the classification system, referred to the dataset identified by the software.

The conditions associated with the achievement of Level 2 are strictly related to the minimum requirements to effectively activate the classification algorithm. In particular, it is reached with a single dataset of at least 5 monitoring points, featuring a value of the determination coefficient equal or higher than 0.85. For this reason, this level usually corresponds to temporary acceleration events, which do not pose any particular risk. However, sometimes it could be a preliminary indication of a more serious event that could potentially evolve over time, reaching higher levels in the classification system during subsequent elaborations.

Level 3

In order to verify the achievement of higher levels, the analysis takes into account the three controlling parameters and checks if one of them overcomes stricter thresholds compared to those previously imposed for Level 2. In particular, this approach generates a total of three different configurations leading to the achievement of Level 3, depending on the parameter that is overcoming the corresponding reference value:

- C1 → a minimum of 2 sensors are activating the IVM procedure at the same time. This condition is intended to represent a situation where the ongoing event is no more localized on a certain depth, but it is detected in different portions of the landslide simultaneously and, therefore, involves a large volume of material.
- C2 → the single dataset defined by the algorithm is composed of at least 6 monitoring points. In this case, the condition refers to a dataset displaying a more consistent accelerating trend, which could be an indication of a more severe event.
- C3 → The linear interpolation performed by the IVM application features a determination coefficient $R^2 \geq 0.92$. This condition corresponds to a more reliable forecasting analysis and, therefore, indicates a trend which is closer to the theoretical pattern represented by a tertiary creep curve.

In the classification structure, the achievement of Level 3 usually implies that the monitored element is showing some kind of activity, which however is not already well defined in terms of effective hazard. Upon receiving the notification of a Level 3 elaboration, the responsible of the monitoring activity should check the available data in order to assess the landslide current behaviour, and keep following the updates regarding the evolution of the displacements experienced by the slope.

Level 4

The same approach adopted for the definition of Level 3 is followed to determine the conditions needed to achieve the following level. In particular, the assessment of Level 4 relies on the simultaneous fulfilment of two conditions among those previously described for Level 3. This concept leads to the definition of three new configurations, depending on the two conditions fulfilled at the same time:

- C1+C2 → the algorithm identifies two different sensors activating the failure forecasting routine, and one of the corresponding datasets features 6 monitoring points.
- C1+C3 → the elaboration returns two positive IVM applications for two different datasets, with a determination coefficient equal or higher than 0.92 for one of the forecasting analyses.
- C2+C3 → the result obtained from the procedure generates a single IVM application on a dataset composed of 6 monitoring points, and featuring a determination coefficient $R^2 \geq 0.92$.
- Additionally, Level 4 is achieved if the automatic elaboration defines 3 datasets activating the IVM analysis at the same time. In this case, conditions previously defined for the other two parameters are still valid, i.e., a minimum of 5 monitoring points and a determination coefficient of at least 0.85.

All these conditions are intended to reflect a situation where the monitored phenomenon is showing several different signs of unusual activity at the same time. Therefore, Level 4 is generally observed in correspondence of substantial movements recorded by monitoring tools installed on site, and should be considered as a sort of pre-alert condition. In fact, even if the

detected event is not immediately leading to a critical state, it still represents a situation which should be investigated and kept under close observation.

Level 5

Level 5 is the highest level achievable by the classification algorithm, and represents a situation where information provided by the monitoring instrumentation highlight an unstable condition of the monitored slope, characterized by an extremely active phenomenon. For this reason, Level 5 corresponds to an actual alert condition and should lead to the activation of predefined safety measures according to the specific case study, as well as further analyses and investigations to verify the evolution over time of the ongoing event in order to identify further signals of potential instabilities.

For what concern the conditions implemented in the algorithm, Level 5 is reached when all configurations described for previous levels are verified at the same time. Therefore, the last level corresponds to an analysis featuring at least two sensors activating the IVM elaboration, with 6 or more monitoring points and $R^2 \geq 0.92$, indicating that the activity detected on the monitored site is showing consistent signals of instability.

5.2. Case studies

As previously observed, the classification algorithm design approach revolves around the necessity to integrate the procedure in an automatic routine for monitoring data elaboration. The present version of the model was included in the software designed for the analysis of displacement data recorded by MUMS-based automatic inclinometers since October 2019. Starting from this date, the algorithm has been continuously applied to 36 monitoring tools installed in several different sites of interest, for a total number of 1250 sensors elaborated by the automatic software. By considering the sampling frequency of each device involved in the monitoring process, varying between 4 and 24 recordings per day depending on the specific case study, it results that the algorithm elaborates roughly 23'000 new datasets every single day in order to identify potentially critical trends, and consequently provide an alert level according to the parameters previously defined.

Table 4. Alert level reached by each classification analysis performed by the algorithm

Alert Level [-]	Number of activations [-]	Percentage [%]
Level 2	66	61%
Level 3	25	23%
Level 4	15	14%
Level 5	2	2%

During this time period, a total number of 676 datasets activated the classification algorithm, which in turn led to the definition of 108 different events (Table 4). It should also be noted that the automatic software generated 285 analyses that returned a time-of-failure forecasting located in the past and were consequently discarded according to the "no-alarm" definition previously discussed.

It is possible to observe that over half of the recorded activations (namely, the 61% of the total amount) stopped at Level 2. The number of Level 3 and Level 4 occurrences are sensibly lower, respectively 23% and 14%, while only two Level 5 activations were obtained throughout the time period considered for this study. Since this represents the higher level achievable by the analysis, and corresponds to a particularly severe condition of the monitored element, it is indeed positive that the automatic software returned such a small number of Level 5 occurrences. Additionally, as emerged by further analyses performed on the two activations in question, in both cases the acceleration trend detected by the algorithm was generated just some days after the installation of the monitoring instrumentation. This is a particularly important information, since the behaviour that follows the installation of an inclinometer (traditional or automatic alike) include a stabilization period, which heavily influences the displacement values recorded by the device (Figure 42).

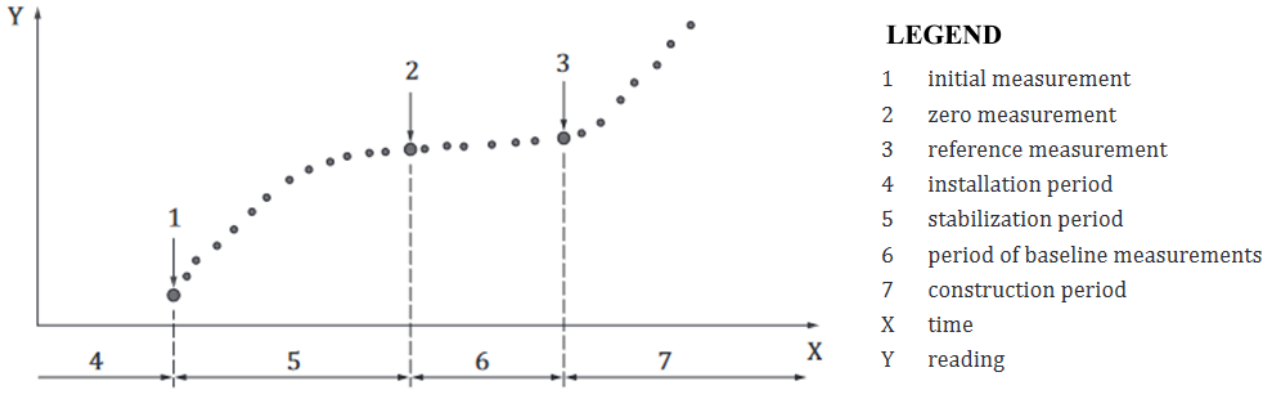

Figure 42. Definition of distinct measuring points after the installation of the monitoring device (modified from ISO 18674-1:2015)

During this specific time interval, monitoring data could not necessarily represent the actual slope deformations, and are usually attributed to adjustments and settling of the inclinometer. Therefore, even if the algorithm returned a high alert level, no action was needed for these specific situations. This is yet another evidence of the role of an expert technician in the monitoring data elaboration process, which should not be appointed exclusively to automatic procedures without any supervision.

The following sections report a series of examples regarding the classification process that followed the identification of an accelerating trend, focusing on the features presented by each dataset and discussing the analysis outcome. Notably, one of the examples included in this chapters refers to a back-analysis performed on displacement data recorded by MUMS instrumentation during an event that effectively led to a collapse of the monitored slope.

5.2.1. Monitored site #1: Landslide in Northern Italy

The first monitoring site is located in a Northern Italy region, characterized by the presence of a construction site of a new transport infrastructure crossing a mountainous and hilly area. In order to control the interaction between the structure and the surrounding environment, the site was equipped with a monitoring system based on MUMS instrumentation. In particular, a

total of 4 Vertical Arrays was installed in different parts of the area of interest to control both displacements and water level variations. Each single Array was produced with specific features, integrating a different number and typology of sensors according to the monitoring plan. Table 5 reports the features of each device installed on site.

Table 5. MUMS-based devices installed on site for case study #1

Array ID [-]	Installation date [gg/mm/yyyy]	Array Typology [-]	Sensors number and typology [-]	Array Length [m]
DT0099	06/03/2019	Vertical Array	20x Tilt Link HR 3D V 2x Piezo Link	20.00
DT0100	05/12/2018	Vertical Array	20x Tilt Link HR 3D V 2x Piezo Link 1x Baro Link	20.00
DT0101	06/03/2019	Vertical Array	20x Tilt Link HR 3D V 1x Piezo Link 1x Baro Link	20.00
DT0102	06/03/2019	Vertical Array	20x Tilt Link HR 3D V 1x Piezo Link	20.00

After their installation and the subsequent definition of the reference date, all Vertical Arrays have continued the monitoring activity to the present day, with a sampling frequency of 6 readings every day. Despite never reaching the highest level of the classification algorithm, the site generated some activations of the automatic procedure achieving lower alert levels. The following paragraphs presents two examples of these occurrences, both measured by Vertical Array DT0101, describing the displacement trend and the corresponding level achieved by the analysis.

Case study #1

The first example refers to a movement observed by the monitoring device in March 2020, when the instrumentation reported an increase of displacement measured by Tilt Link 31, located at 4 m of depth. After the activation of the OOA identification algorithm, which identified the beginning of the accelerating trend on 5 March 2020 11:27 AM, the automatic software processed the selected dataset in order to perform the failure forecasting analysis and evaluate the parameters needed to classify the event. The outcome of this analysis showed that only a single node of the Array (i.e., Tilt Link 31) detected a trend compatible with the requirements imposed to perform the classification analysis. Moreover, the corresponding displacement dataset consisted of 5 monitoring points. The failure forecasting analysis returned a determination coefficient equal to 0.9419, indicating a very good correspondence between inverse of velocity values and the line interpolating the monitoring data. Consequently, according to the value of the three parameters, the automatic software classified this event as a Level 3 (configuration C3).

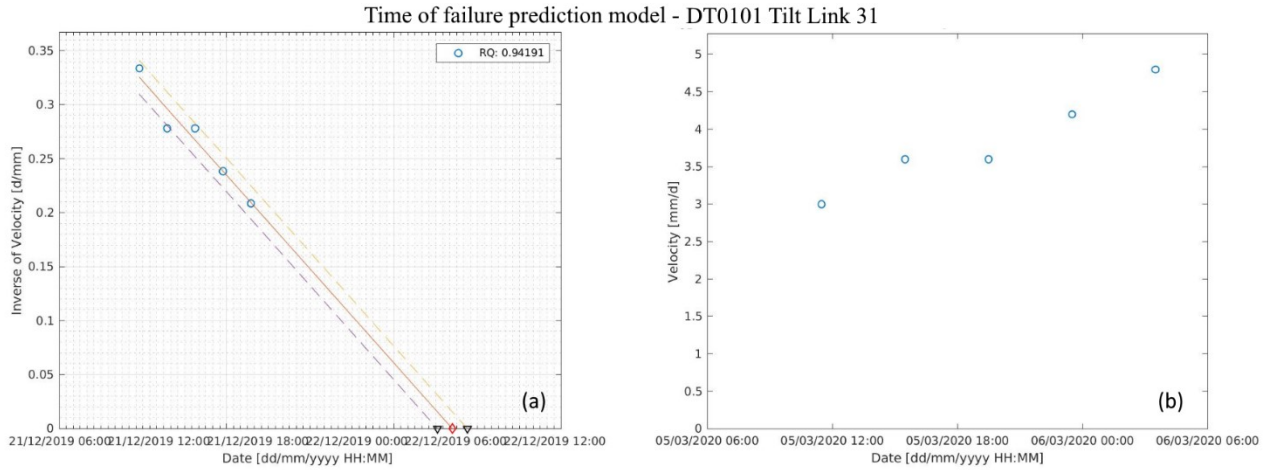

Figure 43. (a) Inverse-Velocity vs Time, and (b) Velocity vs Time calculated from displacement data recorded by DT0101 node 31, with acceleration date on 05 March 2020 11:27 AM

By observing the displacement values recorded by Tilt Link 31 over time (Figure 44), it is possible to notice how the trend actually displays a pattern comparable to a non-linear, increasing curve. However, both displacement and velocity data did not show particularly alarming values, and the following monitoring recordings evidenced a stable condition. Therefore, while the event caused an unusual movement with a total displacement of roughly 6 mm, it did not generate any significant instability, and no alarm was issued.

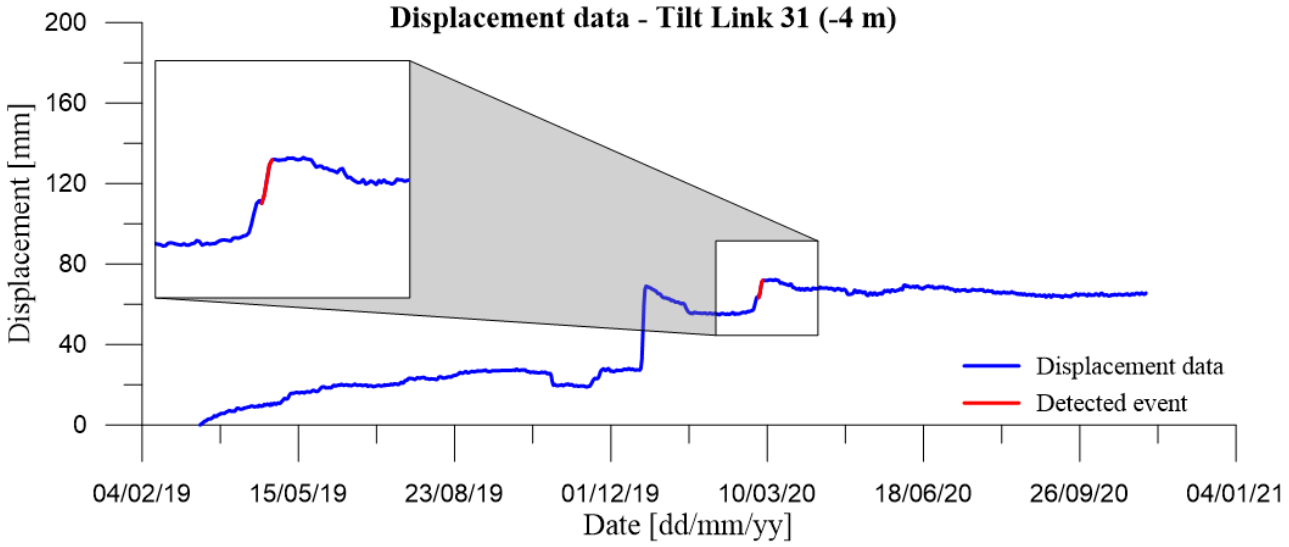

Figure 44. Displacement measured over time by Tilt Link 31, with a detail regarding the event of March 2020 detected by the automatic software

Case study #2

The second example regarding this specific site involves another event, detected once again by Vertical Array DT0101 in December 2019. The instrumentation measured a steep increase of slope displacements on Tilt Links 31 and 35, located respectively 4 and 2 meters below the ground level. In both cases, the automatic software processed the datasets to identify the beginning of the acceleration phase, locating the OOA date on 21 December 2019 10:05 AM, and proceeded to the level evaluation. In this case, since two datasets displayed an accelerating trend starting from the same date, the software performed two separate analyses to compute a

single classification level for the whole event. Monitoring data provided by Tilt Link 31 provided a fairly non-linear trend in the inverse-velocity vs time plot, with the failure forecasting process returning a determination coefficient $R^2 = 0.8777$ evaluated on a 5-point dataset. On the other hand, the application of the IVM algorithm on values recorded by Tilt Link 35 showed a result more consistent with the linear interpolation, generating a determination coefficient of 0.9375. As well as for the other Link, this analysis was also performed on a dataset composed of 5 monitoring points. At the end of the elaboration process, based on the parameters during the analysis, the automatic software classified the event as a Level 4 (specifically a C1+C3 configuration).

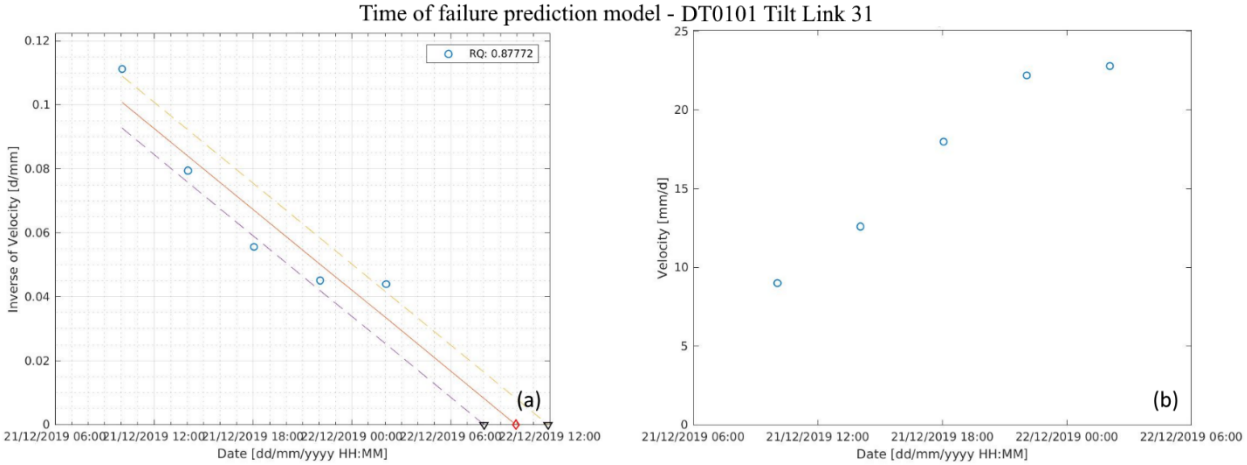

Figure 45. (a) Inverse-Velocity vs Time, and (b) Velocity vs Time calculated from displacement data recorded by DT0101 node 31, with acceleration date on 21 December 2019 10:05 AM

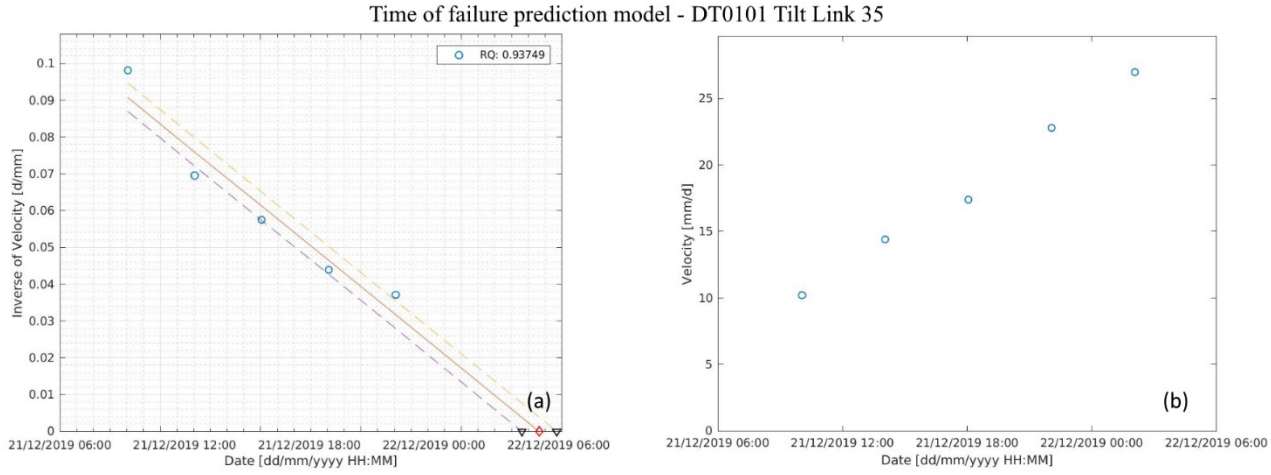

Figure 46. (a) Inverse-Velocity vs Time, and (b) Velocity vs Time calculated from displacement data recorded by DT0101 node 35, with acceleration date on 21 December 2019 10:05 AM

Compared to the example previously reported, the higher level achieved by this event reflects a more serious situation, where the movement identified by the monitoring devices involves different parts of the landslide. Given the fact the two nodes interested by this phenomenon are only 2 meters apart, and considering the similarities between the monitoring data (Figure 47 and Figure 48), it could be assumed that the displacements measured by the two sensors are strictly related. Additionally, by observing the slope displacement vs time plots, it is

noticeable how the magnitude if this event is higher compared to the previous example. In fact, the total displacement generated by the event resulted to be 23.4 mm and 25.6 mm for Tilt Link 31 and Tilt Link 35, respectively. Even if this specific parameter is not involved in the level assessment procedure, it is safe to assume that it played an indirect role in the achievement of this alert level.

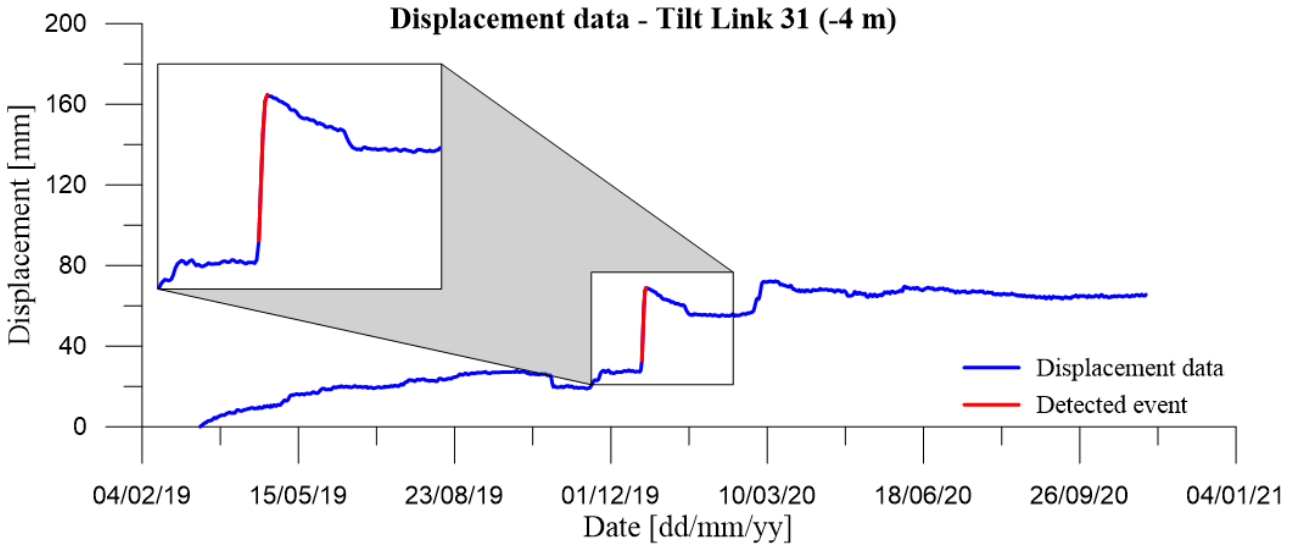

Figure 47. Displacement measured over time by Tilt Link 31, with a detail regarding the event of December 2019 detected by the automatic software

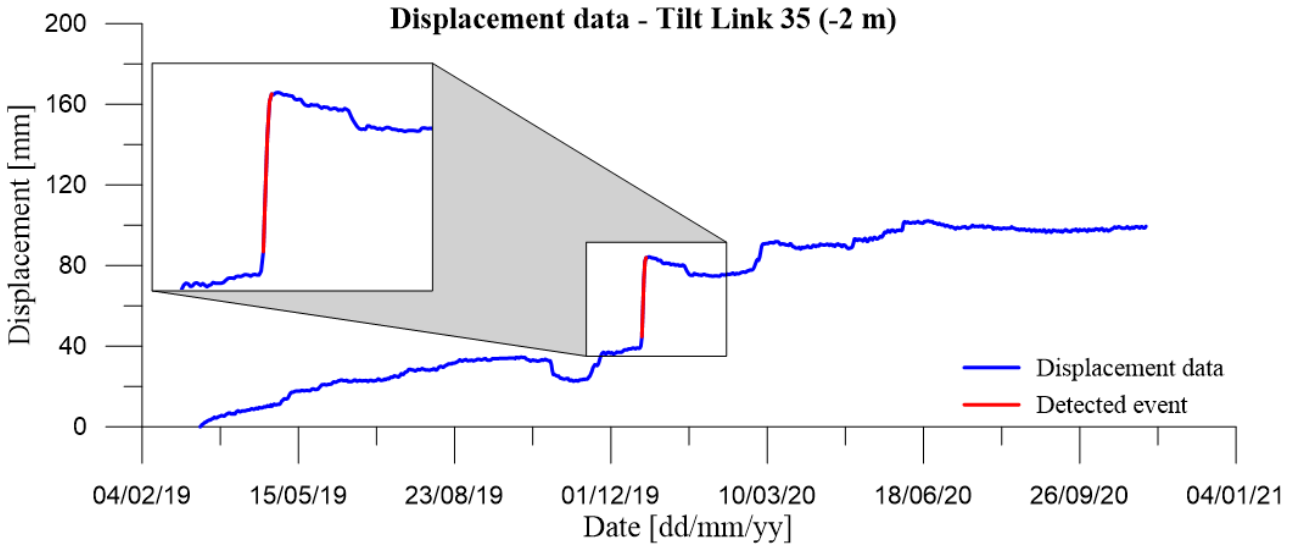

Figure 48. Displacement measured over time by Tilt Link 35, with a detail regarding the event of December 2019 detected by the automatic software

Upon receiving the notification of the achievement of this level, surveillance of monitoring data was increased to identify further signs of potential instabilities. Moreover, data collected by the piezometer showed a slight and sudden variation in the water table level, evidencing a possible correlation with the movement detected by the Array. Following recording evidenced once again the reaching of a stable conditions, with slope displacements following a horizontal trend. The integration of a redundant sensor allowed also to perform a check on the measured movements validity, which were confirmed by the second sensor placed in each Tilt Link

evidencing the same trend both during and after the event. Considering all these information, no further measures were taken, and subsequent on-site inspections performed for maintenance reasons did not evidence any relevant damages on the slope surface.

5.2.2. Monitored site #2: Landslide in Central Italy

The second monitored site regards the control of a landslide located near a state road connecting the Tyrrhenian and Adriatic Seas. Specifically, the area of interest involves a construction site close to the border between two Italian regions, namely Molise and Abruzzo, where several instability phenomena slowed down the construction works over the years (Segalini et al., 2019a). For these reasons, starting from 2016, the site has been equipped with a MUMS-based monitoring system, which was improved during the years with the addition of new Arrays as the monitoring activity progressed. Table 6 summarizes the instrumentation present on site, which was installed in addition to other pre-existing traditional monitoring tools.

Table 6. MUMS-based devices installed on site for case study #2 (modified from Segalini et al., 2019a)

ID [-]	Installation date [gg/mm/yyyy]	Array Typology [-]	Sensors number and typology [-]	Array Length [m]
DT0014	18/11/2016	Vertical Array	50x Tilt Link HR 3D V	35.00
DT0065	07/09/2017	Vertical Array	48x Tilt Link HR 3D V	35.00
DT0094	19/09/2018	Vertical Array	34x Tilt Link HR 3D V	69.00
DT0095	18/09/2018	Vertical Array	47x Tilt Link HR 3D V	95.00
DT0096	20/09/2018	Vertical Array	55x Tilt Link HR 3D V	111.00
DT0097	19/09/2018	Vertical Array	33x Tilt Link HR 3D V	66.00
DT0119	11/11/2020	Vertical Array	50x Tilt Link HR 3D V	100.00
DT0120	14/11/2020	Vertical Array	50x Tilt Link HR 3D V	100.00
DT0121	13/11/2020	Vertical Array	50x Tilt Link HR 3D V	100.00

Case study #1

The first example regarding this site involves the Vertical Array DT0065, which was installed after the damaging experienced by DT0014 (the corresponding event will be discussed in the paragraph regarding Case study #2). The Array included a total of 48 Tilt Link HR 3D V and was set to acquire a new reading every hour. For the first two years of monitoring activity, the instrumentation showed a typical secondary creep pattern, with a constant

displacement rate over time. However, in November 2019, a sudden increase of slope displacements activated the algorithm, leading to the identification of a series of datasets to be processed and analysed. The outcome of the automatic elaboration derived from the analysis of a total of four datasets, and defined the beginning of the acceleration phase on 15 November 2019 12:17 PM. As described in the previous section, the fact that more than three IVM analyses were performed on different monitoring dataset is enough to classify this event as a Level 4. However, the parameters evaluation for each forecasting analysis is necessary to verify the achievement of a higher level, and to acquire useful information for a correct monitoring data interpretation.

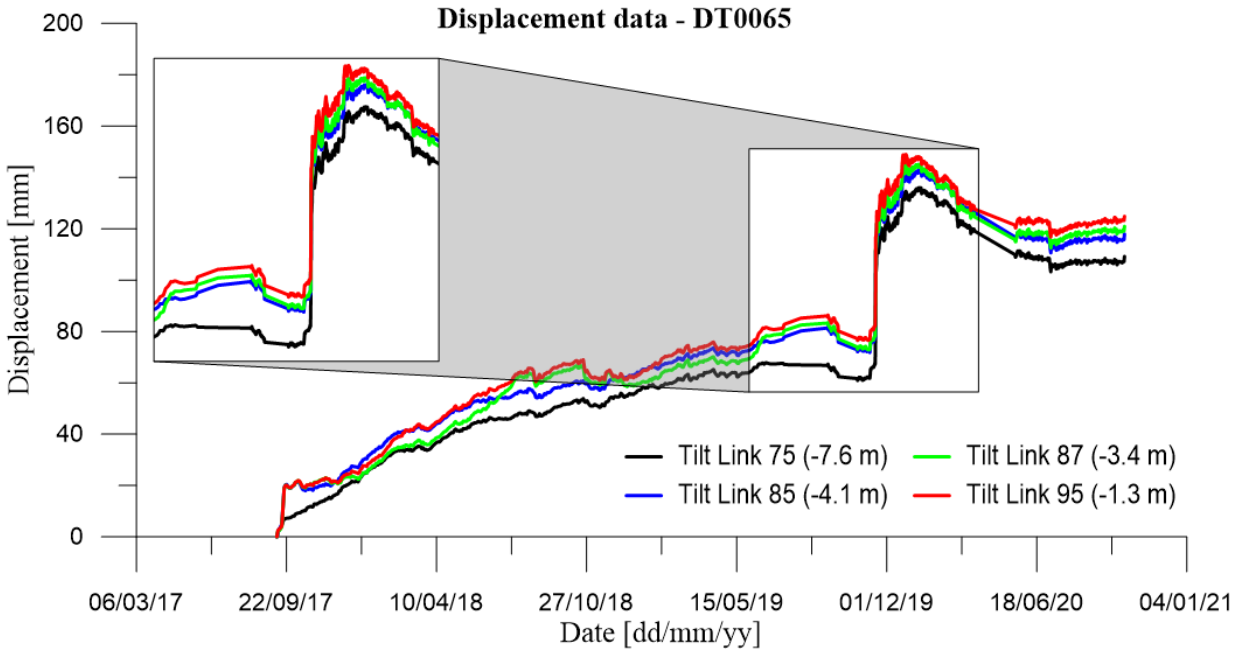

Figure 49. Cumulative displacements measured over time by Vertical Array DT0065 (Tilt Link 75, 85, 87, and 95) with a detail regarding the event of November 2019 detected by the automatic software

By looking at the displacements vs time trend recorded by each sensor (Figure 49), it is possible to derive the following observations:

- The four nodes identified by the algorithm are Tilt Links 75, 85, 87, and 93, respectively located 7.6, 4.1, 3.4, and 1.3 metres below the ground level. Among the corresponding datasets, only the one recorded by node 75 included 5 monitoring points, while each one of the others comprised 6 data. Interestingly, this feature confirms the Level 4 evaluation by fulfilling another configuration, namely C1+C2.
- By observing the displacement and velocity plots recorded by the instrumentation, it is possible to notice how the datasets are extremely similar, even if they are not consecutive in the Array scheme. Since these displacements are cumulative, and derive from local displacements recorded by each single sensor, it is plausible to assume that a localized displacement taking place at a certain depth was propagated along the vertical direction, activating several nodes displaying the same trend. The non-activation of intermediate

Links could be attributed to small differences induced by the local displacement contribution of each sensor.

- As a consequence, the same similarities were observed in the inverse-velocity vs time trends generated by the forecasting analyses. In fact, all four datasets display the same behaviour, characterized by a pronounced non-linear concave trend, usually associated with stabilizing phenomena. Moreover, the corresponding determination coefficient confirmed this observation, presenting values ranging from 0.8693 to 0.8556 for all the considered datasets. In accordance with these evaluations, following this event, monitoring data showed once again a stable behaviour that persisted for the following months.

Case study #2

The second example concerns an event recorded in March 2017, when the Vertical Array DT0014 detected a series of displacement variations involving the first 6 meters of soil. In particular, starting from the end of January 2017, the device showed clear signs of an instability phenomenon taking place on the monitored site, which lead to the gradual damaging of the Array. This resulted in the breaking of the lower part of the instrumentation on 27 February, while the Links placed above 6 metres of depth continued to provide new measures and managed to record the major event that took place on 8 March. Ultimately, the Array functionality was irreversibly compromised, and the monitoring operativity of DT0014 ended on 13 March 2017 due to excessive deformations (Figure 50). At the time of this writing, this is the only event recorded by MUMS instrumentation that ultimately led to the collapse of the monitored element. Main sources for information regarding this case study, as well as for monitoring data discussed below, are Segalini et al. (2019a), and Carri (2019).

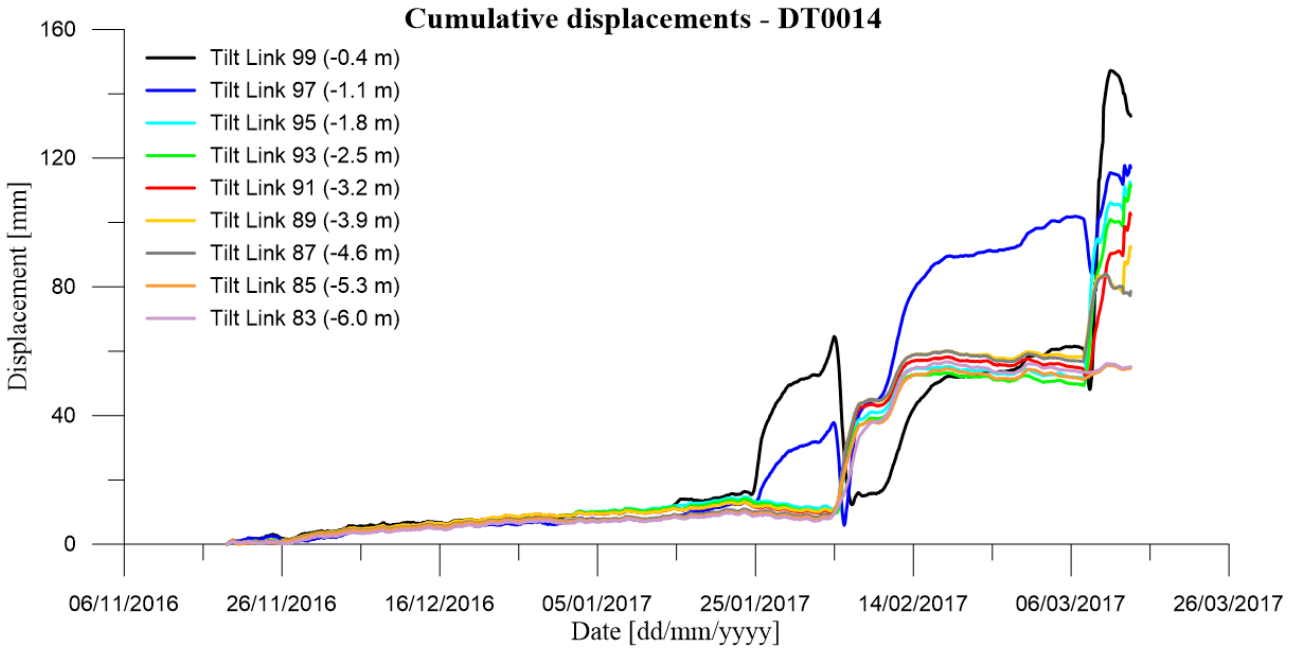

Figure 50. Cumulative displacements recorded by Vertical Array DT0014 down to 6 meters of depth (Tilt Links from 83 to 99) during the entire monitoring period

Figure 51. Installation site of Vertical Array DT0014

At the time the landslide took place, the classification system presented in this thesis was not yet active, and monitoring data were elaborated with an automatic software that included only a previous version of the OOA identification algorithm. Therefore, the discussion regarding the alert level reached by the event is based on a back-analysis performed on available datasets, simulating a real time acquisition and elaboration procedure. However, it is worth noting that the alert procedure active at the time of the event was still able to recognize the critical evolution of the landslide, sending warning messages to authorities responsible of the monitoring activity.

Table 7. Information regarding the different datasets that activated the automatic algorithm, including the estimated OOA, dataset dimension, determination coefficient value, and alert level reached by the analysis

Node ID [-]	**Depth** [m b.g.l.]	**Onset-of-acceleration** [dd/mm/yyyy HH:MM]	**Dataset dimension** [-]	**Determination coefficient R^2** [-]	**Alert Level** [-]
93	2.5	07/03/2017 14:26	5	0.8980	3
95	1.8	07/03/2017 14:26	5	0.8889	
93	2.5	08/03/2017 02:28	7	0.8515	5
95	1.8	08/03/2017 02:28	7	0.9578	
99	0.4	08/03/2017 17:31	6	0.9674	4
91	3.2	09/03/2017 23:28	5	0.9081	2
89	3.9	13/03/2017 06:54	5	0.9395	3

Table 7 summarizes the DT0014 Tilt Links that recorded a dataset activating the algorithm, together with the corresponding onset-of-acceleration evaluated by the automatic software, and the parameters deriving from the IVM application.

The first event identified by the algorithm dates to 7 March 2017, when the automatic software returned a positive result for two Tilt Links, namely 93 and 95, which provided 5-point datasets (Figure 52 and Figure 53, respectively) with an estimated onset of acceleration on the same day at 14:26. These features, together with a determination coefficient lower than 0.92, lead to the achievement of Level 3 due to the presence of two different datasets.

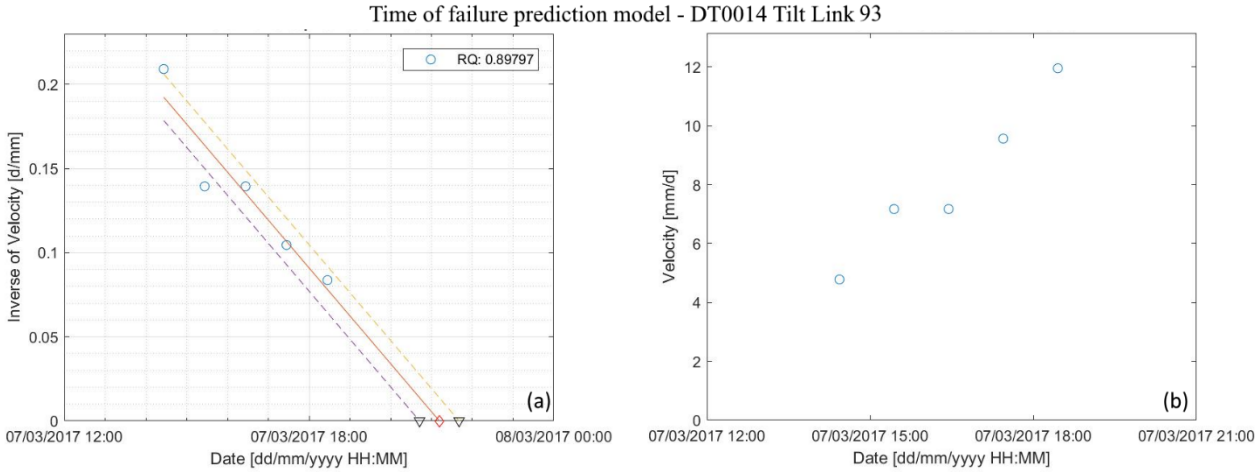

Figure 52. (a) Inverse-Velocity vs Time, and (b) Velocity vs Time calculated from displacement data recorded by DT0014 node 93, with acceleration date on 07 March 2017 14:26

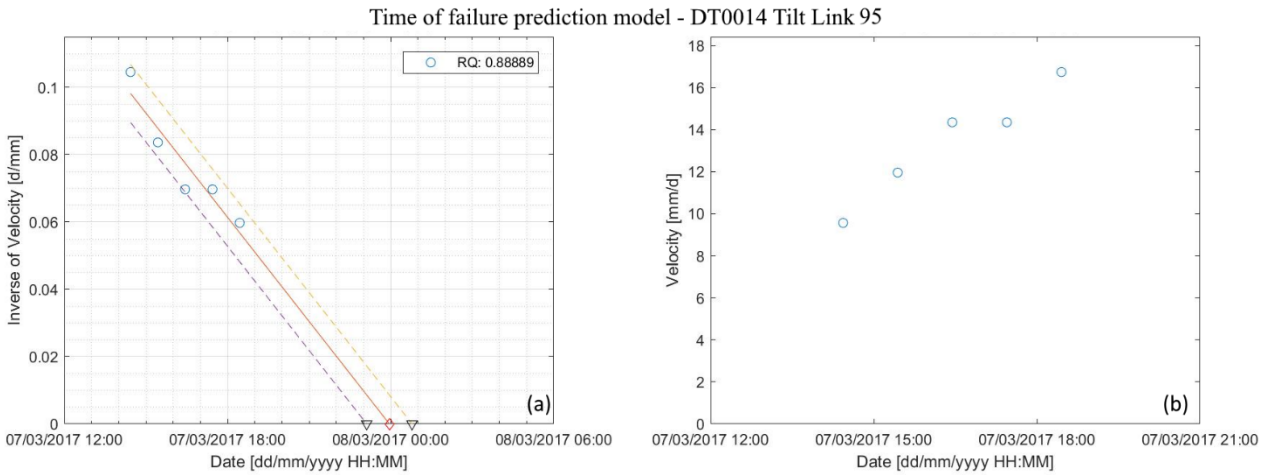

Figure 53. (a) Inverse-Velocity vs Time, and (b) Velocity vs Time calculated from displacement data recorded by DT0014 node 95, with acceleration date on 07 March 2017 14:26

The following activation produced by the software is the most relevant one, since it correctly identified the major event that involved the monitored site and severely damaged the instrumentation. In particular, the elaboration outcomes provided two datasets displaying an accelerating trend, each of them including 7 monitoring values and presenting the same onset of acceleration on 08 March 2017 02:28. As can be noted from the parameters reported in Table 7, there is a relevant difference between the determination coefficient values deriving from the IVM analyses. In particular, the dataset referring to Tilt Link 93 returned $R^2 = 0.8515$ (Figure

54), while the forecasting model applied to Tilt Link 95 achieved a much higher value at 0.9578 (Figure 55). The reason for this behaviour can be identified in the first dataset, which evidences a decrease in displacement rate on the sixth point before showing another increase in the following monitoring data. This occurrence is a good example of the importance of the introduction of a tolerance factor to include values not following a clear accelerating trend, as explained in the previous chapter. In fact, should a single decelerating point be considered enough to stop the dataset definition process, it could lead to discard subsequent monitoring values following the same accelerating trend. On the other hand, displacements recorded by Tilt Link 95 follow a more consistent pattern, thus generating a higher determination coefficient during the inverse-of-velocity vs time interpolation.

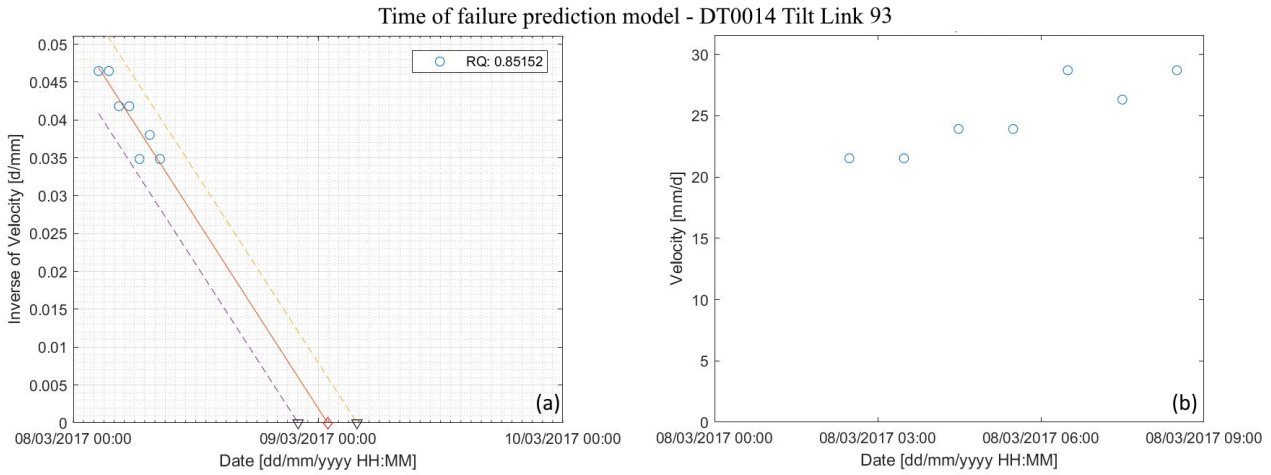

Figure 54. (a) Inverse-Velocity vs Time, and (b) Velocity vs Time calculated from displacement data recorded by DT0014 node 93, with acceleration date on 08 March 2017 02:28

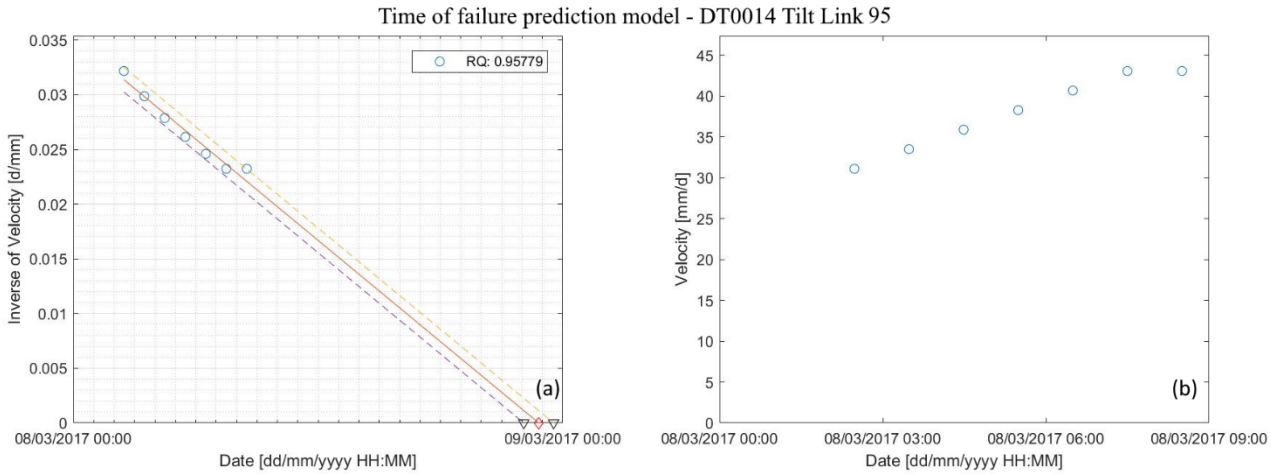

Figure 55. (a) Inverse-Velocity vs Time, and (b) Velocity vs Time calculated from displacement data recorded by DT0014 node 95, with acceleration date on 08 March 2017 02:28

It is also noteworthy that the Level 5 alert involves the very same nodes, namely Tilt Links 93 and 95, that achieved Level 3 less than 24 hours before. Arguably, this occurrence could represent a situation where the main event was previously identified and achieved a lower level, and then evolved to a critical condition that was identified in the subsequent elaboration. While the software does not include a specific procedure to evaluate the presence of relationships

between different alert messages, any technician studying the elaborated data should be able to identify this peculiarity, which further validates the authenticity of the alert issued.

Shortly after the generation of this alert, another node of the Array caused the activation of the algorithm, which identified a new set of monitoring data displaying an accelerating trend. Specifically, Tilt Link 99 (the closest node to the ground surface, located at a depth of 0.4 metres) recorded an increase of displacement rates starting from 08 March 2017 17:31, resulting in a 6-point dataset featuring a determination coefficient of 0.9674 (Figure 56). In this case, the presence of a single dataset leads to the achievement of Level 4. Taking into considerations the behaviour previously highlighted by the monitoring data, this could be interpreted as further confirmation that a critical event is taking place.

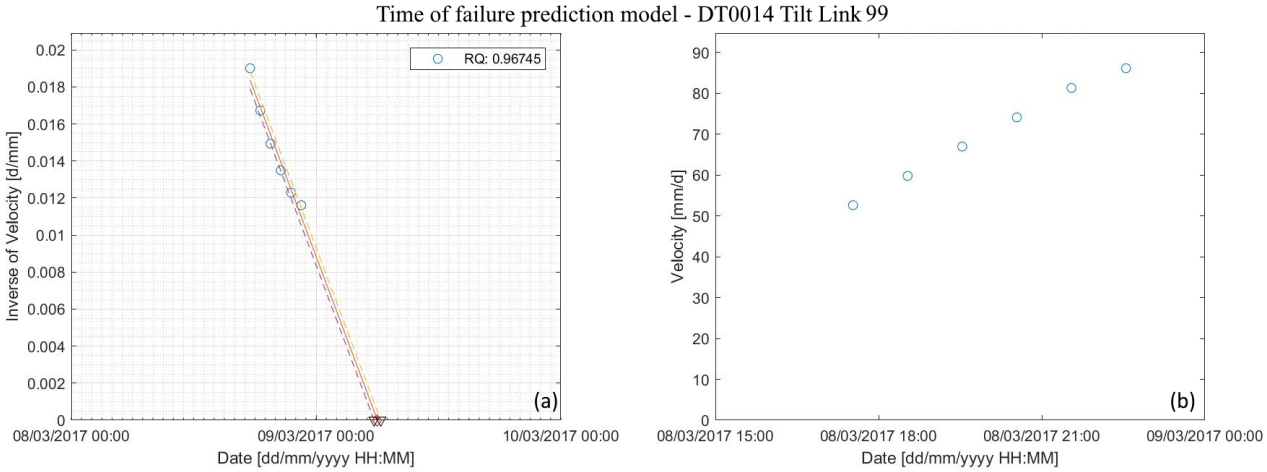

Figure 56. (a) Inverse-Velocity vs Time, and (b) Velocity vs Time calculated from displacement data recorded by DT0014 node 99, with acceleration date on 08 March 2017 17:31

The Vertical Array managed to continue the monitoring activity for five days, and in this time interval the automatic software identified two more datasets activating the OOA algorithm. Both these occurrences involved a 5-point dataset, with Tilt Link 91 achieving Level 2 on March 9th, and Tilt Link 89 (Figure 57) reaching Level 3 on March 13th thanks to a higher R^2 value (0.9081 and 0.9395 respectively). These events could be seen as further indication of a still active site, even if the achievement of lower level could be a sign that the slope is progressing towards a more stable configuration after the major displacements measured in previous days.

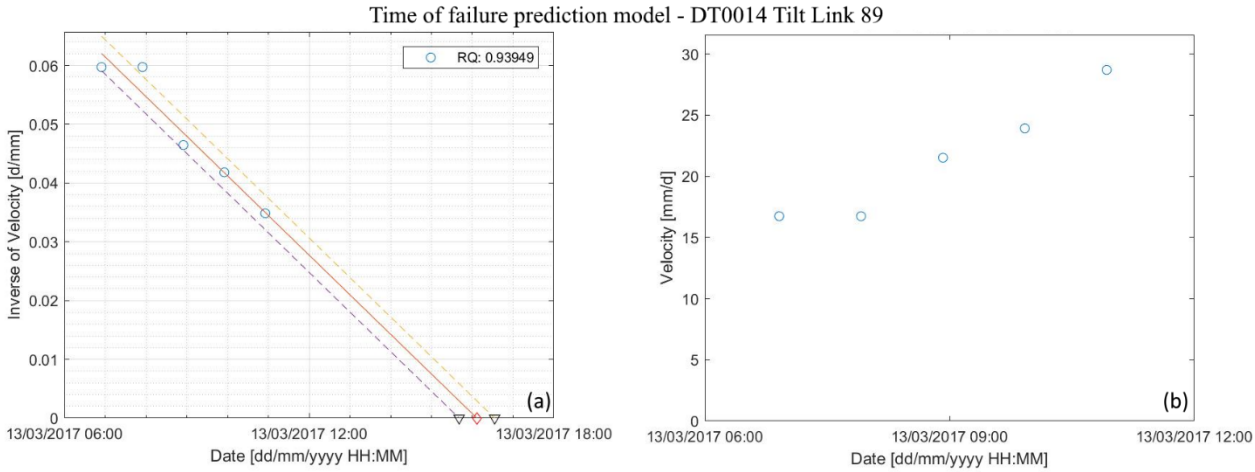

Figure 57. (a) Inverse-Velocity vs Time, and (b) Velocity vs Time calculated from displacement data recorded by DT0014 node 89, with acceleration date on 13 March 2017 06:54

Figure 58. Area surrounding Vertical Array DT0014 as seen during the on-site inspection (Segalini et al., 2019a)

Ultimately, the deformations irreversibly impaired the functionality of Vertical Array DT0014, which recorded the last monitoring data on 13 March 2017 13:56. Following these events, an on-site investigation was carried out to check the monitored area conditions. The inspection confirmed the landslide occurrence, identifying a complex dynamic that included several failures and scarps, settlements, and displacements in the area surrounding the Vertical Array (Figure 58). Moreover, an accurate check of the condition of the monitoring devices reported that all the traditional inclinometer casings were inaccessible due to excessive soil deformations. MUMS devices were the only instrumentation able to identify the landslide and describe its evolution over time, despite being damaged in the process.

Chapter 6. Alert threshold definition

Taking into account the several features that contribute to the correct operation of an Early Warning System, the processes intended to define specific thresholds for the monitored parameters are among the most difficult to tackle. Because of their own nature, these values should be determined with the intent to represent a critical event in the context of the studied phenomenon, in order to be able to disseminate proper warnings if such an occurrence is observed. In particular, for what concern the landslide monitoring framework, critical events are usually associated with slope collapses generated by a situation of irreversible instability of the monitored element. This could be considered as a one-time occurrence, since the effects deriving from a slope failure would have a deep influence on the morphology of the interested area, radically modifying the overall conditions that previously characterized the case study.

As discussed in the previous chapters, the site-specific approach usually followed for the thresholds assessment involves the creation of a numerical model of the landslide, in order to simulate the phenomenon evolution over time and to identify specific values where the monitored element starts the transition towards its failure, or the application of empirical processes. Alternatively, methods based on failure forecasting procedures or deriving from a robust observational basis are considered to be more flexible and can be integrated in different monitoring contexts with good results. Following this line of thought, two new procedures for the assessment of alert thresholds for landslide EWS are described below. The main feature of these methodologies is the overcoming of the site-specific approach, giving the possibility to apply the procedure to a wide range of different case studies.

6.1. Generalized criterion

The first methodology here presented was conceived starting from the idea of identifying a common behaviour in landslides displaying different features in terms of material involved, dimension of the unstable element, failure mechanism, etc. (Segalini et al., 2018). The criterion development followed a series of steps described below, and summarized in Figure 59:

- Collection of monitoring information from historical landslides: this step involved the creation of a database including 26 different landslides reported in scientific literature. For each case study, a dataset consisting of displacement and/or velocity values recorded by different monitoring systems was collected. Case studies included in the database presented relevant differences in terms of volume, failure mechanism, triggering factors, monitoring typology and duration.
- Monitoring values extraction: this passage was performed through the application of a digitizing software on the available plots, in order to generate a series of numerical coordinates representing the displacement vs time trend referred to each case study. Since the recorded data are displayed in different units depending on the specific monitoring approach, all the datasets were converted into a common unit of measurement (mm/d) to be able to compare different cases.

- Failure forecasting: this stage involves the application of the Inverse Velocity Method to evaluate the time-of-failure t_f for each landslide, under the hypothesis of linear relationship between inverse of velocity and time (as discussed in Chapter 2.3). Therefore, the date of collapse is estimated by performing a linear regression in $1/v - t$ plot, corresponding to a constant value of the α parameter in the Fukuzono equation, equal to 2.0.

- Model calibration: the Inverse Velocity Method depends on two main empirical parameters, named A and α. The goal of this step is the calibration of these coefficients in order to improve the model ability to represent the analysed dataset. It is worth noting that this operation involves only the parameters calibration, while the time-of-failure value computed under the linear regression hypothesis is still considered valid. The process aims to minimize the Root Mean Square Error (RMSE) resulting from a comparison between data evaluated by the forecasting model, and recorded by monitoring system installed on-site.

- Velocity curve definition: Taking advantage of the previously calibrated A and α parameters, this step generates a velocity vs time curve for each single case study, representing theoretical behaviour of the landslide during the 30 days preceding the collapse. These curves are computed by exploiting the Fukuzono-Voight equation relating displacement velocity v_{FV} and time t:

$$v_{FV} = \left(A(\alpha - 1)(t_f - t)\right)^{\frac{1}{1-\alpha}} \quad \text{(XXV)}$$

  Each curve computed in this way must be considered site-specific, since the parameters derive from the monitoring data of each specific case study, and each landslide displayed unique displacement and velocity data.

- Normalization of velocity values: The last step of the procedure aims to normalize the velocity curve previously computed, in order to generate a new dimensionless velocity parameter. This would allow the comparison between monitoring data acquired from different case studies and processed with the proposed algorithm. In the following equation, $\mu_{v_{FN}}$ and $\sigma_{v_{FN}}$ are the mean value and standard deviation of v_{FV} values computed at the previous step, respectively.

$$v_n = \frac{v_{FV} - \mu_{v_{FN}}}{\sigma_{v_{FN}}} \quad \text{(XXVI)}$$

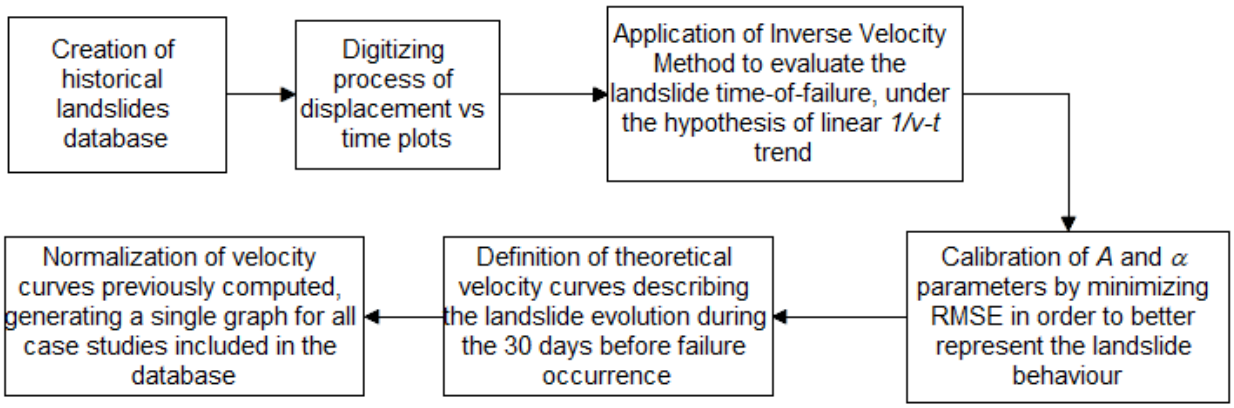

Figure 59. Flow chart summarizing procedure for the development of the generalized criterion (Valletta et al., 2020b)

The application of this process to each dataset available generated a series of dimensionless velocity curves, which can be represented in a single graph evidencing the presence of a common pattern followed by all case studies (Figure 60). One of the features emerging from the normalization process is the negligibility of the A parameter in the definition of the dimensionless velocity curves. This is a particularly interesting aspect, since this parameter can have a wide range of values, up to four orders of magnitude according to results in Segalini et al. (2018). Therefore, a certain degree of uncertainty in the model can be removed by removing this term. Because of this, each curve represented in a dimensionless-velocity versus time plot can be associated to the value of α derived from the calibration of the Fukuzono model. In particular, by taking as a reference the linear case featuring $\alpha = 2.0$, a value of $\alpha > 2.0$ are less concave since the flex point appears earlier, while $\alpha < 2.0$ involves a delayed increasing of normalized velocity.

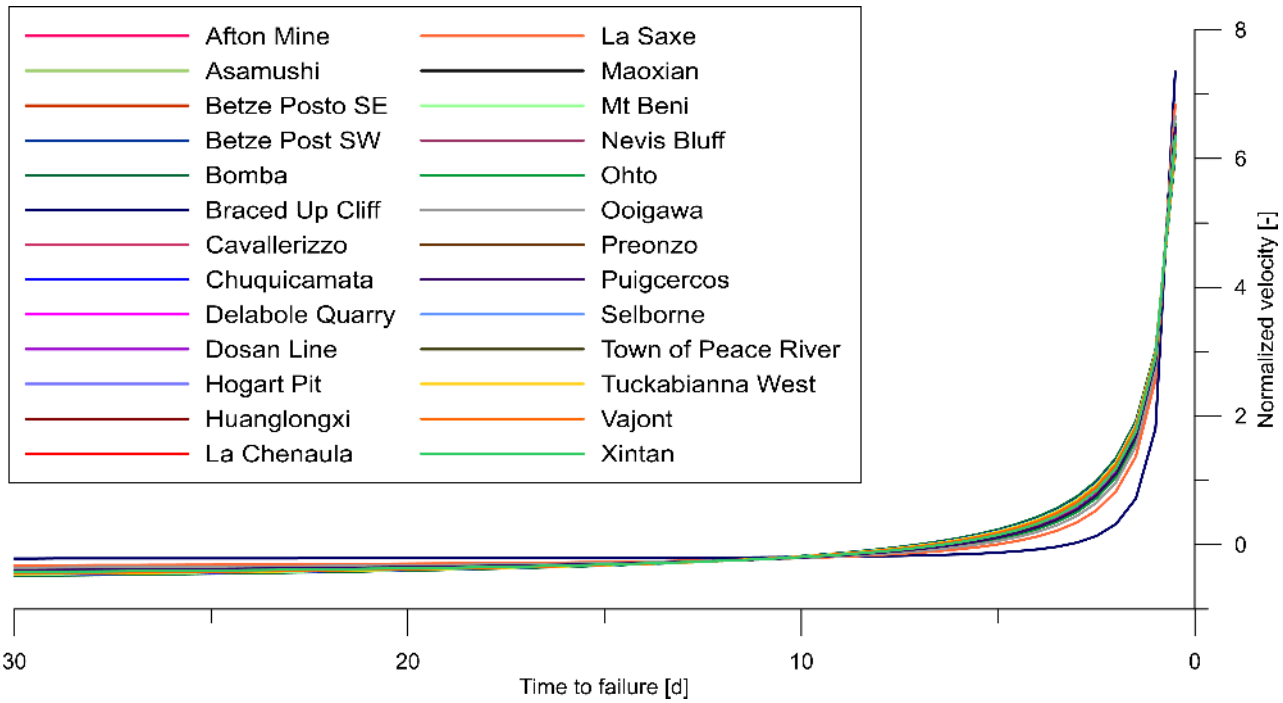

Figure 60. Dimensionless-velocity vs time plot, reporting all the different case studies included in the landslides database (Segalini et al., 2018)

Ultimately, the generalization procedure allowed to evidence a common trend for landslides featuring different attributes. For this reason, the proposed method could be applied to all those phenomena displaying a behaviour that satisfies the Inverse Velocity Method hypotheses, while also sharing some limitations of this method (e.g., difficulty to predict a fast-moving landslide collapse, or necessity to apply it on a tertiary creep phase dataset to obtain a reliable result).

The procedure followed to develop the generalized criterion involved the complete dataset available for each single landslide analysed. As a consequence, the approach previously described should not be considered as representative of a real-time case scenario, where monitoring data become available as the monitoring activity progresses over time. The following sections present a series of applications where real-time sampling and elaboration processes are simulated, in order to test the generalized criterion effectiveness in a real-like context where the dataset expands over time when new information is acquired. These case studies refer to historic landslides retrieved from scientific literature, due to the lack of suitable datasets from MUMS devices to test this specific methodology. However, it is worth noting that these particular landslides, analysed in Valletta et al. (2020b), were not included in the database at the time of its creation.

The progressive acquisition of monitoring data, intended to represent a real-time data acquisition and elaboration, was simulated according to the following procedure:

a) After the identification of the first point of the accelerating phase, the following three displacement data are taken into consideration to generate a 4-point dataset.

b) The Inverse Velocity Method is applied to the selected dataset under the hypothesis of linear $1 / v - t$ relationship, in order to evaluate the landslide time-of-failure t_f

c) Theoretical displacement velocity values are estimated according to the formulation proposed by Fukuzono (1985) and reported below, by using the A and α obtained from the application of IVM under the hypothesis of linearity in $1/v - t$ trend and the t_f calculated at the previous step.

$$\frac{1}{v} = \left(A(\alpha - 1)\left(t_f - t\right)\right)^{\frac{1}{1-\alpha}} \qquad \text{(XXVII)}$$

d) Model parameters A and α are calibrated by minimizing the RMSE value obtained from the comparison between monitoring data and theoretical values calculated in the previous phase.

e) The theoretical velocity curve for the specific case study is generated by implementing the parameters previously evaluated (time-of-failure t_f in step (b), A and α coefficients in step (d) into the Fukuzono-Voight formulation, Eq. XXV).

f) The last value of the dataset provided by the monitoring instrumentation is normalized by applying Eq. XXVI, where mean and standard deviation values derive from the velocity curve determined in the previous step. This gives the possibility to compare the

dimensionless velocity value with one of the theoretical curves generated by the generalized criterion, chosen on the basis of the α parameter obtained during the calibration procedure.

g) If a new monitoring data is available, it is added to the dataset and the procedure is repeated starting from step (b).

6.1.1. Case study #1: New Tredegar colliery

The first case study deals with an unstable slope near the New Tredegar colliery site, located in the Rhymney Valley in Caerphilly County Borough, South Wales. According to the information reported by several authors that studied the area, first evidences of the presence of ground displacements affecting the colliery emerged during the construction of a railway crossing the area in 1856 (Bentley and Siddle, 2000; Carey, 2011; Siddle et al., 2007). In March 1905, a large landslide triggered by extreme rainfall events damaged the railway line and displaced the road laterally up to 50 feet (Knox, 1927).

Following this event, it was decided to start a series of monitoring activities in the site area. In addition, the identification of early movements in the first part of 1930 led to the detection of fissures in the upper part of the slope, causing significant concern. For these reasons, the colliery commissioned daily checks of ground movements. Monitoring operations continued until April 12, 1930, when a catastrophic landslide completely destroyed the colliery and overwhelmed the road (Bentley and Siddle, 2000). Figure 61 represents the surface displacements dataset up to the collapse date, identified at $t = 69$ days in the displacement vs time plot. The beginning of the acceleration phase was identified approximately at $t = 56$ days with respect to the zero-reference. It should be noted that available data do not provide clear information about the primary creep phase, since the monitoring activity started after the identification of previous movements in the area (Carey, 2011).

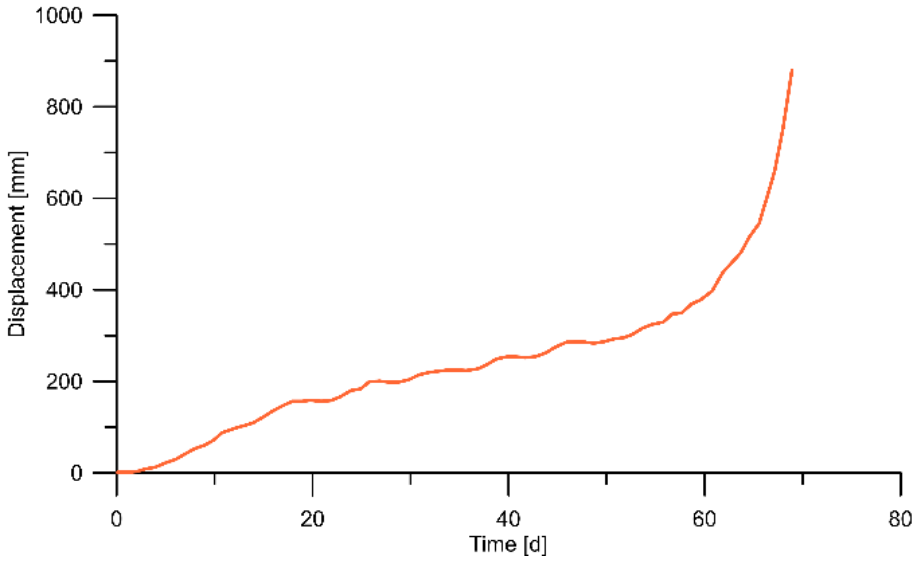

Figure 61. Cumulative displacements at the ground level recorded at the New Tredegar colliery site, date of collapse $t_f = 69$ days from the first measure included in the dataset (Digitized after Siddle et al., 2007)

The application of the generalized criterion, performed according to the procedure previously described, returns the outcomes presented in Table 8. In particular, values resulting from Inverse Velocity Method application, parameters calibration and normalization procedure are included, together with the theoretical warning time represented by the difference between the forecasted time-of-failure and the acquisition date of the last monitoring data available. It possible to observe that the time-of-failure forecasting model returns a value that varies along the monitoring activity duration, getting closer to the actual collapse date as new information are provided by the monitoring system. This is an expected behaviour, since the availability of new data closer to the actual collapse increases the accuracy of failure forecasting methods (Rose and Hungr 2007). Calibration of α parameter shows a similar trend, starting from values close to the linear reference represented by $\alpha = 2.0$, and gradually reaching a final value of 1.94 in correspondence of the last value analysed for this case study.

Table 8. Results obtained from the application of the generalized criterion for New Tredegar dataset

Time [d]	Predicted time-of-failure [d]	Warning time [d]	Calibrated A parameter [-]	Calibrated α parameter [-]	Normalized velocity [-]
59.0	66.6	7.6	0.0096	2.01	-0.0674
60.0	66.6	6.6	0.0099	2.00	-0.0110
61.0	65.5	4.5	0.0111	2.02	0.3022
62.0	66.2	4.2	0.0107	1.99	0.2171
63.0	66.7	3.7	0.0104	1.98	0.2874
64.0	67.4	3.4	0.0101	1.97	0.2943
65.0	68.2	3.2	0.0099	1.95	0.2275
66.0	68.4	2.4	0.0096	1.95	0.7190
67.0	68.4	1.4	0.0097	1.94	1.6706

The calibration procedure is an essential step in the alert threshold assessment process. In fact, the generalized curve to take into account as a theoretical reference for the definition of normalized velocity values should be selected according to the outcome of this procedure. For the case study here discussed, the warning level assessment was performed on the basis of the normalized velocity values extracted from the theoretical curve featuring $\alpha = 1.95$.

Table 9 reports the alert threshold values for this case study, selected by the author in order to illustrate possible implementations of the generalized criterion. In real case applications, it is advised that an expert of the specific case study, such as the monitoring responsible holding adequate knowledge on the monitored site, should address the definition of these values.

Table 9. Warning levels for New Tredegar landslide

Warning level	Theoretical distance from the collapse [d]	Normalized velocity [-]
1	10	-0.1989
2	6	0.0082
3	3	0.5474

Figure 62 shows a graphical comparison between the dimensionless velocity curve featuring $\alpha = 1.95$, and monitoring data after their elaboration and normalization performed by following the procedure developed for the generalized criterion. It is possible to observe that, despite minor inaccuracies, the theoretical curve provides an effective description of the landslide evolution towards collapse. Moreover, Figure 62 also presents a graphical representation of generalized warning levels previously assessed for this case study and reported in Table 9. It can be observed how the first monitoring point is located already above the first threshold, while the second level is consistently exceeded starting from the third normalized velocity value. Finally, the last alert threshold is overcome by two monitoring data, as the landslide gets closer to the collapse day. Table 10 reports the numerical comparison between normalized velocity values and warning levels.

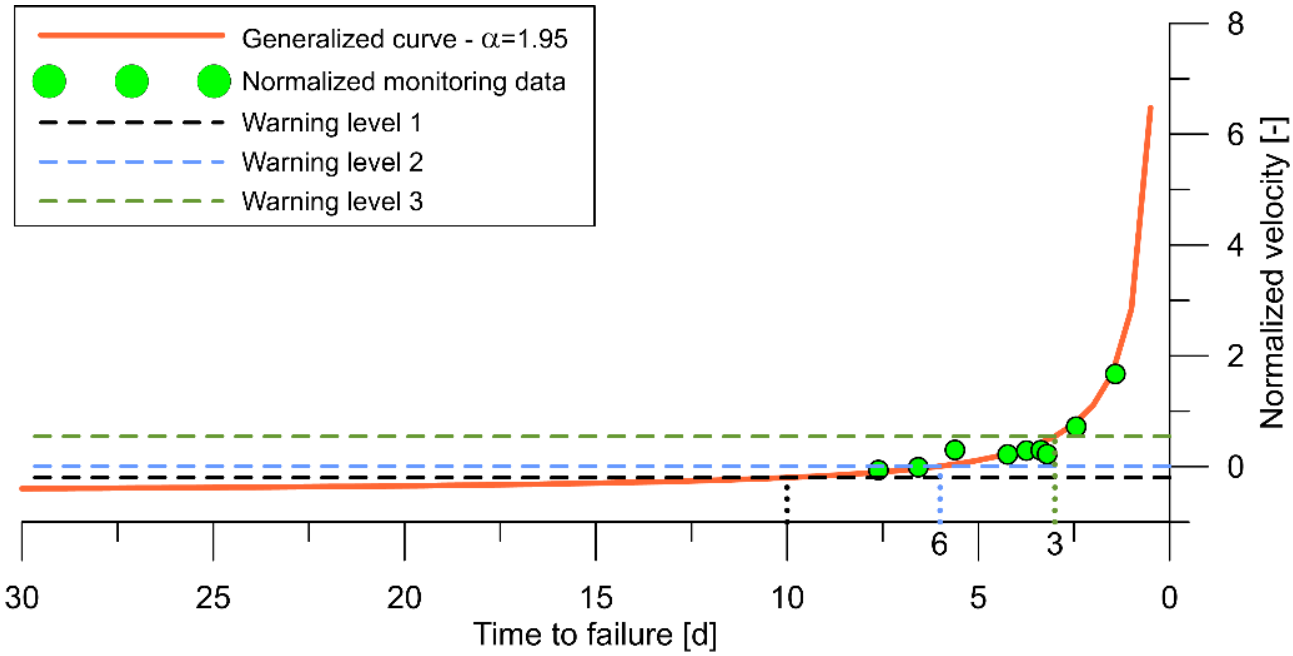

Figure 62. Graphical representation of normalized monitoring data and generalized curve, compared with three warning levels – New Tredegar

Table 10. Warning levels activation at different time during monitoring activity – New Tredegar

Time [d]	Normalized velocity [-]	Alert thresholds overcoming		
		Warning Level 1	Warning Level 2	Warning Level 3
59.0	-0.0674	x		
60.0	-0.0110	x		
61.0	0.3022	x	x	
62.0	0.2171	x	x	
63.0	0.2874	x	x	
64.0	0.2943	x	x	
65.0	0.2275	x	x	
66.0	0.7190	x	x	x
67.0	1.6706	x	x	x

6.1.2. Case study #2: Letlhakane Mine

The second case study involves a collapse observed at the Letlhakane diamond mine, located in Botswana and active since 1975. The landslide occurred on 14 July 2005, in form of a toppling failure with minor sloughing failures in the lower part of the slope, displacing about 233'000 m^3 of material (Kayesa, 2006). The installation on-site of a monitoring system called Geomos (Geodetic Monitoring System), composed of two theodolites located in concrete shelters, allowed to follow the event evolution over time. The system featured an automatic procedure to acquire the position of topographic targets placed in specific locations on the mine wall, aiming to detect slope displacements. Data collected by the sensors are transmitted by radio to the survey office, where a computer fitted with a dedicated Geomos processing software identifies any change with respect to the original position of monitoring targets. The alarm system involves the sending of an email and a text message at the overcoming of a predefined threshold.

First instability signals were recorded at the end of May 2005, when unusual movements of some targets were noted, however an on-site inspection did not highlight any physical signs related to potentially critical displacements. On June 9th, 2005, another investigation reported the appearance of tension cracks in some parts of the monitored slope. Since June 13th, 2005, the instrumentation detected a significant increment of displacement rate, which led to the widening of previously identified cracks. Starting from July 7, after a temporary reduction of ground movements, monitored displacements showed a clear accelerating trend that ultimately led to the slope collapse on July 14th, 2005, corresponding to $t = 127$ days in Figure 63. As reported by Kayesa (2006), the largest crack was measured to be 410 mm wide, and the strike length of the longest crack was estimated to be approximately 183 m.

As previously mentioned, the first dataset comprises the point representing the onset of acceleration of slope displacement, together with the following three points. For this case study, starting point was identified approximately at $t = 114$ days.

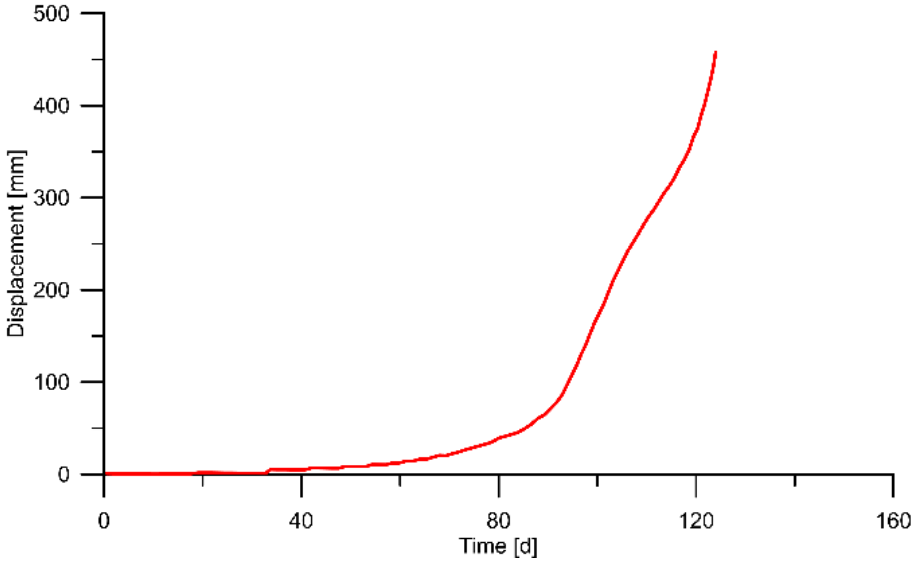

Figure 63. Cumulative displacements at the ground level recorded at Letlhakane diamond mine, date of collapse $t_f = 127$ days from the first measure included in the dataset (digitized after Kayesa, 2006)

Table 11 reports the outcomes of the IVM application, calibration of model parameters, and normalization procedures, including also the warning time represented by the difference between estimated time-of-failure and acquisition date of the monitoring data. In accordance with previous hypotheses expressed for the application of failure forecasting methods, the time-of-failure prediction accuracy significantly increases with the progressing of monitoring activity. In fact, values of t_f initially evidence a relevant fluctuation around the collapse date ($t = 127$ days from the first measure of the available dataset), which is correctly identified in the last part of the dataset analysis, when available information are closer to the slope failure. A similar behaviour can be observed in the calibration procedure of the α parameter, which displays some variations before reaching a stable value of 1.99 in the last three data analysed. However, it should be noted that these are minor differences that have quite less significance with respect of the collapse forecasting variations. On the basis of results obtained in the calibration phase, in the following step it was decided to consider the curve featuring $\alpha = 1.99$.

Table 11. Results obtained from the application of the generalized criterion for Letlhakane dataset

Time [d]	Predicted time-of-failure [d]	Warning time [d]	Calibrated A parameter [-]	Calibrated α parameter [-]	Normalized velocity [-]
117.6	128.5	10.9	0.0107	1.96	-0.2559
118.6	128.4	9.8	0.0100	1.98	-0.1897
119.4	125.1	5.8	0.0122	2.01	0.1860
120.4	128.5	8.1	0.0100	1.97	-0.1959
121.0	126.4	5.4	0.0110	2.00	0.3019
121.8	127.0	5.2	0.0108	1.99	0.0463
122.4	126.8	4.4	0.0108	2.00	0.2575
123.0	127.0	4.0	0.0107	1.99	0.2359
123.5	127.1	3.6	0.0106	1.99	0.3512
123.9	127.0	3.1	0.0106	1.99	0.7473

Table 12. Warning levels for Letlhakane landslide

Warning level	Theoretical distance from the collapse day [d]	Normalized velocity [-]
1	14	-0.2914
2	7	-0.0453
3	3	0.6111

Table 12 reports the hypothetical warning levels considered in the present analysis, while Figure 64 presents the comparison between elaborated monitoring data and the theoretical velocity curve extracted from the generalized criterion, displaying also a graphical representation of the alert thresholds previously assessed. It is possible to note that the velocity curve featuring $\alpha = 1.99$ properly represents the trend displayed by normalized monitoring data. For what concern warning levels, it can be noted how the first data included in the analysis already overcomes the first alert threshold. A significant number of normalized velocity

data exceeds the second warning level, highlighting the accelerating trend of the phenomenon. At the end, the last available monitoring data overcomes the third warning level, confirming that the landslide is getting closer to the collapse date.

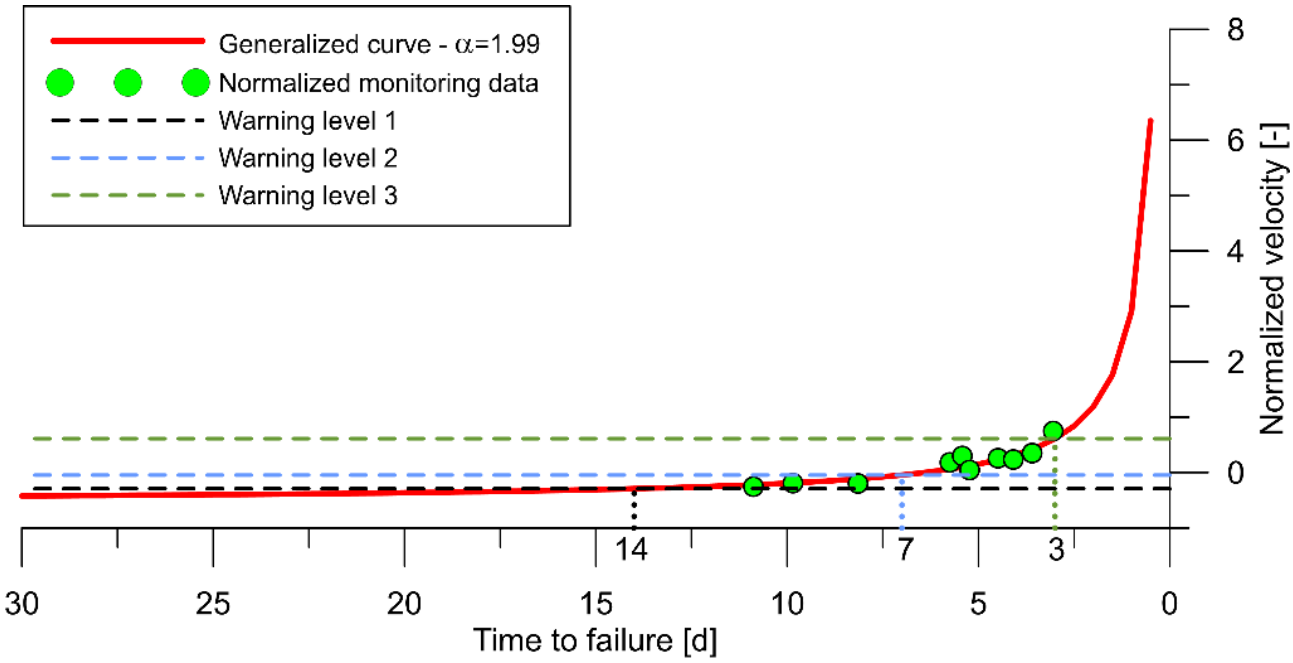

Figure 64. Graphical representation of normalized monitoring data and generalized curve, compared with three warning levels – Letlhakane mine landslide

Numerical values reported in Table 13 show also an unusual behaviour, where the fourth point features a velocity value lower than the previous one, leading to a downgrading from second to first warning level. This singularity could be attributed to a temporary decreasing of displacement rates, causing the forecasting model to calculate a collapse date further in time (125.1 days for the third point and 128.5 days for the fourth point respectively).

Table 13. Warning levels activation at different time during monitoring activity - Letlhakane Mine

Time [d]	**Normalized velocity [-]**	**Alert thresholds overcoming**		
		Warning Level 1	**Warning Level 2**	**Warning Level 3**
117.6	-0.2559	x		
118.6	-0.1897	x		
119.4	0.1860	x	x	
120.4	-0.1959	x		
121.0	0.3019	x	x	
121.8	0.0463	x	x	
122.4	0.2575	x	x	
123.0	0.2359	x	x	
123.5	0.3512	x	x	
123.9	0.7473	x	x	x

Results obtained for both case studies underlined the ability of the proposed method to provide a common tool to interpret the landslide behaviour approaching the slope failure, and to assess warning levels to control its evolution over time. A graphical and numerical comparison with elaborated data permitted to identify a threshold overcoming, indicating that the monitored landslide is progressively approaching the critical state. Nonetheless, it should be always taken into account that several factors affect the model reliability and accuracy. In particular, adequate quality of monitoring data is strongly advised when dealing with failure forecasting and threshold assessment procedures such as the one here described. Moreover, the criterion proved to be an effective tool when applied to case studies displaying a relatively long time period between the onset-of-acceleration and the slope collapse (i.e., days, weeks), while its application to faster displacements did not provide an accurate interpretation of the studied phenomenon.

6.2. Equivalent displacement thresholds

The analysis of time series extracted from monitoring data has always played an important role in the study of landslides evolution. Thanks to more recent technological advancements, as those discussed in Chapter 2.2, nowadays it is much easier to have large amount of information regarding the phenomenon evolution over time. From this perspective, it is possible to rely on displacement time series to provide useful evidence concerning the past behaviour of the monitored element and helping in the interpretation and prediction of possible future trends.

The methodology here presented relates to this concept, aiming to exploit the availability of a large amount of information regarding the past movements of the monitored landslide as a comparison to determine the impact of newly recorded displacements on the slope stability conditions. The main objective of this method is the identification of false alarms generated by events that present a data trend geometrically compatible with an accelerating pattern according to the previous criteria, while featuring a displacement magnitude which does not correspond to a critical occurrence if compared to previously observed events. As previously noted, the introduction of new technologies in the geotechnical monitoring field has notably increased the systems reliability and sampling rate, thus making them able to provide consistently a considerable amount of information regarding the phenomenon evolution. By relying on available monitoring data, it is possible to apply the proposed procedure to assess one or more alert levels not only for any particular case study, but also specifically for each single event identified by the instrumentation and classified according to the criteria previously discussed. The process to define the alert threshold value can be summarized as follows:

- When the software detects a potentially critical event, it extracts the corresponding dataset and evaluates the displacement generated S^* and its duration d^*. Since this event was already processed and validated by the onset-of-acceleration criterion, it is expected to follow an increasing trend in the displacement vs time plot.
- Taking as a reference the date of the first point x included in the dataset, the software retrieves all monitored data sampled by the same sensor during the 30 days preceding the

event. These values are going to serve as a term of comparison for the event identified at the previous step.

- Equivalent displacements are evaluated, i.e., values calculated by considering the available dataset selected in the previous set, and taking d^* as a reference for each displacement. By doing this, the algorithm produces a series of displacements S_n generated in the same time interval d^*. Table 14 reports an example of this procedure for a dataset composed of 6 displacement values.

Table 14. Evaluation of equivalent displacement values for a potentially critical event composed of 6 data

Dimension of the dataset referred to the event of interest = 6	
Event identified	$S^* = d_x - d_{x-5}$
Equivalent displacement 1	$S_1 = d_{x-1} - d_{x-6}$
Equivalent displacement 2	$S_2 = d_{x-2} - d_{x-7}$
Equivalent displacement 3	$S_3 = d_{x-3} - d_{x-8}$
…	…
Equivalent displacement n	$S_n = d_{x-n} - d_{x-5-n}$

- In this step, it is possible to assess an alert threshold S_{th} based on the values of mean μ_S and standard deviation σ_S calculated from the equivalent displacement values:

$$S_{th} = \mu_S + 3\sigma_S \quad \text{(XXVIII)}$$

- Finally, it is possible to compare this outcome with the displacement S^*, in order to verify if the event generated a displacement with a magnitude similar to values previously observed during the considered time period, or if the resulting values overcomes the alert threshold, thus indicating a potentially critical phenomenon.

Since the equivalent displacement threshold assessment follows the identification and classification of a potentially critical event, it has been applied to a wide range of occurrences reaching different warning levels. In the following sections a series of examples are reported, including also a back-analysis on a case study where the detected event led to an actual collapse of the monitored slope (thus representing a "true positive" in terms of early warning).

6.2.1. Case study #1: Landslide in Southern Italy

The first case study here reported involves the monitoring activity of a slope, located in Southern Italy, crossed by a high-speed railway tunnel currently under construction. Following the identification of a quiescent landslide in the area, it was decided to install an automatic monitoring system in order to verify the design hypothesis and control the deformations potentially induced by the excavation works. It included a total of 4 Vertical Array MUMS inclinometers, featuring different lengths (between 30 and 80 metres) and number of sensors (from 31 to 81 3D MEMS) depending on the specific device. Interspace between Links also varied depending on their vertical position, with a distance of 2 metres between each node in

the supposedly stable area, reducing to 0.5 metres in proximity of the sliding surface. Moreover, the system includes 4 Piezo Arrays, each one composed of 2 analog piezometers, to control the water level variations over time. The characteristics of each Array are summarized in Table 15.

During the entire period of the monitoring activity, all Vertical Arrays evidenced a relevant degree of activity of the monitored site, with several datasets triggering the criteria integrated in the elaboration software. However, despite reaching Levels 3 and 4 in some instances, the monitored site did not display any significant evidence of critical instabilities taking place in the area of interest.

Table 15. Features of the monitoring system installed to control displacements and water level variations of a slope located in Southern Italy

ID [-]	Installation date [gg/mm/yyyy]	Array Typology [-]	Sensors number and typology [-]	Array Length [m]
DT0004	18/02/2020	Piezo Array	2x Piezo Link	45.00
DT0111	23/01/2020	Vertical Array	73x Tilt Link V	69.00
DT0005	18/02/2020	Piezo Array	2x Piezo Link	31.70
DT0112	24/01/2020	Vertical Array	81x Tilt Link V	80.00
DT0006	18/02/2020	Piezo Array	2x Piezo Link	52.00
DT0113	14/01/2020	Vertical Array	66x Tilt Link V	80.00
DT0007	22/01/2020	Piezo Array	2x Piezo Link	30.00
DT0114	24/01/2020	Vertical Array	31x Tilt Link V	30.00

The examples presented in the following paragraphs refer to two occurrences identified by two different Vertical Arrays located on site. Datasets recorded by each Tilt Link that identified an unexpected displacement trend were processed with the algorithm previously detailed, assessing an equivalent displacement threshold to verify how the event magnitude compared to the landslide's past behaviour.

The first event was detected on August 13th, 2020, when two 5-point datasets sampled by Tilt Links 47 and 49 activated the acceleration criterion, which identified the onset-of-acceleration for the event at 01:51 of that day. The following elaboration performed by the classification criterion, involving the application of the Inverse Velocity Method, returned a value of the linear determination coefficient equal to 0.8643 and 0.8554 respectively. Therefore, having identified two separate datasets composed of 5 velocity values and featuring $R^2 < 0.92$ from the forecasting analysis, the event achieved a Level 3 rate.

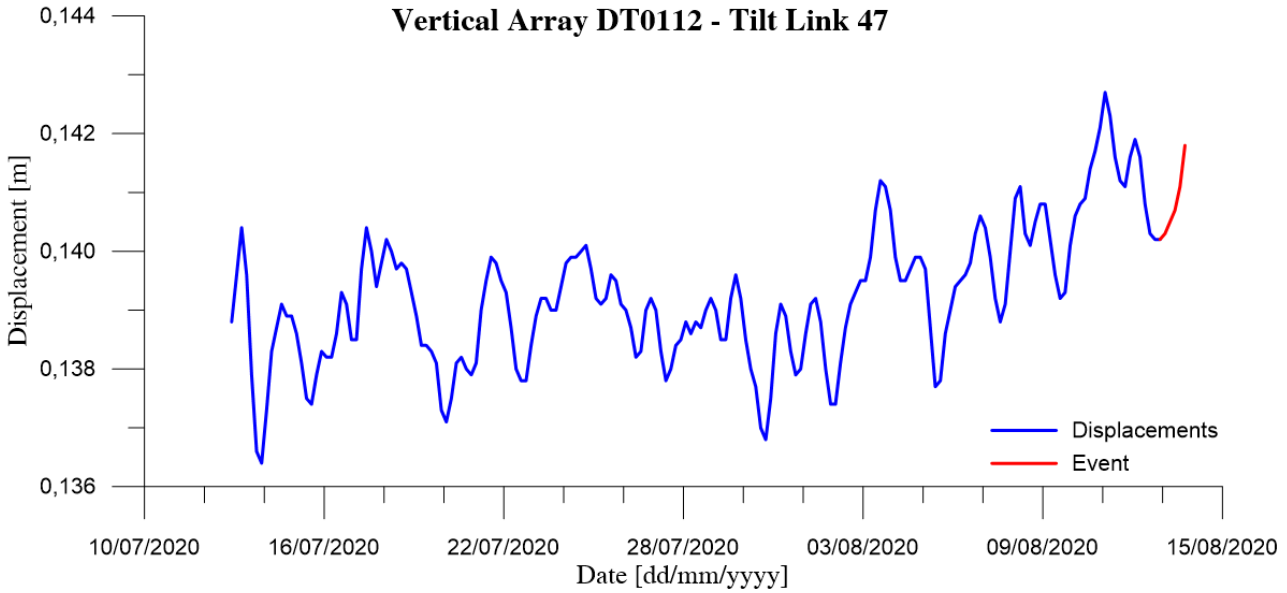

Figure 65. Displacement values measured by Vertical Array DT0112 - Tilt Link 47, referred to the event with OOA on 13/08/2020 01:51, and to the 30 days preceding the event itself

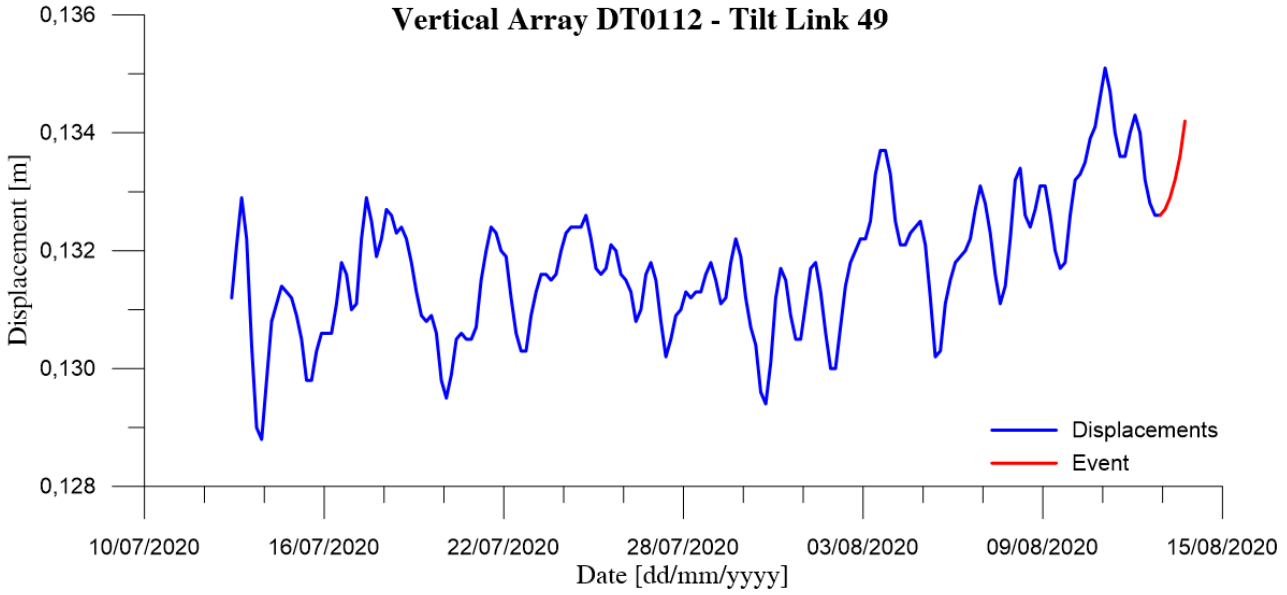

Figure 66. Displacement values measured by Vertical Array DT0112 - Tilt Link 49, referred to the event with OOA on 13/08/2020 01:51, and to the 30 days preceding the event itself

As previously detailed, the first step following the alert level assessment involves the determination of the displacement generated by the event itself. For both datasets available, this corresponds to a value of 1.6 mm over a time period of approximately 20 hours. The subsequent operation consists of retrieving monitoring data from a time period of 30 days preceding the event of interest, in order to assess the equivalent displacements and the correlated threshold for each dataset involved in the analysis. Each displacement value is computed by considering a time interval equal to the one obtained from the event, which in this case equals to 20 hours (corresponding to 6 monitoring values under the hypothesis of constant sampling frequency).

The outcomes of this operation are reported in Table 16, while Figure 67 and Figure 68 present a graphical comparison between equivalent displacements and the threshold computed at the previous step. It is possible to observe how the resulting value referred to the event of interest it is generally comparable to previously recorded displacements for both Links involved, not overcoming the reference value defined with the procedure previously described.

Table 16. Characteristics of the DT0112 Tilt Links and the datasets involved in the analysis, together with the displacement generated by the event and the equivalent displacement threshold

Tilt Link ID	Depth [m]	Dataset dimension	RQ	LEVEL	Displacement generated [mm]	Equivalent displacement threshold [mm]
47	18.00	5	0.8643	3	1.6	2.9
49	17.00	5	0.8554		1.6	2.9

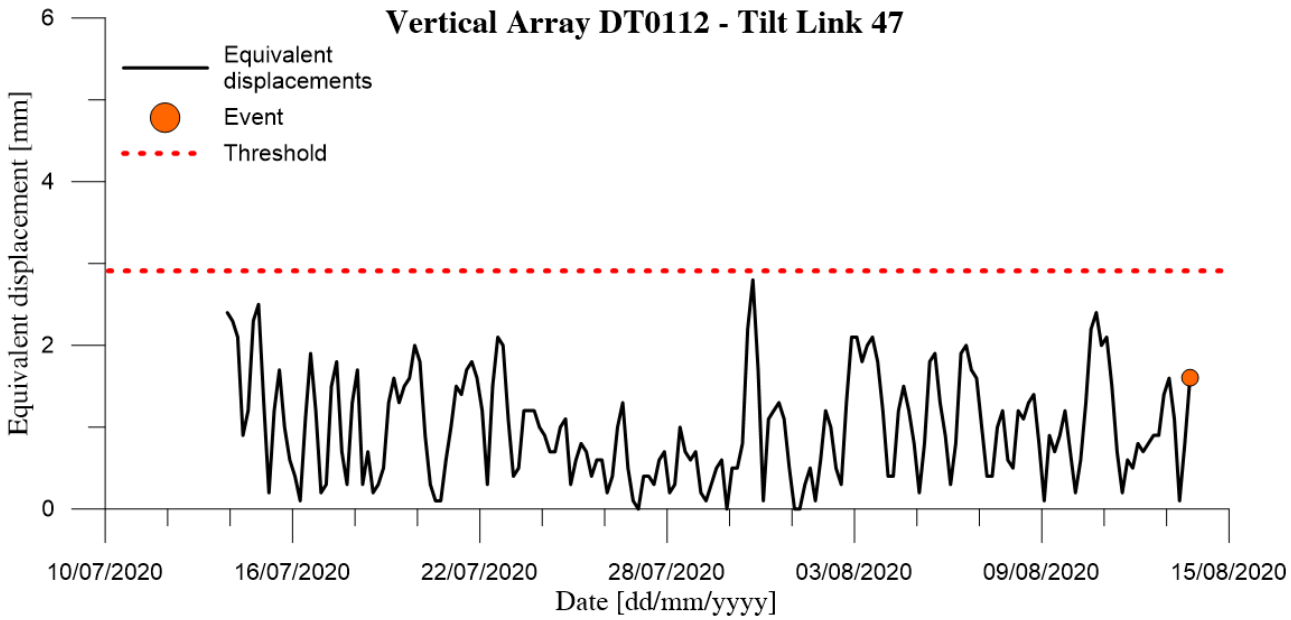

Figure 67. Graphical representation of equivalent displacements referred to the event of interest, the time period of 30 days preceding the event itself, and the threshold evaluated from these values for DT0112 – Tilt Link 47

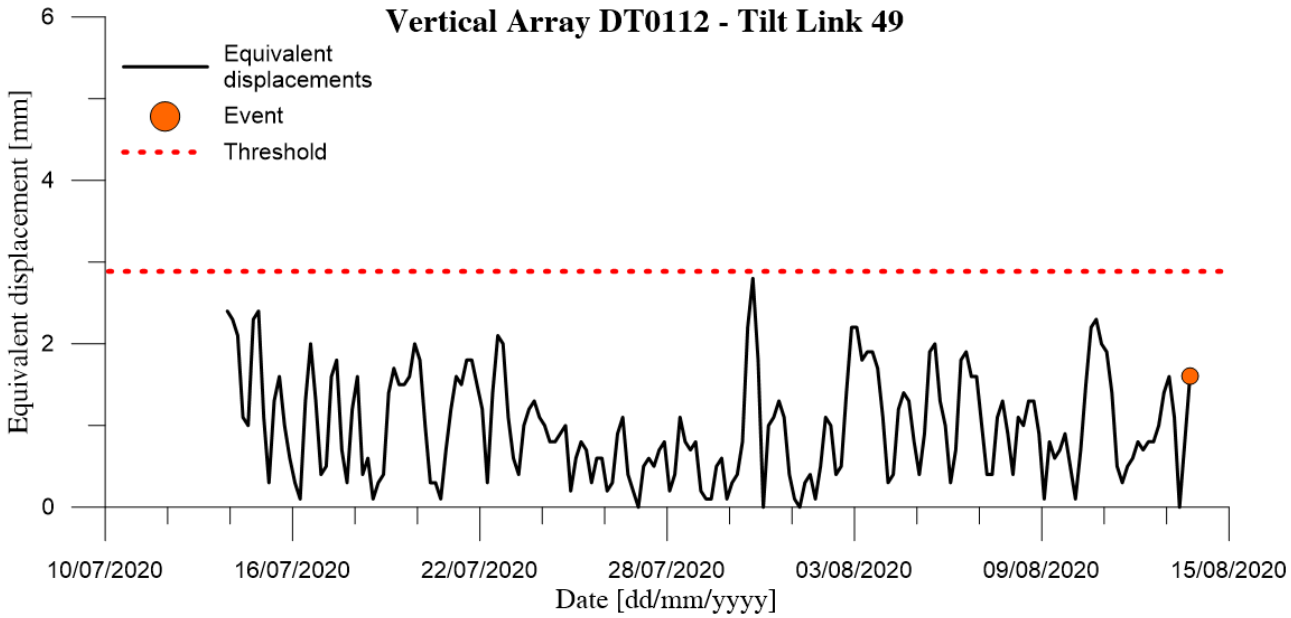

Figure 68. Graphical representation of equivalent displacements referred to the event of interest, the time period of 30 days preceding the event itself, and the threshold evaluated from these values for DT0112 – Tilt Link 49

The second event here analysed was recorded by Vertical Array DT0113 on May 24th, 2020, approximately four months after its installation. In this case, the movement detected by the instrumentation was recorded by Tilt Links 43 and 55, placed respectively at a depth of 12.50 m and 6.50 m, returning two datasets composed of 5 monitoring values each and identifying the OOA at 04:37. However, outcomes of the forecasting analysis evidenced a value of the determination coefficient higher than 0.92 for the Tilt Link 43 dataset, which coupled with a 2-occurrence event allowed the achievement of Level 4 in the classification system.

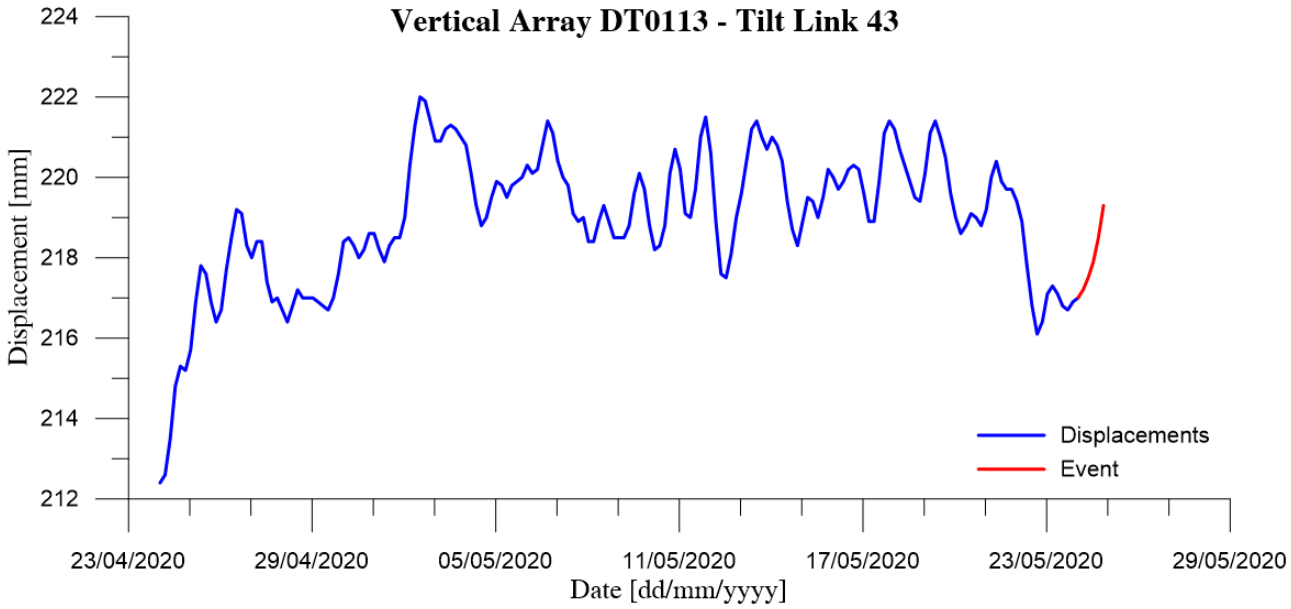

Figure 69. Displacement values measured by Vertical Array DT0113 - Tilt Link 43, referred to the event with OOA on 24/05/2020 04:37, and to the 30 days preceding the event itself

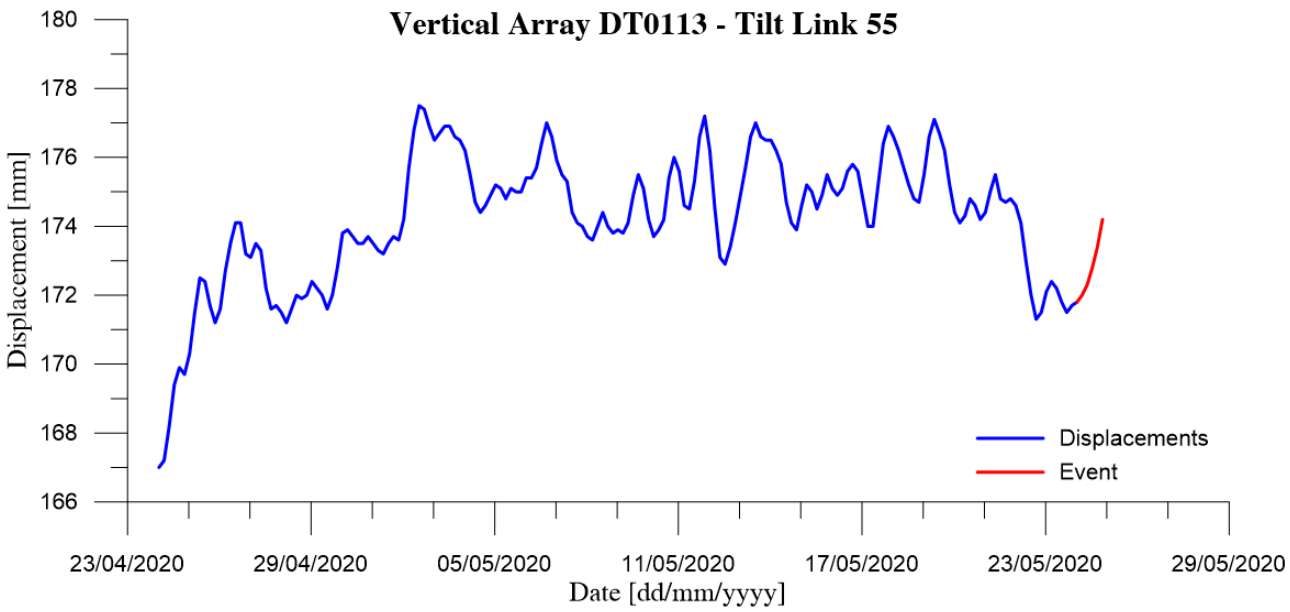

Figure 70. Displacement values measured by Vertical Array DT0113 - Tilt Link 55, referred to the event with OOA on 24/05/2020 04:37, and to the 30 days preceding the event itself

The operations relating to the evaluation of the displacement generated by the event, the extraction of equivalent displacements from previous monitoring data, and the threshold assessment, are summarized in Table 17. It is worth nothing that all Vertical Arrays on this specific site were set on a sampling rate of 4 hours, recording 6 monitoring values each day. Therefore, since each dataset includes 5 velocity values, the time interval to evaluate the equivalent displacements for this example is the same as in the previous case involving DT0112 (i.e., 20 hours). Figure 71 and Figure 72, referring respectively to Tilt Link 43 and 55, present a graphical visualization of the analysis outcomes, evidencing how the detected event did not cause a displacement significant enough to overcome the threshold values assessed for the two Links that activated the alert criteria.

Table 17. Characteristics of the DT0113 Tilt Links and the datasets involved in the analysis, together with the displacement generated by the event and the equivalent displacement threshold

Tilt Link ID	Depth [m]	Dataset dimension	RQ	LEVEL	Displacement generated [mm]	Equivalent displacement threshold [mm]
43	12.50	5	0.9453	4	2.3	3.9
55	6.50	5	0.8997		2.4	4.2

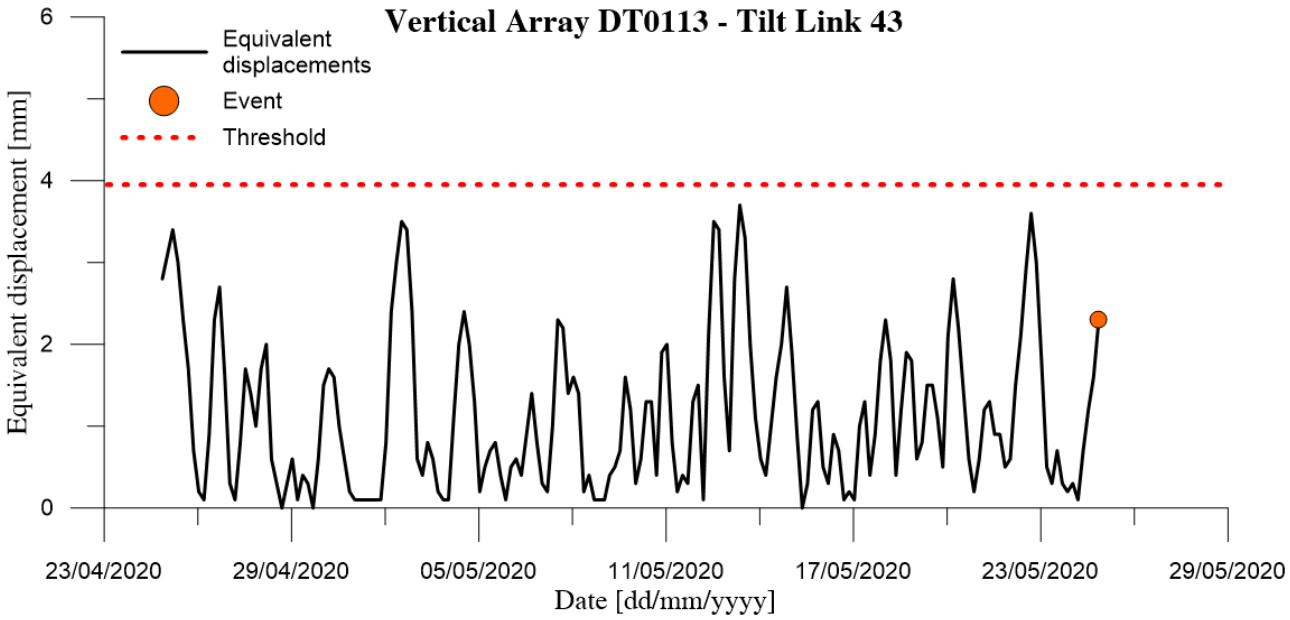

Figure 71. Graphical representation of equivalent displacements referred to the event of interest, the time period of 30 days preceding the event itself, and the threshold evaluated from these values for DT0113 – Tilt Link 43

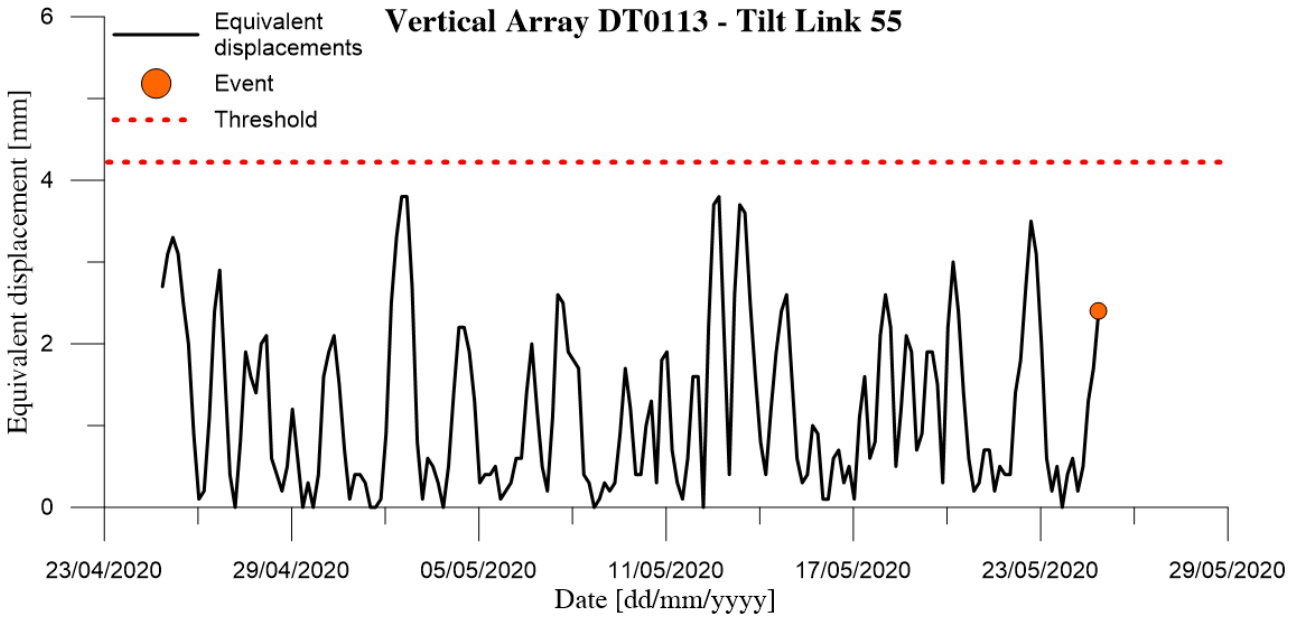

Figure 72. Graphical representation of equivalent displacements referred to the event of interest, the time period of 30 days preceding the event itself, and the threshold evaluated from these values for DT0113 – Tilt Link 55

6.2.2. Case study #2: Landslide in Central Italy

The second case study here discussed refers to the same landslide analysed in Chapter 5.2.2, and focuses on the event that involved the Vertical Array DT0014 some months after its installation, in March 2017. At that time, DT0014 was the only automatic monitoring device present on site, and the acquisition process was set on a sampling frequency of 1 hour. Starting from the end January 2017, the inclinometer recorded a series of displacements involving the first 6 metres of soil, with some datasets activating the early warning criteria implemented in the software. The phenomenon evolution progressed for the following weeks, leading to a major displacement recorded on March 8th that damaged the Array, partially compromising its

functionality. The event was identified by the elaboration software, which issued a series of alert messages to authorities responsible of the monitoring activity. Ultimately, MUMS inclinometer DT0014 became completely inactive on March 13th due to excessive deformations.

As previously specified, only the acceleration criterion (in a slightly different version than the one presented in this thesis) was active during the monitoring activity, hence no classification was available at the time of the event occurrence. Therefore, a back-analysis was performed on the datasets referring to the displacement observed on March 8th, 2017, in order to apply the newly developed methodologies to a real case critical scenario. In particular, the sudden increase of displacement rates was identified by Tilt Links 93 and 95, respectively located 2.5 m and 1.8 m below ground surface. For both Links, the analysis returned a 7-point velocity dataset with the onset-of-acceleration at 02:28 AM of March 8th, while the failure forecasting analysis returned a determination coefficient of 0.8515 for Tilt Link 93, and 0.9578 for Tilt Link 95, therefore qualifying as a Level 5 event.

It is worth noting that this is the only event recorded by MUMS inclinometers that managed to reach the highest level in the classification system, taking into account both real-time and back-analysis evaluations. Another notable detail regards the accuracy of the time of failure assessment, performed through the linear Inverse Velocity Method, which was compared to the date of collapse observed from monitoring data (i.e., the date and time where instrumental data displayed the damaged caused to the Array by soil deformations). As reported in Segalini et al (2019a), both datasets provided a positive prediction of the slope collapse, with a time difference of 3 hours for Tilt Link 93, and 1 hour for Tilt Link 95.

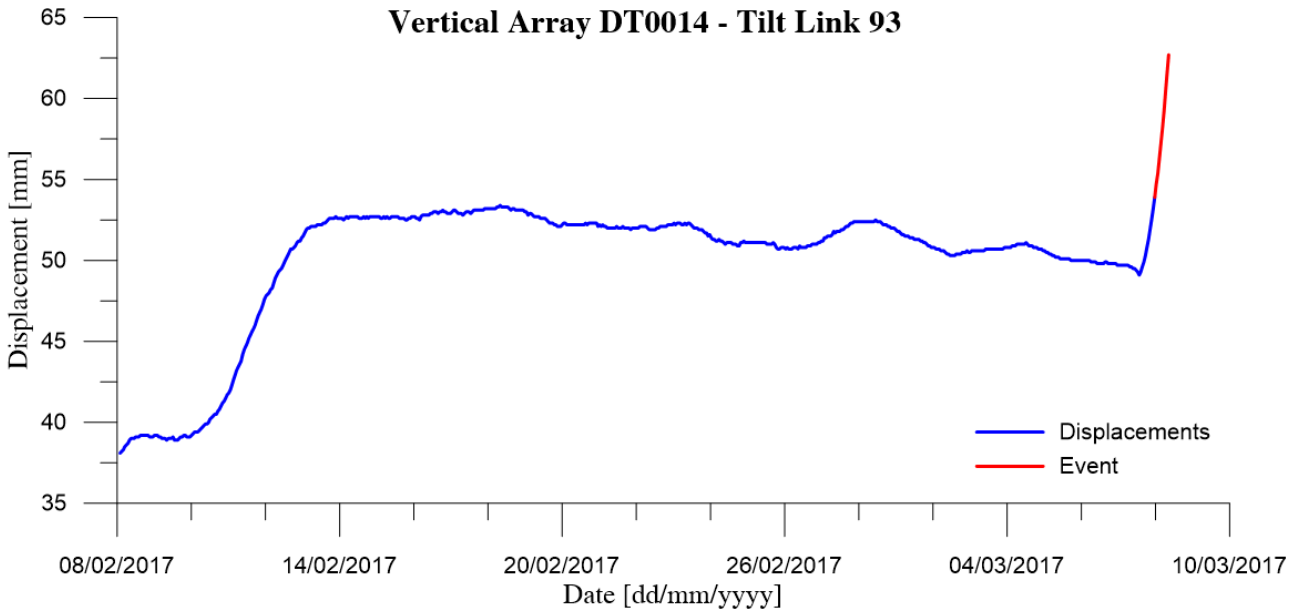

Figure 73. Displacement values measured by Vertical Array DT0014 - Tilt Link 93, referred to the event with OOA on 08/03/2017 02:28, and to the 30 days preceding the event itself

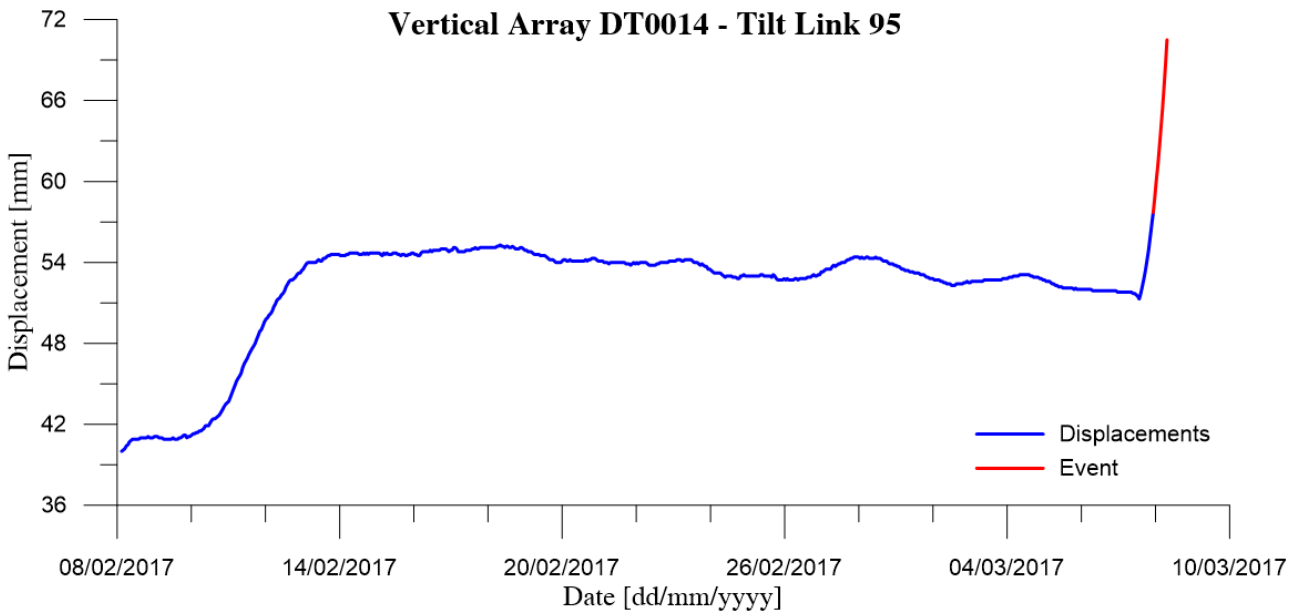

Figure 74. Displacement values measured by Vertical Array DT0014 - Tilt Link 95, referred to the event with OOA on 08/03/2017 02:28, and to the 30 days preceding the event itself

As in previous cases, the available monitoring data were processed in order to evaluate the displacement measured by each Link during the event, and to assess the alert threshold based on the equivalent displacement datasets. Given the 1-hour sampling frequency of the Vertical Array, and since each Tilt Link returned a 7-point dataset, each single equivalent displacement value refers to a time interval of 7 hours.

Table 18. Features of the DT0014 Tilt Links and the datasets involved in the analysis, together with the displacement generated by the event and the equivalent displacement threshold

Tilt Link ID	Depth [m]	Dataset dimension	RQ	LEVEL	Displacement generated [mm]	Equivalent displacement threshold [mm]
93	2.50	7	0.8515	5	7.3	1.9
95	1.80	57	0.9578		11.2	2.4

The outcomes of this procedure are summarized in Table 18, and the graphical representation of the obtained value are displayed in Figure 75 and Figure 76. It is possible to notice how the event caused a displacement that clearly overcomes the threshold value for both datasets, thus confirming that the monitored phenomenon is showing a critical behaviour.

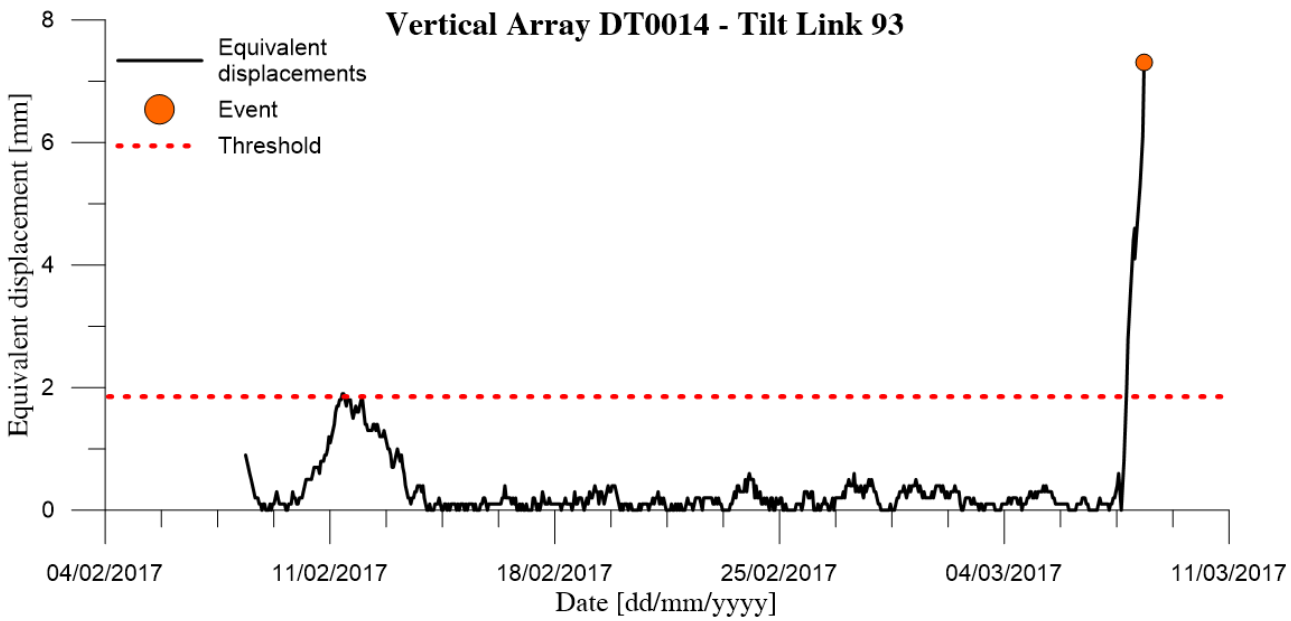

Figure 75. Graphical representation of equivalent displacements referred to the event of interest, the time period of 30 days preceding the event itself, and the threshold evaluated from these values for DT0014 – Tilt Link 93

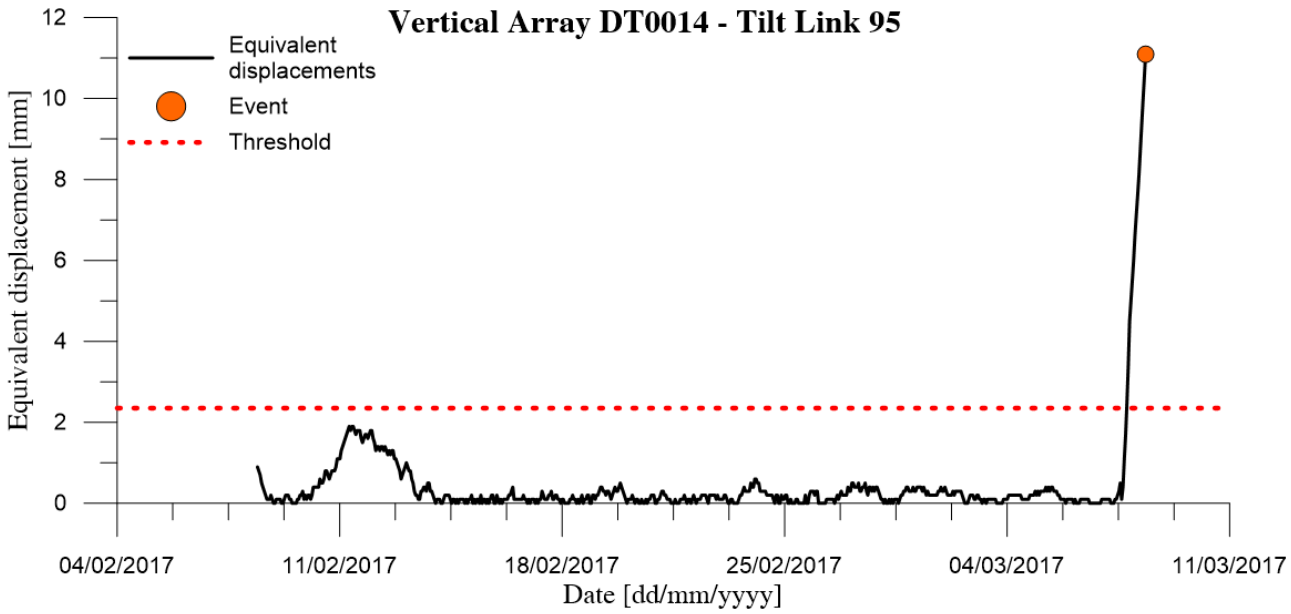

Figure 76. Graphical representation of equivalent displacements referred to the event of interest, the time period of 30 days preceding the event itself, and the threshold evaluated from these values for DT0014 – Tilt Link 95

Chapter 7. Automatic report documents

Technological innovations have resulted into significant improvements over the years in different sectors of the geotechnical monitoring framework, ranging from sensors reliability to data elaboration efficiency. One of the key features that got heavily influenced by the introduction of new approaches in this field is the monitoring data availability. This derives directly from the ability of automatic systems to achieve, and maintain over time, sampling frequencies far higher than those obtainable with manual instrumentation. This approach presents considerable advantages in terms of available knowledge regarding the studied phenomenon, but poses several challenges related to the large amount of data generated.

Several studies highlighted this crucial aspect, observing that the amount of information produced by automatic systems could potentially become so large that it could lead to several issues related to their management and processing (e.g., Allasia et al., 2013; Giordan et al., 2019). While the computational power of modern calculators is far higher than the one available some decades ago, these issues should not be underestimated when dealing with so-called "big data". This term refers not only to a particularly substantial volume of data, but also to a wide range of datasets that cannot be handled with conventional management and processing tools due to their complexity (Cremona and Santos, 2018). Another aspect related to this concept is the importance of a correct presentation of monitoring outcomes. In fact, a large volume of data could lead to difficulties in their representation and visualization, thus causing issues in the interpretation process. Bressani et al. (2018) underlined some relevant aspects related to technical reporting, including the importance of identifying and representing the key parameters involved in the monitoring activity, and the delivery of synthetic and sequential reports. Moreover, as underlined by Giordan et al. (2019), the aspect of scientific data communication has received considerably less attention if compared to technological improvements in this field.

Addressing the issues here discussed, this chapter deals with the need for a dedicated procedure to manage and visualize the considerable volume of data produced by automatic devices installed in several different sites. In particular, the research activity focused on two separate aspects of this problem, concerning the periodic presentation of results and information acquired during the entire monitoring activity period, and the timely reporting of specific outcomes in correspondence of a critical event. In both cases, the software development process exploited the toolbox *Matlab Report Generator*™, which includes a series of functions and APIs (Application Programming Interfaces) that integrate reporting capabilities into MATLAB® applications. This allows to dynamically capture numerical results and figures generated by a MATLAB® code, including them in a single document that can be customized according to each specific application.

7.1. Monitoring report

As previously discussed, the implementation of multi-instrumental landslide monitoring networks is becoming more and more common thanks to the increased availability of automatic sensor designed to measure a wide range of different parameters. These systems are able to

provide a large amount of data at high sampling rates for extended time periods, which should be properly managed to allow the correct interpretation of all available information. The periodic monitoring report here presented was developed with this objective in mind, aiming to summarize in a single document all main information related to the monitored element for a specific time period. It is important to underline that the main purpose of this report is to provide an additional tool for data visualization and interpretation, and it is not aimed to completely replace other representation approaches that allow to browse the monitoring outcomes whenever it is needed.

In the case here presented, the software was designed for MUMS-based instrumentation, which already takes advantage of a dynamic cloud-based visualization platform (called *Geo-Atlas*) that integrates a wide range of different functions, interactive charts, and dedicated figures for each monitored site. Therefore, the design process aimed to the development of a simpler and more synthetic document to summarize the results acquired in a limited time interval, leaving the platform as the main tool for a more comprehensive and extensive data representation. Moreover, the report structure was conceived to adapt to all different monitoring contexts in which MUMS devices could be installed, ranging from landslides to underground constructions, buildings, and geotechnical protection structures. Therefore, starting from a general template including several sections, the software generates a customized report depending on the composition and features of the monitoring system.

7.1.1. Cover pages and initial disclaimer

Figure 77. (a) Cover page and (b) summary of the periodic monitoring report

The first page of the report indicates the name of the monitored site, together with the date when the document was created. The summary, included in the following page, is composed a series of hyperlinks to access any section and subsection of the report directly (Figure 77).

Moreover, before presenting the site information, the document incorporates a short disclaimer to clearly explain the report objectives and its main features. This text is intended to underline that, being automatically generated by a software, the report does not contain any technical evaluation or validation concerning the results measured by the instrumentation installed on site and has the main goal to provide a resume of the main outcomes of the monitoring activity.

7.1.2. Monitoring system description

This section aims to introduce the main components of the monitoring system, including its general structure and the working principles on which it is based. This part is shared by all reports since it is a core feature of any device based on MUMS technology. However, the same section presents a list of all monitoring tools installed on site, as well as any control tools connected to the monitoring system. In particular, for what concern MUMS Arrays, the software is able to identify the devices reported in Table 19.

Table 19. List of MUMS-based Arrays and their main application in a monitoring context

Array/device name	**Application**
Vertical Array	Landslides, embankments, landfills
Piezo Array	
Rain Array	
In Place Array	
Horizontal Array	
Therm Array	Geothermal plants
Vertical Array Structure	Geotechnical structures
Klino Array	Buildings, infrastructures, rock masses
Analog Array	
Cir Array	Tunnels and underground excavations
Rad Array	
PreConv Array	
RockFall Safety Network	Rockfall and debris flow flexible barriers
D-Fence	
Trigger System	
Debris Flow Safety Network	
G-Flow	
ASEcam	Image acquisition

7.1.3. Site features

The following section is intended to frame the main characteristics of the monitored area, indicating the geographical coordinates, and reporting a satellite image of the site location.

Additionally, another figure depicts the detailed position of each control unit and monitoring tool installed in the studied area, in order to summarize the system structure (Figure 78).

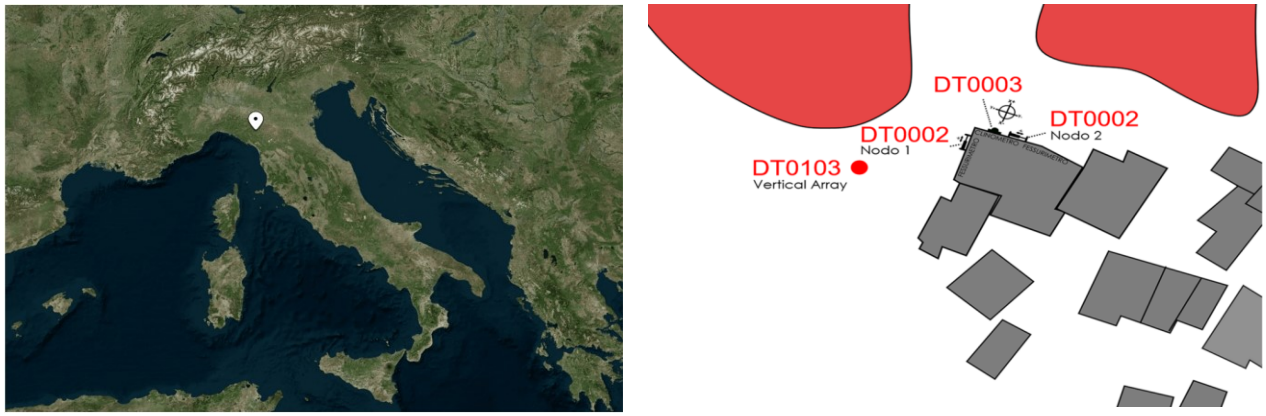

Figure 78. Examples of (a) geographical location of the monitored site; (b) on-site location of the monitoring tools

Moreover, the instrumentation typology and features are reported in a dedicated table, which includes the following information regarding each device present on site:

- Control tool and Array IDs
- First available reading date, referring to the beginning of the monitoring activity
- Reference reading date, representing a time reference where the device can be considered fully operational since no more stabilization movements are observed from sampled data (further information regarding di matter can be found in the International Standard EN ISO 18674-1:2015)
- Array typology, according to the system composition listed in the previous section
- Array length, measured in metres
- Typology of sensors/devices, each one of which is identified as a Link composing the Array (Table 20)
- Total number of sensors/devices included in the Array

Table 20. List of different Links that can be integrated in each typology of Array

Array name	**Link name**
Vertical Array	Tilt Link V, Tilt Link HR 3D V, Piezo Link, Baro Link, Therm Link
Piezo Array	Piezo Link, Baro Link
Rain Array	Rain Link
In Place Array	In Place Link, In Place Link HR,
Horizontal Array	Tilt Link H, Tilt Link HR 3D H
Therm Array	Therm Link
Vertical Array Structure	Tilt Link V, Tilt Link HR 3D V
Klino Array	Klino Link, Klino Link HR

Analog Array	Load Link, Pressure Link, Extensometer Link, 3D Extensometer Link, Wire Extensometer Link, Multi-Point Borehole Extensometer Link, Crack Link, PT100 Link
Cir Array	Tunnel Link
Rad Array	Tunnel Link
PreConv Array	PreConv Link
RockFall Safety Network	RSN Link, RSN Link HR, Load Link
D-Fence	RSN Link, RSN Link HR
Trigger System	Trigger Link
Debris Flow Safety Network	RSN Link, RSN Link HR, G-Shock Link
G-Flow	G-Flow Link

7.1.4. Results - Control Unit

The main objective of this section is to display the monitoring system functionality over time, by reporting the level of the battery connected to each control unit present on site. In fact, as previously discussed, it is fundamental to verify the correct operativity of the power supply system in order avoid failures of the monitoring instrumentation, with potential data losses and missed alerts in case of early warning activities.

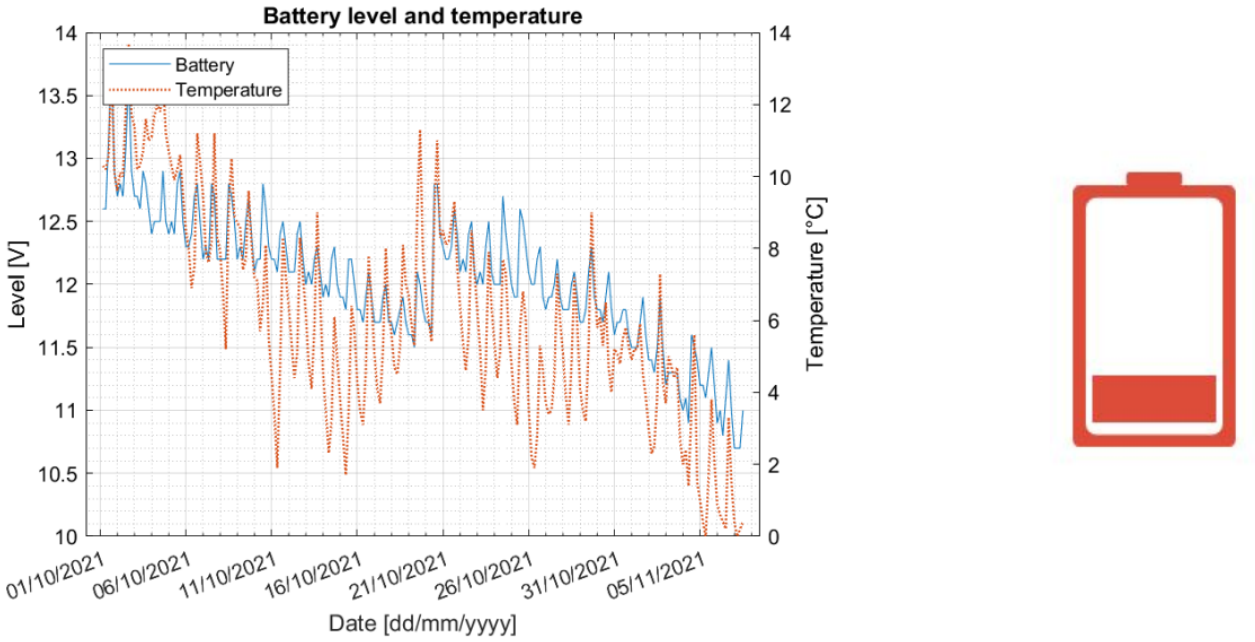

Figure 79. Battery level and control unit temperature variation over time, together with a battery icon displaying the present status of the power supply system

For each datalogger, the report includes a plot displaying the battery level trend over time, as well as the temperature measured by the thermometer integrated in the control unit. Additionally, the graph is paired with an icon representing the status of the power supply system at the time of the report generation, with different levels according to the last value

available. Finally, the numerical value on which this figure is based is specified in a brief paragraph attached to the main plot.

It should be noted that the elaboration software integrates a specific procedure to check the battery level in real time, and it is able to send alert messages if this value falls below a predefined threshold. This process is intended to highlight the presence of an issue that should be immediately addressed to maintain the system functionality. On the other hand, the visualization of the power supply trend over time included in the periodic report is intended to give an overall vision of the system conditions. Therefore, it is especially useful to identify in advance any pattern that could be a symptom of a future power supply failure (i.e., battery level constantly decreasing over time, as in Figure 79), giving the possibility to plan maintenance intervention and restore the system operativity.

7.1.5. Results – Monitoring Tools

This section is the core of the entire document, since it contains the outcomes referred to all monitoring tools installed in the monitored site. It is organized in sub-sections, one for each Array, containing a series of dedicated graphs according to the sensors integrated in the instrumentation. This approach descends from the multi-parametric nature of MUMS tools, which allows to control different physical quantities with a single Array equipping different kind of sensors. On this basis, the software is able to determine the sensor typology and select the most appropriate data representation to include in the report, together with a short comment regarding specific values of interest (e.g., maximum and minimum values, variation over the selected time period, last value available, etc.), in order to give an overall summary of the monitoring activity results referred to a specific time period.

Table 21 lists all supported Links and the corresponding information that can be included in the report, while the following figures display some examples regarding the results representation (namely, Figure 80 and Figure 81 refer to Tilt Link V, Figure 82 to Piezo Link, Figure 83 to Rain Link, and Figure 84 to Klino Link).

Table 21. List of MUMS Links included in the software, together with the corresponding sensor typology and the different information and outcomes included in the automatic report. Monitoring outcomes are related to the reference monitoring period, except where indicated

Link name	**Sensor typology**	**Information included in the report**
Tilt Link V, In Place Link	3D MEMS	▪ 2D local displacements* ▪ 2D cumulative displacements* ▪ Azimuth**
Tilt Link H	3D MEMS	▪ Local subsidence* ▪ Cumulative subsidence*
Piezo Link	Piezometer	▪ Absolute pressure ▪ Water level
Baro Link	Barometer	▪ Atmospheric pressure
Rain Link	Rain gauge	▪ Local Rainfall ▪ Cumulative rainfall**

Therm Link	High-resolution thermometer	▪ Temperature ▪ Maximum and minimum temperature values
Klino Link	3D MEMS	▪ 2D Tilt variation over time ▪ Temperature
Load Link	Load cell	▪ Load variation over time
Pressure Link	Pressure cell	▪ Pressure variation over time
Extensometer Link	1D Extensometer	▪ Deformations ▪ Temperature
3D Extensometer Link	3D Extensometer	▪ 3D deformations
Wire Extensometer Link	Wire Extensometer	▪ Wire length variation over time ▪ Temperature variation over time
Multi-Point Borehole Extensometer (MPBE) Link	Multi-Point Borehole Extensometer	▪ Rod deformations
Crack Link	Crack meter	▪ Crack opening over time
PT100 Link	Resistance thermometer (PT100)	▪ Temperature
Tunnel Link	3D MEMS	▪ 2D Local displacements* ▪ Convergence segments variation over time***
PreConv Link	3D MEMS	▪ 2D Local displacements ▪ 2D Local displacements (pre-convergence phase) ▪ 2D cumulative displacements ▪ 2D cumulative displacements (pre-convergence phase) ▪ Displacement direction
RSN Link	3D MEMS	▪ 2D Tilt variation over time ▪ Temperature
Trigger Link	Electro-mechanical trigger	▪ Trigger activation
G-Shock Link	Shock sensor	▪ Shock sensor activation
G-Flow Link	Accelerometer	▪ 3D acceleration components ▪ Resultant acceleration
ASEcam	Video Camera	▪ Last image acquired by the camera

Related to the reference and entire monitoring periods

**Starting from the reference date*

***Available for Cir Array only*

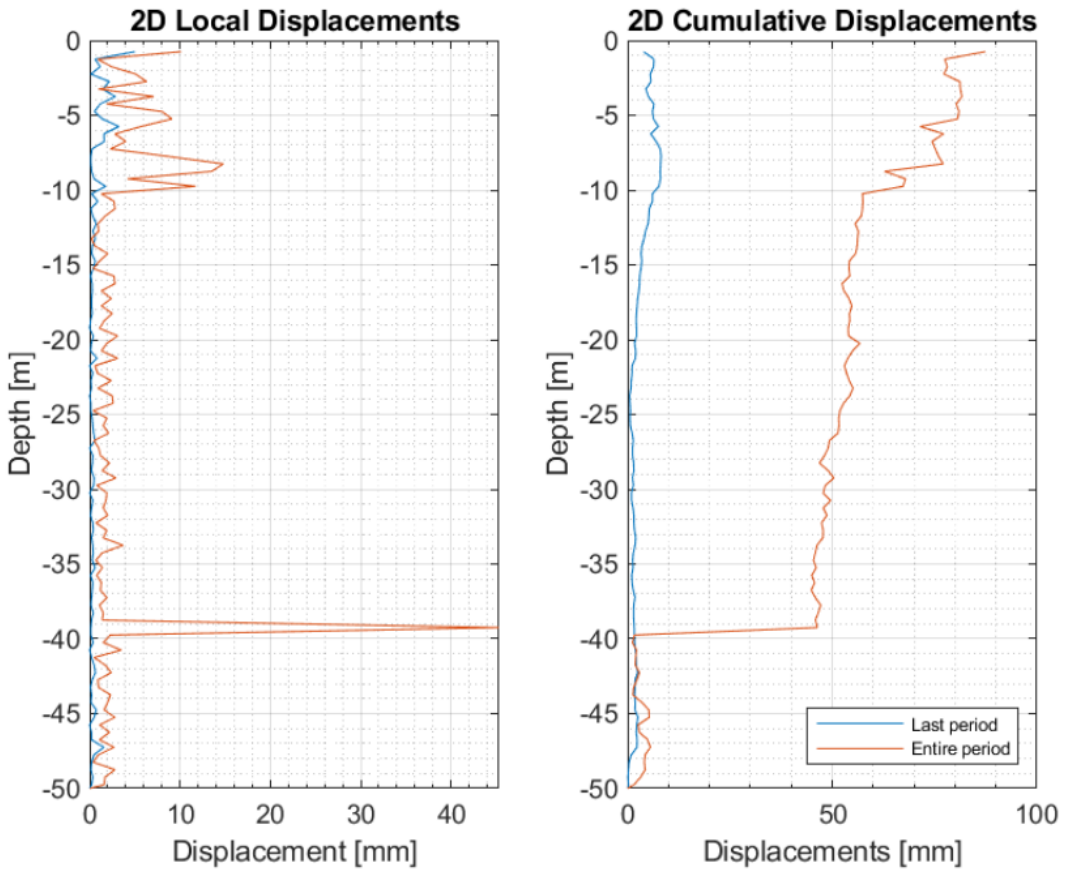

Figure 80. Tilt Link V results: local and cumulative differential displacements along maximum grade direction, related to the reference time period and the entire time period of the monitoring activity

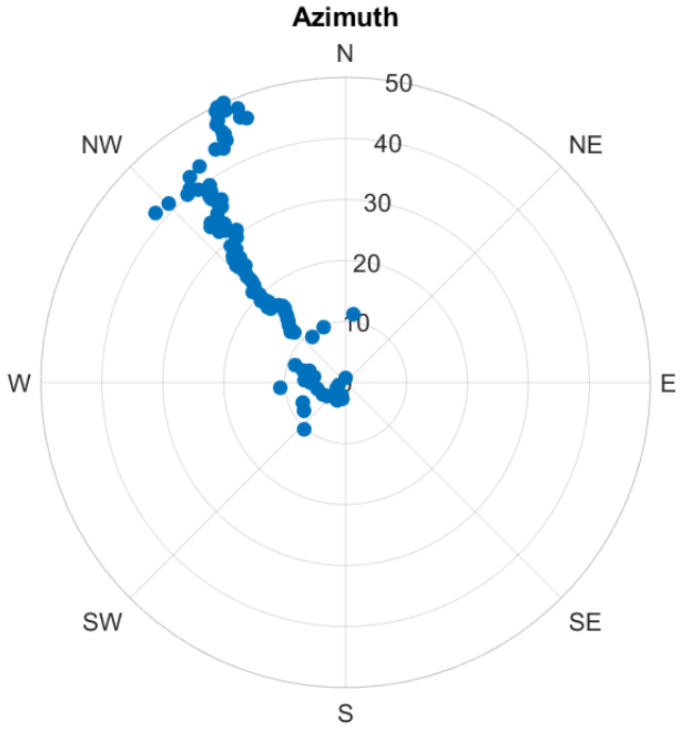

Figure 81. Tilt Link V results: azimuth of cumulative differential displacements vs depth, taking as a reference the beginning of the monitoring activity

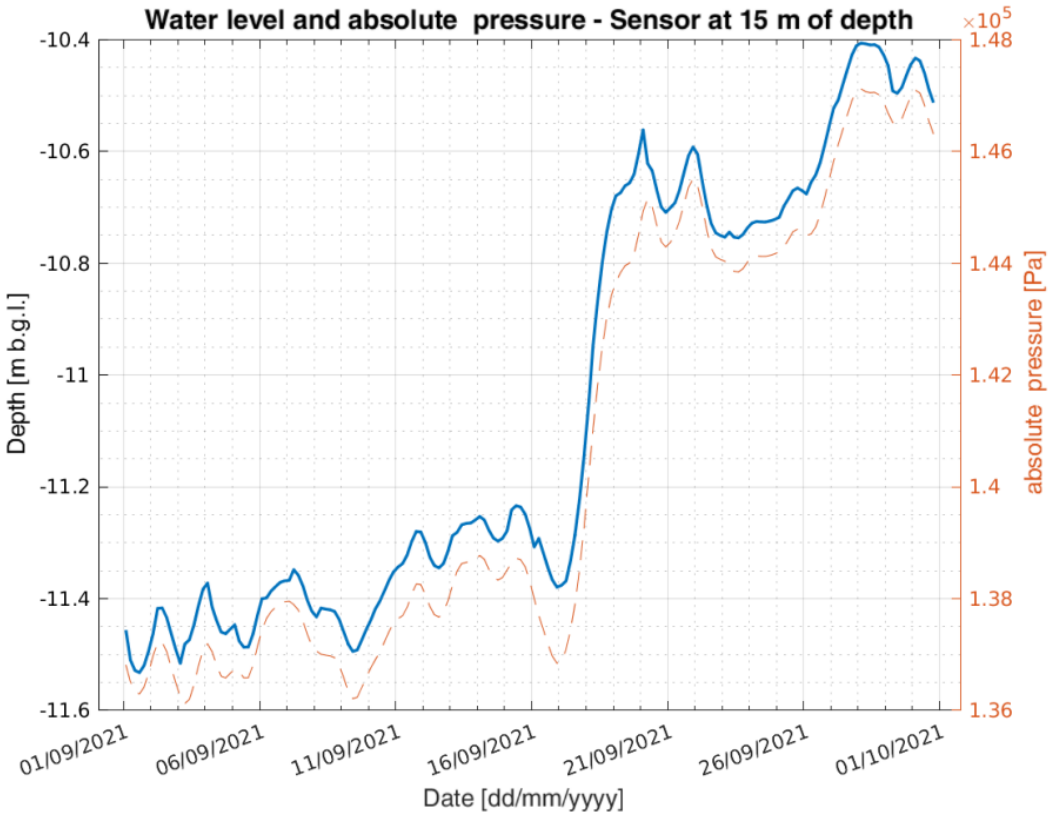

Figure 82. Piezo Link results: water level and absolute pressure values recorded during the reference time period by the sensor placed at a specific depth

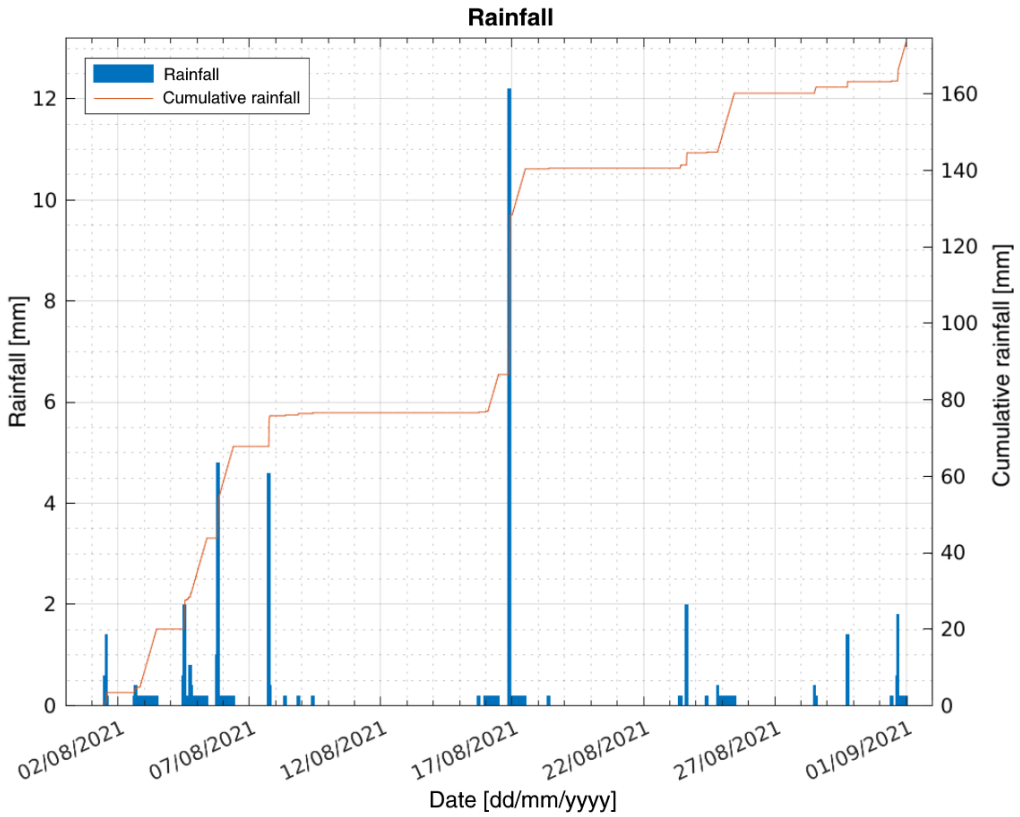

Figure 83. Rain Link results: rainfall trend recorded by the rain gauge during the reference time period, and cumulative rainfall starting from the beginning of the monitoring activity

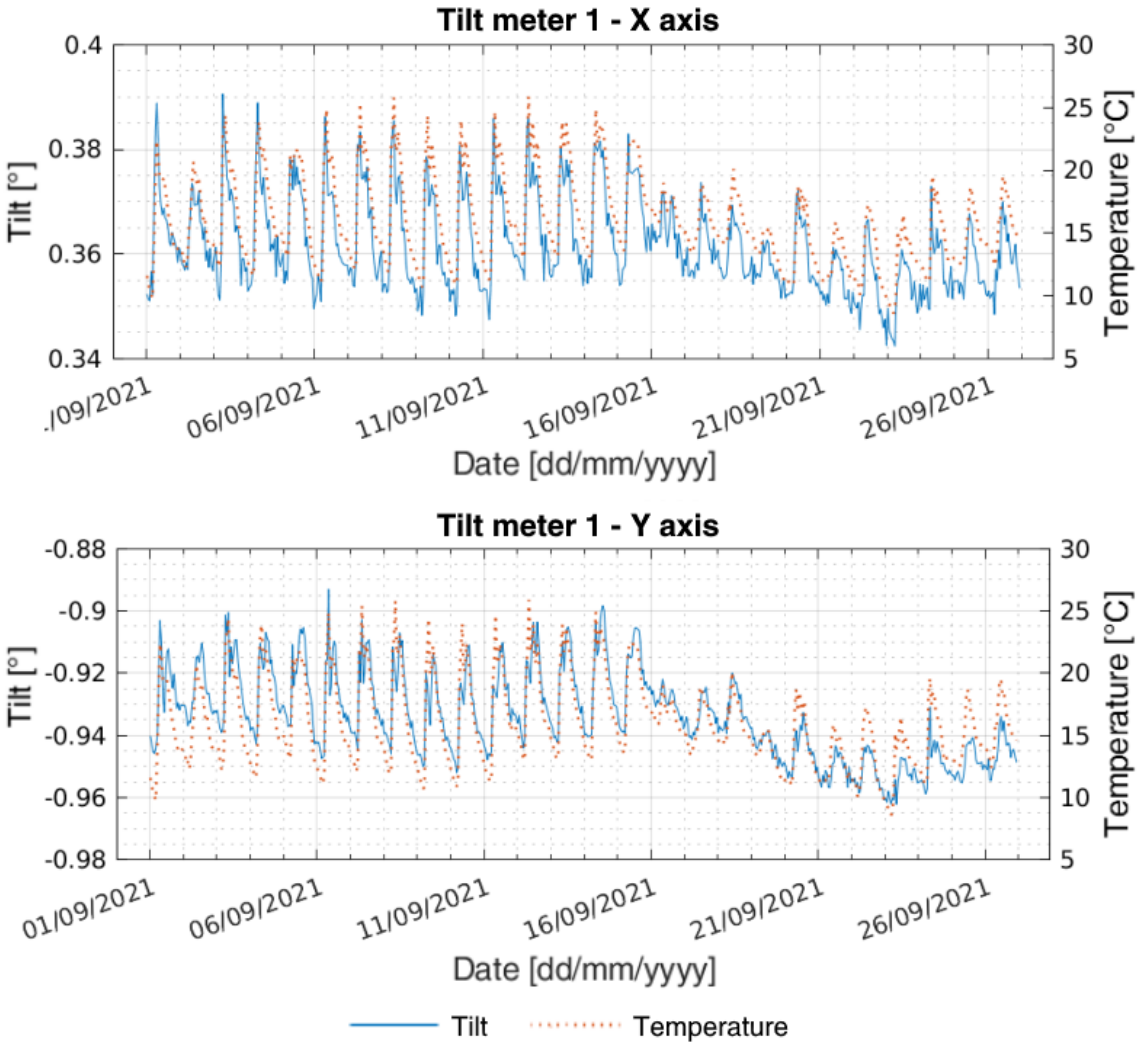

Figure 84. Klino Link results: tilt along X and Y instrumental axes and temperature trend recorded by the MEMS sensor during the reference monitoring period

7.1.6. Results – Correlation between different parameters

This section is strictly related to the previous one, and it is intended to highlight the presence of any possible correlation between the different physical quantities sampled by sensors integrated in the monitoring instrumentation. In order to do so, the software select relevant Links for each Array and compare the sampled values according to pre-defined combinations, aiming to evidence similar patterns and/or cause-effect relationships in the reference time period. The inclusion of these graphical representations is a default operation and does not depend on the actual presence of clear correlations between the parameters of interest. This decision derives from the consideration that such a comparison would provide useful insights on the monitored site behaviour regardless of the positive identification of any correlation between the parameters. Therefore, the identification of actual cause-effect relationships is delegated the user, while the report is intended to provide as much information as possible to assist in this operation.

A list of the cross-correlations that the report can display, with the involved Links and a short description of the objective of each specific representation, is provided in Table 22.

Table 22. List of cross-correlation analyses that can be included in the periodic monitoring report

Links involved	**Parameters**	**Details**
Tilt Link V In Place Link	Displacement	Comparison between the displacement trend measured by the Link (of a specific Array) that recorded the largest displacement during the reference time period, and the water level measured by the piezometer installed in the same Array.
Piezo Link	Water level	
Tilt Link V In Place Link	Displacement	Comparison between the displacement trend measured by the Link (of a specific Array) that recorded the largest displacement during the reference time period, and the rainfall recorded by the rain gauge installed in the same site.
Rain Link	Rainfall	
Piezo Link	Water level	Comparison between the water level variation measured by the piezometer, and the rainfall recorded by the rain gauge installed in the same site.
Rain Link	Rainfall	
Tilt Link V In Place Link	Displacement	Comparison between the displacement trend measured by the Link (of a specific Array) that recorded the largest displacement during the reference time period, the tilt variation of the element monitored with the tilt meter, and the crack opening over time recorded by the crack meter.
Klino Link	Tilt	
Crack Link	Crack opening	
Tilt Link V In Place Link	Displacement	Comparison between the displacement trends measured, for each Array present on site, by the Links that recorded the largest displacement during the reference time period
Tunnel Link (Cir Array)	Displacement	Comparison between displacements recorded by each Array installed on site, referring to specific sectors of the monitored tunnel sections
Tunnel Link (Cir Array)	Displacement	Comparison between displacements measured by the Tunnel Link located at the top of the monitored section, and displacements recorded by the closer PreConv Link installed on the section crown
PreConv Link	Displacement	

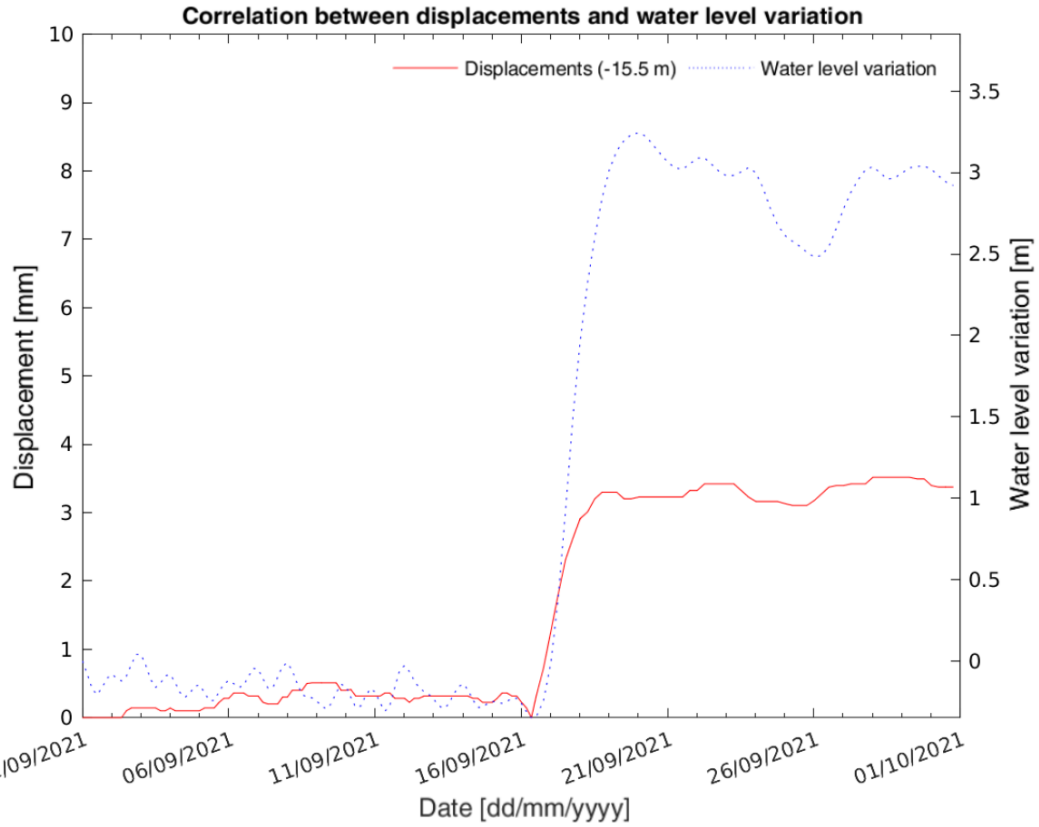

Figure 85. Comparison between the displacement trend measured by the Link that identified the largest displacement during the reference time period, and the water level recorded by the piezometer

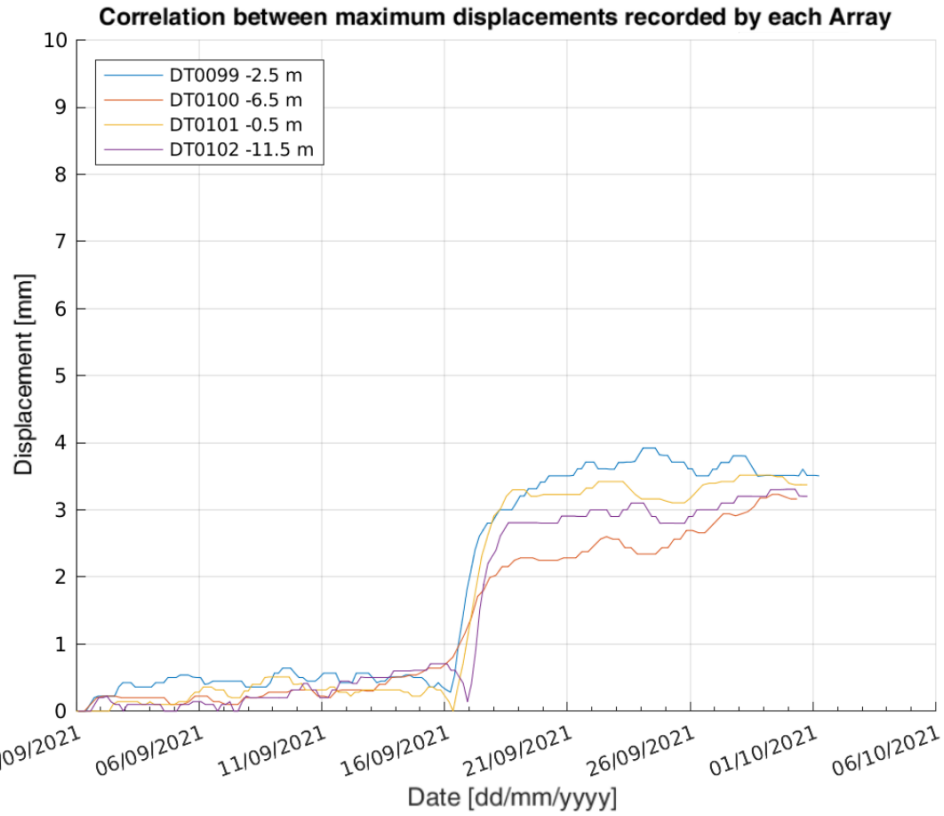

Figure 86. Comparison between maximum displacement data recorded during the reference time period by a series of different Arrays installed in the same monitored site

7.1.7. Appendix

In its last section, the report includes a short description of each monitoring device and sensor located on site. Following a procedure similar to those previously described, the software automatically generates two sub-sections:

- The first one refers to the Arrays typology, and provides a summary of their working principle, elaboration process, and final outcomes.
- The second one is created according to the Arrays previously identified and includes a list of the main features each sensor included in the monitoring instrumentation, outlining also the corresponding physical quantity being measured by it.

7.2. Alert report

While the generation of a periodic report makes for a useful tool to gain insights on the landslide behaviour, providing a general overview on all different quantities monitored, it is not suitable for early warning purposes. In fact, it is essential for an EWS to give the possibility "to take timely action to reduce disaster risks in advance of hazardous events" (United Nations, 2016). It is clear that such an objective could not be achieved with a process applied independently of the occurrence of a potentially critical event, since the relevant information should be delivered as soon as possible after its identification in order to give the possibility to those in charge of the monitoring activity to take proper countermeasures.

With this objective in mind, the toolbox *Matlab Report Generator™* was used to write a software able to generate a more concise document designed for near-real time communications. The so-called "alert report" refers to a specific event and is intended to provide only the essential information needed to understand if the observed phenomenon is evolving towards a potentially hazardous situation. For this reason, its creation takes place in the very last section of the elaboration software, after the application of all criteria and algorithms previously discussed. Unlike the periodic monitoring document, which is customized according to the features of each case study, the alert report takes advantage of a pre-made template designed to include only specific graphs and tables and arranged to fit into a single page.

The different sections of the alert report template are described below, and referenced with the corresponding numbers in Figure 87:

1. Title and date of creation: this section includes the report title (i.e., "Automatic alert report") and the date-time when it was generated by the elaboration software. This information is also included in the file name, in order to avoid duplicates and accidental overwriting.
2. General information: this part of the bulletin summarizes all main information related to the monitoring instrumentation that identified the event under discussion. In particular, the document includes the following details:
    - Name of the monitored site

- ID of the datalogger
- ID of the MUMS Vertical Array
- Number and depth of the node (Tilt Link) that measured the displacement
- OOA date of the identified event

3. Activity level indicator: the alert report includes a coloured logo to assess immediately the activity level represented by the identified event. According to the outcomes of the classification criterion and the comparison with the equivalent displacement threshold, the report is able to show three different colours:
   - Green → Level 5, displacement below the equivalent displacement threshold
   - Orange → Level 4, displacement above the equivalent displacement threshold
   - Red → Level 5, displacement above the equivalent displacement threshold
4. Displacement vs time trend: this section includes the displacements measured in the 30 days preceding the first value included in the potentially critical dataset, evidencing also the OOA date assessed by the acceleration criterion. This graph has the main goal to provide a visual representation to help in the understating of the landslide behaviour, as recorded by the same node that recorded the event of interest, and to have a first evaluation of the entity of the recorded movement.
5. Equivalent displacement vs time trend: the second graph included in the alert report displays the equivalent displacement values, calculated by following the procedure detailed in Chapter 6.2, including the value obtained for the event of interest. It also gives a graphical representation of the equivalent displacement threshold, in order to provide another easily readable indication of the event magnitude.
6. Numerical values: this table reports the main numerical outcomes of the data elaboration, focusing on few key values referred to displacements measured by the Tilt Link indicated in Section 1:
   - Total displacement measured over the reference time period (i.e., 30 days preceding the event of interest)
   - Displacement generated by the event, calculated from the dataset identified by the acceleration criterion
   - Equivalent displacement threshold, evaluated with the procedure previously discussed
7. Legend: in this section it is possible to find a list of all symbols included in both graphs of the alert report, namely:
   - Displacements

- Onset-of-acceleration
- Equivalent displacements
- Displacement generated by the event
- Equivalent displacement threshold

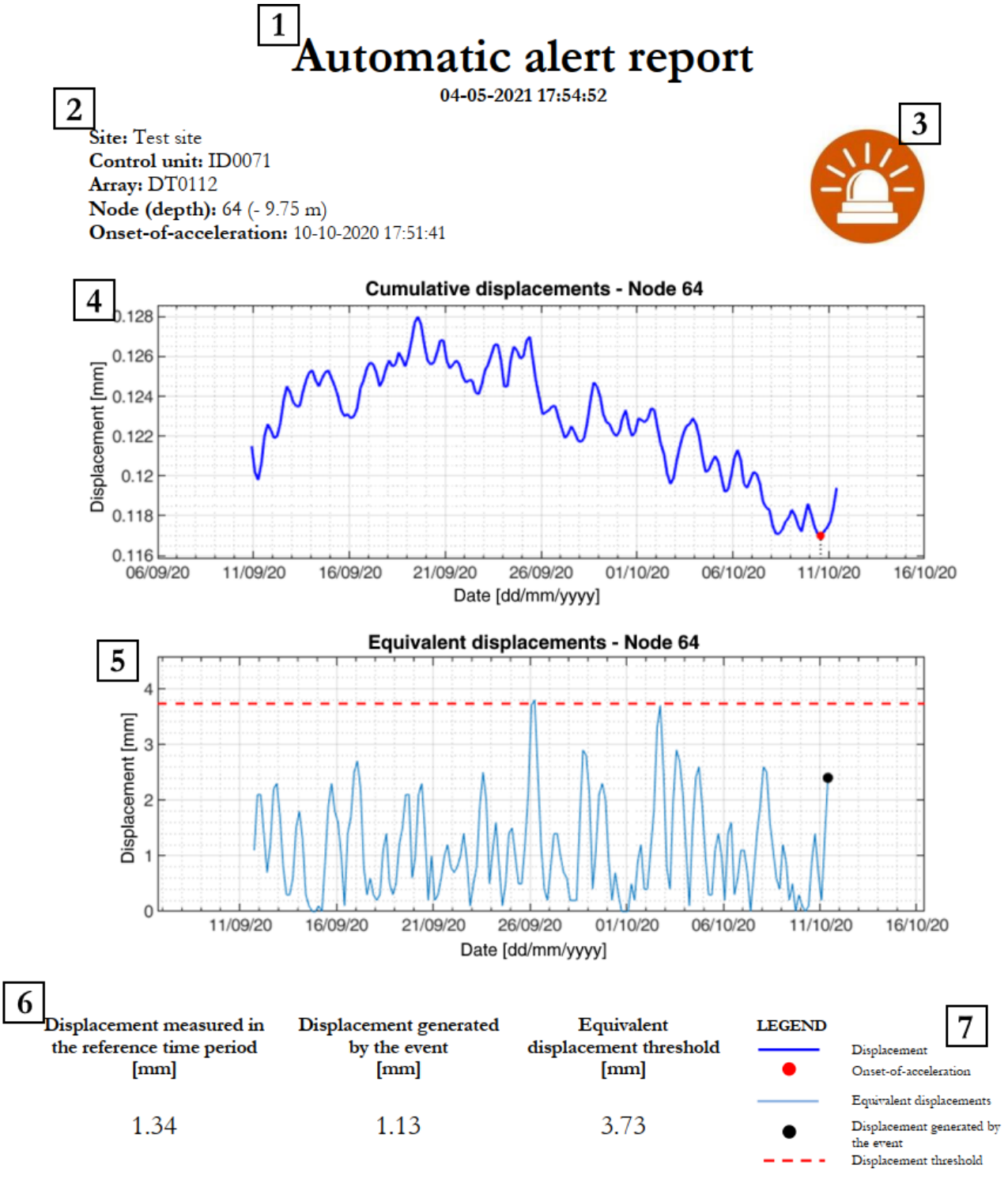

Figure 87. Example of an automatically generated alert report, with indicated the pre-defined sections: 1. Title and date of creation; 2. General information; 3. Activity level indicator; 4. Displacement vs time trend; 5. Equivalent displacement vs time trend; 6. Numerical values; 7. Legend

Chapter 8. Conclusions

8.1.Summary and conclusions

The present work focused on the development, validation, and application of a series of methodologies intended to analyse the occurrence of potentially critical landslide events. In particular, the main objective of this thesis involved the automatic analysis of monitoring data, the application of several algorithms to assess the hazard posed by the event, and the subsequent dissemination of appropriate alert messages. Figure 88 summarizes the thesis structure, defining the main topics and highlighting the connection between the different components.

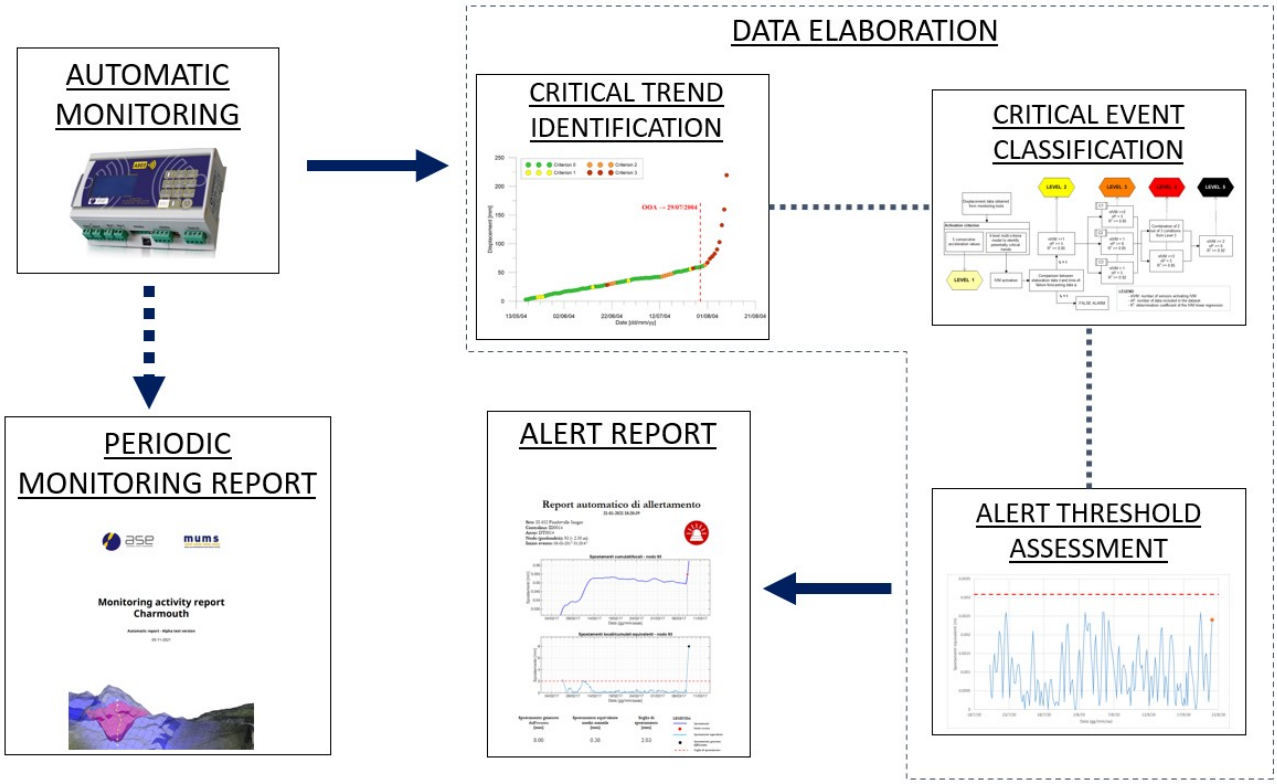

Figure 88. Flow diagram summarizing the different topics included in the thesis

After describing the main theoretical elements on which the work is based, the thesis focused on the advantages deriving from the application of automatic monitoring systems. Particular attention is dedicated to instrumentation based on IoNH (Internet of Natural Hazards) approach, representing a design concept where the implementation of Internet of Things principles allows different components of the system to interact and exchange data. The advantages of this approach are reported through a series of examples provided by monitoring devices based on MUMS (Modular Underground Monitoring System) technology. MUMS was initially designed as an automatic inclinometer, and has been subsequently developed to adapt to different geotechnical scenarios, keeping the IoNH structure as the core working principle. This approach permits a constant check of instrumentation functionality, both in terms of sensor operativity and control unit conditions. Moreover, the high sampling frequency achievable by IoNH-based devices gives the possibility to introduce statistical analyses in the

elaboration process, in order to validate the monitoring outcomes. Other features involve the remote control of the power supply system conditions, the assessment of reliable cause–effect relationships related to multi-parameter information, and the activation of alert procedures and external devices.

The first step in the data elaboration process relies on a multi-criteria algorithm able to identify automatically an accelerating trend starting from displacement monitoring data. Specifically, the proposed approach relies on a drop-down sequence composed of four steps applied to each single data sample, with the objective of identifying specific variations in the landslide behaviour. The development process involved a series of parametric analyses, aimed to calibrate the main parameters included in the algorithm. The final result is a four-level process that allows to identify the OOA (onset-of-acceleration) point referred to the accelerating trend. A real-time acquisition was simulated for three case studies, where a collapse was observed, taken from historical landslides studied in scientific literature. Outcomes of the analyses performed on available displacement datasets underlined the algorithm ability to identify two different stages of the phenomenon evolution over time. Moreover, the comparison of the estimated OOA point with the acceleration curves reported for each case study underlined the positive result of the multi-criteria methodology in locating the beginning of the critical acceleration phase.

Following the critical trend identification, a classification procedure was introduced to define the alert level for the event of interest. The evaluation depends on three different features, namely the number of values included in each dataset, the number of positive outcomes generated by the OOA identification process, and the value of the determination coefficient obtained from the application of the linear Inverse Velocity Method to the monitoring data. Each one of these parameters represents a specific aspect of the landslide behaviour, and their increment corresponds to an increasingly critical condition. In fact, datasets including a higher number of points corresponds of a more consistent accelerating trend, and multiple OOA identifications are an indication that the displacement is involving different sectors of the monitored element. Finally, the determination coefficient refers to the application of a forecasting method to the selected dataset, therefore higher values of R^2 represent a more reliable outcome of the forecasting analysis. All these parameters are arranged in a 5-level structure to automatically provide a classification of the potentially critical events, according to the features resulting from the analysis. The algorithm has been continuously tested over time on several monitored sites, elaborating roughly 23’000 datasets each day for several months. The present work reports four events, referred to two different case studies, displaying for each one the corresponding level and underlining the ability of the proposed approach to provide further information regarding the event entity. Among these, it is also included a back-analysis of the only event that achieved the highest alert level (namely Level 5), which is also the only event recorded by MUMS-based instrumentation that ultimately led to a slope collapse.

After the classification procedure, the data elaboration goes through a comparison with alert thresholds defined according to two different methodologies. The first approach aims to provide

a generalized criterion useful to compare events with different features and to help defining reference values for specific case studies. This is achieved through a normalization of available monitoring data, resulting in a dimensionless parameter deriving from velocity values recorded by monitoring instrumentation. The method is applied by simulating a real-time acquisition of monitoring data taken from two case studies reported in scientific literature. Results obtained for both landslides underlined the ability of the proposed method to provide a reliable tool to describe the accelerating trend of a landslide approaching failure. After the normalization procedure, monitoring data were in good agreement with generalized velocity curves, allowing to use them as a reference to assess warning levels.

The second algorithm was designed with the express purpose of identifying any false alarm coming out of the classification algorithm. In order to achieve this task, this thesis introduces the concept of equivalent displacement, defined as the displacement generated in a time interval equal to the one showed by the potentially critical event. When referred to data sampled prior to the event of interest, they can give an indication of the past behaviour of the monitored element. Therefore, they are able to establish a term of comparison in order to understand if the recorded event generated a displacement magnitude which does not correspond to a critical occurrence if compared to previously observed events a data trend, despite being geometrically compatible with an accelerating pattern. The thesis reports a series of examples referring to different alert levels obtained from the classification algorithm, underlining the ability of the proposed model to define an effective threshold value to compare the potentially critical event with previously observed trends. In particular, the Level 5 event previously discussed is analysed in this phase, and represents the only case study where the recorded displacements overcame the assessed threshold, furtherly confirming the exceptional nature of the recorded event.

Finally, the work focuses its attention on the development of new approaches for the dissemination of relevant information obtained from the previously described methodologies. This regards not only the features of a potentially critical event, but also the large amount of knowledge acquired over the entire monitoring period thanks to the implementation of automatic instrumentation, which is fundamental to have a proper comprehension of the studied phenomenon. For this reason, the first algorithm presented in this work aims to produce a periodic report intended to provide a general overview of monitoring outcomes sampled over a predefined time period. The document structure comprises several sections, which are dynamically integrated according to the monitoring system features. The algorithm, based on the toolbox *Matlab Report Generator™,* is able to represent data deriving from more than 20 different sensors and dataloggers, including also the most relevant numerical values recorded during the reference time period. Moreover, depending on the instrumentation installed on-site, the report can include, in the same graph, monitoring results coming from different type of devices with the objective to evidence the presence of any correlation between parameters of interest.

Being generated periodically, this document was designed as a practical tool for the global understating of the monitored site behaviour, and therefore not suitable for early warning

applications. Instead, the second algorithm presented in this thesis was specifically developed for this purpose, with the intention to concentrate all relevant data regarding a potentially critical event in a short report, able to provide the essential information for a first interpretation of the event of interest. The result is a 1-page bulletin, automatically created following the fulfilment of all conditions introduced by previously described criteria. After listing the main features of the monitored site, the alert report displays two graphs, namely the slope displacement and the equivalent displacement trends measured in the reference time period (i.e., 30 days) preceding the event of interest. Moreover, a table includes the numerical values for the total displacement measured over the reference time period, the displacement generated by the event, and the equivalent displacement threshold, in order to help the user to evaluate the entity of the observed phenomenon.

8.2. Future developments

Starting from the results of the present work, future research activities could focus on different aspects, from the selection process of the monitoring instrumentation to the implementation of other algorithms in the elaboration procedure.

As previously noted, the real-time application of the proposed methodologies involved the application of a specific set of monitoring systems, namely MUMS-based instrumentation. Nonetheless, there are several other devices that are able to achieve the requirements needed for early warning purposes, and are capable to provide the parameters needed for the application of the algorithms here described. Therefore, a potential development would involve the integration of the elaboration process into monitoring systems based on different sensors, in order to test the compatibility of the approach with data sampled by other typologies of monitoring instrumentation. Moreover, this could provide additional data and information to refine the criteria parameters, further improving their reliability and robustness.

Another interesting aspect to investigate is the integration of forecasting methodologies based on Machine Learning (ML) algorithms and Neural Network models for the prediction of landslide deformations. Thanks to more recent technological advancements, the implementation of Artificial Intelligence (AI) for the analysis of monitoring data has gained increasing attention, providing positive outcomes in several case studies (e.g., Jiang et al., 2021; Ma et al., 2020; Lian et al., 2014; Wang et al 2021; Zhu et al 2018). From this perspective, it would be possible to rely on displacement time series to provide useful information concerning the past behaviour of the monitored element and helping in the interpretation and prediction of possible future trends. For these reasons, the implementation of AI-based procedures would greatly improve the system ability to describe the phenomenon evolution. Additionally, it could be possible to apply the developed methodologies to displacements forecasted with Machine Learning algorithms, thus being able to identify further in advance the onset of potentially critical events.

Acknowledgements

Upon the hearth the fire is red,
Beneath the roof there is a bed;
But not yet weary are our feet,
Still round the corner we may meet
A sudden tree or standing stone
That none have seen but we alone.

J.R.R. Tolkien – The Lord of the Rings

The past three years have been full of great experiences, stimulating challenges, and inspiring collaborations, all culminating in the work here presented. It is safe to say that I would have never been able to achieve any of this without the help of those who supported and encouraged me during this journey.

For these reasons, my heartfelt gratitude goes firstly to prof. Andrea Segalini, who introduced me to these fascinating topics and motivated me with new ideas and challenges throughout the duration of my Ph.D. course. I would like also to thank prof. Marian Drusa and the entire team of the University of Žilina for their hospitality during my stay in Slovakia.

During these years I was lucky enough to work with an amazing team of colleagues and friends, sharing many days of hard work as well as a lot of fun moments. Therefore, I would like to thank Roberto, Edoardo, and especially Andrea, for their invaluable presence and contribution to what I have done and to who I am today. I am sure that our collaboration will go on, so keep the whiteboard clean and check that those sharpies are still working, I could have some new ideas I would like to discuss with you guys!

A special thanks goes also to the group of my long-time friends from my hometown, with whom I shared so many unforgettable experiences over the years. We may have chosen different paths, but in the end we always managed to keep our friendship alive and thriving, and this means a lot to me.

The final and most important thanks go to my family. The importance of their continuous support cannot be emphasized enough, and I will be always grateful for their trust and encouragements over all these years.

References

Abraham, M.T., Satyam, N., Pradhan, B., Alamri, A.M., 2020. *IoT-Based Geotechnical Monitoring of Unstable Slopes for Landslide Early Warning in the Darjeeling Himalayas.* Sensors 20, 2611. https://doi.org/10.3390/s20092611

Alam, M.R., Zain, M.F.M., Kaish, A.B.M.A., Jamil, M., 2015. *Underground soil and thermal conductivity materials based heat reduction for energy-efficient building in tropical environment.* Indoor and Built Environment 24, 185–200. https://doi.org/10.1177/1420326X13507591

Allasia, P., Godone, D., Giordan, D., Guenzi, D., Lollino, G., 2020. *Advances on Measuring Deep-Seated Ground Deformations Using Robotized Inclinometer System.* Sensors 20, 3769. https://doi.org/10.3390/s20133769

Allasia, P., Manconi, A., Giordan, D., Baldo, M., Lollino, G., 2013. *ADVICE: A New Approach for Near-Real-Time Monitoring of Surface Displacements in Landslide Hazard Scenarios.* Sensors 13, 8285–8302. https://doi.org/10.3390/s130708285

Angeli, M.-G., Gasparetto, P., Silvano, S., Tonnetti, G., 1988. *An automatic recording system to detect the critical stability conditions in slopes.* Proceeding of the 5th International Symposium on Landslides (ISL), Lausanne, 1988. Vol. 1 375–378.

Angeli, M.-G., Pasuto, A., Silvano, S., 2000. *A critical review of landslide monitoring experiences.* Engineering Geology 55, 133–147. https://doi.org/10.1016/S0013-7952(99)00122-2

Arbanas, Ž., Jagodnik, V., Ljutić, K., Vivoda, M., Dugonjić Jovančević, S., Peranić, J., 2014. *Remote monitoring of a landslide using an integration of GPS, TPS and conventional geotechnical monitoring methods.* 1st Regional Symposium on Landslides in the Adriatic-Balkan Region "Landslide and Flood Hazard Assessment"

Ardizzone, F., Cardinali, M., Galli, M., Guzzetti, F., Reichenbach, P., 2007. *Identification and mapping of recent rainfall-induced landslides using elevation data collected by airborne Lidar.* Natural Hazards and Earth System Sciences 7, 637–650. https://doi.org/10.5194/nhess-7-637-2007

Assis Dias, M.C. de, Saito, S.M., Alvalá, R.C. dos S., Seluchi, M.E., Bernardes, T., Camarinha, P.I.M., Stenner, C., Nobre, C.A., 2020. *Vulnerability index related to populations at-risk for landslides in the Brazilian Early Warning System (BEWS).* International Journal of Disaster Risk Reduction 49, 101742. https://doi.org/10.1016/j.ijdrr.2020.101742

Atzori, L., Iera, A., Morabito, G., 2010. *The Internet of Things: A survey.* Computer Networks 54, 2787–2805. https://doi.org/10.1016/j.comnet.2010.05.010

Bai, D., Tang, J., Lu, G., Zhu, Z., Liu, T., Fang, J., 2020. *The design and application of landslide monitoring and early warning system based on microservice architecture.*

Geomatics, Natural Hazards and Risk 11, 928–948. https://doi.org/10.1080/19475705.2020.1766580

Barra, A., Monserrat, O., Mazzanti, P., Esposito, C., Crosetto, M., Mugnozza, G.S., 2016. *First insights on the potential of Sentinel-1 for landslides detection.* Geomatics, Natural Hazards and Risk 7, 1874–1883. https://doi.org/10.1080/19475705.2016.1171258

Bazin, S., 2012. *Guidelines for landslide monitoring and early warning systems in Europe - Design and required technology (Deliverable No. D4.8).* Living with landslide risk in Europe: Assessment, effects of global change, and risk management strategies. ICG - International Centre of Geohazards.

Bentley, S.P., Siddle, H.J., 2000. *New Tredegar landslide, Rhymney Valley.* In: Landslides and Landslide Management in South Wales, Geological Series N° 18. Siddle H.J., Bromhead E.N., Bassett M.G. (eds), National Museum and Galleries of Wales, Cardiff, pp. 71–74.

Bonnard, C., Steinmann, G., 1990. *Continuous measurement of landslide movements.* Presented at the Conference geotechnical Instrumentation in Civil Engineering Projects, Thomas Telford, London, pp. 177–189.

Bozzano, F., Cipriani, I., Mazzanti, P., Prestininzi, A., 2014. *A field experiment for calibrating landslide time-of-failure prediction functions.* International Journal of Rock Mechanics and Mining Sciences 67, 69–77. https://doi.org/10.1016/j.ijrmms.2013.12.006

Bozzano, F., Cipriani, I., Mazzanti, P., Prestininzi, A., 2011. *Displacement patterns of a landslide affected by human activities: insights from ground-based InSAR monitoring.* Natural Hazards 59, 1377–1396. https://doi.org/10.1007/s11069-011-9840-6

Bozzano, F., Mazzanti, P., Moretto, S., 2018. *Discussion to: 'Guidelines on the use of inverse velocity method as a tool for setting alarm thresholds and forecasting landslides and structure collapses' by T. Carlà, E. Intrieri, F. Di Traglia, T. Nolesini, G. Gigli and N. Casagli.* Landslides 15, 1437–1441. https://doi.org/10.1007/s10346-018-0976-2

Brabb, E.E., 1993. *Proposal for worldwide landslide hazard maps.* Proceedings of the Seventh International Conference and Field Workshop on Landslides, Czech and Slovak Republics, August 28-September 15, 1993, pp. 15–27.

Brawner, C.O., Stacey, P.F., 1979. *Chapter 21 - Hogarth Pit Slope Failure, Ontario, Canada.* In: Voight, B. (Ed.), Developments in Geotechnical Engineering, Rockslides and Avalanches, 2. Elsevier, pp. 691–707. https://doi.org/10.1016/B978-0-444-41508-0.50029-6

Bressani, L.A., Simoes, E.B., Ogura, A.T., Boesing, I.J., Hanaeur, D.S., Balbinot, G., 2018. *A Monitoring System for Landslides and Geotechnical Works Using Statistical and Artificial Intelligence Model.* In: Proceedings from the 10th International Symposium on Field Measurements in Geomechanics (FMGM2018), SESSION 2 - Remote System, Emerging Technology and Environmental Monitoring. Presented at the International Symposium on FIeld Measurements in Geomechanics, Rio de Janeiro, 16-20 July 2018.

Brox, D., Newcomen, W., 2003. *Utilizing Strain Criteria to Predict Highwall Stability Performance.* In: Proceedings of ISRM 2003 -Technology Roadmap for Rock Mechanics, Sandton, South Africa. 8-12 September. South African Institute of Mining and Metallurgy, Johannesburg.

Calvello, M., d'Orsi, R.N., Piciullo, L., Paes, N., Magalhaes, M., Lacerda, W.A., 2015. *The Rio de Janeiro early warning system for rainfall-induced landslides: Analysis of performance for the years 2010–2013.* International Journal of Disaster Risk Reduction 12, 3–15. https://doi.org/10.1016/j.ijdrr.2014.10.005

Carey, J., 2011. *The progressive development and post-failure behaviour of deep-seated landslide complexes.* Doctoral Thesis, Durham University.

Carlà, T., Farina, P., Intrieri, E., Botsialas, K., Casagli, N., 2017a. *On the monitoring and early-warning of brittle slope failures in hard rock masses: Examples from an open-pit mine.* Engineering Geology 228, 71–81. https://doi.org/10.1016/j.enggeo.2017.08.007

Carlà, T., Intrieri, E., Di Traglia, F., Nolesini, T., Gigli, G., Casagli, N., 2017b. *Guidelines on the use of inverse velocity method as a tool for setting alarm thresholds and forecasting landslides and structure collapses.* Landslides 14, 517–534. https://doi.org/10.1007/s10346-016-0731-5

Carri, A., 2019. *Innovative monitoring instrumentations and methods for landslide risk management and mitigation.* Doctoral Thesis, Università degli Studi di Parma.

Carri, A., Chiapponi, L., Giovanelli, R., Segalini, A., 2016. *Integrated analysis of data collected by an innovative monitoring system and results of a 3D numerical model in Boschetto landslide.* In: Aversa, S., Cascini, L., Picarelli, L., Scavia, C. (Eds.), Landslides and Engineered Slopes. Experience, Theory and Practice. 31 July 2016, CRC Press, London.

Carri, A., Valletta, A., Cavalca, E., Savi, R., Segalini, A., 2021. *Advantages of IoT-Based Geotechnical Monitoring Systems Integrating Automatic Procedures for Data Acquisition and Elaboration.* Sensors 21, 2249. https://doi.org/10.3390/s21062249

Carri, A., Valletta, A., Segalini, A., Savi, R., 2019. *On-site applications of innovative tools for deformation monitoring in underground excavations.* In: Fontoura, S.A.B., Rocca, J.R., Pavòn Mendoza, J. (Eds.), Rock Mechanics for Natural Resources and Infrastructure Development. Proceedings of the 14th International Congress on Rock Mechanics and Rock Engineering (ISRM 2019), Foz do Iguassu, Brazil.

Casagli, N., Guzzetti, F., Jaboyedoff, M., Nadim, F., Petley, D., 2017. *Hydrological risk: landslides.* In: Poljanšek, K., Marín Ferrer, M., De Groeve, T., Clark, I. (Eds.), Science for Disaster Risk Management 2017: Knowing Better and Losing Less., EUR 28034 EN. Publications Office of the European Union, Luxembourg, p. 19.

Castagnetti, C., Bertacchini, E., Corsini, A., Capra, A., 2013. *Multi-sensors integrated system for landslide monitoring: critical issues in system setup and data management*. European Journal of Remote Sensing 46, 104–124. https://doi.org/10.5721/EuJRS20134607

Chaturvedi, P., Thakur, K.K., Mali, N., Kala, V.U., Kumar, S., Yadav, S., Dutt, V., 2018. *A Low-Cost IoT Framework for Landslide Prediction and Risk Communication*. In: Quasay, H. (Ed.), Internet of Things A to Z. John Wiley & Sons, Ltd, pp. 593–610. https://doi.org/10.1002/9781119456735.ch21

Coe, J.A., Ellis, W.L., Godt, J.W., Savage, W.Z., Savage, J.E., Michael, J.A., Kibler, J.D., Powers, P.S., Lidke, D.J., Debray, S., 2003. *Seasonal movement of the Slumgullion landslide determined from Global Positioning System surveys and field instrumentation, July 1998–March 2002.* Engineering Geology, Remote sensing and monitoring of landslides 68, 67–101. https://doi.org/10.1016/S0013-7952(02)00199-0

Corcoran, J., Davies, C.M., 2018. *Monitoring power-law creep using the Failure Forecast Method*. International Journal of Mechanical Sciences 140, 179–188. https://doi.org/10.1016/j.ijmecsci.2018.02.041

Corominas, J., Moya, J., Lloret, A., Gili, J.A., Angeli, M.G., Pasuto, A., Silvano, S., 2000. *Measurement of landslide displacements using a wire extensometer*. Engineering Geology 55, 149–166. https://doi.org/10.1016/S0013-7952(99)00086-1

Corsini, A., Castagnetti, C., Bertacchini, E., Rivola, R., Ronchetti, F., Capra, A., 2013. *Integrating airborne and multi-temporal long-range terrestrial laser scanning with total station measurements for mapping and monitoring a compound slow moving rock slide*. Earth Surface Processes and Landforms 38, 1330–1338. https://doi.org/10.1002/esp.3445

Cremona, C., Santos, J., 2018. *Structural Health Monitoring as a Big-Data Problem*. Structural Engineering International 28, 243–254. https://doi.org/10.1080/10168664.2018.1461536

Crippa, C., Franzosi, F., Zonca, M., Manconi, A., Crosta, G.B., Dei Cas, L., Agliardi, F., 2020. *Unraveling Spatial and Temporal Heterogeneities of Very Slow Rock-Slope Deformations with Targeted DInSAR Analyses*. Remote Sensing 12, 1329. https://doi.org/10.3390/rs12081329

Crosetto, M., Monserrat, O., Cuevas-González, M., Devanthéry, N., Crippa, B., 2016. *Persistent Scatterer Interferometry: A review. ISPRS Journal of Photogrammetry and Remote Sensing*. Theme issue "State-of-the-art in photogrammetry, remote sensing and spatial information science" 115, 78–89. https://doi.org/10.1016/j.isprsjprs.2015.10.011

Crosta, G.B., Agliardi, F., 2002. *How to obtain alert velocity thresholds for large rockslides.* Physics and Chemistry of the Earth, Parts A/B/C 27, 1557–1565. https://doi.org/10.1016/S1474-7065(02)00177-8

Crosta, G.B., Agliardi, F., Rivolta, C., Alberti, S., Dei Cas, L., 2017. *Long-term evolution and early warning strategies for complex rockslides by real-time monitoring*. Landslides 14, 1615–1632. https://doi.org/10.1007/s10346-017-0817-8

Crozier, M.J., 1995. *Landslide hazard assessment, theme report.* In: Bell, D. (Ed.) Landslides: Proceedings of the 6th International Symposium on Landslides, 10-14 February 1992, Christchurch, Vol. 1. Balkema, Rotterdam, pp. 1843–1848.

Cruden, D.M., Masoumzadeh, S., 1987. *Accelerating creep of the slopes of a coal mine*. Rock Mechanics and Rock Engineering 20, 123–135. https://doi.org/10.1007/BF01410043

Dai, F.C., Lee, C.F., Ngai, Y.Y., 2002. *Landslide risk assessment and management: an overview*. Engineering Geology 64, 65–87.

Dasenbrock, D.D., Abdoun, T., Bennett, V., 2012. *Real-Time Structural Health Monitoring of Landslides and Geotechnical Assets with ShapeAccelArrays.* Advances in Geotechnical Engineering - Proceedings of the Geo-Frontiers 2011 Conference, pp. 1585–1594. https://doi.org/10.1061/41165(397)162

Depietri, Y., 2020. *The social–ecological dimension of vulnerability and risk to natural hazards*. Sustainability Science 15, 587–604. https://doi.org/10.1007/s11625-019-00710-y

Di Biagio, E., Kjekstad, O., 2007. *Early Warning, Instrumentation and Monitoring Landslides* In: Proceedings of the 2nd Regional Training Course, RECLAIM II, Phuket, Thailand.

Di Matteo, L., Romeo, S., Kieffer, D.S., 2017. *Rock fall analysis in an Alpine area by using a reliable integrated monitoring system: results from the Ingelsberg slope (Salzburg Land, Austria).* Bulletin of Engineering Geology and the Environment 76, 413–420. https://doi.org/10.1007/s10064-016-0980-5

Dick, G.J., Eberhardt, E., Cabrejo-Liévano, A.G., Stead, D., Rose, N.D., 2015. *Development of an early-warning time-of-failure analysis methodology for open-pit mine slopes utilizing ground-based slope stability radar monitoring data*. Canadian Geotechnical Journal 52, 515–529. https://doi.org/10.1139/cgj-2014-0028

Drusa, M., Bulko, R., 2016. *Rock Slide Monitoring by Using TDR Inclinometers*. Civil and Environmental Engineering 12, 137–144. https://doi.org/10.1515/cee-2016-0019

Dunnicliff, J., 1988. *Geotechnical Instrumentation for Monitoring Field Performance*. John Wiley & Sons, Ltd, New York.

Dunnicliff, J., Marr, W.A., Standing, J., 2012. *Chapter 94 Principles of geotechnical monitoring*. In: ICE Manual of Geotechnical Engineering: Volume II, ICE Manuals. Thomas Telford Ltd, pp. 1363–1377. https://doi.org/10.1680/moge.57098.1363

Eberhardt, E., 2013. *Extensometers*. In: Bobrowsky, P.T. (Ed.), Encyclopedia of Natural Hazards. Springer Netherlands, Dordrecht, pp. 306–307. https://doi.org/10.1007/978-1-4020-4399-4_127

Eidsvig, U.M.K., Papathoma-Köhle, M., Du, J., Glade, T., Vangelsten, B.V., 2014. *Quantification of model uncertainty in debris flow vulnerability assessment*. Engineering Geology 181, 15–26. https://doi.org/10.1016/j.enggeo.2014.08.006

Fabris, M., 2019. *Coastline evolution of the Po River Delta (Italy) by archival multi-temporal digital photogrammetry.* Geomatics, Natural Hazards and Risk 10, 1007–1027. https://doi.org/10.1080/19475705.2018.1561528

Federico, A., Popescu, M., Elia, G., Fidelibus, C., Internò, G., Murianni, A., 2012. *Prediction of time to slope failure: a general framework*. Environmental Earth Sciences 66, 245–256. https://doi.org/10.1007/s12665-011-1231-5

Fell, R., 1994. *Landslide risk assessment and acceptable risk*. Canadian Geotechnical Journal 31(2), April 1994. https://doi.org/10.1139/t94-031

Frigerio, S., Schenato, L., Bossi, G., Cavalli, M., Mantovani, M., Marcato, G., Pasuto, A., 2014. *A web-based platform for automatic and continuous landslide monitoring: The Rotolon (Eastern Italian Alps) case study.* Computers & Geosciences 63, 96–105. https://doi.org/10.1016/j.cageo.2013.10.015

Frodella, W., Ciampalini, A., Gigli, G., Lombardi, L., Raspini, F., Nocentini, M., Scardigli, C., Casagli, N., 2016. *Synergic use of satellite and ground based remote sensing methods for monitoring the San Leo rock cliff (Northern Italy).* Geomorphology 264, 80–94. https://doi.org/10.1016/j.geomorph.2016.04.008

Froese, C.R., Moreno, F., 2014. *Structure and components for the emergency response and warning system on Turtle Mountain, Alberta, Canada*. Natural Hazards 70, 1689–1712. https://doi.org/10.1007/s11069-011-9714-y

Fujisawa, K., Marcato, G., Nomura, Y., Pasuto, A., 2010. *Management of a typhoon-induced landslide in Otomura (Japan).* Geomorphology, Recent advances in landslide investigation 124, 150–156. https://doi.org/10.1016/j.geomorph.2010.09.027

Fukui, K., Okubo, S., 1997. *Life expectancy and tertiary creep for rock*. In: Proceedings of Fall Meeting of Mining and Materials Processing Institute of Japan, Mining and Materials Processing Institute of Japan, Tokyo, pp. 91–94

Fukuzono, T., 1985. *A new method for predicting the failure time of a slope*. In: Proceedings of the Fourth International Conference and Field Workshop on Landslides. Tokyo University Press, Tokio, pp. 145–150.

Gamperl, M., Singer, J., Thuro, K., 2021. *Internet of Things Geosensor Network for Cost-Effective Landslide Early Warning Systems*. Sensors 21, 2609. https://doi.org/10.3390/s21082609

Ganjalipour, K., 2021. *Review of Inclinometer Errors and Provide Correction Methods for Bias shift Error and Depth Position Error of the Probe*. Geotechnical and Geological Engineering 39, pp. 4017-4034. https://doi.org/10.1007/s10706-021-01743-w

Gazibara, S.B., Krkač, M., Arbanas, S.M., 2019. *Landslide inventory mapping using LiDAR data in the City of Zagreb (Croatia).* Journal of Maps 15, 773–779. https://doi.org/10.1080/17445647.2019.1671906

Gigli, G., Morelli, S., Fornera, S., Casagli, N., 2014. *Terrestrial laser scanner and geomechanical surveys for the rapid evaluation of rock fall susceptibility scenarios.* Landslides 11, 1–14. https://doi.org/10.1007/s10346-012-0374-0

Giordan, D., Wrzesniak, A., Allasia, P., 2019. *The Importance of a Dedicated Monitoring Solution and Communication Strategy for an Effective Management of Complex Active Landslides in Urbanized Areas.* Sustainability 11, 946. https://doi.org/10.3390/su11040946

Giorgetti, A., Lucchi, M., Tavelli, E., Barla, M., Gigli, G., Casagli, N., Chiani, M., Dardari, D., 2016. *A Robust Wireless Sensor Network for Landslide Risk Analysis: System Design, Deployment, and Field Testing.* IEEE Sensors Journal 16, 6374–6386. https://doi.org/10.1109/JSEN.2016.2579263

Giusto, D., Iera, A., Morabito, G., Atzori, L., 2010. *The Internet of Things: 20th Tyrrhenian Workshop on Digital Communications.* Springer-Verlag, New York. https://doi.org/10.1007/978-1-4419-1674-7

Glastonbury, J., Fell, R., 2002. *Report on the analysis of the deformation behaviour of excavated rock slopes.* Studies from the School of Civil and Environmental engineering. University of New South Wales, School of Civil Engineering, Sydney.

Gracchi, T., 2019. *Wireless sensor networks for landslide monitoring: application and optimization by visibility analysis on 3D point clouds.* Doctoral Thesis, Université de Lausanne, Faculté des géosciences et de l'environnement.

Green, G.E., Mikkelsen, P.E., 1988. *Deformation measurements with inclinometers.* Transportation Research Record 1169.

Guzzetti, F., 2005. *Landslide hazard and risk assessment - concepts, methods and tools for the detection and mapping of landslides, for landslide susceptibility zonation and hazard assessment, and for landslide risk evaluation.* Doctoral Thesis, Mathematisch-Naturwissenschaftlichen Fakultät der Rheinischen Friedrich-Wilhelms-Universität University of Bonn, Bonn.

Guzzetti, F., Gariano, S.L., Peruccacci, S., Brunetti, M.T., Marchesini, I., Rossi, M., Melillo, M., 2020. *Geographical landslide early warning systems.* Earth-Science Reviews 200, 102973. https://doi.org/10.1016/j.earscirev.2019.102973

Hao, S., Liu, C., Lu, C., Elsworth, D., 2016. *A relation to predict the failure of materials and potential application to volcanic eruptions and landslides.* Scientific Reports 6, 27877. https://doi.org/10.1038/srep27877

Helmstetter, A., Sornette, D., Grasso, J.-R., Andersen, J.V., Gluzman, S., Pisarenko, V., 2004. *Slider block friction model for landslides: Application to Vaiont and La Clapière landslides.* Journal of Geophysical Research 109, Issue B2. https://doi.org/10.1029/2002JB002160

Hunt, R.E., 1984. *Geotechnical engineering investigation manual.* McGraw-Hill, New York.

Intrieri, E., Carlà, T., Gigli, G., 2019. *Forecasting the time of failure of landslides at slope-scale: A literature review.* Earth-Science Reviews 193, 333–349. https://doi.org/10.1016/j.earscirev.2019.03.019

Intrieri, E., Gigli, G., 2016. *Landslide forecasting and factors influencing predictability.* Natural Hazards and Earth System Sciences 16, 2501–2510. https://doi.org/10.5194/nhess-16-2501-2016

Intrieri, E., Gigli, G., Casagli, N., Nadim, F., 2013. *Brief communication "Landslide Early Warning System: toolbox and general concepts."* Natural Hazards and Earth System Sciences 13, 85–90. https://doi.org/10.5194/nhess-13-85-2013

ISO 18674-1:2015, 2015. *Geotechnical investigation and testing. Geotechnical monitoring by field instrumentation -Part 1: General rules.*

Jaboyedoff, M., Derron, M.-H., 2020. *Chapter 7 - Landslide analysis using laser scanners.* In: Tarolli, P., Mudd, S.M. (Eds.), Developments in Earth Surface Processes, Remote Sensing of Geomorphology. Elsevier, pp. 207–230. https://doi.org/10.1016/B978-0-444-64177-9.00007-2

Jakob, M., Stein, D., Ulmi, M., 2012. *Vulnerability of buildings to debris flow impact.* Natural Hazards 60, 241–261. https://doi.org/10.1007/s11069-011-0007-2

Jiang, Y., Xu, Q., Lu, Z., Luo, H., Liao, L., Dong, X., 2021. *Modelling and predicting landslide displacements and uncertainties by multiple machine-learning algorithms: application to Baishuihe landslide in Three Gorges Reservoir, China.* Geomatics. Natural Hazards and Risk 12(1):741–762. https://doi.org/10.1080/19475705.2021.1891145

Kalybekov, T., Yunussov, R., Rysbekov, K.V., Soltabayeva, S.T., 2018. *Control of reserves readiness and quality characteristics of ore in open pit mining.* In: Proceedings of the 25th World Mining Congress 2018, Astana, Kazakhstan, pp. 220–226.

Karnawati, D., Fathani, T.F., Andayani, B., Suharto, 2010. *The Hybrid Socio-Technical Approach as a Strategic Program for Social Development in Geo-disaster Prone Area in Indonesia.* International Journal of Humanities and Social Sciences 4, 800–804.

Kayesa, G., 2006. *Prediction of slope failure at Letlhakane mine with the Geomos slope monitoring system.* In: Proceedings of the International Symposium on Stability of Rock Slopes in Open Pit Mining and Civil Engineering Situations, The South African Institute of Mining and Metallurgy, Cape Town, pp. 602–622.

Kilburn, C.R.J., Petley, D.N., 2003. *Forecasting giant, catastrophic slope collapse: lessons from Vajont, Northern Italy*. Geomorphology, Studies on Large Volume Landslides 54, 21–32. https://doi.org/10.1016/S0169-555X(03)00052-7

Klein, E., Coccia, S., 2020. *Early warning systems for slope instabilities: concepts, feedback and perspectives*. Ineris - 201176 - 2176123 - v1.0. Institut national de l'environnement industriel et des risques.

Knox, G., 1927. *Landslides in South Wales valleys.* In: Proceedings of the South Wales Institute of Engineers, 43 (1927), pp. 161-247

Kramp, T., van Kranenburg, R., Lange, S., 2013. *Introduction to the Internet of Things.* In: Bassi, A., Bauer, M., Fiedler, M., Kramp, T., van Kranenburg, R., Lange, S., Meissner, S. (Eds.), Enabling Things to Talk: Designing IoT Solutions with the IoT Architectural Reference Model. Springer, Berlin, Heidelberg, pp. 1–10. https://doi.org/10.1007/978-3-642-40403-0_1

Krkač, M., Špoljarić, D., Bernat, S., Arbanas, S.M., 2017. *Method for prediction of landslide movements based on random forests.* Landslides 14, 947–960. https://doi.org/10.1007/s10346-016-0761-z

Lane, S.N., James, T.D., Crowell, M.D., 2000. *Application of Digital Photogrammetry to Complex Topography for Geomorphological Research*. The Photogrammetric Record 16, 793–821. https://doi.org/10.1111/0031-868X.00152

Li, H., Xu, Q., He, Y., Deng, J., 2018. *Prediction of landslide displacement with an ensemble-based extreme learning machine and copula models*. Landslides 15, 2047–2059. https://doi.org/10.1007/s10346-018-1020-2

Lian, C., Zeng, Z., Yao, W., Tang, H., 2014. *Ensemble of extreme learning machine for landslide displacement prediction based on time series analysis*. Neural Computing & Applications 24, 99–107 (2014). https://doi.org/10.1007/s00521-013-1446-3

Lienhart, W., 2017. *Geotechnical monitoring using total stations and laser scanners: critical aspects and solutions*. Journal of Civil Structural Health Monitoring 7, 315–324. https://doi.org/10.1007/s13349-017-0228-5

Lin, Q., Wang, Y., Liu, T., Zhu, Y., Sui, Q., 2017. *The Vulnerability of People to Landslides: A Case Study on the Relationship between the Casualties and Volume of Landslides in China*. International Journal of Environmental Research and Public Health 14. https://doi.org/10.3390/ijerph14020212

Liu, Z., Gilbert, G., Cepeda, J.M., Lysdahl, A.O.K., Piciullo, L., Hefre, H., Lacasse, S., 2021. *Modelling of shallow landslides with machine learning algorithms*. Geoscience Frontiers 12, 385–393. https://doi.org/10.1016/j.gsf.2020.04.014

Lo, H.-C., Hsu, S.-M., Chou, P.-Y., Ke, C.-C., 2020. *Mitigating drought and landslide simultaneously for mountain tribes of Taiwan: hydrogeological investigation, modelling, and*

development of an intelligent hazard prevention system. Natural Hazards 103, 3101–3121. https://doi.org/10.1007/s11069-020-04121-6

Loew, S., Gschwind, S., Gischig, V., Keller-Signer, A., Valenti, G., 2017. *Monitoring and early warning of the 2012 Preonzo catastrophic rockslope failure.* Landslides 14, 141–154. https://doi.org/10.1007/s10346-016-0701-y

Lollino, G., Arattano, M., Cuccureddu, M., 2002. *The use of the automatic inclinometric system for landslide early warning: the case of Cabella Ligure (North-Western Italy).* Physics and Chemistry of the Earth, Parts A/B/C 27, 1545–1550. https://doi.org/10.1016/S1474-7065(02)00175-4

Lovisolo, M., Della Giusta, A., 2005. *Precision of D.M.S. columns from real time in-place measurements and improvement in micro-movements analysis with early warning function.* WIT Transactions on Modelling and Simulation 41, 10.

Ma, J., Liu, X., Niu, X., Wang, Y., Wen, T., Zhang, J., Zou, Z., 2020. *Forecasting of Landslide Displacement Using a Probability-Scheme Combination Ensemble Prediction Technique.* International Journal of Environmental Research and Public Health. 2020; 17(13):4788. https://doi.org/10.3390/ijerph17134788

Manconi, A., Giordan, D., 2016. *Landslide failure forecast in near-real-time.* Geomatics, Natural Hazards and Risk 7, 639–648. https://doi.org/10.1080/19475705.2014.942388

Manconi, A., Giordan, D., 2015. *Landslide early warning based on failure forecast models: the example of the Mt. de La Saxe rockslide, northern Italy.* Natural Hazards and Earth System Sciences 15, 1639–1644. https://doi.org/10.5194/nhess-15-1639-2015

Marsella, M., Baldi, P., Coltelli, M., Fabris, M., 2012. *The morphological evolution of the Sciara del Fuoco since 1868: reconstructing the effusive activity at Stromboli volcano.* Bulletin of Volcanology 74, 231–248. https://doi.org/10.1007/s00445-011-0516-6

Mavrouli, O., Corominas, J., Jaboyedoff, M., 2015. *Size Distribution for Potentially Unstable Rock Masses and In Situ Rock Blocks Using LIDAR-Generated Digital Elevation Models.* Rock Mechanics and Rock Engineering 48, 1589–1604. https://doi.org/10.1007/s00603-014-0647-0

Mazzanti, P., Bozzano, F., Brunetti, A., Esposito, C., Martino, S., Prestininzi, A., Rocca, A., Scarascia Mugnozza, G., 2015a. *Terrestrial SAR Interferometry Monitoring of Natural Slopes and Man-Made Structures.* In: Lollino, G., Manconi, A., Guzzetti, F., Culshaw, M., Bobrowsky, P., Luino, F. (Eds.), Engineering Geology for Society and Territory - Volume 5. Springer International Publishing, Cham, pp. 189–194. https://doi.org/10.1007/978-3-319-09048-1_37

Mazzanti, P., Bozzano, F., Cipriani, I., Prestininzi, A., 2015b. *New insights into the temporal prediction of landslides by a terrestrial SAR interferometry monitoring case study.* Landslides 12, 55–68. https://doi.org/10.1007/s10346-014-0469-x

Mazzanti, P., Schilirò, L., Martino, S., Antonielli, B., Brizi, E., Brunetti, A., Margottini, C., Scarascia Mugnozza, G., 2018. *The Contribution of Terrestrial Laser Scanning to the Analysis of Cliff Slope Stability in Sugano (Central Italy).* Remote Sensing 10, 1475. https://doi.org/10.3390/rs10091475

Medina-Cetina, Z., Nadim, F., 2008. *Stochastic design of an early warning system.* Georisk: Assessment and Management of Risk for Engineered Systems and Geohazards 2, 223–236. https://doi.org/10.1080/17499510802086777

Mentes, Gy., 2012. *A new borehole wire extensometer with high accuracy and stability for observation of local geodynamic processes.* Review of Scientific Instruments 83, 015109. https://doi.org/10.1063/1.3676652

Michoud, C., Bazin, S., Blikra, L.H., Derron, M.-H., Jaboyedoff, M., 2013. *Experiences from site-specific landslide early warning systems.* Natural Hazards and Earth System Sciences 13, 2659–2673. https://doi.org/10.5194/nhess-13-2659-2013

Miele, P., Di Napoli, M., Guerriero, L., Ramondini, M., Sellers, C., Annibali Corona, M., Di Martire, D., 2021. *Landslide Awareness System (LAwS) to Increase the Resilience and Safety of Transport Infrastructure: The Case Study of Pan-American Highway (Cuenca–Ecuador).* Remote Sensing 13, 1564. https://doi.org/10.3390/rs13081564

Mikkelsen, P., 2003. *Advances in inclinometer data analysis.* In: Myrvoll, F. (Ed.), Proceedings of the 6th International Symposium on Field Measurements in Geomechanics, Oslo, Norway.

Moret, D., López, M.V., Arrúe, J.L., 2004. *TDR application for automated water level measurement from Mariotte reservoirs in tension disc infiltrometers.* Journal of Hydrology 297, 229–235. https://doi.org/10.1016/j.jhydrol.2004.04.003

Moretto, S., Bozzano, F., Esposito, C., Mazzanti, P., Rocca, A., 2017. *Assessment of Landslide Pre-Failure Monitoring and Forecasting Using Satellite SAR Interferometry.* Geosciences 7, 36. https://doi.org/10.3390/geosciences7020036

Moulat, M.E., Debauche, O., Mahmoudi, S., Brahim, L.A., Manneback, P., Lebeau, F., 2018. *Monitoring System Using Internet of Things For Potential Landslides.* Procedia Computer Science, The 15th International Conference on Mobile Systems and Pervasive Computing (MobiSPC 2018) / The 13th International Conference on Future Networks and Communications (FNC-2018) / Affiliated Workshops 134, 26–34. https://doi.org/10.1016/j.procs.2018.07.140

Mufundirwa, A., Fujii, Y., Kodama, J., 2010. *A new practical method for prediction of geomechanical failure-time.* International Journal of Rock Mechanics and Mining Sciences 47, 1079–1090. https://doi.org/10.1016/j.ijrmms.2010.07.001

Nor Diana, M.I., Muhamad, N., Taha, M.R., Osman, A., Alam, M.M., 2021. *Social Vulnerability Assessment for Landslide Hazards in Malaysia: A Systematic Review Study.* Land 10, 315. https://doi.org/10.3390/land10030315

Oppikofer, T., Jaboyedoff, M., Blikra, L., Derron, M.-H., Metzger, R., 2009. *Characterization and monitoring of the Åknes rockslide using terrestrial laser scanning*. Natural Hazards and Earth System Sciences 9, 1003–1019. https://doi.org/10.5194/nhess-9-1003-2009

Petley, D.N., 2004. *The evolution of slope failures: mechanisms of rupture propagation*. Natural Hazards and Earth System Sciences 4, 147–152. https://doi.org/10.5194/nhess-4-147-2004

Piciullo, L., 2016. *Performance analysis of landslide early warning systems at regional scale.* Doctoral Thesis, Università degli Studi di Salerno.

Piciullo, L., Calvello, M., Cepeda, J.M., 2018. *Territorial early warning systems for rainfall-induced landslides.* Earth-Science Reviews 179, 228–247. https://doi.org/10.1016/j.earscirev.2018.02.013

Pollock, W., Wartman, J., 2020. *Human Vulnerability to Landslides*. GeoHealth 4, e2020GH000287. https://doi.org/10.1029/2020GH000287

Pouloupatis, P.D., Florides, G., Tassou, S., 2011. *Measurements of ground temperatures in Cyprus for ground thermal applications.* Renewable Energy 36, 804–814. https://doi.org/10.1016/j.renene.2010.07.029

Prakash, N., Manconi, A., Loew, S., 2021. *A new strategy to map landslides with a generalized convolutional neural network*. Sci Rep 11, 9722. https://doi.org/10.1038/s41598-021-89015-8

Prasad, R., Dixit, M., 2020. *Performance Monitoring Of Dams through Piezometers - A Case Study.* International Journal of Engineering and Applied Sciences (IJEAS) 7.

Pumo, D., Francipane, A., Lo Conti, F., Arnone, E., Bitonto, P., Viola, F., La Loggia, G., Noto, L.V., 2015. *The SESAMO early warning system for rainfall-triggered landslides*. Journal of Hydroinformatics 18, 256–276. https://doi.org/10.2166/hydro.2015.060

Raspini, F., Bianchini, S., Ciampalini, A., Del Soldato, M., Montalti, R., Solari, L., Tofani, V., Casagli, N., 2019. *Persistent Scatterers continuous streaming for landslide monitoring and mapping: the case of the Tuscany region (Italy).* Landslides 16, 2033–2044. https://doi.org/10.1007/s10346-019-01249-w

Reid, M.E., Baum, R.L., Ellis, R.G.L.& W.L., 2008. *Capturing landslide dynamics and hydrologic triggers using near-real-time monitoring*. In: Chen, Z., Zhang, J-M., Ho, K., Wu, F-Q. (Eds.) Landslides and Engineered Slopes. From the Past to the Future. Proceedings of the 10th International Symposium on Landslides and Engineered Slopes, 30 June - 4 July 2008, Xi'an, China. CRC Press, London. https://doi.org/10.1201/9780203885284-14

Reid, W.V., 2005. *Millennium Ecosystem Assessment: Ecosystems and Human Well-Being—Synthesis Report.* World Resources Institute, 2005

Rengers, F.K., Rapstine, T.D., Olsen, M., Allstadt, K.E., Iverson, R.M., Leshchinsky, B., Obryk, M., Smith, J.B., 2021. *Using High Sample Rate Lidar to Measure Debris-Flow Velocity and Surface Geometry.* Environmental and Engineering Geoscience 27, 113–126. https://doi.org/10.2113/EEG-D-20-00045

Reyes-Carmona, C., Barra, A., Galve, J.P., Monserrat, O., Pérez-Peña, J.V., Mateos, R.M., Notti, D., Ruano, P., Millares, A., López-Vinielles, J., Azañón, J.M., 2020. *Sentinel-1 DInSAR for Monitoring Active Landslides in Critical Infrastructures: The Case of the Rules Reservoir (Southern Spain).* Remote Sensing 12, 809. https://doi.org/10.3390/rs12050809

Roncella, R., Forlani, G., Fornari, M., Diotri, F., 2014. *Landslide monitoring by fixed-base terrestrial stereo-photogrammetry.* ISPRS Annals of the Photogrammetry, Remote Sensing and Spatial Information Sciences, II–5, 297–304. https://doi.org/10.5194/isprsannals-II-5-297-2014

Rose, N.D., Hungr, O., 2007. *Forecasting potential rock slope failure in open pit mines using the inverse-velocity method.* International Journal of Rock Mechanics and Mining Sciences 44, 308–320. https://doi.org/10.1016/j.ijrmms.2006.07.014

Ryan, T., Call, R., 1993. *Applications of rock mass monitoring for stability assessment of pit slope failure.* International Journal of Rock Mechanics and Mining Sciences & Geomechanics Abstracts 30, A57. https://doi.org/10.1016/0148-9062(93)90607-F

Saito, M., 1969. *Forecasting Time of Slope failure by Tertiary Creep.* In: Proceedings of the 7th International Conference on Soil Mechanics and Foundation Engineering, 2 (1969), pp. 677–683.

Saito, M., 1979. *Evidential study on forecasting occurrence of slope failure.* Trans. of the Dept. of Geomech. Armenian Academy of Sciences, Yerevan, URSS.

Saito, M., Uezawa, H., 1961. *Failure of soil due to creep.* In: Proceedings of the 5th International Conference on Soil Mechanics and Foundation Engineering, Mexico City, pp. 315–318.

Sassa, K., Canuti, P., 2008. *Landslides - Disaster Risk Reduction.* Springer Science & Business Media, Berlin, Heidelberg. https://doi.org/10.1007/978-3-540-69970-5

Savi, R., Carri, A., Cavalca, E., Valletta, A., Segalini, A., 2019. *Application of innovative monitoring tools for safety and alert procedures in road tunnels.* Transportation Research Procedia, TRANSCOM 2019 13th International Scientific Conference on Sustainable, Modern and Safe Transport 40, 1540–1547. https://doi.org/10.1016/j.trpro.2019.07.213

Savvaidis, P.D., 2003. *Existing landslide monitoring systems and techniques.* Presented at "From Stars to Earth and Culture, In honor of the memory of Professor Alexandros Tsioumis", The Aristotle University of Thessaloniki, Thessaloniki, Greece, pp. 242–258.

Scheidl, C., Rickenmann, D., Chiari, M., 2008. *The use of airborne LiDAR data for the analysis of debris flow events in Switzerland.* Natural Hazards and Earth System Sciences 8, 1113–1127. https://doi.org/10.5194/nhess-8-1113-2008

Segalini, A., Carini, C., 2013. *Underground Landslide Displacement Monitoring: A New MMES Based Device.* In: Margottini, C., Canuti, P., Sassa, K. (Eds.), Landslide Science and Practice: Volume 2: Early Warning, Instrumentation and Monitoring. Springer, Berlin, Heidelberg, pp. 87–93. https://doi.org/10.1007/978-3-642-31445-2_11

Segalini, A., Carri, A., Savi, R., 2017. *Role of geotechnical monitoring: state of the art and new perspectives.* In: Proceedings of the GEO-EXPO 2017, Geotechnical Society of Bosnia and Herzegovina. https://doi.org/10.35123/GEO-EXPO_2017_3

Segalini, A, Carri, A., Valletta, A., Martino, M., 2019a. *Innovative Monitoring Tools and Early Warning Systems for Risk Management: A Case Study.* Geosciences 9, 62. https://doi.org/10.3390/geosciences9020062

Segalini, A., Chiapponi, L., Pastarini, B., Carini, C., 2014. *Automated Inclinometer Monitoring Based on Micro Electro-Mechanical System Technology: Applications and Verification.* In: Sassa, K., Canuti, P., Yin, Y. (Eds.), Landslide Science for a Safer Geoenvironment. Springer International Publishing, Cham, pp. 595–600. https://doi.org/10.1007/978-3-319-05050-8_92

Segalini, A., Savi, R., Cavalca, E., Valletta, A., Carri, A., 2021. *Innovative Application of IoT Technologies to Improve Geotechnical Monitoring Tools and Early Warning Performances.* In: Rotaru, A. (Ed.), Critical Thinking in the Sustainable Rehabilitation and Risk Management of the Built Environment, Springer Series in Geomechanics and Geoengineering. Springer International Publishing, Cham, pp. 142–146. https://doi.org/10.1007/978-3-030-61118-7_12

Segalini, A., Valletta, A., Carri, A., 2018. *Landslide time-of-failure forecast and alert threshold assessment: A generalized criterion.* Engineering Geology 245, 72–80. https://doi.org/10.1016/j.enggeo.2018.08.003

Segalini, A., Valletta, A., Carri, A., Cavalca, E., 2019b. *Monitoring of a retaining wall with innovative multi-parameter tools.* In: Proceedings of the 4th Regional Symposium on Landslides in the Adriatic—Balkan Region, Sarajevo, Bosnia and Herzegovina. https://doi.org/10.35123/ReSyLAB_2019_5

Shah, S.K., Aye, L., Rismanchi, B., 2019. *Undisturbed ground temperature in Melbourne.* AIP Conference Proceedings 2121, 080001. https://doi.org/10.1063/1.5115928

Siddle, H.J., Moore, R., Carey, J., Petley, D.N., 2007. *Pre-failure behaviour of slope materials and their significance in the progressive failure of landslides.* In: McInnes, R., Jakeways, J., Fairbank, H., Mathie, E. (Eds.), Proceedings of the International Conference on Landslides and Climate Change, Ventnor, Isle of Wight, UK, 21-24 May 2007. CRC Press, London. https://doi.org/10.1201/NOE0415443180

Singer, J., Thuro, K., Sambeth, U., 2006. *Development of a continuous 3D-monitoring system for unstable slopes using TDR.* Felsbau, 2006, n. 3, v. 24

Singh, V.K., Ansari, T.A., Vishal, V., Singh, T.N., 2020. *Landslide Susceptibility Analysis Using Numerical and Neural Network, Near Kedarnath, Uttarakhand, India*. American Journal of Environmental Sciences 16, 8–20. https://doi.org/10.3844/ajessp.2020.8.20

Smethurst, J.A., Smith, A., Uhlemann, S., Wooff, C., Chambers, J., Hughes, P., Lenart, S., Saroglou, H., Springman, S.M., Löfroth, H., Hughes, D., 2017. *Current and future role of instrumentation and monitoring in the performance of transport infrastructure slopes.* Quarterly Journal of Engineering Geology and Hydrogeology 50, 271–286. https://doi.org/10.1144/qjegh2016-080

Stähli, M., Sättele, M., Huggel, C., McArdell, B.W., Lehmann, P., Van Herwijnen, A., Berne, A., Schleiss, M., Ferrari, A., Kos, A., Or, D., Springman, S.M., 2015. *Monitoring and prediction in early warning systems for rapid mass movements.* Natural Hazards and Earth System Sciences 15, 905–917. https://doi.org/10.5194/nhess-15-905-2015

Stark, T.D., Choi, H., 2008. *Slope inclinometers for landslides*. Landslides 5, 339. https://doi.org/10.1007/s10346-008-0126-3

Stumpf, A., Malet, J.-P., Allemand, P., Pierrot-Deseilligny, M., Skupinski, G., 2015. *Ground-based multi-view photogrammetry for the monitoring of landslide deformation and erosion.* Geomorphology 231, 130–145. https://doi.org/10.1016/j.geomorph.2014.10.039

Suwa, H., Mizuno, T., Ishii, T., 2010. *Prediction of a landslide and analysis of slide motion with reference to the 2004 Ohto slide in Nara, Japan*. Geomorphology, Recent advances in landslide investigation 124, 157–163. https://doi.org/10.1016/j.geomorph.2010.05.003

Swarbrick, G.E., Clarke, S.J., 2015. *Shape Accel Arrays — comparative performance in a mining application*. Presented at the Ninth International Symposium on Field Measurements in Geomechanics, 2015 9-11 September, Sydney, Australian Centre for Geomechanics. https://doi.org/10.36487/ACG_rep/1508_10_Swarbrick

Tarchi, D., Casagli, N., Moretti, S., Leva, D., Sieber, A.J., 2003. *Monitoring landslide displacements by using ground-based synthetic aperture radar interferometry: Application to the Ruinon landslide in the Italian Alps.* Journal of Geophysical Research: Solid Earth 108. https://doi.org/10.1029/2002JB002204

Tavenas, F., Leroueil, S., 2011. *Creep and failure of slopes in clays.* Canadian Geotechnical Journal. https://doi.org/10.1139/t81-010

Terzaghi, K., Peck, R., 1996. *Soil Mechanics In Engineering Practice, 1996th ed.* John Wiley & Sons, Ltd.

Thiebes, B., 2012. *Landslide Analysis and Early Warning Systems: Local and Regional Case Study in the Swabian Alb, Germany*. Springer Theses. Springer-Verlag, Berlin Heidelberg. https://doi.org/10.1007/978-3-642-27526-5

Tinti, F., Carri, A., Kasmaee, S., Valletta, A., Segalini, A., Bonduà, S., Bortolotti, V., 2018. *Ground temperature monitoring for a coaxial geothermal heat exchangers field: practical aspects and main issues from the first year of measurements*. Rudarsko-geološko-naftni zbornik 33, 47–57. https://doi.org/10.17794/rgn.2018.5.5

Tofani, V., Raspini, F., Catani, F., Casagli, N., 2013. *Persistent Scatterer Interferometry (PSI) Technique for Landslide Characterization and Monitoring*. Remote Sensing 5, 1045–1065. https://doi.org/10.3390/rs5031045

Tremblay, M., 1989. *Pore Pressure Measurement - Reliability of Different Systems*. SGI - Swedish Geotechnical Institute Report n°37.

Trigila, A., Iadanza, C., Bussettini, M., Lastoria, B., 2018. *Dissesto idrogeologico in Italia: pericolosità e indicatori di rischio – Edizione 2018.* ISPRA - Istituto Superiore per la Protezione e la Ricerca Internazionale.

UNDRR, 2019. *2018: Extreme weather events affected 60m people*. Press release: embargo 11.00 CET, January 24 No. 2019/01.

UNISDR, 2006. *Developing early warning systems, a checklist*. Presented at the Third International Conference on Early Warning (EWC III), Bonn, Germany.

United Nations, 2016. *Report of the open-ended intergovernmental expert working group on indicators and terminology relating to disaster risk reduction* (No. A/71/644).

Uysal, M., Toprak, A.S., Polat, N., 2015. *DEM generation with UAV Photogrammetry and accuracy analysis in Sahitler hill*. Measurement 73, 539–543. https://doi.org/10.1016/j.measurement.2015.06.010

Valletta A., Carri A., Savi R., Cavalca E., Segalini A., 2020a. *Definition of a new multi-level early warning procedure for landslide risk management.* EGU General Assembly 2020, Online, 4-8 May 2020, EGU2020-13777. https://doi.org/10.5194/egusphere-egu2020-13777

Valletta, A., Carri, A., Segalini, A., 2021. *Definition and application of a multi-criteria algorithm to identify landslide acceleration phases*. Georisk: Assessment and Management of Risk for Engineered Systems and Geohazards 0, 1–15. https://doi.org/10.1080/17499518.2021.1952610

Valletta, A., Carri, A., Segalini, A., 2019. *Innovative monitoring instruments as support tools for natural risks management*. ROL – Rendiconti Online della Società Geologica Italiana, 48/2019. https://doi.org/10.3301/ROL.2019.44

Valletta, A., Segalini, A., Carri, A., 2020b. *Application of a Generalized Criterion: Time-of-Failure Forecast and Alert Thresholds Assessment for Landslides.* In: De Maio, M., Tiwari, A.K. (Eds.), Applied Geology: Approaches to Future Resource Management. Springer International Publishing, Cham, pp. 283–298. https://doi.org/10.1007/978-3-030-43953-8_17

Van Asch, T., Malet, J.-P., Van Beek, L., Amitrano, D., 2007. *Techniques, advances, problems and issues in numerical modelling of landslide hazard*. Bulletin de la Société Géologique de France (2007) 178 (2): 65–88. https://doi.org/10.2113/gssgfbull.178.2.65

VanDine, D.F., Moore, G.D., Wise, M., Program, B.C.F.S., 2004. *Landslide Risk Case Studies in Forest Development Planning and Operations*. British Columbia, Forest Science Program.

Varnes, D.J., 1982. *Time-deformation relations in creep to failure of earth materials*. In: Proceedings of the 7th Southeast Asia Geotechnical Conference, Hong Kong, pp. 107–130.

Varnes, D.J., 1984. *Landslide hazard zonation: a review of principles and practice*. Natural Hazards, 3 (1984).

Voight, B., 1988. *A method for prediction of volcanic eruptions*. Nature 332, 125–130. https://doi.org/10.1038/332125a0

Voight, B., 1989. *A Relation to Describe Rate-Dependent Material Failure*. Science 243, 200–203. https://doi.org/10.1126/science.243.4888.200

Voight, B., Kennedy, B.A., 1979. *Chapter 17 - Slope Failure of 1967–1969, Chuquicamata Mine, Chile*. In: Voight, B. (Ed.), Developments in Geotechnical Engineering, Rockslides and Avalanches, 2. Elsevier, pp. 595–632. https://doi.org/10.1016/B978-0-444-41508-0.50025-9

Walstra, J., Chandler, J.H., Dixon, N., Dijkstra, T.A., 2007. *Aerial photography and digital photogrammetry for landslide monitoring*. Geological Society, London, Special Publications 283, 53–63. https://doi.org/10.1144/SP283.5

Wang, H., Zhang, L., Yin, K., Luo, H., Li, J., 2021. *Landslide identification using machine learning*. Geoscience Frontiers, Volume 12, Issue 1, 2021, Pages 351-364, ISSN 1674-9871, https://doi.org/10.1016/j.gsf.2020.02.012.

Wang, T., Zhao, Y., Wang, Z., Nan, L., Yu, Z., Zan, Z., 2015. *Research on Safety monitoring network of the city subway engineering*. In: Proceedings of the 4th International Conference on Information Technology and Management Innovation, Atlantis Press, pp. 420–425. https://doi.org/10.2991/icitmi-15.2015.66

Wilson, M., Landrø, M., Davis, T.L., 2019. *Geophysical Techniques*. In: Geophysics and Geosequestration. Cambridge University Press, Cambridge, pp. 71–194.

Wortmann, F., Flüchter, K., 2015. *Internet of Things*. Business & Information Systems Engineering volume 57, pages 221–224. https://doi.org/10.1007/s12599-015-0383-3

WP/WLI, 1990. *A suggested method for reporting a landslide*. Bulletin of the International Association of Engineering Geology 41, 5–12. https://doi.org/10.1007/BF02590201

WP/WLI, 1991. *A suggested method for a landslide summary*. Bulletin of the International Association of Engineering Geology 43, 101–110. https://doi.org/10.1007/BF02590177

Wrzesniak, A., Giordan, D., 2017. *Development of an algorithm for automatic elaboration, representation and dissemination of landslide monitoring data.* Geomatics, Natural Hazards and Risk 8, 1898–1913. https://doi.org/10.1080/19475705.2017.1392369

Xie, Y., Liu, J., 2017. *Analysis of early-warning threshold for metro construction collapse risk based on D-S evidence theory and rough set.* Wuhan University Journal of Natural Sciences 22, 510–516. https://doi.org/10.1007/s11859-017-1281-y

Xu, Q., Yuan, Y., Zeng, Y., Hack, R., 2011. *Some new pre-warning criteria for creep slope failure.* Science China Technological Sciences 54, 210–220. https://doi.org/10.1007/s11431-011-4640-5

Zhang, H., Wu, Y., 2017. *Removing spike noise from track alignment irregularities measures using an iteration filter.* AIP Conference Proceedings 1834, 030007. https://doi.org/10.1063/1.4981572

Zheng, X., Yang, X., Ma, H., Ren, G., Yu, Z., Yang, F., Zhang, H., Gao, W., 2019. *Integrative Landslide Emergency Monitoring Scheme Based on GB-INSAR Interferometry, Terrestrial Laser Scanning and UAV Photography.* Journal of Physics: Conference Series 1213, 052069. https://doi.org/10.1088/1742-6596/1213/5/052069

Zhou, C., Yin, K., Cao, Y., Ahmed, B., Fu, X., 2018. *A novel method for landslide displacement prediction by integrating advanced computational intelligence algorithms.* Scientific Reports 8, 7287. https://doi.org/10.1038/s41598-018-25567-6

Zhu, X., Xu, Q., Tang, M., Li, H., Liu, F., 2018. *A hybrid machine learning and computing model for forecasting displacement of multifactor-induced landslides.* Neural Computing & Applications 30, 3825–3835 (2018). https://doi.org/10.1007/s00521-017-2968-x